Nuclear Science
NEA/NSC/WPFC/DOC(2012)17
June 2012
www.oecd-nea.org

OECD

Benchmarking of thermal-hydraulic loop models for lead-alloy-cooled advanced nuclear energy systems

Phase I: Isothermal forced convection case

AEN
NEA

NUCLEAR ENERGY AGENCY

Benchmarking of thermal-hydraulic loop models for lead-alloy-cooled advanced nuclear energy systems

Phase I: Isothermal forced convection case

NUCLEAR ENERGY AGENCY
ORGANISATION FOR ECONOMIC CO-OPERATION AND DEVELOPMENT

ORGANISATION FOR ECONOMIC CO-OPERATION AND DEVELOPMENT

The OECD is a unique forum where the governments of 34 democracies work together to address the economic, social and environmental challenges of globalisation. The OECD is also at the forefront of efforts to understand and to help governments respond to new developments and concerns, such as corporate governance, the information economy and the challenges of an ageing population. The Organisation provides a setting where governments can compare policy experiences, seek answers to common problems, identify good practice and work to co-ordinate domestic and international policies.

The OECD member countries are: Australia, Austria, Belgium, Canada, Chile, the Czech Republic, Denmark, Estonia, Finland, France, Germany, Greece, Hungary, Iceland, Ireland, Israel, Italy, Japan, Luxembourg, Mexico, the Netherlands, New Zealand, Norway, Poland, Portugal, the Republic of Korea, the Slovak Republic, Slovenia, Spain, Sweden, Switzerland, Turkey, the United Kingdom and the United States. The European Commission takes part in the work of the OECD.

OECD Publishing disseminates widely the results of the Organisation's statistics gathering and research on economic, social and environmental issues, as well as the conventions, guidelines and standards agreed by its members.

NUCLEAR ENERGY AGENCY

The OECD Nuclear Energy Agency (NEA) was established on 1 February 1958. Current NEA membership consists of 30 OECD member countries: Australia, Austria, Belgium, Canada, the Czech Republic, Denmark, Finland, France, Germany, Greece, Hungary, Iceland, Ireland, Italy, Japan, Luxembourg, Mexico, the Netherlands, Norway, Poland, Portugal, the Republic of Korea, the Slovak Republic, Slovenia, Spain, Sweden, Switzerland, Turkey, the United Kingdom and the United States. The European Commission also takes part in the work of the Agency.

The mission of the NEA is:

- to assist its member countries in maintaining and further developing, through international co-operation, the scientific, technological and legal bases required for a safe, environmentally friendly and economical use of nuclear energy for peaceful purposes, as well as
- to provide authoritative assessments and to forge common understandings on key issues, as input to government decisions on nuclear energy policy and to broader OECD policy analyses in areas such as energy and sustainable development.

Specific areas of competence of the NEA include the safety and regulation of nuclear activities, radioactive waste management, radiological protection, nuclear science, economic and technical analyses of the nuclear fuel cycle, nuclear law and liability, and public information.

The NEA Data Bank provides nuclear data and computer program services for participating countries. In these and related tasks, the NEA works in close collaboration with the International Atomic Energy Agency in Vienna, with which it has a Co-operation Agreement, as well as with other international organisations in the nuclear field.

Foreword

Under the auspices of the NEA Nuclear Science Committee (NSC), the Working Party on Scientific Issues of the Fuel Cycle (WPFC) has been established to co-ordinate scientific activities regarding various existing and advanced nuclear fuel cycles, including advanced reactor systems, associated chemistry and flowsheets, development and performance of fuel and materials and accelerators and spallation targets. The WPFC has different expert groups to cover a wide range of scientific issues in the field of nuclear fuel cycle.

The Task Force on Lead-Alloy-Cooled Advanced Nuclear Energy Systems (LACANES) was created in 2006 to study thermal-hydraulic characteristics of heavy liquid metal coolant loop. The objectives of the task force are to (1) validate thermal-hydraulic loop models for application to LACANES design analysis in participating organisations, by benchmarking with a set of well-characterised lead-alloy coolant loop test data, (2) establish guidelines for quantifying thermal-hydraulic modelling parameters related to friction and heat transfer by lead-alloy coolant and (3) identify specific issues, either in modelling and/or in loop testing, which need to be addressed via possible future work.

Nine participants from seven different institutes participated in the first phase of the benchmark. This report provides details of the benchmark specifications, method and code characteristics and results of the preliminary study: pressure loss coefficient and Phase-I. A comparison and analysis of the results will be performed together with Phase-II.

Acknowledgements

The NEA Secretariat expresses its sincere gratitude to Mr. V. V. Kuznetsov from the International Atomic Energy Agency for giving his best effort and support to collaborate with Russian experts and to the NUTRECK of Seoul National University of the Republic of Korea for sharing valuable experimental data.

Table of contents

Chapter 1: Introduction 11
Chapter 2: Benchmark specifications 13
2.1 Design feature of the HELIOS...13
2.2 Geometrical data 15
2.3 Guidelines for pressure loss coefficient evaluation 20
2.3.1 Definition of pressure loss coefficients 20
2.3.2 Procedures for pressure loss coefficient evaluation 20
2.3.3 Report format for evaluated pressure loss coefficients under isothermal forced convection conditions 21
Chapter 3: Method of the benchmark.. 22
3.1 KIT/IKET, Germany...22
3.1.1 Code description 22
3.1.2 Mesh structure and local form loss coefficients 24
3.2 RSE, Italy 28
3.3 ENEA, Italy 37
3.3.1 RELAP5 code version for HLM 37
3.3.2 Models and nodalisation...37
3.3.3 Preliminary results 41
3.4 Seoul National University, Korea 42
3.4.1 Computer code characteristics 42
3.4.2 Nodalisation of HELIOS 43
3.4.3 Pressure loss lodels in MARS-LBE 3.11 [1]...43
3.5 GIDROPRESS, Russian Federation 48
3.6 IPPE, Russian Federation 49
3.6.1 Calculating code HYDRA for carrying out calculation of a hydraulic network...49
3.6.2 HELIOS model 51
3.7 RRC KI, Russian Federation..54
3.7.1 Definition of pressure loss coefficients and relative pressure all over the loop 54
3.7.2 Procedures for pressure loss coefficients evaluation 54
3.7.3 Results of calculation of pressure loss coefficients and pressure distribution along HELIOS loop under isothermal flow conditions 55
3.8 KIT/INR, Germany 56
3.8.1 Description of TRACE 56
3.8.2 Wall drag and pressure loss models 56
3.8.3 TRACE nodalisation and calculation of the HELIOS loop 59
Chapter 4: HELIOS experiments and results.. 62
4.1 Setup 62
4.2 Instrumentation 62

4.3 Procedure 66
4.4 Results 68
Chapter 5: Comparison and discussion 71
5.1 Benchmark plan 71
5.2 Result of system code simulation 71
5.3 Result of CFD simulation 75
5.3.1 Core 75
5.3.2 Gate valve 78
5.3.3 Orifice 79
5.4 Comparison and discussion 81
5.4.1 Core 81
5.4.2 Orifice 84
5.4.3 Gate valve 84
5.4.4 Heat exchanger 85
5.4.5 Expansion tank 88
5.4.6 Straight and 45° and 90° elbow pipes 89
5.4.7 Gasket 92
5.4.8 Tee 93
Chapter 6: Summary and conclusion 96
6.1 Summary 96
6.2 Conclusion 97
Appendix A 105
Appendix B 120
Appendix C 158

List of figures

Figure 2.1: Schematic diagram of PEACER-300 13
Figure 2.2: Schematic (left) and photograph (right) of HELIOS (Heavy Eutectic liquid metal Loop for Integral test of Operability and Safety of PEACER) 14
Figure 2.3: Component numbers 16
Figure 3.1: Form loss coefficient of T-junction [3] 27
Figure 3.2: Form loss coefficient of bending pipe [3] 27
Figure 3.3: Flow expansion and contraction [3] 27
Figure 3.4: Form loss coefficient of flow contraction [3] 27
Figure 3.5: LegoPC graphical interface 29
Figure 3.6: Translation of the component links into a non-linear equation system 29
Figure 3.7: LegoPC simulation user interface 30
Figure 3.8: HELIOS model main components 30
Figure 3.9 Gasket between flanges 31
Figure 3.10: Single bend 31
Figure 3.11: S-shaped bend with flow in one plane 32
Figure 3.12: Rehme modified drag coefficient 33
Figure 3.13: Thin-plate orifice 34
Figure 3.14: Gate valve 34
Figure 3.15: LegoPC HELIOS preliminary model 35
Figure 3.16: Nodalisation scheme of Helios loop for RELAP5 code 39

Figure 3.17: Pressure distribution in HELIOS loop at high-flow conditions 42
Figure 3.18: Nodalisation of the HELIOS...43
Figure 3.19: Sudden expansion (left) and contraction (right)...45
Figure 3.20: A_1 (left figure) and B_1 (right figure) for elbow form factor............................45
Figure 3.21: Geometry of tee (left figure) and form factor (right figure) 46
Figure 3.22: Geometry of the orifice...47
Figure 3.23: Grid form factor, C_v...47
Figure 3.24: TRACE nodding for an abrupt contraction (a), an abrupt expansion (b) and a thin-plate orifice (c) [5] 59
Figure 3.25: TRACE nodalisation scheme of the HELIOS loop..60
Figure 4.1: Three-dimensional diagram of the HELIOS forced convection test setup....63
Figure 4.2: Location of Type K thermocouples (T/C) in the HELIOS 64
Figure 4.3: Location of five differential pressure transducers (DP) in the HELIOS..........65
Figure 4.4: Pressure difference at orifice region and temperature at all positions at a different pump speed...67
Figure 4.5: Pressure loss at core region 68
Figure 4.6: Pressure loss at gate valve 69
Figure 4.7: Pressure loss at orifice region...69
Figure 5.1: Overall procedures of LACANES benchmark...71
Figure 5.2: Comparison of the total and partial pressure loss at high-mass flow rate case(13.57kg/s) 73
Figure 5.3: Comparison of the accumulated pressure loss at high-flow rate case (G/V: Gate Valve, E/T: Expansion Tank, H/X: Heat Exchanger) 74
Figure 5.4: Comparison between CFD and experiment result 75
Figure 5.5: Schematic diagram of HELIOS core and flow path...76
Figure 5.6: Pressure distribution at the centre plane of the core (a) results of Star-CD® (b) results of CFX®...77
Figure 5.8: Schematic diagram of gate valve 78
Figure 5.9: Pressure distributions at gate valve..79
Figure 5.10: Pressure change due to the gate valve 79
Figure 5.11: Schematic diagram of orifice...80
Figure 5.12: Pressure distribution at orifice 80
Figure 5.13: Pressure change due to the orifice...81
Figure 5.14: Pressure loss in the core at the high mass flow rate case............................81
Figure 5.15: Schematic diagram of core spacer based on orifice shape 82
Figure 5.16: Drag coefficient (C_v) of Rehme correlation for predicted pressure loss of grid spacer; modified new one based on measured data and four set used in benchmarking 83
Figure 5.17: Pressure loss in the core using equation 5.1 83
Figure 5.18: Pressure loss in the orifice at the high-mass flow rate 84
Figure 5.19: Pressure loss in the gate valve at the high-mass flow rate (other participants used manufacturer's data) 85
Figure 5.20: Accumulated pressure loss in the heat exchanger at high-flow rate..........86
Figure 5.21: Geometry and pressure loss coefficients of entrance in a vessel and discharge into a pipe [2]...87
Figure 5.22: Accumulated pressure loss in the heat exchanger at high-flow rate using Figure 5.21 88
Figure 5.23: Pressure loss in the expansion tank at the high-mass flow rate (left) and schematic diagram of expansion tank (right) 88

Figure 5.24: Sum of pressure loss in the straight pipe (15m) at high-flow rate..............91
Figure 5.25: Sum of pressure loss in the 45° elbow pipes (9ea) at high-flow rate 91
Figure 5.26: Sum of pressure losses in the 90° elbow pipes (4ea) at high-flow rate 92
Figure 5.27: Pressure loss at gasket area at the high-flow rate...92
Figure 5.28: Schematic diagram of tee-straight (left) and tee-branch (right) 93
Figure 5.29: Sum of pressure loss in tee-straight (8ea) at high-flow rate........................94
Figure 5.30: Pressure loss in tee-branch pipe at high-flow rate.......................................94
Figure A-1: 3D View of component #1 core vessel...106
Figure A-2: 3D View of component #2 pipe with tee..107
Figure A-4: 3D View of component #4 pipe with tee and elbows....................................108
Figure A-10: 3D View of component #10 expansion tank..109
Figure A-12: 3D View of component #12 pipe with tee and elbow.................................110
Figure A-14: 3D View of component #14 pipe with tee..111
Figure A-15: 3D View of component #15 heat exchanger..112
Figure A-16: 3D View of component #16 pipe with tee and elbow.................................113
Figure A-18: 3D View of component #18 pipe with tee..114
Figure A-20: 3D View of component #20 pipe with tee and elbow.................................115
Figure A-21: 3D View of component #21 pipe with elbow...116
Figure A-23: 3D View of component #23 pipe with tee and elbow.................................117
Figure A-24: 3D View of component #24 pipe with tee, elbow and valve 118
Figure A-25: 3D View of component #25 core..119
Figure B-1..121
Figure B-2..122
Figure B-3..123
Figure B-4..124
Figure B-5..125
Figure B-6..126
Figure B-7..127
Figure B-8..128
Figure B-9..129
Figure B-10..130
Figure B-11..131
Figure B-12..132
Figure B-13..133
Figure B-14..134
Figure B-15..135
Figure B-16..136
Figure B-17..137
Figure B-18..138
Figure B-19..139
Figure B-20..140
Figure B-21..141
Figure B-22..142
Figure B-23..143
Figure B-24..144
Figure B-25..145

Figure B-26 146
Figure B-27 147
Figure B-28 148
Figure B-29 149
Figure B-30 150
Figure B-31 151
Figure B-32 152
Figure B-33 153
Figure B-34 154
Figure B-35 155
Figure B-36 156
Figure B-37 157

List of tables

Table 1.1: List of participants and code for the OECD/NEA benchmark on LACANES 12
Table 2.1: Comparison of design parameters for PEACER-300 and for HELIOS 15
Table 2.2: List of components and parts (component number is given in Figure 2.3) 17
Table 2.3: Recommended conditions for the evaluation of pressure loss coefficients under forced convection tests at 250 °C 20
Table 3.1: Cell information 25
Table 3.2: Single bend, values of A 31
Table 3.3: Single bend, values of B 32
Table 3.4: Single bend, values of K_{re}- 32
Table 3.5: S-shaped bend, values of C 33
Table 3.6: Gate valve, values of K_1 34
Table 3.7: Flow meter calibration data 35
Table 3.8: Orifice data 35
Table 3.9: Main component pressure loss at low-mass flow rate 36
Table 3.10: Main component pressure loss at high-mass flow rate 36
Table 3.11: RELAP5 Correlations for friction factors 40
Table 3.12: Singular pressure loss coefficient for flow area variation 41
Table 3.13: Form loss coefficient for sudden area change in MARS-LBE code 44
Table 3.14: k_{Re} for elbow form factor 45
Table 3.15: λ for elbow form factor 46
Table 3.16: Form loss coefficient of the components 48
Table 3.17: Formulas for calculation of form loss coefficients and friction loss coefficients 50
Table 3.18: Nodalisation of HELIOS model 51
Table 3.19: Suggested conditions for the evaluation of pressure loss coefficients at 250 °C 55
Table 3.20: Values of K for different components depending on the mass flow rate 58
Table 4.1: Specification of differential pressure transducer, Rosemount model 3051 CD3A 65
Table 4.2: Correlations with function of mass flow rate (Q) and pressure loss (DP) 70
Table 4.3: Pressure losses at different mass flow rates 70
Table 5.1: Description on 11 main components and available data 72

Table 5.7: Pressure loss distribution in the core (from CFX® simulation) 77
Table 5.2: Value of A_1 for equation 5.4 89
Table 5.3: Value of B_1 for equation 5.4 89
Table 5.4: Value of k_{Re} for equation 5.4 90
Table 5.5: Value of λ for equation 5.4 90
Table 5.6: The recommended form loss coefficient for the tee-branch 93
Table 6.1: Recommended correlations in the LACANES benchmarking phase-I 98
Table C-1: Friction loss coefficient (1) at low-mass flow rate condition - ENEA, ERSE, GIDROPRESS 159
Table C-2: Friction loss coefficient (II) at low-mass flow rate condition - IAEA, IPPE, KIT/INR 166
Table C-3: Friction loss coefficient (III) at low-mass flow rate condition - RRC KI, SNU 173
Table C-4: Form loss coefficient (I) at low-mass flow rate condition - ENEA, ERSE, GIDROPRESS, IPPE 183
Table C-5: Form loss coefficient (II) at low-mass flow rate condition - KIT/INR, RRC KI, SNU 189
Table C-6: Friction loss coefficient (1) at high-mass flow rate condition - ENEA, ERSE, GIDROPRESS 197
Table C-7: Friction loss coefficient (II) at high-mass flow rate condition - IAEA, IPPE, KIT/IKET 204
Table C-8: Friction loss coefficient (III) at high-mass flow rate condition - KIT/INR, RRC KI, SNU 211
Table C-9: Form loss coefficient (I) at high-mass flow rate condition - ENEA, ERSE, GIDROPRESS, IPPE 218
Table C-10: Form loss coefficient (II) at high-mass flow rate condition - KIT/IKET, KIT/INR, RRC KI, SNU 225
Table C-11: Form loss coefficient of IAEA at low-and high-mass flow rate condition.......229

Chapter 1: Introduction

Lead-alloys are very attractive nuclear coolants because of their low melting temperature, high boiling temperature, chemical stability and neutron transparency. In addition, Lead-bismuth eutectic (LBE) itself is a very efficient spallation target for neutron generation via a high-energy proton accelerator. Thus, lead and lead-alloy coolants continue to be the subject of considerable research in the USA, Europe and Asia as well as the Russian Federation, focusing on accelerator-driven transmutation systems and lead and lead-alloy-cooled fast reactors (LFR).

In 2007, the OECD Nuclear Energy Agency published a comprehensive handbook on lead-bismuth eutectic alloy and lead properties, materials compatibility, thermal hydraulics and technologies [1] to integrate available information on such heavy liquid metals (HLM). Meanwhile, a systematic study on HLM was proposed which covers thermal-hydraulic safety issues of lead-alloy-cooled advanced nuclear energy systems (LACANES). This study mainly addresses thermal-hydraulic behaviours of those LACANES under the steady-state forced and natural convection, which is of critical importance for the system design development effort, while such studies have been extensively carried out for sodium coolants.

Experimental data can be examined and qualified for use in benchmarking of these models utilising large-scale lead-alloy coolant loop test facilities. Hence, the reference of benchmark is large-scale lead-bismuth (Pb-Bi) coolant loop test facility HELIOS (Heavy Eutectic liquid metal Loop for Integral test of Operability and Safety of PEACER[1]) of the Seoul National University in the Republic of Korea.

According to the HELIOS test results, two phases of approach are suggested:

- Phase I - Isothermal steady-state forced convection case
- Phase II - Non-isothermal natural circulation case

Prior to the Phase I, a comparative study on the pressure loss coefficient of each part of HELIOS under isothermal conditions is performed as well. All thermo-physical properties of Lead-bismuth eutectic (LBE) coolant are based on the OECD/NEA LBE handbook.

This report contains characteristics of the HELIOS, the specification of benchmark Phase I [2] and method of benchmark and preliminary results from the participants mostly on the pressure loss coefficient.

The complete list of participants and codes used are shown in Table 1.1.

[1] Proliferation-resistant, environment-friendly, accident-tolerant, continuable and economical reactor

Table 1.1: List of participants and code for the OECD/NEA benchmark on LACANES

Country	Institute	Participant	Code*
Italy	ENEA	Paride MELONI and Francesco Saverio NITTI	RELAP5-Version HLM
Italy	RSE	Vincenzo CASAMASSIMA	LEGOPST
Russian Federation	GIDROPRESS	Alexander V. DEDUL	TRIANA
	IAEA	Vladimir V. KUZNETSOV	
Russian Federation	IPPE	Oleg KOMLEV	HYDRA
Germany	KIT/IKET	Abdalla BATTA, Xu CHENG, and Andreas CLASS	HETRAF, STAR-CD®
Germany	KIT/INR	Wadim JÄGER	TRACE
Russian Federation	RRC KI	Alexey SEDOV	
Republic of Korea	Seoul National University	Il Soon HWANG and Jae Hyun CHO	MARS-LBE, CFX®

* References for employed computer codes are given in Chapter 3.

References

[1] OECD/NEA (2007), "Handbook on Lead-bismuth Eutectic Alloy and Lead Properties, Materials Compatibility, Thermal hydraulics and Technologies".

[2] OECD/NEA,"Benchmarking of thermal-hydraulic loop models for Lead alloy-cooled advanced nuclear energy systems (LACANES) - Task Guideline for Phase 1: Characterisation of HELIOS".

Chapter 2: Benchmark specifications

2.1 Design features of the HELIOS

Figure 2.1 is the schematic diagram of PEACER-300 and Figure 2.2 is HELIOS loop which is down scaled by the factor of ~5 000 based on non-dimensionalised energy balance equations of Ishii and Kataoka [1]. Various thermal-hydraulic characteristics under accident scenarios of the PEACER have been studied by HELIOS, which includes isothermal forced circulation, LOFA (Loss of Flow Accident) and natural circulation behaviour [2-3]. It was found that HELIOS can give the good indication for safety feature of LBE-cooled system and the key safety function of lead-alloy advanced cooled nuclear energy system (LACANES) often relies on their natural circulation ability. Table 2.1 shows the scale-down parameters of PEACER and HELIOS.

Figure 2.1: Schematic diagram of PEACER-300

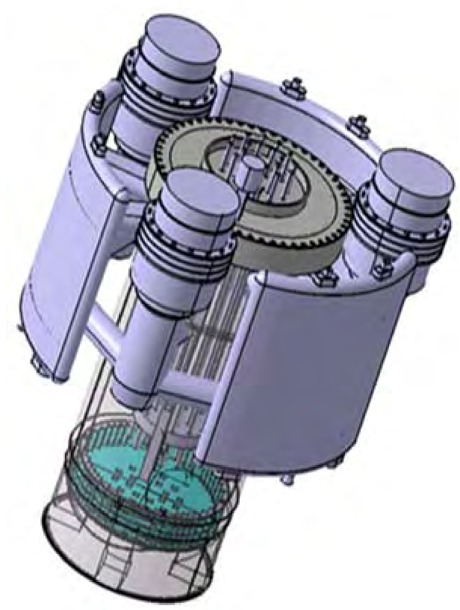

Figure 2.2: Schematic (left) and photograph (right) of HELIOS (Heavy Eutectic liquid metal Loop for Integral test of Operability and Safety of PEACER)

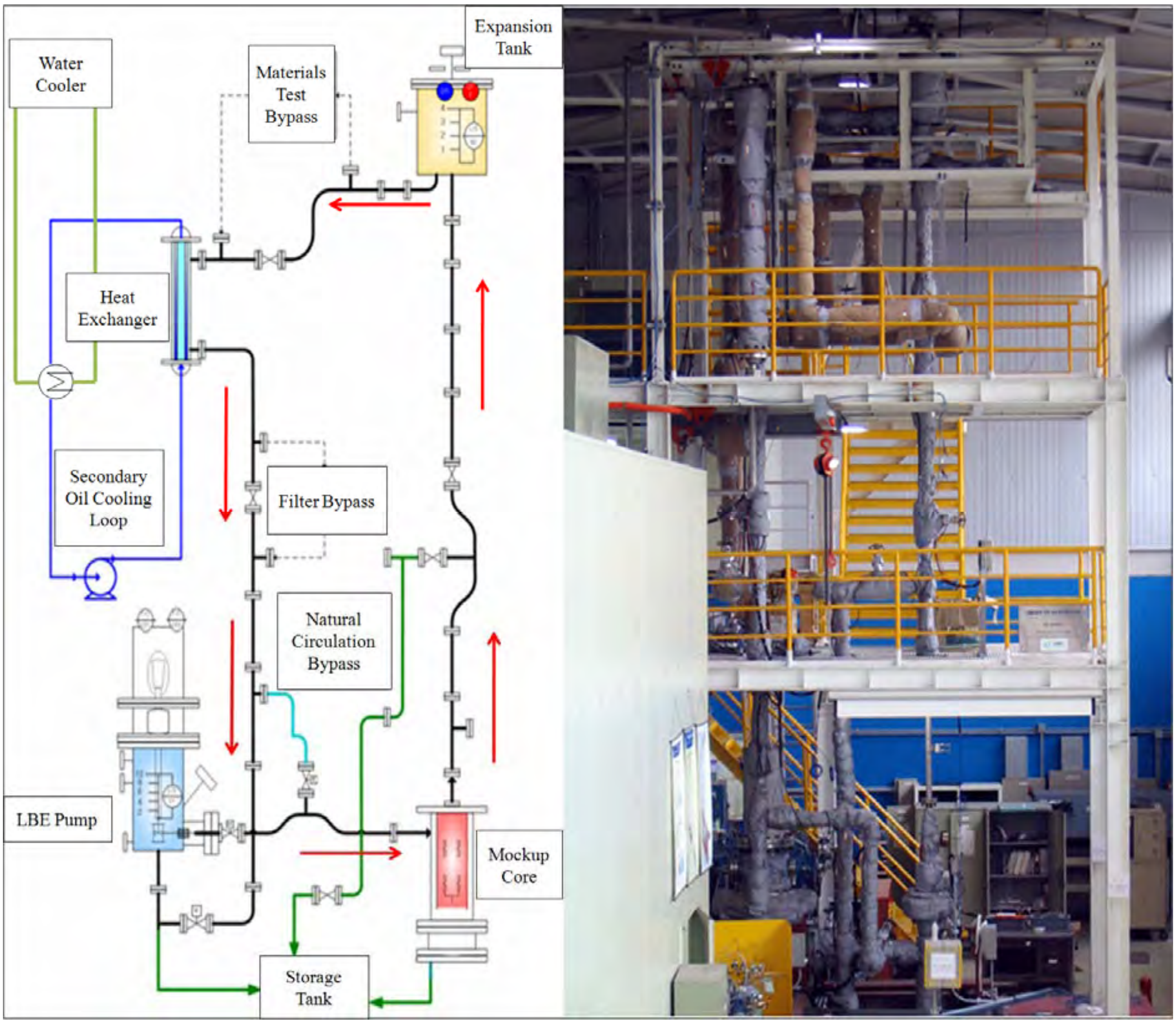

Table 2.1: Comparison of design parameters for PEACER-300 and for HELIOS

Parameter	PEACER-300	HELIOS	Ratio of PEACER-300 to HELIOS
Number of loops	3	1	
Decay heat [MWt] (10% of normal power)	85.0	0.0174	4 885
Number of rods	77280	4	19 320
LBE flow area [m^2]	6.92	0.00142	4 873
Cross sectional heated area [m^2]	4.20	0.000507	8 284
Natural circulation flowrate [kg/s]	12550	2.40	5 229
ΔT (between hotleg and coldleg) [^oC]	46.8	49.4	0.95
Representative flow velocity at core [m/s]	0.176	0.173	1.02
Elevation difference between thermal centers [m]	8.0	7.6	1.05
Total loss coefficient	30.4	24.5	1.24
Richardson number	15.2	12.2	1.25

2.2 Geometrical data

The HELIOS facility consists of pipes, tanks and associated components that are mostly made of Type 316 L stainless steel. Figure 2.3 shows the segment number and description of the components. In the case of forced-convection, the LBE enters from component No.24 into the LBE pump and piping to the mock-up core (Component No.1). In the case of natural circulation, the LBE bypasses the LBE pump to flow directly from Components No.20 to No.24 and returns to component 1.

Table 2.2 provides precise data for the components and associated parts. Three-dimensional plans of the components are given in Appendix A. Appendix B provides the two-dimensional plans of each part of the component. Dimensions of the plans are shown in *mm*.

Figure 2.3: Component numbers

(: closed, : open)

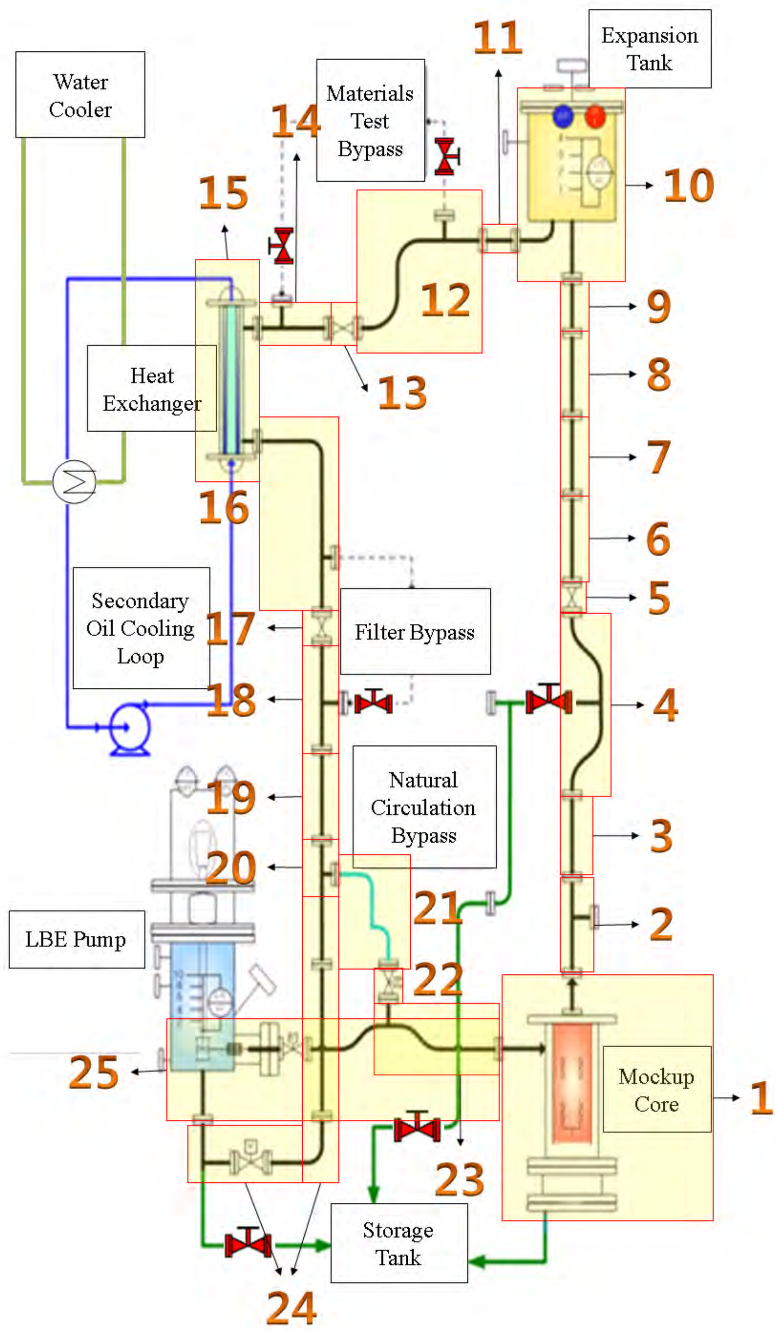

Table 2.2: List of components and parts (component number is given in Figure 2.3)

Component number	Part name	Reference length [mm]	Component 3D plan (Appendix A)	Part drawings and data (Appendix B)
1	Core vessel	3633.1	A-1	B-1
	Barrel			B-2
	Rod			B-3
	Bottom			B-4
	Gasket [between flanges]	4.5		B-34
2	Pipe [one side flange]	300	A-2	B-16
	Tee	127		B-27
	Pipe [one side flange]	300		B-16
	Gasket [between flanges]	4.5		B-34
3	Pipe [both side flange]	1 000	-	B-24
	Gasket [between flanges]	4.5		B-34
4	45 Degree elbow [one side flange]	82.5	A-4	B-29
	Pipe	180.68		B-11
	45 Degree elbow	60		B-28
	Pipe	718.86		B-21
	Tee	127		B-27
	Pipe	171.11		B-10
	45 Degree elbow	60		B-28
	Pipe	180.68		B-11
	45 Degree elbow [one side flange]	82.5		B-29
	Gasket [between flanges]	4.5		B-34
5	Glove valve	216	-	B-31
	Gasket [between flanges]	4.5		B-34
6	Pipe [both side flange]	1 000	-	B-24
	Gasket [between flanges]	4.5		B-34
7	Pipe [both side flange]	1 000	-	B-24
	Gasket [between flanges]	4.5		B-34
8	Pipe [one side flange]	200	-	B-12
	Orifice	400		B-32, B-33
	Pipe [one side flange]	200	-	B-12
	Gasket [between flanges]	4.5		B-34
9	Pipe[both side flange]	500	-	B-20
	Gasket [between flanges]	4.5		B-34
10	Expansion tank	872.7	-	B-5
	Gasket [between flanges]	4.5		B-34
11	Pipe [both side flange]	500	-	B-20
	Gasket [between flanges]	4.5		B-34

Table 2.2: List of components and parts (continued)

Component number	Part name	Reference length [mm]	Component 3D plan (Appendix A)	Part drawings and data (Appendix B)
12	Pipe [one side flange]	300	A-12	B-16
	Tee	127		B-27
	Pipe	305.41		B-17
	90 Degree elbow	120		B-30
	90 Degree elbow	120		B-30
	Pipe[one side flange]	200		B-12
	Gasket [between flanges]	4.5		B-34
13	Glove valve	216	-	B-31
	Gasket [between flanges]	4.5		B-34
14	Pipe [one side flange]	200	A-14	B-12
	Tee	127		B-27
	Pipe [one side flange]	382.32		B-18
	Gasket [between flanges]	4.5		B-34
15	Heat exchanger vessel	2415.5	A-15	B-6
	Heat exchanger 2nd line	-		B-7
	Gasket [between flanges]	4.5		B-34
16	Pipe [one side flange]	219.75	A-16	B-14
	90 Degree elbow	120		B-30
	Pipe	785.5		B-23
	Tee	127		B-27
	Pipe [one side flange]	500		B-19
	Gasket [between flanges]	4.5		B-34
17	Glove valve	225	-	B-31
	Gasket [between flanges]	4.5		B-34
18	Pipe[one side flange]	500	A-18	B-19
	Tee	127		B-27
	Pipe [one side flange]	500		B-19
	Gasket [between flanges]	4.5		B-34
19	Pipe [both side flange]	1 000	-	B-24
	Gasket [between flanges]	4.5		B-34
20	Pipe[one side flange]	500	A-20	B-19
	Tee	127		B-27
	Pipe [one side flange]	100		B-9
	Gasket [between flanges]	4.5		B-34
21	Pipe [one side flange]	757.12	A-21	B-22
	90 Degree elbow	120		B-30
	Pipe	1204.62		B-26
	90 Degree elbow	120		B-30
	Pipe [one side flange]	276.25		B-15
	Gasket [between flanges]	4.5		B-34

Table 2.2: List of components and parts (continued)

Component number	Part name	Reference length [mm]	Component 3D plan (Appendix A)	Part drawings and data (Appendix B)
22	Glove valve	216	-	B-31
	Gasket [between flanges]	4.5		B-34
23	Pipe [one side flange]	100	A-23	B-9
	Tee	127		B-27
	45 Degree elbow	60		B-28
	Pipe	180.68		B-11
	45 Degree elbow [one side flange]	82.5		B-29
	Gasket [between flanges]	4.5		B-34
24	Pipe [one side flange]	1 000	A-24	B-25
	Pipe[both side flange]	1 000		B-24
	Pipe [one side flange]	52.27		B-8
	90 Degree elbow	120		B-30
	45 Degree elbow	60		B-28
	Pipe [one side flange]	217.2		B-13
	Glove valve	216		B-31
	Pipe [one side flange]	300		B-16
	Tee	127		B-27
	Pipe [one side flange]	300		B-16
	Gasket [between flanges]	4.5		B-34
25	Sump tank	977.4	A-25	B-35, B-36, B-37
	Gasket [between flanges]	4.5		B-34
	Glove valve	216		B-31
	Gasket [between flanges]	4.5		B-34
	45 Degree elbow [one side flange]	82.5		B-29
	Pipe	180.68		B-11
	45 Degree elbow	60		B-28
	Tee	127		B-27
	45 Degree elbow	60		B-28
	Pipe	180.68		B-11
	45 Degree elbow [one side flange]	82.5		B-29
	Gasket [between flanges]	4.5		B-34

2.3 Guidelines for pressure loss coefficient evaluation

2.3.1 Definition of pressure loss coefficients

The total pressure drop of the HELIOS, ΔP_{total}, can be calculated by summing up the pressure drop of each component:

$$\Delta P_{total} = \frac{1}{2}\rho\sum_i V^2{}_{i(average)}\left(f\frac{L}{D}+K\right)_i \qquad (2.1)$$

where P, i, ρ, V, f, L, D and K are pressure, the number of components, fluid density, average flow velocity, friction factor, the length, the diameter of a component and the form loss coefficient, respectively. The last term in the right hand side of Equation (1) is defined as:

$$\text{Pressure loss coefficient} = \left(f\frac{L}{D}+K\right) \qquad (2.2)$$

where $f\frac{L}{D}$ is the friction loss coefficient for a component with no change in cross-sectional dimensions.

2.3.2 Procedures for pressure loss coefficient evaluation

The pressure loss coefficient of a part or a component defined in Equation (2), can be evaluated using correlations available from various literature data including hydraulic design handbooks. They can also be determined from three-dimensional computational fluid dynamics simulations. Each participant of this benchmark has agreed to evaluate pressure loss coefficients by selecting methods that are judged to be most appropriate for given conditions, together with detailed descriptions of the employed method. Pressure loss coefficients are usually dependent not only on geometries but on flow conditions such as the Reynolds number and surface roughness. Using the procedure, participants are requested to calculate the pressure loss coefficient for two different flow rate cases: a low and a high flow, respectively. Table 2.3 provides the conditions of each case from the isothermal (250 °C) flow test. It is recommended that the measured value Root-Mean-Square (RMS) surface roughness is used.

Table 2.3: Recommended conditions for the evaluation of pressure loss coefficients under forced convection tests at 250 °C

Condition	Mass flow rate (kg/sec)	Surface roughness (μm, RMS)
Low flow	3.27	2.53
High flow	13.57	2.53

2.3.3 Report format for evaluated pressure loss coefficients under isothermal forced convection conditions

Based on the procedure described in the previous section, evaluated pressure loss coefficients of each component of HELIOS at two different flow rates are requested to be inputted using a format given in Appendix C.

References

[1] I.S. Hwang (2006), "A Sustainable Regional Waste Transmutation System: P E A C E R", *Plenary Invited Paper,* ICAPP '06, Reno, NV, USA. 4-6 June 2006.

[2] S. H. Jeong, C. B. Bahn, S. H. Chang, Y. J. Oh, W. C. Nam, K. H. Ryu, H. O. Nam, J. Lim, N. Y. Lee and I. S. Hwang (2006), "Operation Experience of LBE loop: HELIOS", Paper #6284, *Proceedings of ICAPP '06,* Reno, NV, USA. 4-6 June 2006.

[3] J. Lim, S. H. Jeong, Y. J. Oh, H. O. Nam, C. B. Bahn, S. H. Chang, W. C. Nam, K. H. Ryu, T. H. Lee, S. G. Lee, N. Y. Lee and I. S. Hwang (2007), "Progresses in the Operation of Large Scale LBE Loop : HELIOS", Paper #7536, *Proceedings of ICAPP*, Nice, France, 13-18 May 2007.

Chapter 3: Method of the benchmark

3.1 KIT/IKET, Germany

3.1.1 Code description

In order to study the dynamic behaviour of the HELIOS cooling system, the HETRAF code is used, which was originally developed for the safety analysis and for investigating the dynamic behaviour of cooling systems for superconducting magnets cooled by super-critical helium. It has been successfully verified by experimental data and analytical results [1]. The HETRAF code has been extended to Pb-Bi applications [2]. Thermal and hydraulic characteristics of individual flow cells are modelled, which makes it possible to simulate any kind of distributions of heat source and flow resistance in the flow domain. The code is capable of simulating a multi-loop system with thermal coupling between the loops, e.g. heat exchangers. There are modules for different kinds of components, e.g. pumps and bypass. This code can be easily modified for the application of any specific purpose.

Along the main flow direction, each loop is divided into loop sections (or cells), which are characterised as an annular pipe with its inner and outer diameter, inner and outer wall thickness, length and orientation. The cell length is identical as the real loop section. The cell diameters are selected according to the criterion that the flow area of the cell is the same as the loop section. The orientation is determined to keep the elevation difference between both ends of the cell the same as in the real loop. Some main features of the HETRAF code are summarised as follows:

- 1-D configuration (flow cell with two bounding walls);
- single phase;
- multi-loop system with thermal coupling;
- individual pump characteristics;
- individual pressure control systems;
- individual source term (energy, momentum);
- bypass;
- unlimited number of boundary coupling (thermal).

Some important models used for the LACANES benchmark are summarised as follows:

Friction pressure drop

Friction pressure drop is calculated by

$$\Delta P_f = C_f \cdot f \frac{l}{d_h} \frac{G^2}{2\rho} \qquad (3.1)$$

The multiplier C_f is introduced to account the deviation of the hydraulic diameter between the HETRAF model and the real system, i.e.

$$C_f = \left(\frac{d_{h,m}}{d_{h,P}} \right)^{1+n} \quad (3.2)$$

Where n=0.25 is the exponent in the Blasius equation. Two equations are available for computing the friction factor, i.e. the Blasius equation

$$f = 0.3164\,\mathrm{Re}^{-0.25} \quad (3.3)$$

and the equation of Colebrook

$$f = \left\{ -2.0 \log\left(\frac{2.51}{\mathrm{Re}\sqrt{f}} \right) + \frac{r}{3.71D} \right\}^{-2.0} \quad (3.4)$$

Heat transfer between fluid and solid wall

The amount of heat transferred is determined by

$$Q = C_h F_h \cdot \alpha \cdot \Delta T$$

The multiplier for heat transfer C_h corrects the deviation of the hydraulic diameter between the HETRAF model and the real system and is determined by:

$$C_h = \frac{d_{h,m}^{2-n}}{d_{h,P}^{1-n} \cdot d_{ht,P}} \quad (3.5)$$

Here n is the exponent in the Dittus-Boelter equation (0.8), d_h the hydraulic diameter and d_{ht} the equivalent heated diameter.

Thermal coupling

Thermal coupling between a cell and its environment or between cells is considered in the code. An additional thermal resistance between both coupled cells can be taken into consideration. This option provides the code with more feasibility for various kinds of applications. The counterpart of the thermal coupling can be one cell of the same loop, or a cell of another loop, or an external system. The HETRAF code considers more than one thermal coupling of each cell. For a coupling with an external system, the temperature of the counterpart is a required input.

Bypass

The present version allows maximum two parallel flow paths for each bypass section. The user has to define one of them as the main flow path, the other as a bypass. All the elements in bypasses must have higher identification number as all the elements in the main flow path. The following boundary conditions are fulfilled to determine flow conditions in each flow path:

- Mass conservation: In each flow path, mass flow is constant. The sum of mass flow in all parallel flow paths gives the total mass flow, which is constant in the entire loop.
- Pressure condition: The pressure is the same for both flow paths at their connecting points.
- The fluid temperature into each flow path is the same as that at their connecting point.

Pump characteristics

Five options are at present available in the code. An extension to additional options can be easily realised by using a user-subroutine. The five options are:

- constant pump head;
- constant mass flow rate;

- a time table for the pump head;
- a time table for the mass flow rate is given;
- pump head is dependent on mass flow rate and time.

Further boundary conditions

A reference pressure has to be given at a fixed point. This is either a constant value or a time dependent parameter. Furthermore, the code user has the possibility to give a timetable for the fluid temperature at one fixed point.

A user subroutine is provided for additional boundary conditions specified by the user. This subroutine contains all the important variables, which can be changed for any specific application

3.1.2 Mesh structure and local form loss coefficients

Table 3.1 indicates the number of cells, the corresponding ID-number of the components, the cell length and the cell height (elevation).

Table 3.1: Cell information

Mesh No.	A-No.	B-No.	Name	Length m	Height m	Form factor
1	A-1		core inlet	0.181	0	1.92
2 to 7	A-1		downcomer	1.2228	-1.2228	0
8	A-1		lower plenum-down	0.144	-0.144	1
9	A-1		lower plenum-up	0.144	0.144	0.2
10 to 15	A-1		core to inlet level	1.2228	1.2228	5.586
16	A-1		to core end	0.1792	0.1792	0.07
17 to 19	A-1		upper plenum	0.5391	0.5391	0
20	A-2			0.7315	0.7315	0.05
21	A-3			1.0045	1.0045	0
22	A-4			1.6679	1.53782	0.49
23	A-5			0.2205	0.2205	1
24	A-6			1.0045	1.0045	0
25	A-7			1.0045	1.0045	0
26	A-8			1.0045	1.0045	2.384
27	A-9			0.5045	0.5045	0
28	A-10		up to tank bottom	0.334	0.334	1
29	A-10		inside tank	0.361	0	0
30	A-10		tank outer pipe	0.1779	-0.1299	0.5
31	A-11			0.5045	0	0
32	A12			1.1808	-0.1523	0.39
33	A13			0.2205	0	1
34	A14			0.7138	0	0.05
35	A15 HEX inlet			0.202	0	1.72
36 to 45	HEX			2.01	-2.01	5.79
46	HEX outlet			0.206	0	1.975
47	A16+A17			1.977	-1.7137	1.22
48	A18			1.1315	-1.1315	0.05
49	A19			1.0045	-1.0045	0
50	A20			0.5	-0.5	0
51	A20			0.127	-0.127	0.05
52	A24	B25+B24+B34		2.009	-2.009	0
53	A24	B8+B30+B28+B13+B34		0.4536	-0.1285	0.28
54	A24	B31		0.2205	0	1
55	A24+Pump			1.2052	0.84171	1.3
56	A25	B31		0.2205	0	1
57	A25	to middle point of the T junction		0.3867	0	0.245
58	A25			0.3912	0	0.245

The local form loss coefficients of various parts are mostly determined according to the Handbook of the German Engineer Association (VDI-Wärmeatlas) [3]. The local form loss coefficient of various parts is also presented in Table 3.1.

T-junction

Part B27 is a T-junction. As shown in Figure 3.1 the loss coefficient can be determined according to the direction and the flow rates of both inflow and outflow.

Bending pipe

Parts B28, B29 and B30 are bending pipes with different bending angles. The local form loss coefficients can be determined according to Figure 3.2.

Flow expansion and contraction

For flow area expansion [Figure 3.3(a)], the following equation is applied:

$$\zeta = \left(1 - \frac{f_1}{f_2}\right)^2 \qquad (3.6)$$

For flow area contraction [Figure 3.3(b)], the form loss coefficient is determined by Figure 3.4.

Spacers

For all spacers in both the heated bundle of the core and the tube bundle of the heat exchanger, the correlation of Rehme [4] is applied.

$$\zeta = 7 \cdot \left(\frac{A_s}{A}\right)^2 \qquad (3.7)$$

Figure 3.1: Form loss coefficient of T-junction [3]

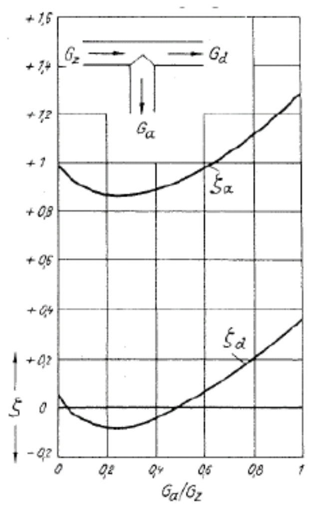

Figure 3.2: Form loss coefficient of bending pipe [3]

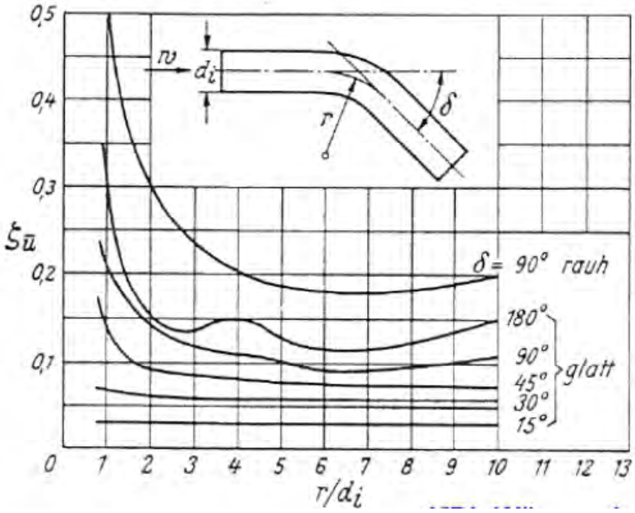

Figure 3.3: Flow expansion and contraction [3]

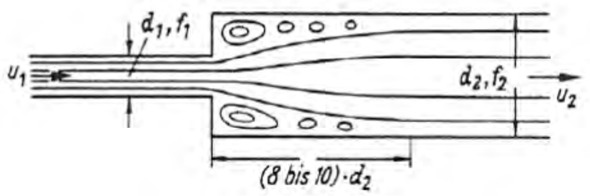

(a)

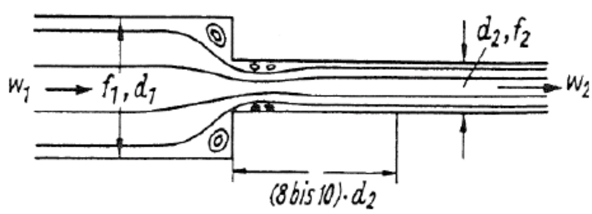

(b)

Figure 3.4: Form loss coefficient of flow contraction [3]

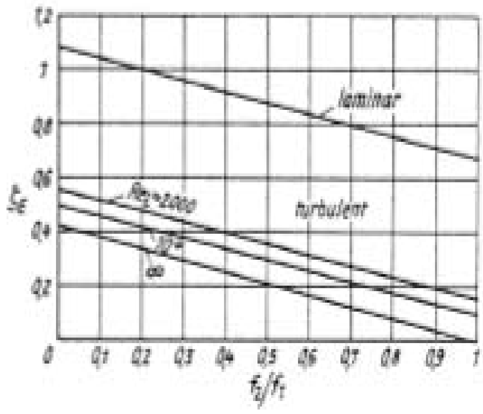

References

[1] X. Cheng, Numerical analysis of thermally induced transients in forced flow of supercritical helium, Cryogenics, Vol.34 (1994), No.3, 195-201.

[2] X. Cheng, A. Class, (2008), Analysis of Dynamic Behavior of MEGAPIE Cooling System, ICAPP'08, 8-12 June 2008, Anaheim, CA, USA, paper 8106.

[3] Verein Deutscher Ingenieure, VDI-Wärmeatlas 3.0, Springer Verlag, Berlin Heidelberg, 2006.

[4] K. Rehme (1973), Pressure Drop Correlations for Fuel Element Spacers, Nuclear Technology, Vol.17, pp.15-23.

3.2 RSE, Italy

Lego plant simulation tools

In the field of real time power plant dynamic simulation, the RSE developed an integrated software environment, named "Lego Plant Simulation Tools" (LegoPST), capable of modelling the whole plant, from the field (plant process and machinery) to the Human Machine Interface. LegoPST was successfully used to build dynamic plant simulators both in nuclear (LWR) and conventional field [1-5], in order to verify plant control and automation system and to perform plant operation transient analysis and plant operators training.

In the frame of the European Project ELSY, the extension of the LegoPST ability to liquid metal fast reactor plants simulation is ongoing. Models of plant components (drums pipes, pumps, valves, etc.) able to simulate liquid metal loops were developed and LegoPST libraries of the fluids physical properties were extended to liquid lead and lead-bismuth. The participation in benchmarking the thermal-hydraulic loop models for LACANES is part of the planned code validation activities.

Lego PST packages

LegoPST suite consists of: 1) a master solver for non-linear differential and algebraic equation systems; 2) an expandable library of mathematical models of plant components; 3) integrated tools covering all plant simulator building steps, from design to final simulator, including debugging, monitoring and configuration. In particular, as for tools: Lego Process CAD (LegoPC) is useful in developing and testing process models; Lego Automation CAD (LegoAC) allows full graphic editing of automation schemes; LegoHMI is specific for Plant Display and Operating Window building and configuration; Lego Simulation Manager (LegoSM) runs the whole simulator, managing multiple links among process, automation and HMI models. To model HELIOS facility and carry out the benchmark simulations only LegoPC tool is required. It runs both under Red Hat Enterprise Linux 4.0 and Windows XP.

Lego master solver

Lego master solver manages non-linear equation systems which include algebraic and ordinary differential equation with respect to time. The semi-implicit time integration algorithm uses the Newton-Raphson iterative method to handle non-linear equations and MA28 package suitable for large sparse matrices.

Models library

The models library consists in an expandable set of mathematical models of the plant components (valves, pipes, etc.) and physical properties of various fluids (water, gases, liquid metals, etc.). All the mathematical models are based on the mass, momentum and energy conservation equations, developed in lumped parameter approach, in one-dimension geometry. The related equation system is closed by coupling material properties correlations and fluid state equations.

Process CAD

The process model builder LegoPC covers and sequences all the phases of the process model building and testing: models topology build-up, input assignment, steady-state and transient calculation and output analysis. The plant model is built by selecting the plant components from the models library, placing it on a graphical page and linking the components input-output terminals to draw the plant section (Figure 3.5). The plant drawing is translated into a global non-linear algebraic and differential equations system (Figure 3.6) solved by the master solver.

Figure 3.5: LegoPC graphical interface

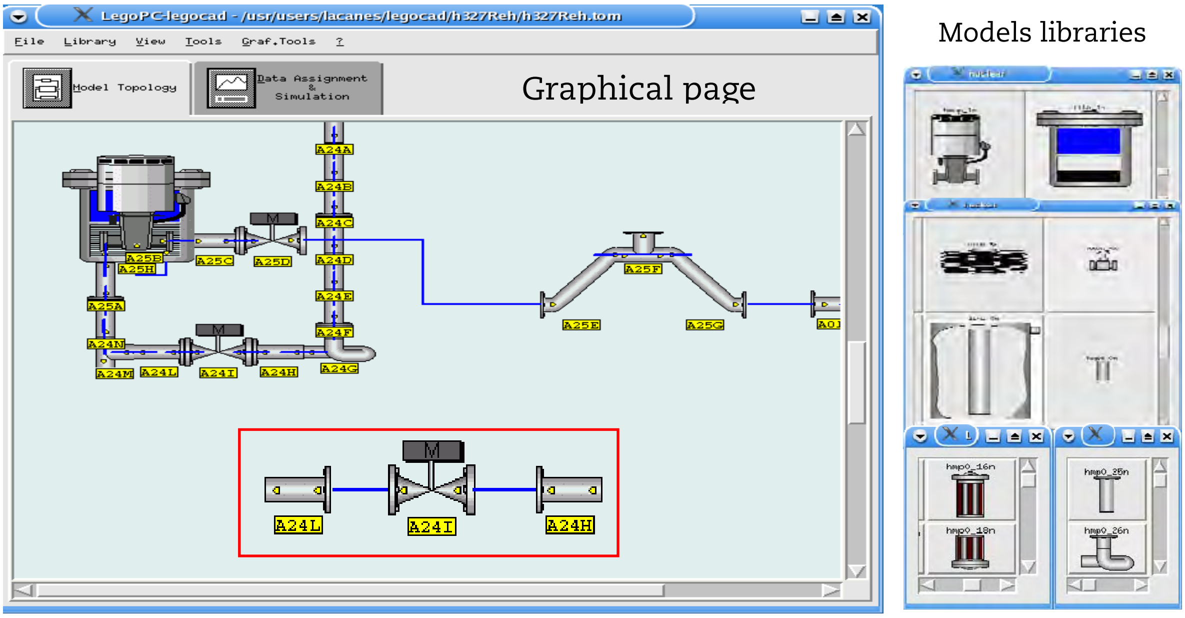

Figure 3.6: Translation of the component links into a non-linear equation system

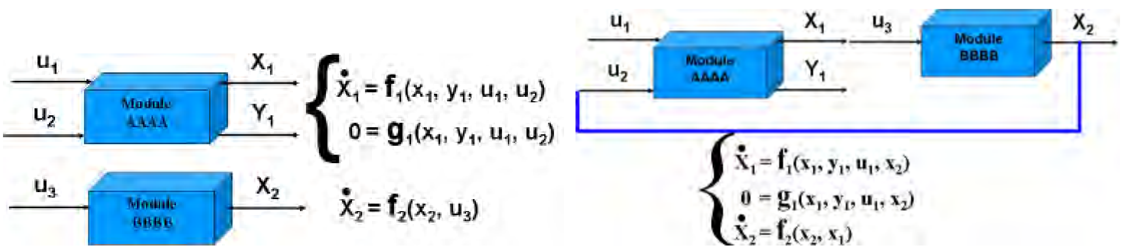

Dynamic simulation and transient analysis can be performed interactively (Figure 3.7) by the embedded LegoSM, which allows to set simulation speed (real, accelerated or step by step) and time step integration, to freeze and restart simulation from a "snapshot" previously recorded, to perturb boundary conditions and show variables trend.

Figure 3.7: LegoPC simulation user interface

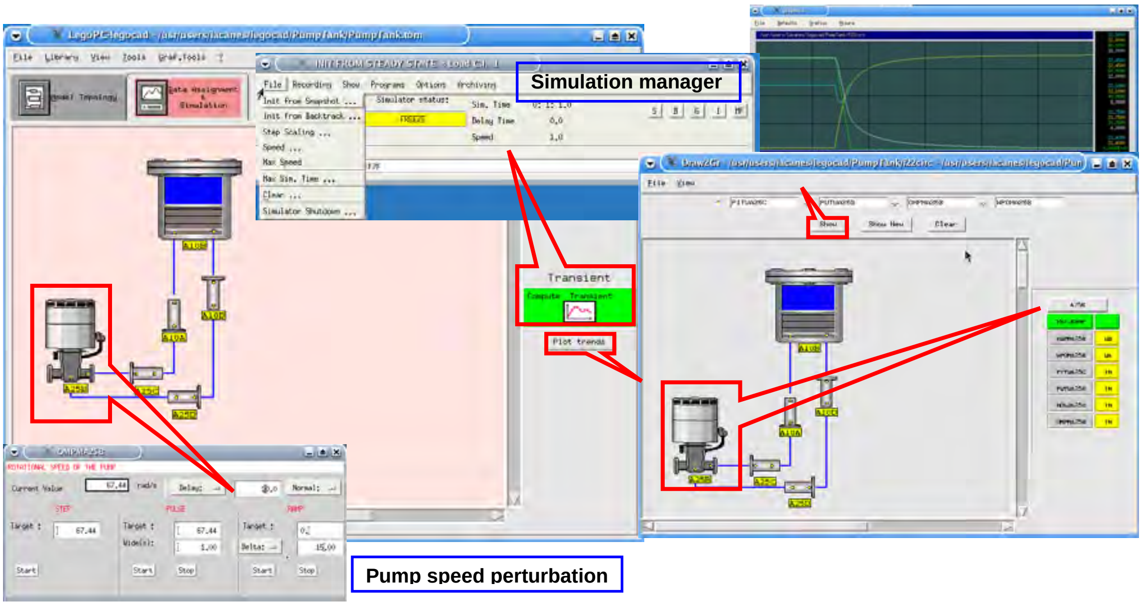

The main loop component taken into account in modelling HELIOS facility is resumed in Figure 3.8. The valve and flow meter models calculate the pressure drop only and neglect the mass accumulation and energy dissipation (fluid expansion is considered isenthalpic). The pump model also neglects the mass accumulation, but takes into account the energy dissipation. All the other models use all the three (mass, momentum and energy) conservation equations.

Lead-bismuth physical property correlations and state equations, needed to close the equation system, come from reference [6].

Figure 3.8: HELIOS model main components

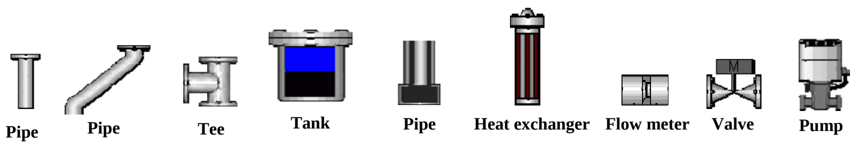

To deal with pressure losses, friction factor and form loss coefficients for the most common pipe shape and geometry variations can be calculated.

The available configurations are related to pipe entrance or exit, sudden expansion or contraction, merging of streams, change of stream direction, spacers or grids, orifices and valves [7-9]

Friction factor

The reference for the evaluation of the friction factor is the Moody chart [7]. For the laminar flow, the friction factor is calculated by the Hagen-Poiseuille correlation:

$$f = \frac{64}{\mathrm{Re}} \qquad \left[0 \le \mathrm{Re} \le 2000\right] \tag{3.8}$$

Otherwise, by solving the Colebrook interpolation formula:

$$\frac{1}{f^{\frac{1}{2}}} = -2.0\log_{10}\left(\frac{\frac{\varepsilon}{d}}{3.7} + \frac{2.51}{\mathrm{Re}\, f^{\frac{1}{2}}}\right) \qquad [\mathrm{Re} > 2000] \tag{3.9}$$

via the Newton-Raphson iterative method.

Gasket between flanges

The form loss coefficient for a gasket between flanges is calculated as sequence of a sudden expansion and contraction (Figure 3.9), assuming Re > 10^4.

Figure 3.9 Gasket between flanges

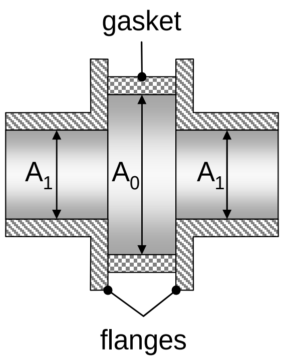

$$K_G = \left(1 - \frac{A_1}{A_0}\right)^2 + 0.5\left(1 - \frac{A_1}{A_0}\right)^{3/4} \qquad [\mathrm{Re} > 10000] \tag{3.10}$$

A = cross-sectional area [m^2]

Bends

Various bends are taken into account: single, doubly S-shaped and doubly U-shaped (Figure 3. 10). In the case of single and doubly S-shaped bends with flow in one plane, the value of the form loss coefficient is calculated by the following formulas:

Single bend

Figure 3.10: Single bend

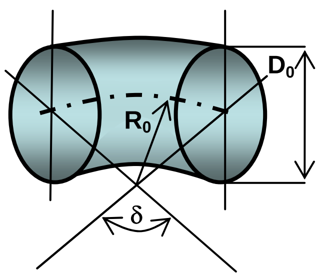

$\mathbf{R_0/D_0} < 3.0$ - $0 < \delta < 180°$

$$K_{sb} = K_{R_e} \cdot A \cdot B \tag{3.11}$$

Table 3.2: Single bend, values of A

δ	0	20	30	45	60	75	90	110	130	150	180
A	0	0.31	0.45	0.6	0.78	0.9	1.0	1.13	1.20	1.28	1.40

Table 3.3: Single bend, values of B

R_0/D_0	0.5	0.6	0.7	0.8	0.9	1.	1.25	1.5	2.	3.	4.	6.	8.	10.	15	20	25
B	1.18	0.77	0.51	0.37	0.28	0.21	0.19	0.17	0.15	0.12	0.11	0.09	0.07	0.07	0.06	0.05	0.05

R_0/D_0	30	35	40	50
B	0.04	0.04	0.03	0.03

Table 3.4: Single bend, values of K_{re}-

$R_e \times 10^{-5}$ / R_0/D_0	*0.1*	*0.14*	*0.2*	*0.3*	*0.4*	*0.6*	*0.8*	*1.0*	*1.4*	*2.0*	*3.0*	*4.0*	
[0.5 ÷ 0.55]	1.4	1.33	1.26	1.19	1.14	1.09	1.06	1.04	1.0	1.0	1.0	1.0	
] 0.55 ÷ 0.7]	1.67	1.58	1.49	1.4	1.34	1.26	1.21	1.19	1.17	1.14	1.06	1.0	$\mathbf{K_{Re}}$
> 0.7	2.0	1.89	1.77	1.64	1.56	1.46	1.38	1.3	1.15	1.02	1.0	1.0	

Tables 3.2-3.4 give the form loss coefficient dependence on the angle of the bend δ, the relative radius of curvature R_0/D_0, the straight distance length L_e between the bends and the Reynold number Re.

Figure 3.11: S-shaped bend with flow in one plane

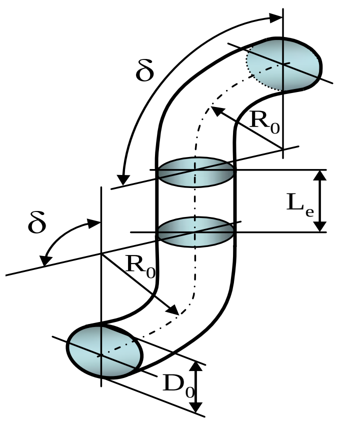

Doubly S-shaped bend with flow in one plane

$$K_{db} = C \cdot K_{sb} \tag{3.12}$$

Table 3.5: S-shaped bend, values of C

δ \ L_e/D_0	0	1	2	3	4	6	8	10	12	14	16	18	20	25	40÷50	
15	0.20	0.42	0.60	0.78	0.94	1.16	1.20	1.15	1.08	1.05	1.02	1.00	1.10	1.25	2.00	
30	0.40	0.65	0.88	1.16	1.2	1.18	1.12	1.06	1.06	1.15	1.28	1.40	1.50	1.70	2.00	
45	0.60	1.06	1.20	1.23	1.20	1.08	1.03	1.08	1.17	1.30	1.42	1.55	1.65	1.80	2.00	
60	1.05	1.38	1.37	1.28	1.15	1.06	1.16	1.30	1.42	1.54	1.66	1.76	1.85	1.95	2.00	C
75	1.5	1.58	1.46	1.30	1.27	1.30	1.37	1.47	1.57	1.68	1.75	1.80	1.88	1.97	2.00	
90	1.70	1.67	1.40	1.37	1.38	1.47	1.55	1.63	1.70	1.76	1.82	1.88	1.92	1.98	2.00	
120	1.78	1.64	1.48	1.55	1.62	1.70	1.75	1.82	1.88	1.90	1.92	1.95	1.97	1.99	2.00	

Spacers

The form loss coefficient for spacers is calculated by the Rehme correlation.

Figure 3.12: Rehme modified drag coefficient

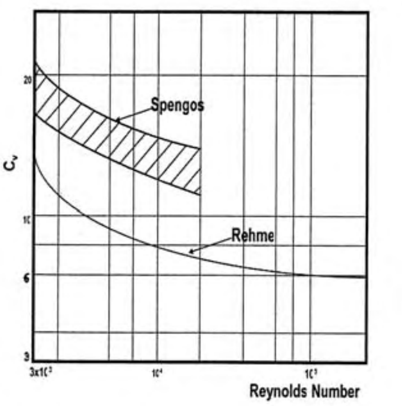

$$K_{sp} = C_v \left(\frac{A_s}{A_v} \right)^2 \tag{3.13}$$

A_s=projected frontal area of the spacer

A_v=unrestricted flow area away from the spacer

C_v= modified drag coefficient (Figure 3.8)

The modified drag coefficient is evaluated by the following interpolation formula:

$$C_v = C_0 \left(\log\left(\frac{\mathrm{Re}}{2000} \right) \right)^{\frac{1}{C_1}} + \left(\log\left(\frac{\mathrm{Re}}{2000.} \right) \right)^{C_2} + C_3 \tag{3.14}$$

C_0=-14.51728, C_1=7.88567, C_2=-1.38061, C_3=23.41088

Orifice

The flow meter model refers to a thin-plate orifice type flow meter (Figure 3.13). In the Reynolds number range $10^4 < Re < 10^7$, the value of the form loss coefficient is given by:

Figure 3.13: Thin-plate orifice

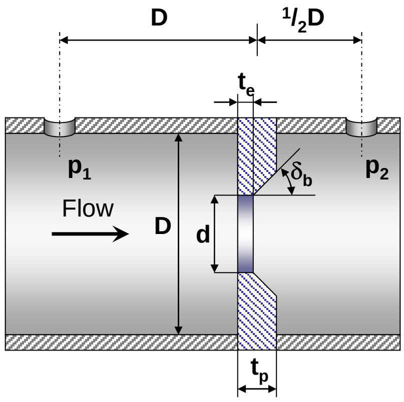

$$K_o = \frac{1-\beta^4}{C_d^2} \tag{3.15}$$

Where

$$\beta = \frac{d}{D}$$

$$C_d = f(\beta) + 91.71\beta^{2.5}\,\mathrm{Re}_D^{-0.75} + \frac{0.09\beta^4}{1-\beta^4}F_1 - 0.0337\beta^3 F_2$$

$$f(\beta) = 0.5959 + 0.0312\beta^{2.1} - 0.184\beta^8$$

The Reynolds number Re_D is related to the unperturbed flow. The value of the correction factors F_1 and F_2 depends on the position of the taps for the pressure measures. The default is $F_1 = 0.4333$ and $F_2=0.47$, characteristic values for taps position of D-$^1/_2$D (Figure 3. 13).

Valve

Figure 3.14 reports the section of the type of gate valve arranged in the HELIOS loop. According to [9], when the valve is fully open, the form loss coefficient of this type of valve is given by the contribution due to the sudden contraction and expansion, adjusted by a factor K_1, which depends on the dimensions of the inlet-outlet and transition zones.

Figure 3.14: Gate valve

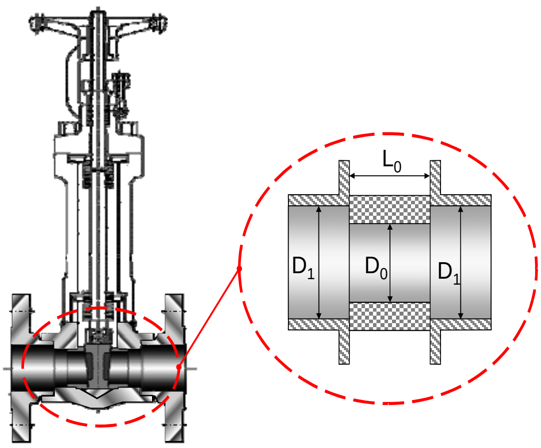

$$K_{GV} = K_1 \cdot K_G \tag{3.16}$$

The contraction expansion contribution K_G is given by Equation (3.16). Table 3.6 gives the adjustment factor K_1.

Table 3.6: Gate valve, values of K_1

D_1/D_0 \ L_0/D_0	0.5	0.6	0.7	0.8	1.0	1.4	≥2.0	
1.25	1.02	1.01	1.0	1.0	1.0	1.0	1.0	K_1
1.5	1.06	1.03	1.02	1.01	1.0	1.0	1.0	
1.75	-	1.1	1.06	1.04	1.01	1.0	1.0	
≥2.0	-	1.15	1.1	1.08	1.04	1.03	1.0	

LegoPC HELIOS model

Figure 3.15 shows the LegoPC display of the HELIOS facility model. The pipes and heat exchangers models are based on lumped parameter approach. The average length of their computational grid is 50 mm. The pump model, based on similarity rules, is characterised by the actual pump characteristic curves. The flow meter model is adjusted to the available calibration values as follows:

Table 3.7: Flow meter calibration data

Calibration data				
Mass flow rate W [kg/s]	Density ρ [kg/m^3]	Pressure P_1 [Pa]	Pressure P_2 [Pa]	ΔP [Pa]
4	10403.54	601 729	599 227	2 502
13	10403.54	618 250	591 823	26 427

Table 3.8: Orifice data

Orifice data				
D [m]	d [m]	$A_d=\pi d^2/4$ [m^2]	Re	K_0
0.0529	0.03246	0.000827	149853.75	2.309

Figure 3.15: LegoPC HELIOS preliminary model

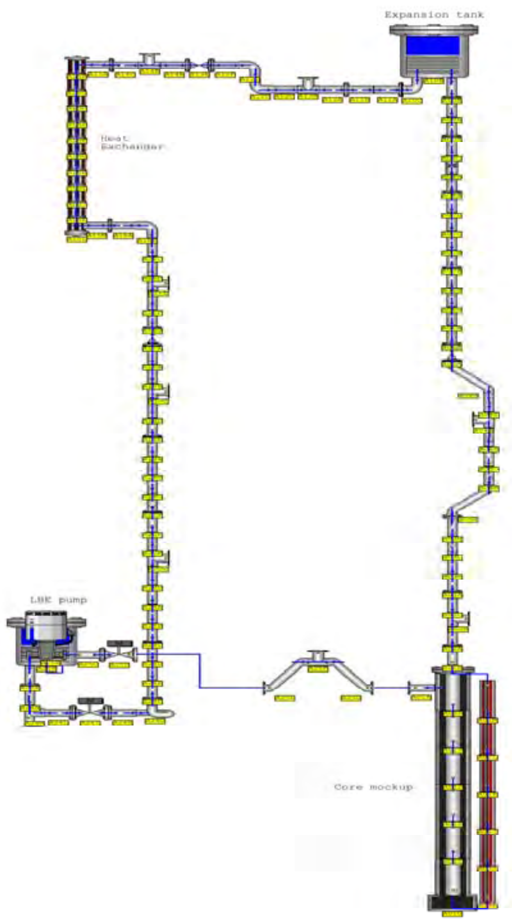

The Darcy pressure loss correlation can be written as:

$$\Delta P = \frac{\xi K_0}{2\rho A_d^2} W^2 = \frac{K^*}{2\rho A_d^2} W^2 \tag{3.17}$$

Where ξ is an adjustment factor and K^* can be assumed as a modified orifice form loss coefficient. When no information is available about the flow meter calibration, the ξ default value is ξ =1 and the two coefficient are an identity ($K^* = K_0$). If some flow meter calibration data in the range of the simulation are available, as the data reported in the previous tables, the adjustment factor ξ and the modified form loss coefficient K^* can be easily calculated:

$$\xi = \frac{2\rho A_d^2 \Delta P}{K_0 W^2} = .965 \tag{3.18}$$

$$\boldsymbol{K^* = \xi K_0} = 2.228$$

Now, we may use the adjusted coefficient K^* to obtain the flow meter pressure loss related to the high-mass flow rate (W=13.57 kg/s).

$$\Delta P = \frac{K^*}{2\rho A_d^2} W^2 = 28830{,}54 \tag{3.19}$$

The following table summarises most loop components form loss coefficient, reference fluid velocity and pressure loss related to low-and high-mass flow rate.

Table 3.9: Main component pressure loss at low-mass flow rate

Component		Low-mass flow rate 3.27 kg/s						
		Velocity [m/s]	$f\frac{l}{D}$	ΔP_f [Pa]	K	ΔP_k [Pa]	$f\frac{l}{D}+K$	ΔP [Pa]
Gasket between flanges		0.082	0.0015	0.0536	0.545	19.025	0.545	19.08
Bends	S-shaped 45°	0.163	0.154	21.28	0.19	26.26	0.344	47.54
	Single 90°	0.163	0.053	7.32	0.263	36.35	0.316	43.67
Core spacer		0.222	-	-	1.85	474.79	1.85	474.79
Flow meter		0.38	-	-	2.225	1669.8	2.225	1669.8
Gate valve		0.292	-	-	0.589	262	0.589	262

Table 3.10: Main component pressure loss at high-mass flow rate

Component		High-mass flow rate 13.57 kg/s						
		Velocity [m/s]	$f\frac{l}{D}$	ΔP_f [Pa]	K	ΔP_k [Pa]	$f\frac{l}{D}+K$	ΔP [Pa]
Gasket between flanges		0.34	0.0011	0.68	0.545	327.63	0.546	328.3
Bends	S-shaped 45°	0.678	0.115	274.98	0.133	318.03	0.248	593.01
	Single 90°	0.678	0.04	95.65	0.184	439.97	0.224	535.62
Core spacer		0.92	-	-	1.566	6894.7	1.566	6894.7
Flow meter		1.576	-	-	2.229	28800.66	2.229	28800.66
Gate valve		1.213	-	-	0.577	4419.3	0.577	4419.3

References

[1] S. Spelta (1981), Confrontation du model LEGO-REP 900 MW CP2 avec l'essai d'ilotage de St. Laurent B1 du 22/7/81, SEPTEN (EDF), *Internal Report TH-85-09 A (DF07)*.

[2] S. Spelta (1985), An application of the LEGO Packages to PWR Power Plant Modelling, *Proc. of the Fifth International Conference on Mathematical Modelling, Berkley*, California.

[3] G.Garbossa, R.Mosca, S.Spelta, R.Cori, P.Cento (1989), A model of Alto Lazio boiling water reactor using the Lego code: Nuclear Steam Supply System Simulation, *Seventh Power Plant Dynamics, Control and Testing Symposium, Knoxville, Tenn.* (USA), 15-17 may 1989.

[4] S.Spelta, G.Garbossa, P.Cento, L.Ferrari (1989), A model of Alto Lazio boiling water reactor using the Lego code: Balance of Plant Simulation, *Seventh Power Plant Dynamics, Control and Testing Symposium, Knoxville, Tenn.* (USA), 15-17 may 1989.

[5] R. Cori, G. Migliavacca, S. Spelta (1997), A new approach to LEGO steady state calculation for power plants dynamic models – 15th *IMACS World Congress on Scientific Computation Modeling Applied Mathematics, Berlin*, August 1997.

[6] OECD/NEA (2007), Handboook on Lead-bismuth Eutectic Alloy and Lead Properties, Materials Compatibility, thermal-hydraulics and Technologies.

[7] Frank M. White (1986), Fluid Mechanics 2nd edition, McGraw-Hill.

[8] K.Rehme (1973), Pressure drop correlations for fuel elements spacers, Nuclear Technology, 43:17.

[9] I.E. Idelchik, G.R. Malyavskaya, O.G. Martynenko, E. Fried (1986), Handbook of Hydraulic Resistance, 2nd edition, Hemisphere Pub. Corp.

[10] A. Guagliardi, V. Casamassima (2008), A modular approach to lead-cooled reactors modelling, *Journal of Nuclear Materials,* Vol 376/3 pp 293-296, DOI: 10.1016/j.jnucmat.2008.02.085.

3.3 ENEA, Italy

ENEA participation in the benchmark aims to assess the RELAP5 code specifically modified for treating heavy metal cooling fluids. This code is the ENEA's reference tool for transient and accident analyses in heavy liquid metal (HLM) cooled systems. Both Mod3.2 and Mod3.3, the latest versions of RELAP, have been applied in the first part of the benchmark with almost identical results. Therefore RELAP5 Mod3.3 has been chosen as the reference code for the ENEA's participation in the benchmark.

3.3.1 RELAP5 code version for HLM

Modification for heavy metal fluid

The RELAP5 code was developed for LWR LOCA analysis, extensively validated and worldwide used as a best estimate code for LWRs. The thermo-hydraulic system code is based on a 6-equation 2-fluid model describing mass, momentum and energy balances of separated steam and liquid phases. This code [1] was chosen in the frame of the Italian research programme on ADS (TRASCO) as the reference code for the thermal-hydraulics analysis of Pb and Pb-Bi-cooled systems.

This original version was modified generating the physical and thermodynamic properties for Pb, Pb-Bi (soft sphere model) and for diathermic oil and updating several original routines in order to implement new correlations for heavy liquid metal. Moreover, specific heat transfer correlations were added: convective heat transfer for heavy liquid metals evaluated according to Seban-Shimazky (pipe) or Subbotin-Ushakov (tube bundle), and for oil helical path (Gnielinsky).

Assessment activity

The modifications that mainly concern Pb and Pb-Bi physical properties and thermal exchange correlations have been validated against experimental data. The qualification was mainly based on an experimental programme carried out at the ENEA Research Centre of Brasimone (Italy) in support of XADS design and MEGAPIE experiment:

- ability to simulate a two-component, two-phase mixture of liquid lead-bismuth and steam successfully assessed using EGTAR-3 experiment (ANSALDO);
- ability to simulate LBE natural circulation in a loop successfully assessed on CHEOPE experimental facility (Brasimone- Italy) [2];
- ability to simulate a two-component, two-phase mixture of liquid lead-bismuth and gas successfully assessed using the CIRCE gas-lifting tests (Brasimone Italy) [3];
- validation of thermal-exchage correlations against MEGAPIE single-pin tests (Brasimone) and integral tests (PSI) [4].

3.3.2 Models and nodalisation

RELAP5 nodalisation

The objective of the ENEA's participation in the LACANES benchmark is to assess both the code used for transient analysis and the procedure followed to build the code model of the heavy metal-cooled system to be analysed. For this reason, the nodalisation of the Helios loop has been developed with the simulation detail adopted in the reactor applications, moreover, the models for the computation of the singular pressure drops have been drawn from the hydraulic handbook usually used as a reference [5].

The nodalisation scheme of the RELAP5 model is reported in Figure 3.16. It represents a complete one-dimension description of the forced flow path of the Helios loop. The 250 hydraulic meshes range between 0.05 m and 0.15 m in order to join sufficient detail in the description with an acceptable computation time. That implies an error in calculating the punctual value of the parameters like pressure and temperature due to the averaging process in the mesh.

As the first part of the benchmark is purely hydraulic, neither pipe walls nor internal structure have been simulated for the time being, so the calculation concerns a completely adiabatic system. In order to avoid the simulation of the pump dissipation heat the RELAP5 pump module has not been used and the lead-bismuth flowrate has been imposed by a boundary condition.

Figure 3.16: Nodalisation scheme of Helios loop for RELAP5 code

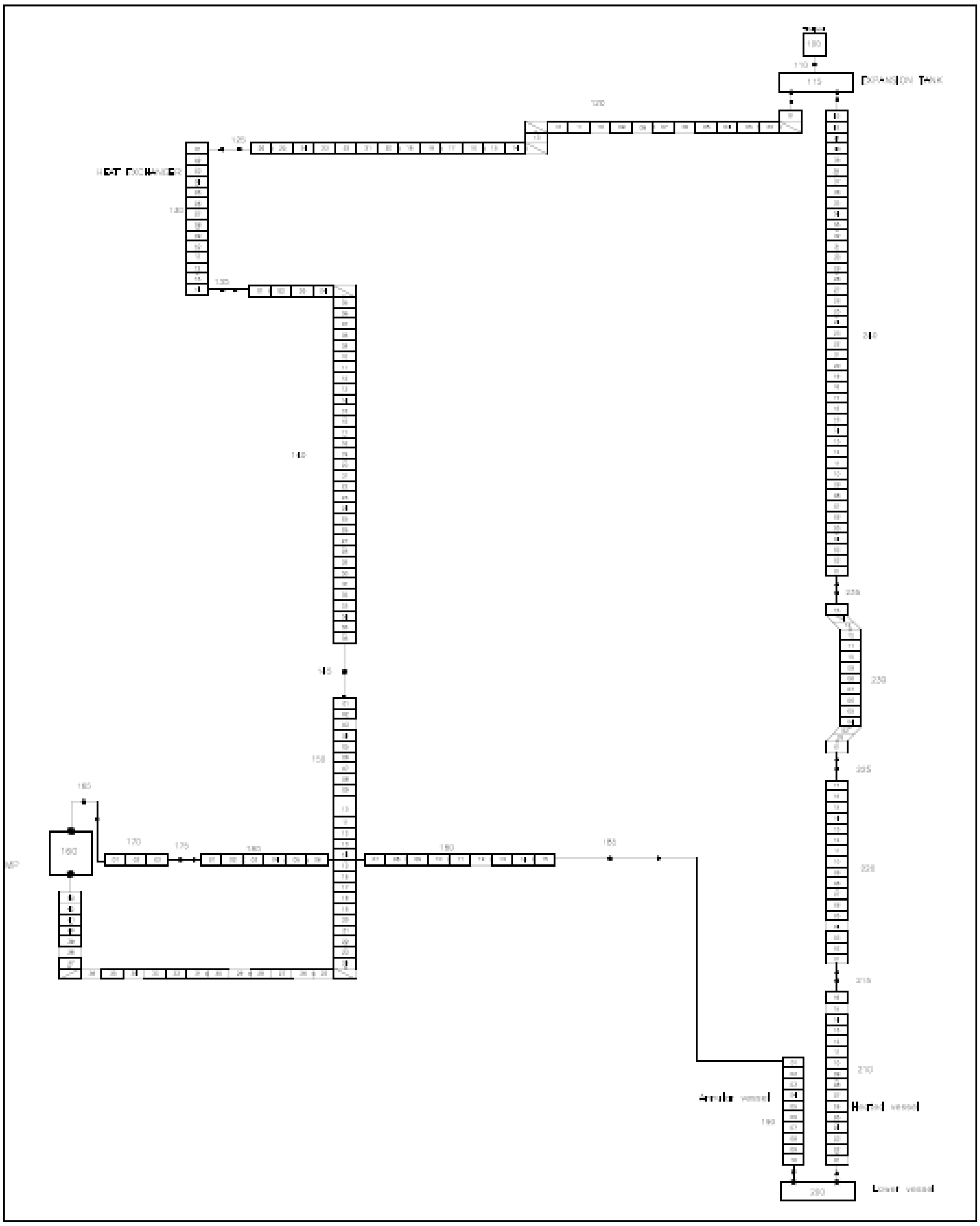

Distributed friction losses

The friction loss coefficients are calculated directly by the RELAP5 code. To perform the calculation of Darcy-Weisbach friction factor for the distributed friction loss inside the loop, the code utilises the different correlations reported in Table 3.11 at different flow regimes. In detail, it uses correlations for laminar flow regime, for turbulent flow regime and for transition flow regime from laminar to turbulent. The turbulent friction factor is given by the Zigrang-Sylvester engineering approximation to the Coolebrook-White correlation. The first one has the advantage that it is an explicit relation for the friction factor, while the second one is a transcendental function requiring iteration for the friction factor calculation.

Table 3.11: RELAP5 Correlations for friction factors

Laminar flow regime	$\lambda_L = \frac{64}{\mathrm{Re}\,\Phi_s}$	$0 \le \mathrm{Re} \le 2200$
Turbulent flow regime	$\frac{1}{\sqrt{\lambda_T}} = -2\log_{10}\left\{\frac{\varepsilon}{3{,}7D} + \frac{2{,}51}{\mathrm{Re}}\left[1{,}14 - 2\log_{10}\left(\frac{\varepsilon}{D} - \frac{21{,}25}{\mathrm{Re}^{0{,}9}}\right)\right]\right\}$	$\mathrm{Re} > 3000$
Transition flow regime	$\lambda_{L,T} = \left(3{,}75 - \frac{8250}{\mathrm{Re}}\right)\left(\lambda_{T,3000} - \lambda_{T,2200}\right) + \lambda_{T,2200}$	$2200 \le \mathrm{Re} \le 3000$

Φ_s Shape factor for noncircular flow channel, ε Surface roughness, D Hydraulic diameter,

$\lambda_{L,2200}$ Laminar friction factor at Re=2 200, $\lambda_{L,3000}$ Laminar friction factor at Re=3 000

Concentrated friction losses

The flow area variations as well as elbows, orifices and grids are taken into account in the RELAP5 model by means of concentrated pressure drops ($\frac{1}{2}\zeta\rho V^2$). The pressure losses coefficients are pre-calculated by means of correlations mainly drawn by the IDELCHIK book [5] and introduced in the corresponding junctions of the RELAP5 nodalisation. The following correlations are briefly described:

Bend loss coefficients

The general loss coefficient formula used is the following:

$$\zeta = k_\Delta k_{\mathrm{Re}} \zeta_M + \zeta_f \quad \text{where} \quad \zeta_M = A_1 B_1 C_1 \quad \text{and} \quad \zeta_f = 0.0175\lambda \frac{R}{D}\delta^\circ$$

The values A_1, B_1, C_1, λ, k_Δ, k_{Re} are determined by diagrams/tables as a function of Re, Δ, R/D, and δ°. The above relations are valid for bends with roughness Δ>0, 0.5<R/D<1.5 and $0 < \delta^\circ \le 180$

Sudden changes in flow area

The relations in Table 3.12 [5] had been used for all concerned flow situations and in several particular cases:

- Heat exchanger inlet - The exit area A_1 calculated with a radius r equal to distance between the axis of inlet pipe and the top of heat exchanger.
- Heat exchanger outlet - Exit area A_1 calculated with a radius r equal to the distance between the axis of outlet pipe and the bottom of heat exchanger.
- Core inlet - Exit area A_1 calculated with a radius r equal to distance between the axis of inlet pipe and the top of core vessel.
- Gasket - There are a lot of pipe connections with gaskets along the loop, so it is important to calculate the pressure drop on each one. The shape of path flow between connection flanges and gasket has been treated like a sudden expansion followed by a sudden contraction. The limitations of this approach could be the fact that the relations are valid for a completely developed flow, whereas before the sudden contraction this is not the case, nevertheless, such a consideration can be made in several other loop locations.
- Pump outlet - The pump outlet shows a complex situation from the point of view of change flow area variation. The system is made up of a pump outlet section plus a valve

and two connection gaskets. It was schematised like a sequence of sudden expansion and contraction sections.

Heat exchanger and core grids

The pressure drop coefficients on the grids are calculated by Rehme correlation [6] reported in Table 3.12.

Orifice

The pressure drop on the orifice was calculated by means of a formula in Table 3.12 [5].

Glove valves

The valves were totally open in the loop configuration considered for the first phase of the benchmark. The total pressure loss coefficient provided by the manufacture (ζ= 0.973) is introduced in the nodalisation junctions corresponding to the valve locations.

Table 3.12: Singular pressure loss coefficient for flow area variation

Sudden change in flow area	$\zeta = \left(1 - \frac{A_0}{A_1}\right)^2$	Sudden expansion	A_0 smallest area A_1 biggest area
	$\zeta = 0.5\left(1 - \frac{A_0}{A_1}\right)$	Sudden contraction	
Grids	$\varsigma = C_V \varepsilon^2$	$C_V = 3{,}5 + \frac{73{,}5}{R_e^{0,264}} + \frac{2{,}79*10^{10}}{R_e^{2,79}}$	A_V Grid area A_S Flow area without grid
		$\varepsilon = \frac{A_V}{A_S}$	
Orifice	$\zeta = \left(1 + 0{,}707\sqrt{1 - \frac{F_0}{F_1}} - \frac{F_0}{F_1}\right)^2 \left(\frac{F_1}{F_0}\right)^2$	$R_e \geq 10^5$	F_0 smallest area F_1 biggest area

3.3.3 Preliminary results

The RELAP5 model here described has been used to simulate the two steady-state conditions at high (13.57 kg/s) and low (3.27 kg/s) mass flow rate proposed to characterise the HELIOS facility pressure drops. The singular pressure drop coefficients that depend on flow conditions through the Reynolds number like the bend loss coefficients and the grid coefficients are calculated and introduced in the model for each mass flow rate.

Figure 3.17: Pressure distribution in HELIOS loop at high-flow conditions

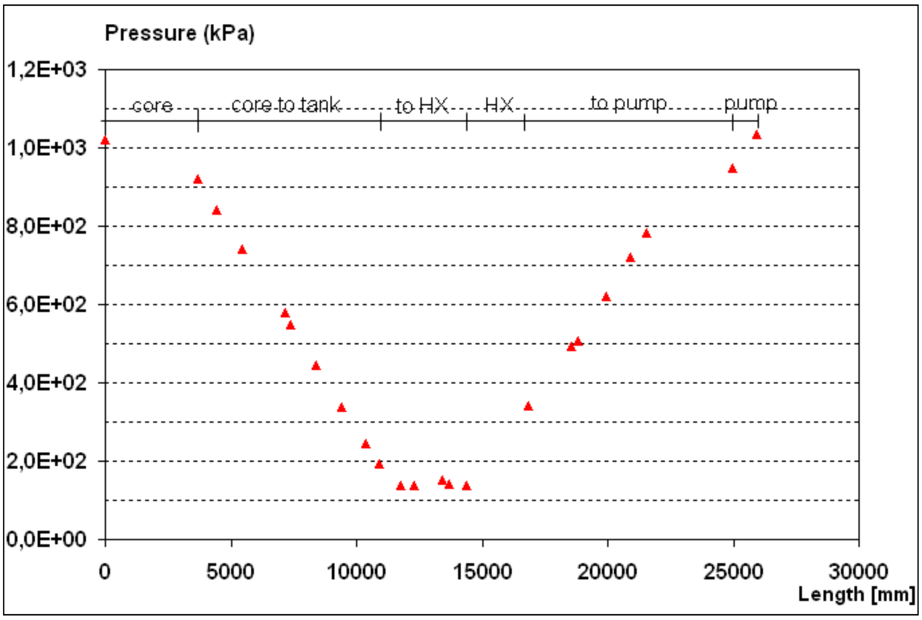

As an example of the results obtained, the pressure distribution along the loop is reported in Figure 3.17 for the high-mass flowrate conditions. RELAP5 has calculated that the head of 1.439 bar has to be supplied by the pump to have a LBE mass flowrate of 13.57 kg/s in the Helios loop. It has to be noted that the absolute values of the pressure depend on the level imposed in the upper tank (0.3 m) as a boundary condition for the calculations.

Reference

[1] P. Meloni *et al.* (2001), "Implementation and Preliminary Verification of the RELAP5/PARCS Code for Pb-Bi Cooled Subcritical System", *Proc. of the International Conference on Accelerator Applications* AccApp01, Nuclear American Society, Reno, USA.

[2] P.Meloni *et al.* (2002), "Natural circulation of Lead-Bismuth in a one-dimensional loop: experiments and code predictions", *Proc. of the International Conference ICONE-10*, Arlington, USA.

[3] P.Meloni *et al.* (2004), "Investigation of RELAP5 Capability to simulate the LBE Cooling System Thermal-Hydraulic", *Proc. of the 8th Information Exchange Meeting on Transmutation and Partitioning (IEMTP),* Las Vegas, USA.

[4] P.Meloni *et al.* (2008), "Verification of the RELAP5 Code against the MEGAPIE Irradiation Experiment", presented at the *10th Information Exchange Meeting on Transmutation and Partitioning (IEMTP)*, 6-10 October 2008, Mito, Japan.

[5] I.E. Idelchik (2003), "Handbook of Hydraulic Resistance", 3rd Edition, Published by Jaico Publishing House.

[6] K. Rheme (1973), "Pressure drop correlations for fuel element spacers", Nuclear Technology Review, Vol. 17 January.

3.4 Seoul National University, Republic of Korea

3.4.1 Computer code characteristics

The SNU used MARS-LBE version 3.11 code (Multi-dimensional Analysis Reactor Safety for LBE coolant), which is a revised version of MARS 3.1 code by updating hydraulics and heat transfer correlations for LBE fluid modelling. The MARS code was originally developed by KAERI (KOREA Atomic Energy Research Institute) based on RELAP5 and COBRA-TF codes for LWR thermal-hydraulic analysis [1]. Recently, the MARS code has been improved to analyse sodium-cooled fast reactor (SFR) and lead-bismuth-cooled fast reactor (LBFR). The RELAP5 code analyses one-dimensional fluid flow model including modelling of two-phase flow, thermal hydraulics and component characteristics. It also includes the point kinetics model with versatile and robust features. The COBRA-TF code is a three-dimensional analysis tool which can also handle two-phase flow with re-flood heat structure model on flexible noding schemes.

3.4.2 Nodalisation of HELIOS

Figure 3.18 shows nodalisation of the HELIOS. The MARS-LBE code has two options for standard components: PIPE and JUNCTION modules. The PIPE module models pipes of the HELIOS and the JUNCTION module links two PIPE modules which can be divided into smaller volumes. For instance, the PIPE at node number 100 has 5 volumes in Figure 3.18. The JUNCTION module is non-volume segment and uses K-factor (form loss coefficient) to represent geometric change such as 45 or 90 degree elbows, etc. For each module, initial conditions of temperature and mass flow rate should be defined.

The node number 750 JUNCTION between node 700 PIPE and node 100 PIPE represents the pump of the HELIOS. For the benchmark study, the pressure loss in the pump was ignored and the net head increase by the pump was taken into account.

Figure 3.18: Nodalisation of the HELIOS

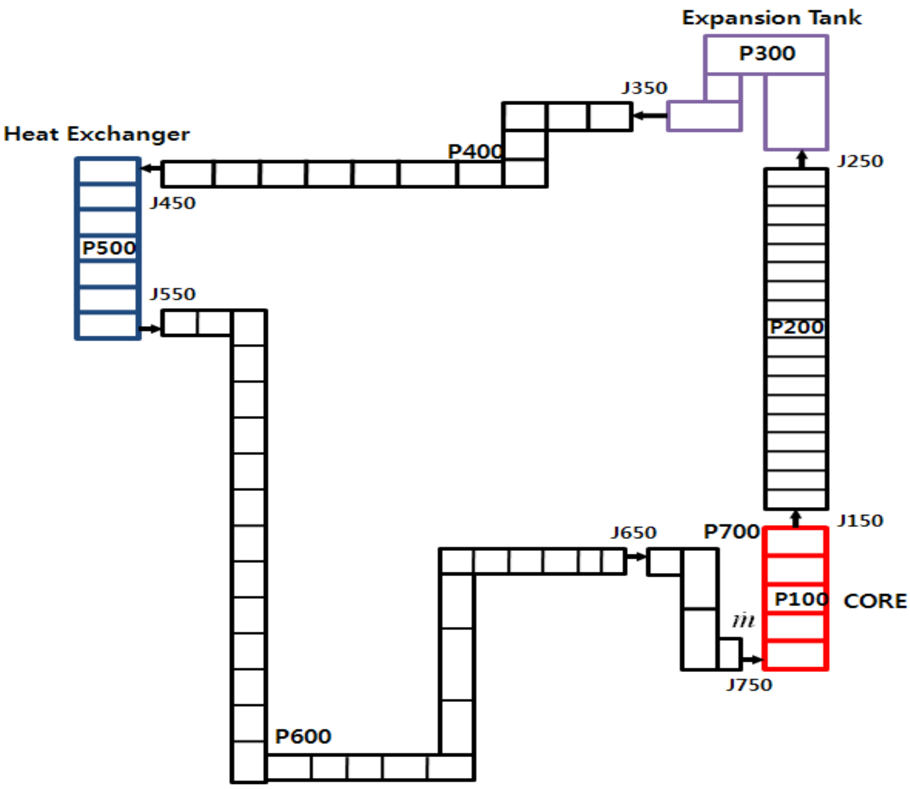

3.4.3 Pressure loss lodels in MARS-LBE 3.11 [1]

Friction factor (f)

Three friction factor models were used: laminar; laminar-turbulent transition; and turbulent flow regimes. The laminar friction factor is:

$$f = \frac{64}{\mathrm{Re}\Phi_S} \quad \text{for} \quad 0 \le \mathrm{Re} \le 2200$$

where Re is the Reynolds number and Φ_S is a shape factor for noncircular flow channels.

The friction factor in the transition region between laminar and turbulent flows could be computed by the reciprocal interpolation

$$f = (3.75 - \frac{8250}{\mathrm{Re}})(f_{T,3000} - f_{L,2200}) + f_{L,2200} \quad \text{for} \quad 2200 \le \mathrm{Re} \le 3000$$

where $f_{L,2200}$ is the laminar factor at a Reynolds number of 2200, $f_{T,3000}$ is the turbulent friction factor at a Reynolds number of 3 000 and the interpolation factor is defined to lie between 1 and 0.

The turbulent friction factor is given by the Zigrang-Sylvester approximation to the Colebrook-White correlation:

$$\frac{1}{\sqrt{f}} = -2\log_{10}\{\frac{\varepsilon}{3.7D} + \frac{2.51}{\mathrm{Re}}[1.14 - 2\log_{10}(\frac{\varepsilon}{D} - \frac{21.25}{\mathrm{Re}^{0.9}})]\}$$

where ε is the surface roughness. Unlike the Colebrook-White correlation, which is a transcendental function and requires internal iteration to determine the friction factor, the Zigrang-Sylvester equation has advantage of explicit relation scheme.

Sudden area change

The form factor (K) and dynamic head loss (ΔP_L) of the sudden area changes can be obtained by the Borda-Carnot assumption. The velocity at the smaller section is the reference velocity for pressure drop calculation.

Table 3.13: Form loss coefficient for sudden area change in MARS-LBE code

Change type	Expansion	Contraction
Form factor	$K = (1 - \frac{A_1}{A_2})^2$	$K = (1 - \frac{A_2}{A_c})^2$
Pressure drop	$\Delta P_L = \frac{1}{2}\rho(1 - \frac{A_1}{A_2})^2 v_1^2$	$\Delta P_L = \frac{1}{2}\rho(1 - \frac{A_2}{A_C})^2 v_2^2$

where, A_2 is downstream area, A_1 is upstream area, $\frac{A_c}{A_2} = 0.62 + 0.38(\frac{A_2}{A_1})^3$

Figure 3.19: Sudden expansion (left) and contraction (right)

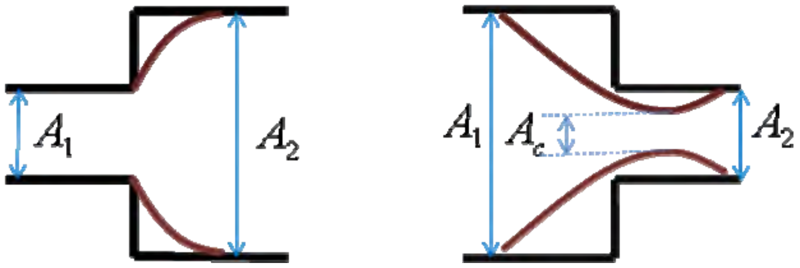

Other form loss coefficients were set by user defined values. Form loss coefficients of gasket, glove valve, expansion tank were calculated based on sudden area changes. Form loss coefficients of 45 or 90 degree elbows, tee-junction, orifice, core spacer, heat exchanger spacer were obtained from Handbook of hydraulic resistance [2] and nuclear system [3].

45 or 90 degree elbows

$$\zeta = k_{\mathrm{Re}} k_{loc} + 0.0175 \delta \lambda \frac{R_0}{D_h}$$

where, k_{loc}= A_1B_1 and δ is angle in degree, D_h is hydarulic diameter.

Figure 3.20: A_1 (left figure) and B_1 (right figure) for elbow form factor

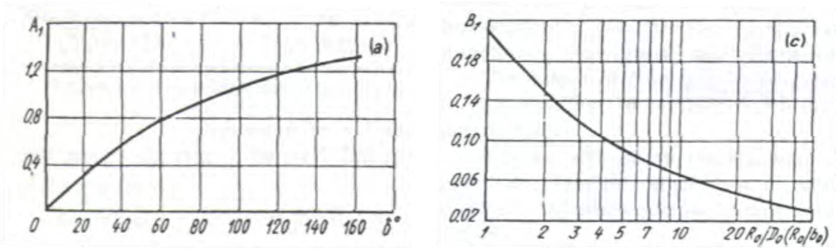

Table 3.14: k_{Re} for elbow form factor

k_{Re}						
R_0/D_0 (R_0/b_0)	Re × 10^{-5}					
	0.1	0.14	0.2	0.3	0.4	0.6
0.5-0.55	1.40	1.33	1.26	1.19	1.14	1.09
>0.55-0.70	1.67	1.58	1.49	1.40	1.34	1.26
>0.70	2.00	1.89	1.77	1.64	1.56	1.46
R_0/D_0 (R_0/b_0)	Re × 10^{-5}					
	0.8	1.0	1.4	2.0	3.0	4.0
0.5-0.55	1.06	1.04	1.0	1.0	1.0	1.0
>0.55-0.70	1.21	1.19	1.17	1.14	1.06	1.0
>0.70	1.38	1.30	1.15	1.02	1.0	1.0

where R_o is radius of curvature and D_o is diameter

Table 3.15: λ for elbow form factor

λ									
$\bar{\Delta}=\frac{\Delta}{D_h}$	Re								
	3×10^3	4×10^3	6×10^3	10^4	2×10^4	4×10^4	6×10^4	10^5	2×10^5
0.0008	0.043	0.040	0.036	0.032	0.027	0.024	0.023	0.022	0.020
0.0006	0.046	0.040	0.036	0.032	0.027	0.023	0.022	0.021	0.018
0.0004	0.036	0.040	0.036	0.032	0.027	0.023	0.022	0.020	0.018
0.0002	0.036	0.040	0.036	0.032	0.027	0.022	0.021	0.019	0.017
0.0001	0.036	0.040	0.036	0.032	0.027	0.022	0.021	0.019	0.017
0.00005	0.036	0.040	0.036	0.032	0.027	0.022	0.021	0.019	0.016
0.00001	0.036	0.040	0.036	0.032	0.027	0.022	0.021	0.019	0.016
0.000005	0.036	0.040	0.036	0.032	0.027	0.022	0.021	0.019	0.016

△ is roughness

Tee-junction

Figure 3.21: Geometry of tee (left figure) and form factor (right figure)

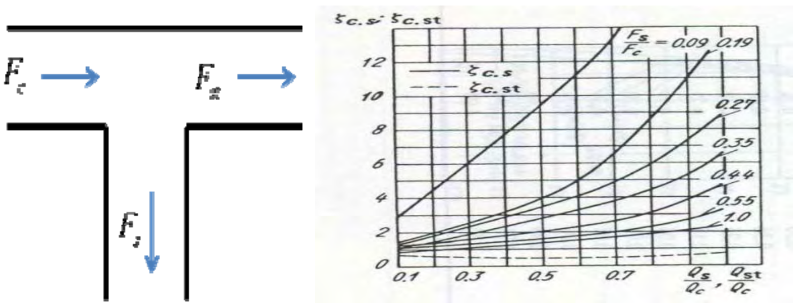

F is cross-sectional area,

Subscript c, st, and s means converging, straight passage and side branch, respectively,

ζ is form factor.

Orifice

$$K=\left(1+0.707\sqrt{1-\frac{F_0}{F_1}}-\frac{F_0}{F_1}\right)^2\left(\frac{F_1}{F_0}\right)^2 \quad \text{for} \quad \mathrm{Re}>10^5$$

Figure 3.22: Geometry of the orifice

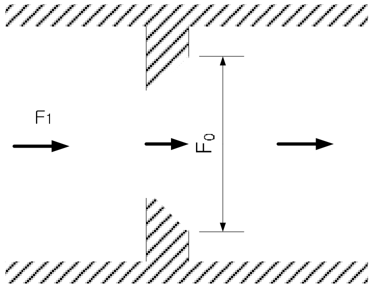

Grid (core, heat exchanger) - Rehme's data for square arrays

Δp_s is pressure drop in spacer grids which are located in core and heat exchanger.

$$\Delta p_s = C_v(\rho V_v^2 / 2)(\frac{A_s}{A_v})^2$$

Where, v is bundle fluid. The C_v could be obtained from Figure 3.23.

Figure 3.23: Grid form factor, C_v

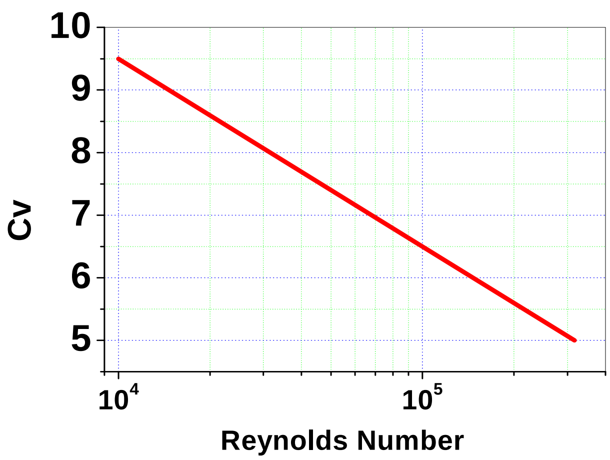

Table 3.16 shows form loss coefficient of components which were used for the MARS-LBE simulation.

Table 3.16: Form loss coefficient of the components

Type of Component		Low mass flow rate (3.27 kg/s)		High mass flow rate (13.57 kg/s)	
		Ref. velocity (m/s)	*K*	Ref. velocity (m/s)	*K*
Elbow	45 degree	0.163	0.19	0.678	0.13
	90 degree	0.163	0.32	0.678	0.22
Tee	Straight	0.163	0.70	0.678	0.70
	Branch	0.163	2.80	0.678	2.80
Grid	CORE(#3)	0.222	6.35	0.92	4.94
	HX[2](#6)	0.029	6.35	0.121	5.10
Gasket	Pipe to gasket	0.163	0.25	0.678	0.25
	Gasket to pipe	0.163	0.25	0.678	0.25
Orifice		0.163	10.43	0.678	10.43
Gate valve		0.292	0.51	1.213	0.49
Expansion tank		0.163	1.64	0.678	1.54

References

[1] KAERI (2006), Thermal Hydraulic Safety Research Department of KAERI, MARS CODE Manual Volume I – Code structure, System Models, and Solution Methods.

[2] I.E. Idelchik (2000), Handbook of Hydraulic Resistance 3rd Edition, CRC.

[3] N. E. Todreas, M. S. Kazimi (1990), Nuclear system, Hemisphere Publishing Corporation.

3.5 GIDROPRESS, Russian Federation

Computer codes were not applied in "GIDROPRESS" calculations of pressure losses in HELIOS loop. Such decision has been made because of the following key reasons:

- a simple configuration of a loop;
- known value of the flow rate;
- factors of local hydraulic resistance are used as the initial data for computer codes;
- procedure of pressure loss comparison on separate circuit parts conflicts with nodalisation schemes of computer codes.

Recommendations of [1] were used in calculations of pressure losses. Properties of lead-bismuth coolant were used according to recommendations of [2].

It is supposed to use computer code TRIANA at phase II of HELIOS benchmark for computation of natural circulation level. TRIANA code is developed in "GIDROPRESS" for

[2] HX: Heat Exchanger

calculations of transients and safety assessment of lead-bismuth cooled reactor facilities. Constitutive relations for pressure losses in TRIANA code are based on [1].

Reference

[1] I.E. Idelchik (1975), Hydraulic resistance handbook, Moscow, "Mashinostroeniye", (in Russian).

[2] P.L. Kirillov, M.I. Terentjeva, N.B. Deniskin (2007), Thermophysical properties of nuclear engineering materials, (2nd edition), Moscow, IzdAt, (in Russian).

3.6 IPPE, Russian Federation

3.6.1 Calculating code HYDRA for carrying out calculation of a hydraulic network

Problem definition

Code HYDRA is intended for engineering calculation of a hydraulic network (N). Hydraulic network is considered as a set of interconnected elements (e_i). The state of hydraulic network element e_i is defined by the values of parameters (p_{ij}) and characteristics (h_{ik}). Parameters p_{ij} are specified as input data. Types of element characteristics are identical for all hydraulic network elements (e.g. pressure, temperature, coolant velocity etc.). Some element characteristics are used to interconnect elements in the hydraulic network N ($h_{ik}, k \in R_i$) by continuity conditions. For each element there are two non-overlapping subsets of characteristics: one which is input data ($h_{ik}, k \in R_i^{in} \subset R_i$) and another one ($h_{ik}, k \in R_i^{out} \subset R_i$) that is determined from $h_{ik}, k \in R_i^{in}$ by element specific functions f_{ik} :[3]

$$h_{ik} = f_{ik}(p_{ij}, h_{im}), k \in R_i^{out}, m \in R_i^{in}, i \in [1, I], j \in J_i, \qquad (3.20)$$

where I - number of elements in the network N, J_i - number of parameters for the i-th element.

Code HYDRA is intended for two types of calculations: pressure drop calculation on the basis of given flow rate and flow rate calculation on the basis of given pressure drops. The mathematical problem in carrying out these calculations can be formulated as solution of the following system of the nonlinear Equations:

$$\begin{cases} \hat{P}_{IN}\vec{h} = \hat{P}_{OUT}\vec{h}, \\ \hat{P}_{OUT}\vec{h} = \vec{f}(\vec{p}, \hat{P}_{IN}\vec{h}), \end{cases} \qquad (3.21)$$

where $\vec{h} = col\{h_{ik}\}$ - a vector of definitely ordered characteristics of all elements of the network; $\vec{p} = \{p_{ij}\}$ - a vector of definitely ordered parameters of all elements of the network; $\hat{P}_{IN}\vec{h}$ ($\hat{P}_{OUT}\vec{h}$) – a vector made of components of vector $\vec{h}$ which are input (output) element characteristics (equation $\hat{P}_{IN}\vec{h} = \hat{P}_{OUT}\vec{h}$ expresses a continuity of corresponding variables); $\vec{f} = col\{f_{ik}\}$ - a vector of definitely ordered functions f_{ik} from the system of the nonlinear equations (3.20).

[3] For the sake of simplicity influence of the rest of elements is not shown.

Definition of pressure loss coefficients

Functions f_{ik} from (3.20) for isothermal flows are basically determined by pressure drops in hydraulic network elements:

$$\Delta P_i = (\zeta_i^{FORM} + \zeta_i^{FRIC})\frac{\rho_i w_i^2}{2} - \rho_i g \Delta h_i = (\zeta_i^{FORM} + \zeta_i^{FRIC})\frac{\rho_i}{2}\left(\frac{Q_i}{F_i}\right)^2 - \rho_i g \Delta h_i, \quad (1.22)$$

where ΔP_i - pressure drop on i-th element (between the element's output and input); ζ_i^{FORM} - form loss coefficient for i-th element; ζ_i^{FRIC} - friction loss coefficient for i - th element; ρ_i - coolant density in i-th element; $w_i = \dfrac{Q_i}{F_i}$ - coolant velocity in i-th element; Q_i - volume flow rate in i-th element; F_i - the area of characteristic section in i-th element; g - acceleration of gravity; Δh_i - difference of heights between the element's output and input.

References to formulas for calculation of form loss coefficients and friction loss coefficients used in code HYDRA are presented in Table 3.17.

Table 3.17: Formulas for calculation of form loss coefficients and friction loss coefficients

#	Type of element	References
1	Direct pipe	Item 30, p. 65
2	Direct ring pipe	Diagram (2-7), [1]
3	Direct ring pipe with ribs	Diagram (2-7), [1]
4	Pipe bundle, square lattice	Formulas (1.7) and (1.18), [1]
5	Suction tee	Diagram (7-4), [1]
6	Supply tee	Diagram (7-18), [1]
7	Sudden narrowing	Diagrams (4-9), (4-10), [1]
8	Sudden widening	Diagrams (4-2), (4-6) and (4-1), [1]
9	Direct pipe inlet	Diagram (3-1), [1]
10	Direct pipe with barrier	Diagrams (4-14), (4-15) and (4-19), [1]
11	Direct pipe with cannelures	Diagram (2-12), [1]
12	Bend	Diagrams (6-1), (6-2) and (2-1), [1]
13	S-shaped spatial connected bends	Diagram (6-19), [1]
14	S-shaped flat connected bends	Diagram (6-18), [1]

Numerical solution

For the numerical solution of the nonlinear equation system (3.21), software package KINSOL is used. Software package KINSOL is intended for solution systems of the nonlinear equations of kind $\vec{F}(\vec{u}) = 0$. Code HYDRA is written in C++ language with the object-oriented approach: elements of a hydraulic network, a hydraulic network, solver of systems of the equations, properties of the coolant, etc. are C++ objects. HYDRA's source code counts ~5 000 lines.

3.6.2 HELIOS model

Basic assumptions

The following basic assumptions are accepted while HELIOS model build up:

- description of the elements of the hydraulic network is taken from Appendix B;
- the pump interior was not taken into account, calculated pressure rise is used instead;
- the temperature and density of the coolant were accepted by constants in the elements;
- mutual influence of form loss coefficients, as a rule, was not taken into account (an exception - connected bends).

To make phase I results more accurate and to carry out calculation of phase II (natural circulation) it is necessary to specify geometry of HELIOS' loop in whole (i.e. spatial placing of elements of the loop - pipes, bends, tees, etc.).

Nodalisation of HELIOS model

Nodalisation of HELIOS model is presented in Table 3.18.

Table 3.18: Nodalisation of HELIOS model

#	Sub part No.	Sub part name	Element chain (types from Table 3.17).
1	1-1	Core inlet	1, 5
2	1-2	Downcomer	2, 7, 3, 8
3	1-3	Lower plenum	2, 9
4	1-4	Core	4, 10, 4, 10, 4, 10, 4, 8
5	1-5	Upper plenum	1
6	1-6	Gasket [between flanges]	11
7	2-1	Pipe [one side flange]	1
8	2-2	Tee	1
9	2-3	Pipe [one side flange]	1
10	2-4	Gasket [between flanges]	11
11	3-1	Pipe [both side flange]	1
12	3-2	Gasket [between flanges]	11
13	4-1	45 Degree elbow [one side flange]	1, 12
14	4-2	Pipe	1
15	4-3	45 Degree elbow	12
16	4-4	Pipe	1
17	4-5	Tee	1
18	4-6	Pipe	1
19	4-7	45 Degree elbow	12
20	4-8	Pipe	1
21	4-9	45 Degree elbow [one side flange]	12, 1
22	4-10	Gasket [between flanges]	11

#	Sub part No.	Sub part name	Element chain (types from Table 3.17).
23	5-1	Glove valve	1, 7, 1, 8, 1
24	5-2	Gasket [between flanges]	11
25	6-1	Pipe [both side flange]	1
26	6-2	Gasket [between flanges]	11
27	7-1	Pipe [both side flange]	1
28	7-2	Gasket [between flanges]	11
29	8-1	Pipe [one side flange]	1, 11
30	8-2	Orifice	1, 10, 1, 11
31	8-3	Pipe [one side flange]	1
32	8-4	Gasket [between flanges]	11
33	9-1	Pipe [both side flange]	1
34	9-2	Gasket [between flanges]	11
35	10-1	Expansion tank	1, 8, 7, 1, 12, 1
36	10-2	Gasket [between flanges]	11
37	11-1	Pipe [both side flange]	1
38	11-2	Gasket [between flanges]	11
39	12-1	Pipe [one side flange]	1
40	12-2	Tee	1
41	12-3	Pipe	1
42	12-4	90 Degree elbow	13
43	12-5	90 Degree elbow	
44	12-6	Pipe[one side flange]	1
45	12-7	Gasket [between flanges]	11
46	13-1	Glove valve	1, 7, 1, 8, 1
47	13-2	Gasket [between flanges]	11
48	14-1	Pipe [one side flange]	1
49	14-2	Tee	1
50	14-3	Pipe [one side flange]	1
51	14-4	Gasket [between flanges]	11
52	15-1	Heat exchangner vessel inlet	1, 5
53	15-2	Heat exchangner internal	4, 10, 4, 10, 4, 10, 4, 10, 4, 10, 4, 10, 4, 6
54	15-3	Heat exchangner outlet	1
55	15-4	Gasket [between flanges]	11
56	16-1	Pipe [one side flange]	1
57	16-2	90 Degree elbow	12
58	16-3	Pipe	1
59	16-4	Tee	1

#	Sub part No.	Sub part name	Element chain (types from Table 3.17).
60	16-5	Pipe [one side flange]	1
61	16-6	Gasket [between flanges]	11
62	17-1	Glove valve	1, 7, 1, 8, 1
63	17-2	Gasket [between flanges]	11
64	18-1	Pipe[one side flange]	1
65	18-2	Tee	1
66	18-3	Pipe [one side flange]	1
67	18-4	Gasket [between flanges]	11
68	19-1	Pipe [both side flange]	1
69	19-2	Gasket [between flanges]	11
70	20-1	Pipe[one side flange]	1
71	20-2	Tee	1
72	24-1	Pipe [one side flange]	1
73	24-2	Gasket [between flanges]	11
74	24-3	Pipe[both side flange]	1
75	24-4	Gasket [between flanges]	11
76	24-5	Pipe [one side flange]	1
77	24-6	90 Degree elbow	12
78	24-7	45 Degree elbow	12
79	24-8	Pipe [one side flange]	1
80	24-9	Gasket [between flanges]	11
81	24-10	Glove valve	1, 7, 1, 8, 1, 11
82	24-11	Pipe [one side flange]	1
83	24-12	Tee	1, 5
84	24-13	Pipe [one side flange]	1
85	25-1	Gasket [between flanges]	11
86	25-2	Sump tank	-
87	25-3	Gasket [between flanges]	11
88	25-4	Glove valve	1, 7, 1, 8, 1
89	25-5	Gasket [between flanges]	11
90	25-6	45 Degree elbow [one side flange]	1, 12
91	25-7	Pipe	1
92	25-8	45 Degree elbow	12
93	25-9	Tee	1
94	25-10	45 Degree elbow	12
95	25-11	Pipe	1
96	25-12	45 Degree elbow [one side flange]	12, 1

#	Sub part No.	Sub part name	Element chain (types from Table 3.17).
97	25-13	Gasket [between flanges]	11

References

[1] I.E. Idelchik (1992), Hydraulic Resistance Handbook, Moscow, "Mashnostroenie".

[2] P.L. Kirillov, Y.S. Yuriev, V.P. Bobkov (1990), Heat-Hydraulic Calculation Handbook, Moscow, "Energoatomizdat".

[3] A. M. Collier, A. C. Hindmarsh, R. Serban, and C. S. Woodward (2004), "User Documentation for KINSOL v2.2.0", LLNL technical report UCRL-SM-208116, November 2004.

[4] OECD/NEA (2007), Benchmarking of thermal-hydraulic loop models for lead alloy-cooled advanced nuclear energy systems, NEA/NSC/DOC (2007)14.

3.7 RRC KI, Russian Federation

3.7.1 Definition of pressure loss coefficients and relative pressure all over the loop

Current pressure in *i*-th point of the HELIOS loop, P_i, relatively to the point of inlet of the section A1 (point 1), can be calculated by summing the pressure drops of each component from the point 1 up to the current point *i* as follows:

$$P_i = \rho \sum_{k=1}^{i} (\bar{V}_k^2 f_k \frac{L_k}{D_k} + V_{k_{ref}}^2 K_k) \tag{3.23}$$

where

P, - current pressure in the point i;

ρ_k, f_k, L_k, D_k and K_k - are respectively fluid density, friction factor, length, hydraulic diameter and form loss coefficient of components k ($1 \le k \le i$);

$\bar{V}_k$ - average flow velocity of the part k;

$V_{k_{ref}}$ - reference velocity, related to the form loss coefficient K_k at the part *k*.

3.7.2 Procedures for pressure loss coefficients evaluation

The pressure loss coefficients of the part or the component are found from various literature data including handbooks [6-20]. Pressure loss coefficients are usually dependent not only on geometries but on flow conditions such as the Reynolds number or inner surface roughness. Two different flow rate cases are calculated: low and high flow. Table 3.19 provides the conditions for both cases from the HELIOS experiment on the isothermal (250 °C) flow test. It is noted that the Root-Mean-Square (RMS) surface roughness has been measured.

Table 3.19: Suggested conditions for the evaluation of pressure loss coefficients at 250 °C

Condition	Mass flow rate (kg/s)	Surface roughness (μm, RMS)
Low flow	3.27	2.53
High flow	13.57	2.53

3.7.3 Results of calculation of pressure loss coefficients and pressure distribution along HELIOS loop under isothermal flow conditions

The pressure loss coefficients of each part of HELIOS have been evaluated for two different flow rates, indicated in Table 3.20 and presented in the Table of Appendix C.

It has been shown in [21] that for the relative surface roughness less than 0.0004 there is no dependence of friction factor in straight channels on Reynolds number when Re > 40 000. Because in the most parts of HELIOS loop the Reynolds number exceeds $4*10^4$ and relative surface roughness rarely exceeds 0.0004 for both low-and high-flow cases, then in calculations of friction factors and loss coefficients we supposed that there is no dependence of these coefficients on Re number for the flow rates more than 3.27 kg/s and quadratic low of pressure loss on velocity is valid. So, the values of friction factors and loss coefficients given in Table of Appendix C characterise both cases of low and high flow.

The results of calculation of friction and form loss coefficients as well as pressure distribution along the HELIOS loop are presented for the both cases: low-mass flow rate of 3.27 kg/s and high-mass flow rate of 13.57 kg/s. Values of pressure in i-th points of HELIOS loop have been calculated with the use of Equation 3.23. The resulting plots of dependence of relative coolant pressure in HELIOS loop on distance from the inlet of Section A-1 to the current point *i* is shown in Figure 5.3 (for the case of high-mass flow rate). The results of low-mass flow rate are shown in Appendix C.

Total hydraulic resistance, calculated for the both flow rate cases amounts 135 kPa for the flow rate of 13.57 kg/s and 7.8 kPa for the flow rate of 3.27 kg/s.

References

[1] OECD/NEA (2007), "Summary Record of the first meeting of the benchmarking of thermal-hydraulic loop models for lead alloy-cooled advanced nuclear energy systems (LACANES)", OECD Nuclear Energy Agency, NEA/NSC/WPFC/DOC(2007)7.

[2] OECD/NEA (2007), "Handbook on Lead-bismuth Eutectic Alloy and Lead Properties, Materials Compatibility, Thermal-hydraulics and Technologies".

[3] I.S. Hwang (2006), "A Sustainable Regional Waste Transmutation System: P E A C E R", *Plenary Invited Paper,* ICAPP '06, Reno, NV, U.S.A. 4-6 June 2006.

[4] S. H. Jeong, C. B. Bahn, S. H. Chang, Y. J. Oh, W. C. Nam, K. H. Ryu, H. O. Nam, J. Lim, N. Y. Lee and I. S. Hwang (2006), "Operation Experience of LBE loop: HELIOS", Paper #6284, *Proceedings of ICAPP '06*, Reno, NV, U.S.A. 4-6 June 2006.

[5] J. Lim, S. H. Jeong, Y. J. Oh, H. O. Nam, C. B. Bahn, S. H. Chang, W. C. Nam, K. H. Ryu, T. H. Lee, S. G. Lee, N. Y. Lee and I. S. Hwang (2007), "Progresses in the Operation of Large Scale LBE Loop HELIOS", Paper #7536, *Proceedings of ICAPP*, Nice, France, 13-18 May 2007.

[6] P.M. Slissky (1983), Methodical Recommendations to Calculation of Friction Factors in Tubes for Transition Zone, *Proc. of Sc.-Tech. Hydraulics*, M. pp. 31-44.

[7] A.S. Gynevsky, E.E. Solodkin (1961), Hydraulic Resistance of Ring Channels Industrial Aerodynamics, M. Iss. 20, pp. 202-215.

[8] A.V. Sheinina (1967), Hydraulic Resistance of Rod Bundles in Axial Liquid Flow, Liquid Metals, M. pp. 210-223.

[9] G.N. Abramovich (1935), Air Dynamics of Local Drags, Industrial Air-Dynamics, M. Iss. 21, pp. 65-150.

[10] S.Yu (1972), Hydraulic Calculation of Plastic Pipes, HydroTechnics and Melioration, Offengenden, #1, pp. 24-28.

[11] M.Taliev (1952), Calculation of Drag Coefficients of Tee Connectors, M. Mashgiz, p. 52.

[12] I.E. Idelchik (1948), Discharge Losses in Flow with Nonuniform Velocity Profile, *Proc. of ZAGI*, Iss. 662, pp. 1-24.

[13] I.E. Idelchik, I.L.Hinsburg (1968), Hydraulic Resistance of Ring Turns of 180°, J. Teploenergetika, #4, pp. 87-90.

[14] I.E.Idelchik (1954), Hydraulic Resistance (physical mechanics foundations), M. Mashgiz, p. 316.

[15] I.E.Idelchik (1960), Account of Viscosity in Hydraulic Resistance of Baffles and Spacers, J. Teploenergetika, # 9, pp. 75 – 80.

[16] R. Rapp, R.W.Alperi (1970), Pressure Loss in Convolution Pipes // Building systems Design, April, pp. 26-28.

[17] V.M. Zusmanovich (1953), Resistance of Tees of Sink Gas- and Water- Pipes, Problems of Heat Supply and Ventilation, M. pp. 10 – 30.

[18] G.N. Abramovich (1935), Air Dynamics of Local Drags // Industrial AirDynamics, M. Iss. 21, pp. 65-150.

[19] B.I.Ianshin (1965), HydroDynamic Characteristics of Valves and Pipes // Mashgiz, M. p. 260.

[20] V.N.Karev (1953), Pressure Losses at Pipe Sudden Contraction and Influence of Local Drags for Flow Disturbance // Oil Economy, #8, pp. 3-7.

[21] J. Nikuradze (1933), Stromungsgesetze in rauchen Rohrcn // VD1. N 361. pp. 16-53.

3.8 KIT/INR, Germany

3.8.1 Description of TRACE

The system code TRACE (TRACE/RELAP Advanced Computational Engine) is the thermal hydraulics reference code of the US Nuclear Regulatory Commission (US NRC) and under continuous development [1]. It has been developed by the Los Alamos National Laboratory (LANL), the Information Systems Laboratory (ISL) and the Penn State University (PSU). The INR takes part in the validation of TRACE in the frame of the ongoing validation and qualification process of system codes within the CAMP agreement (Code Assessment and Maintenance Project). TRACE is a 3D, two-phase flow `Best-Estimate' code for modelling plant/system components, by solving the mass, energy and momentum conservation equations in the frame of a finite volume method. Up to now TRACE has mostly been used and validated for light-water reactor. Since TRACE includes, in addition to water sodium, lead-bismuth and different gases as working fluids, INR started investigations to qualify TRACE regarding its application to lead-cooled fast systems. This work is at an early stage but progressing [2, 3 and 4]. The LACANES benchmark will be appropriate for validating different pressured drop and heat transfer models relevant to liquid metal reactors.

3.8.2 Wall drag and pressure loss models

The following correlations are part of the TRACE source code. The complete procedure of handling the wall drag can be found in the TRACE theory manual [5], where the following correlations were taken out.

For the friction factor TRACE employs the Churchill formulation [5] [6] since it is applicable to all ranges of Re and Δ/d (Δ = wall roughness).

$$f = 8 \cdot \left[\left(\frac{8}{Re} \right)^{12} + \frac{1}{(A+B)^{1.5}} \right]^{1/12} \tag{3.24}$$

where

$$A = \left\{ 2.457 \cdot ln \left[\left(\frac{7}{Re} \right)^{0.9} + 0.27 \cdot \left(\frac{\Delta}{d} \right) \right] \right\}^{16}$$

$$B = \left(\frac{37530}{Re} \right)^{16}$$

For abrupt changes in the flow area TRACE uses the following two expressions

$$K = \left(1 - \frac{A_j}{A_{j+1}} \right)^2 \tag{3.25}$$

for an abrupt expansion and

$$K = 0.5 - 0.7 \cdot \left(\frac{A_{j+1}}{A_j} \right) + 0.2 \cdot \left(\frac{A_{j+1}}{A_j} \right)^2 \tag{3.26}$$

for an abrupt contraction.

In addition to the implemented correlations [Equations (3.24)-(3.26)], others are needed since some components and geometrical variations (e.g. elbows) are not considered within TRACE. These correlations are shown below. For the calculation of the K-factor of an orifice a correlation according to Idelchik [7] is used.

$$K = K' \cdot \left(1 - \frac{A_{j+1/2}}{A_j} \right) + \left(1 - \frac{A_{j+1/2}}{A_{j+1}} \right)^2 + \tau \cdot \sqrt{1 - \frac{A_{j+1/2}}{A_j}} \cdot \left(1 - \frac{A_{j+1/2}}{A_{j+1}} \right) + K_{fr} \tag{3.27}$$

For the definition of the areas/interfaces used in the above displayed correlations please refer to Figure 2.3. The handbook of Idelchik was also used for the calculation of K-factors for the bends of the loop.

$$K = k_{\Delta} \cdot k_{Re} \cdot K_{loc} + K_{fr} \tag{3.28}$$

where

$$K_{loc} = A_1 \cdot B_1 \cdot C_1$$

$$K_{fr} = 0.0175 \cdot \frac{R_0}{d} \cdot \delta \cdot \lambda$$

Values for k_{Δ}, k_{Re}, K_{fric}, K', A_1, B_1, C_1, τ and λ can be taken out of tables and diagrams provided by the handbook of Idel'Chik. As for the spacer grids in the core part and the heat exchanger, formulations derived by Rehme [8] will be used.

$$K = C \cdot \varepsilon \tag{3.29}$$

$$C = 3.5 + \left(\frac{73.5}{Re^{0.264}}\right) + \left(\frac{2.79 \cdot 10^{10}}{Re^{2.79}}\right)$$

$$\varepsilon = \frac{A_{grid}}{A_u}$$

Some of the calculated values of K are shown in Table 3.20.

Table 3.20: Values of K for different components depending on the mass flow rate

Component		Low-mass flow rate (3.27 kg/s)		High-mass flow rate (13.57 kg/s)	
		Ref. vel. (m/s)	K	Ref. vel. (m/s)	K
Elbow	45°	0.1632	0.2289	0.6774	0.1593
	90°	0.1632	0.3174	0.6774	0.2223
Tee	Straight	0.1632	0.4000	0.6774	0.4000
	Branch	0.1632	0.0000	0.6774	0.4000
Grid	Core	0.2216	3 x 2.1834	0.9200	3 x 1.7618
	HX	0.0292	6 x 2.0804	0.1210	6 x 1.6267
Expansion tank	Inlet	0.1632	0.9993	0.6774	0.9993
	Outlet	0.1632	0.4818	0.6774	0.4818
HX	Inlet	0.1632	0.9500	0.6774	0.9500
	Outlet	0.1632	0.9500	0.6774	0.9500
Core	to lower plenum	0.0324	0.3780	0.1342	0.3780
	from lower plenum	0.2216	0.4690	0.9196	0.4690
Orifice		0.1429	7.4015	0.5932	7.3826
Glove valve		0.2918	0.974	1.2125	0.974

Figure 3.24: TRACE nodding for an abrupt contraction (a) an abrupt expansion (b) and a thin-plate orifice (c) [5]

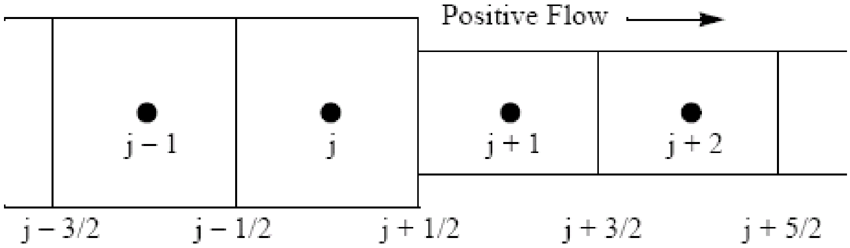

(a)

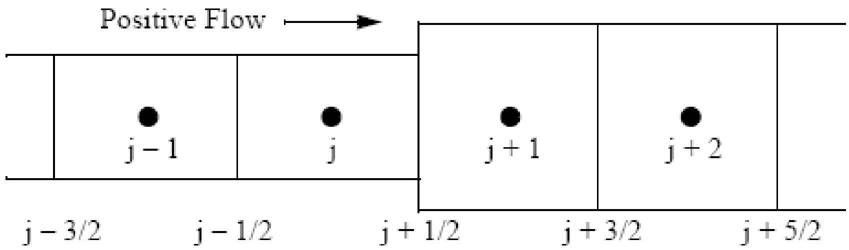

(b)

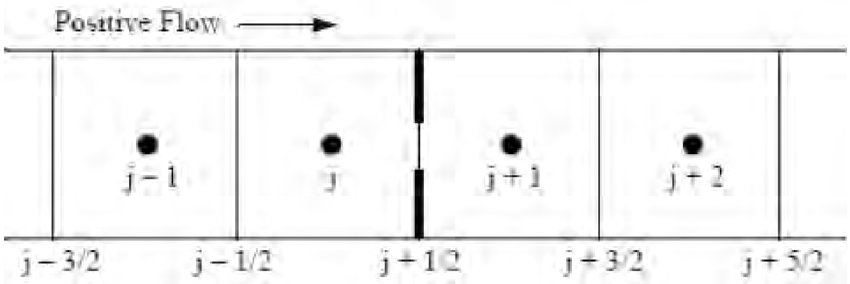

(c)

3.8.3 TRACE nodalisation and calculation of the HELIOS loop

The TRACE model of the Helios loop (see Figure 3.25) consists of several components of different nature. Four different component types were used - PIPE, BREAK, VALVE, PUMP. The whole model contains 23 components (16 x PIPE, 1 x BREAK, 5 x VALVE, 1 x PUMP) with a total number of 2 530 cells. The number of cells is relatively high since the average cell length is in the order of 10-15 mm. The reason for this fine meshing is due to the fact that the gaskets (length = 4.5 mm) were represented in the model. To avoid big jumps in the cell length of adjacent cells, since this is a common cause for numerical instabilities, the lengths of the cells were reduced to 10-15 mm.

The PIPE components were used to model the piping system of the HELIOS loop (straight pipes, tees, elbows, etc.) and also to model the lower plenum of the core, the expansion tank as well as the sump tank. The BREAK component serves as boundary condition for the pressure, simulating the ambiance conditions. The VALVE component was used to model the glove-valves of the loop. Since phase II of the LACANES benchmark deals with steady-state conditions the pump was modelled as a mass flow controlled time dependent junction with fixed mass flow rates.

As a first approach, the calculations were conducted as steady-state runs. The convergence criterion for the outer-iteration pressure calculation and the steady-state calculation were set to values of 10^{-6}. Since the code converges within 1*s*, the calculations were repeated but this time as transient scenario to obtain more time dependent values of the components. The computational effort for 20 s real time is 2 500 cpu seconds for the low-mass flow case and 11 000 cpu seconds for the high-mass low case on an Intel Core 2 Duo CPU P8400 @ 2.26 GHz, 3.9 GB RAM, operated with openSUSE 11.0.

Figure 3.25: TRACE nodalisation scheme of the HELIOS loop

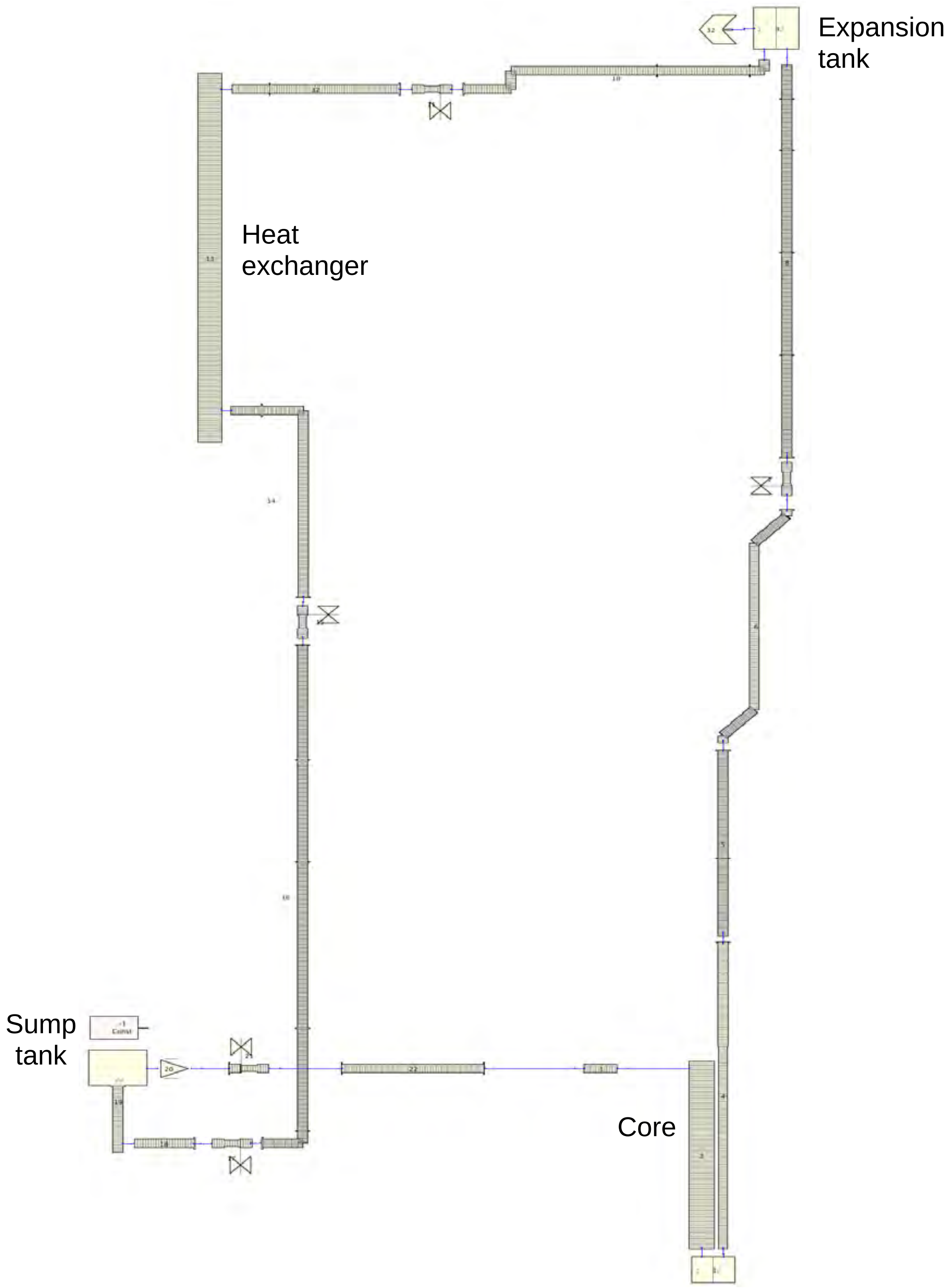

Notation

f	friction factor	d	diameter (m)
K	form loss coefficient	A_j	flow area befor area change
Re	Reynolds number	$A_{j+1/2}$	flow area inside the orifice
Δ	wall roughness (m)	A_{j+1}	flow area after area change
δ	angle (°) of the bend	A_{grid}	projected cross-section of the spacer grid
λ	hydraulic friction coefficient	A_u	undisturbed flow area

References

[1] US Nuclear Regulatory Commission (2007), TRACE V5.0 User's Manual, Washington, DC, 20555-0001.

[2] W. Jaeger, V. Sánchez (2008), "Analyses of a LBE-Diphyl THT heat exchanger with the system code TRACE", *Proc. of the 16th International Conference on Nuclear Engineering, ICONE-16,* Orlando, USA.

[3] W. Jaeger and V. Sánchez (2008), "Influence of oxide layers on the cladding material in a liquid lead environment: a comparison between MATRA and TRACE", *Proc. of the International Conference on Reactor Physics, PHYSOR-08,* Interlaken, Switzerland.

[4] W. Jaeger, V. Sánchez and B. Feng (2008), "Analysis of an XADS target with the system code TRACE", *Proc. of the International Youth Nuclear Congress, IYNC-08,* Interlaken, Switzerland.

[5] US Nuclear Regulatory Commission (2007), TRACE V5.0 Theory Manual. Filed Equations, Solution Methods and Physical Models, Washington, DC, 20555-0001.

[6] D.J. Zigrang, N.D. Sylvester (1982), "Explicit approximations to the solution of Colebrook's friction factor equation", AIChE Journal, Vol. 28, No. 3, pp. 514-515.

[7] I.E.Idelchik (1986), "Handbook on Hydraulic Resistance", 2nd Edition, Hemisphere Publishing Corporation, Washington, USA.

[8] K. Rehme (1973), "Pressure drop correlations for fuel element spacers", Nuclear Technology, Vol. 17, pp. 15-23.

Chapter 4: HELIOS experiments and results

4.1 Setup

As shown in Table 2.3, the phase I of LACANES benchmarking using HELIOS experiment includes two mass flow rates in isothermal forced convection case. In the case of isothermal forced convection experiments, the mechanical pump was operated in order to measure the pressure loss and pressure loss coefficient in the main components such as core, gate valve and orifice which shows large pressure loss and gives large impact on the total pressure loss.

The HELIOS consists of primary and secondary loops similar to the PEACER design. The primary loop is filled with LBE (44.5% of the lead and 55.5% of the bismuth) and the secondary loop is filled with single phase oil. The heat is exchanged from the heat exchanger. As shown in Figure 4.1, the primary loop consists of core, expansion tank, heat exchanger, mechanical pump, storage tank, valves, orifice, etc. Four electric heaters in lattice type are installed in the mock-up core with the maximum power of 60 kW total. The heat exchanger is installed at the top of the HELIOS. Two tubes are placed in the cylindrical shell of the heat exchanger. The LBE of the primary loop flows down in the shell and the oil of the secondary loop flows up in the tube. The average elevation of the heat exchanger is 7.4 m higher than the mock-up core. The expansion tank is also located at the top of the facility to adjust the LBE level in the loop and to control the dissolved oxygen concentration in LBE. The LBE is used to drain into the storage tank under the mock-up core after the loop test.

4.2 Instrumentation

In order to perform the forced convection test, the following three instruments were needed:

Thermocouple

Type K thermocouples sheathed with stainless steel 304 were used to measure the fluid and external wall temperature. The locations of the thermocouples (T/C#) are shown in Figure 4.2. The thermocouples were calibrated with an accuracy of ±0.5 K in the temperature range between -200 °C and 900°C.

Differential pressure transducer

Based on the preliminary analysis, it was found that that the main pressure loss in the HELIOS occurred in the core, orifice, and gate valve area. The core was expected to have the largest pressure loss due to the three spacers in the core which is only about 37% of inlet pipe flow area (49.5 mm of inner diameter). The gate valve and the orifice were also expected to have large pressure drop due to the sudden expansions and contractions. Figure 4.3 shows location of differential pressure transducers. The specification of the differential pressure transducer is given in Table 4.1.

Flow meter

The orifice flow meter was used to measure the LBE flow rate. The mass flow rate was calibrated by using differential pressure transducer at the orifice region (DP 9-10 of Figure 4.3).

Figure 4.1: Three-dimensional diagram of the HELIOS forced convection test setup

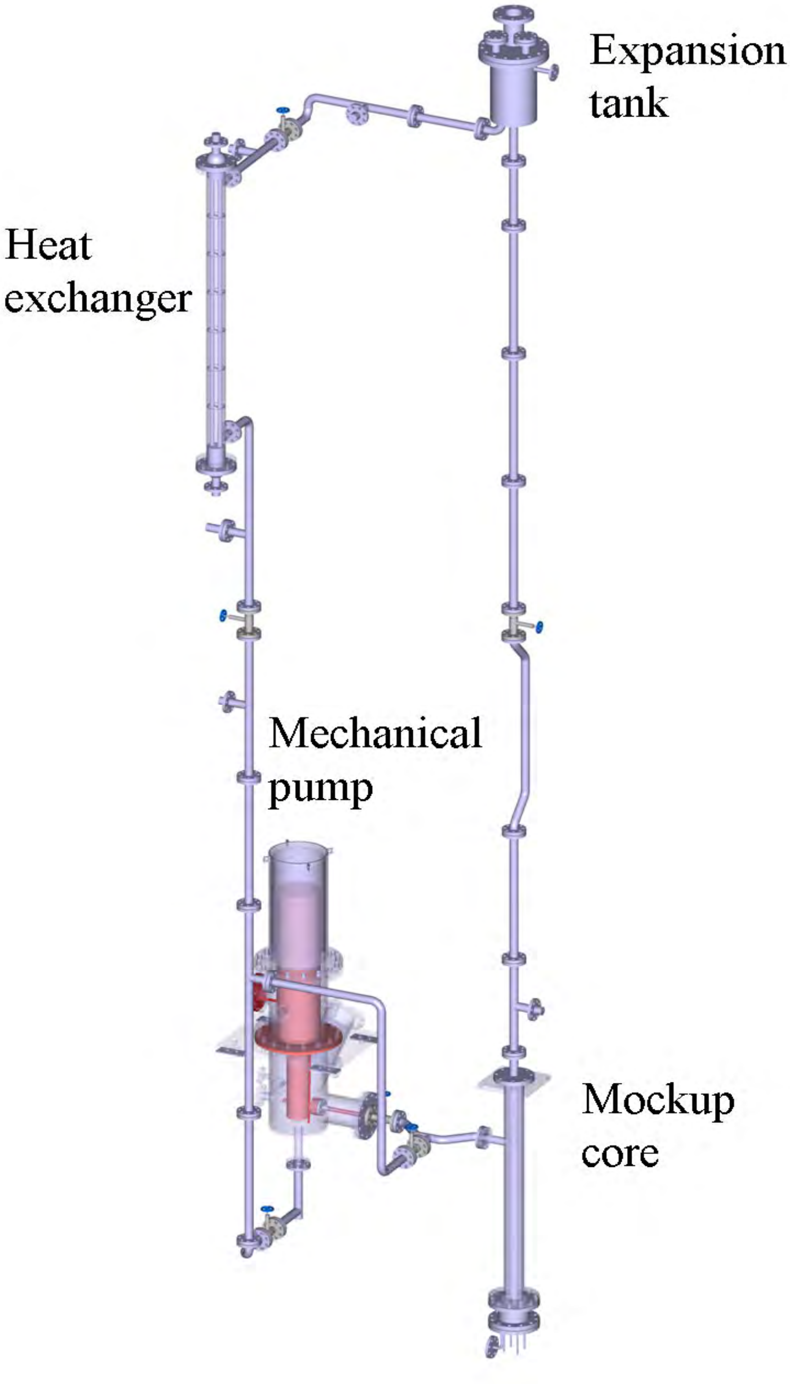

Figure 4.2: Location of Type K thermocouples (T/C) in the HELIOS

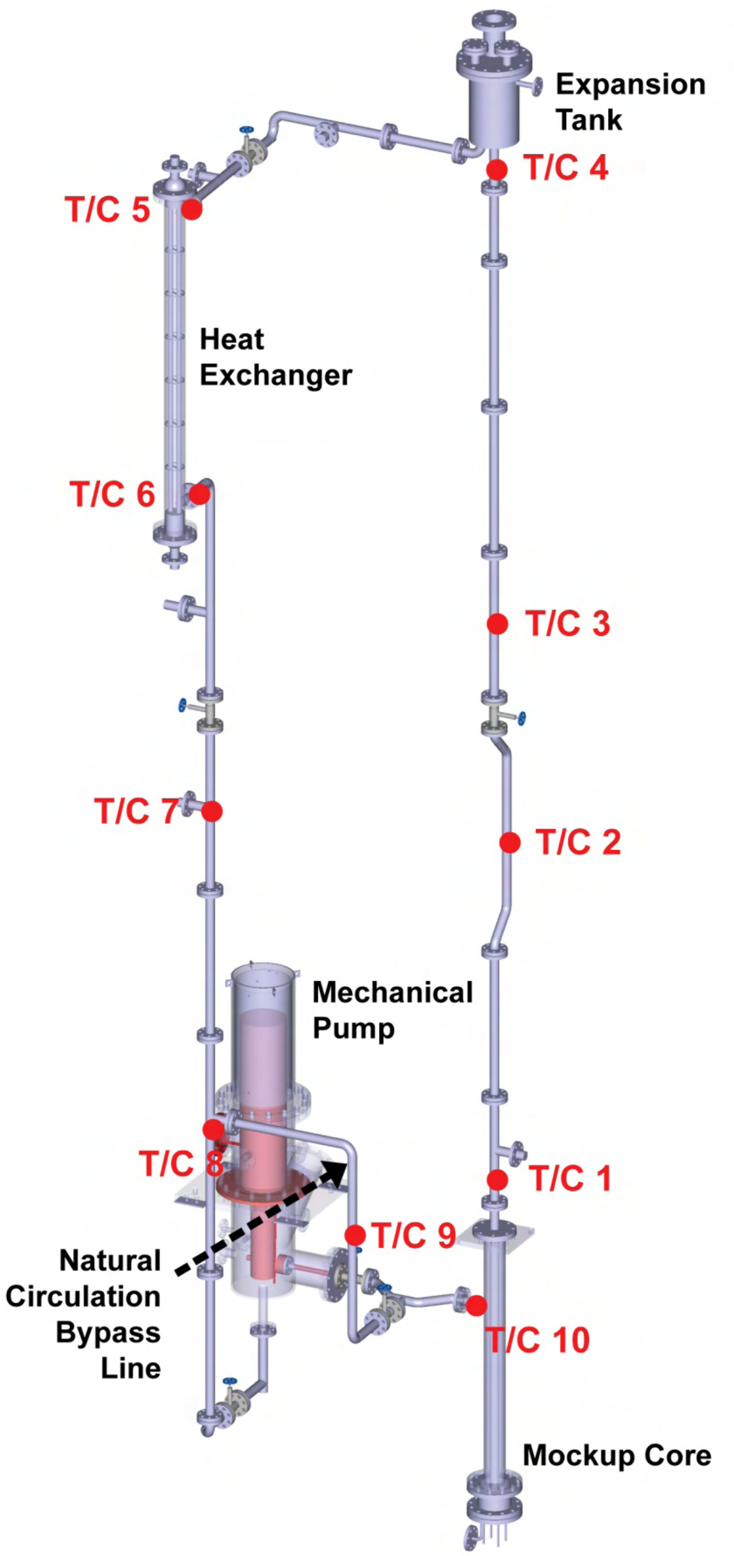

Figure 4.3: Location of five differential pressure transducers (DP) in the HELIOS

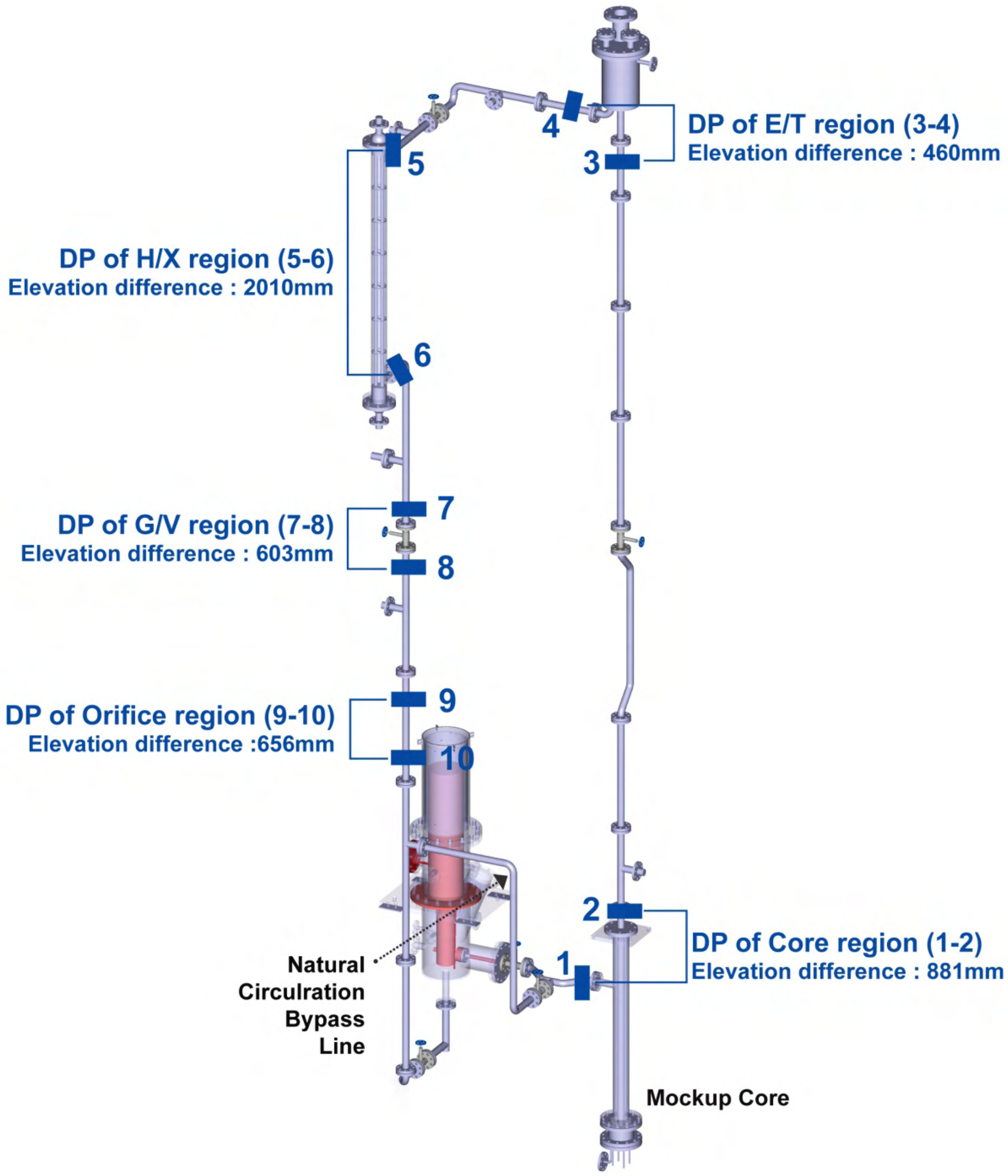

Table 4.1: Specification of differential pressure transducer, Rosemount model 3051 CD3A

Model	Rosemount model 3051 CD3A
Diaphragm	Type 316L stainless steel
Pressure transport fluid	DC 704 oil
Measurement span	1.5 bar (core region, orifice region, gate valve region, and expansion tank region) 2.5 bar (heat exchanger region)
Accuracy (% full scale)	±0.065%
Maximum estimated error	±97.5 Pa(core region, orifice region, gate valve region, and expansion tank region), ±162.5 Pa (heat exchanger region)
Temperature range	-10^{o}C to 320^{o}C

4.3 Procedure

Prior to pumping the LBE into the loop, the loop was filled with argon gas and pre-heated up to 250°C, higher than the melting point of the LBE (125°C). When pre-heating was completed, the loop was filled with LBE by pressuring the LBE storage tank with argon gas. In order to maintain the steady-state with no mass flow, all the gates valves remain closed while LBE is filled in the loop.

The isothermal boundary condition could be obtained by maintaining constant temperature at the loop pipe wall surface (250°C) which is constantly heated by the line and jacket heaters with temperature controllers at ten different sections. When isothermal boundary condition was reached, all the pressure transducers were reset to zero to eliminate hydrostatic pressure effect. Then, the gate valves were opened and regulated for the forced convection. Finally, the required flow rate was achieved by the pumping power and pressure loss data could be collected as a function of mass flow rate.

The experiment procedure of the isothermal forced convection test is summarised as follows:

1. pre-heat the loop to 250°C;
2. fill the loop with argon gas with 4% hydrogen;
3. monitor gas leakage during 24 hrs;
4. produce the vacuum to 10^{-3} torr;
5. melt LBE in the storage tank (350°C);
6. fill the loop with argon gas;
7. configure of the loop valves;
8. release the main drain valve;
9. pressurise the LBE storage tank with argon gas to fill the loop with the LBE;
10. adjust LBE level in the pump sump tank and expansion tank by argon gas pressure in the LBE storage tank;
11. close the main drain valve and vent the argon gas in the LBE storage tank,
12. configure the valves for test;
13. maintain constant LBE temperature (250 °C) by heating the loop pipe;
14. reset all DP meters to zero under no flow condition;
15. pump LBE and record differential pressure, temperature, and flow rate as a function of time;
16. stop pumping;
17. re-configure valves under no flow;
18. release the main drain valve to drain LBE;
19. turn off the heaters.

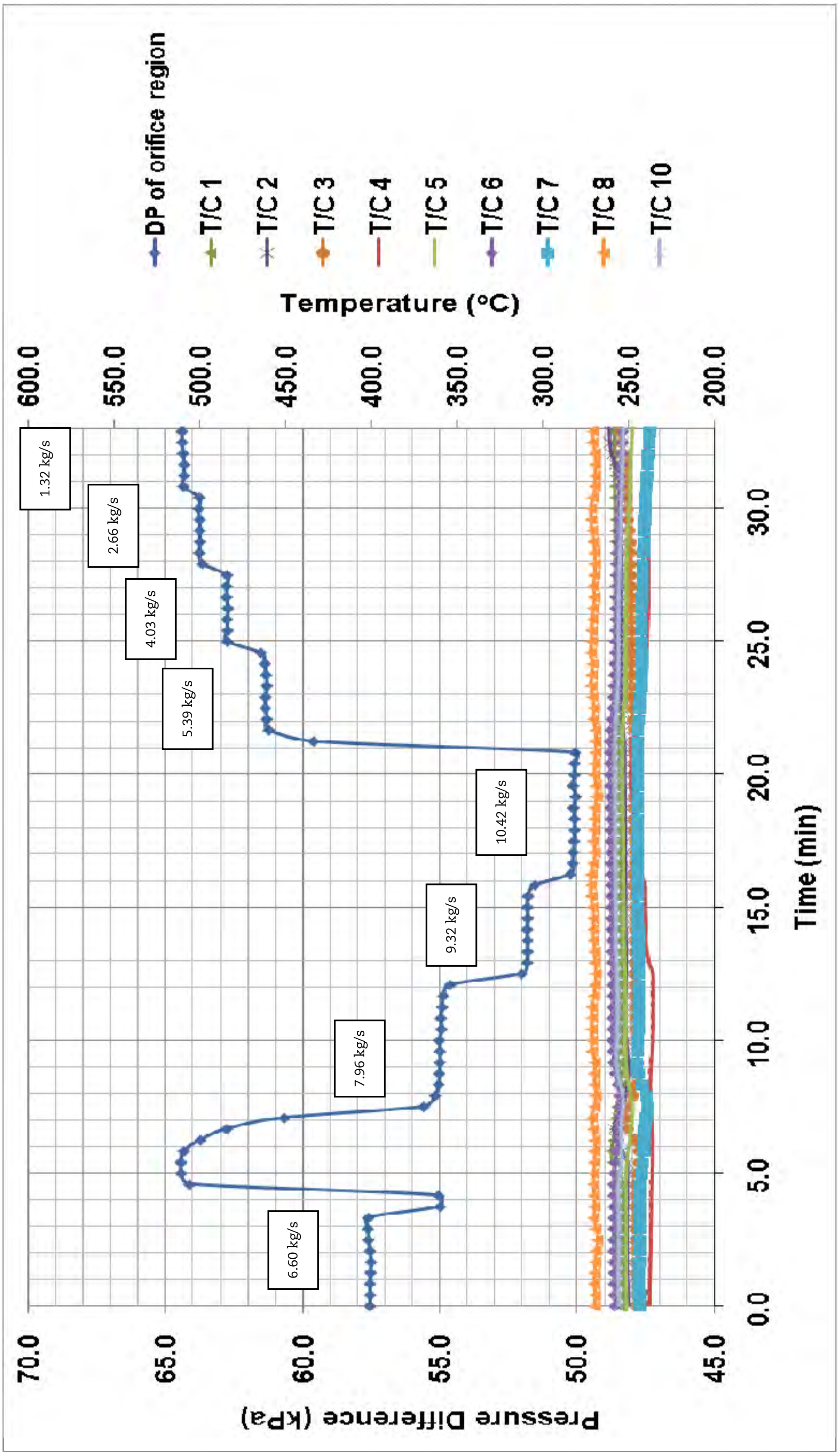

Figure 4.4: Pressure difference at orifice region and temperature at all positions at a different pump speed

4.4 Results

Figure 4.4 shows the measured raw data of the isothermal forced convection test. As the pump speed increases, pressure difference between both sides of orifice also increases. The temperature of most of positions remains constant (250°C) during the test.

Figures 4.5, 4.6 and 4.7 show pressure losses of the core, gate valve and orifice region, respectively. Measurement error of the gate valve pressure difference was in the range of 100 to 200 Pa but those of the core and the orifice region were negligible. Table 4.2 shows derived correlation of pressure loss as a function of mass flow rate and Table 4.3 shows measured values of pressure loss at different mass flow rates.

Figure 4.5: Pressure loss at core region

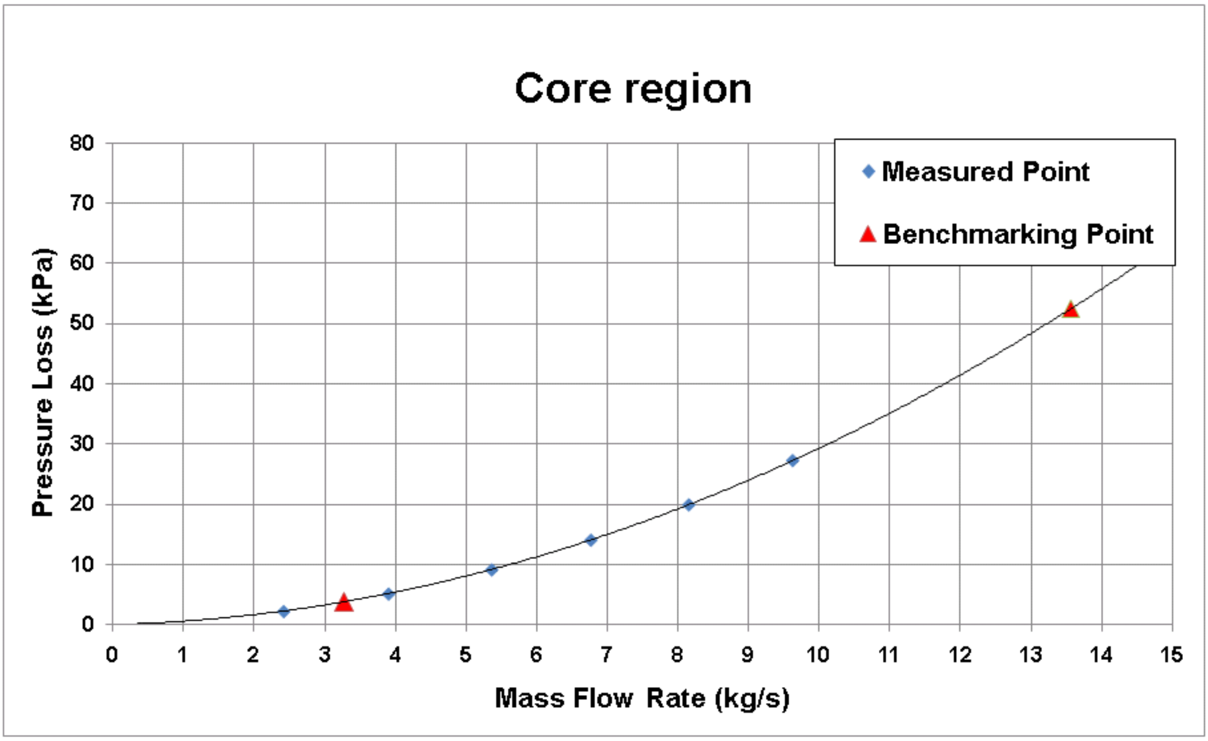

Figure 4.6: Pressure loss at gate valve

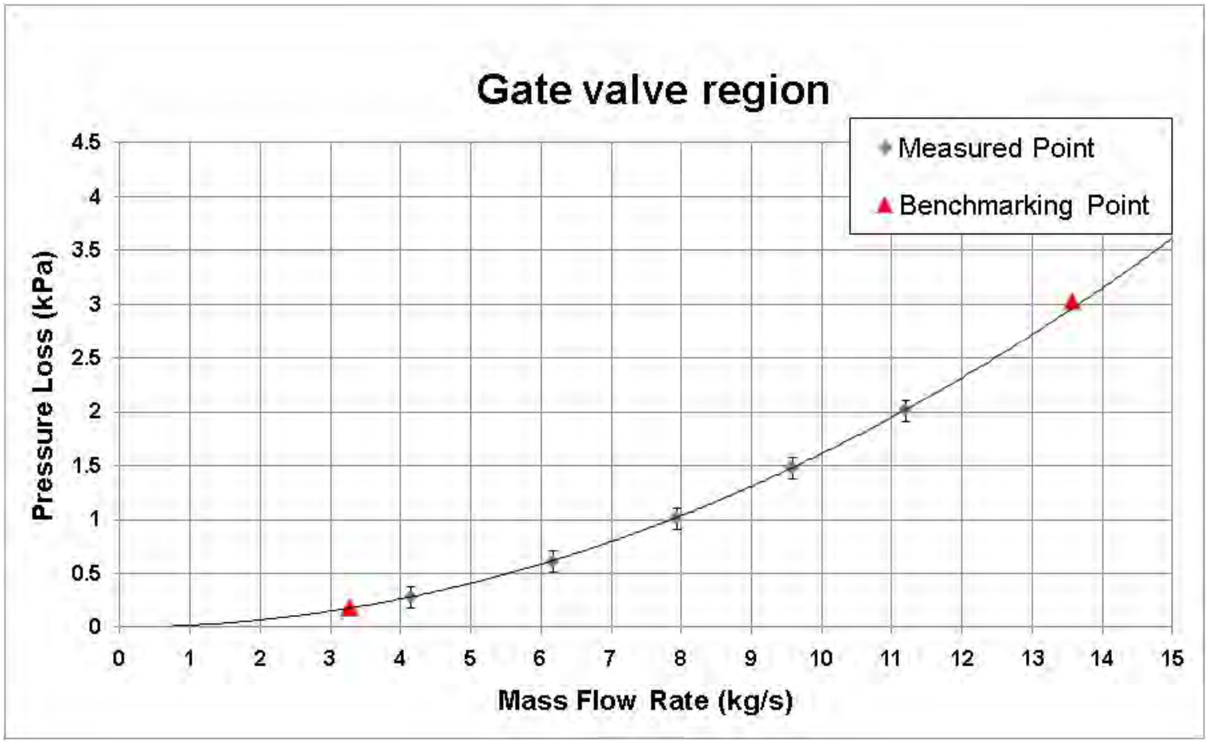

Figure 4.7: Pressure loss at orifice region

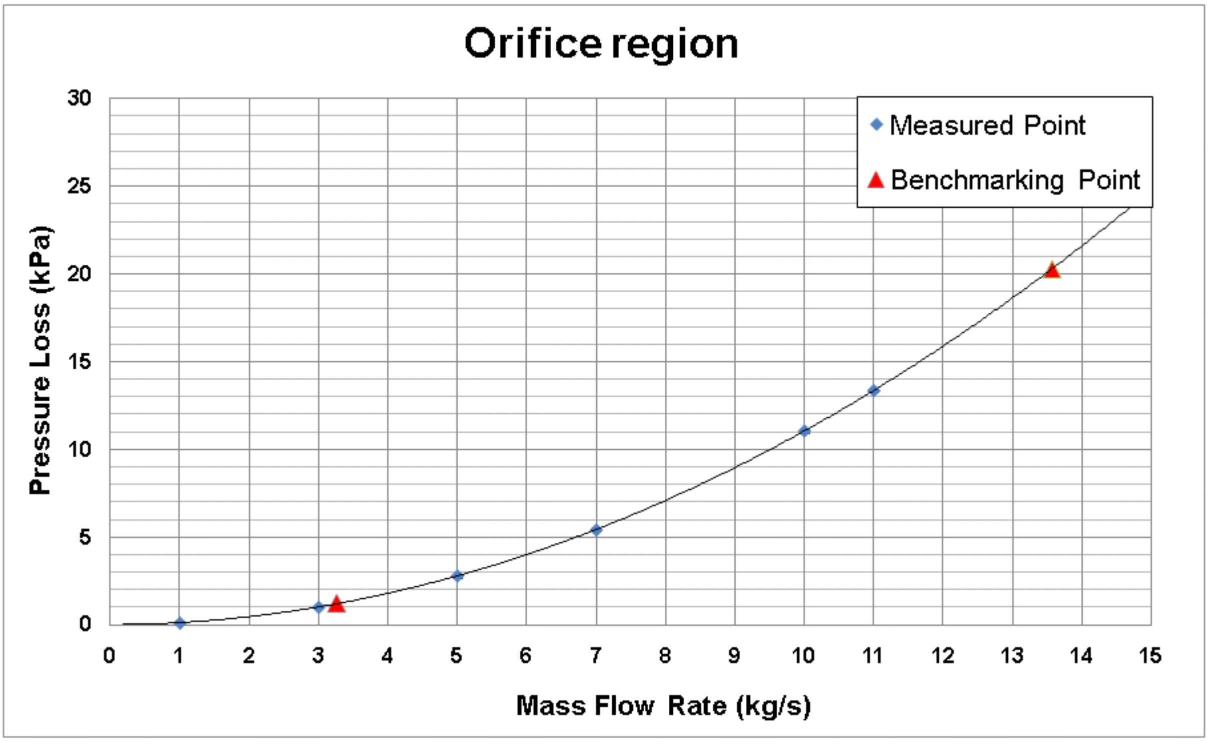

Table 4.2: Correlations with function of mass flow rate (Q) and pressure loss (DP)

Region	Pressure loss x: Q [kg/s], y: DP [Pa]	R^2
Core region	$y=263.32\ x^2+295.23\ x$	0.9994
Gate valve region	$y=16.25\ x^2+2.41\ x$	1.0000
Orifice region	$y=109.47\ x^2+7.47\ x$	0.9999

Table 4.3: Pressure losses at different mass flow rates

Mass flow rate (kg/s)		Measured pressure loss (kPa)		
		Core region	Gate valve region	Orifice region
Low	3.27	3.781	0.182	1.194
High	13.57	52.491	3.025	20.247

Chapter 5: Comparison and discussion

5.1 Benchmark plan

Figure 5.1 shows a schematic diagram of the entire benchmark plan. Based on the specification [1], participants performed preliminary analysis using well-known correlations and performed the blind computer simulation by thermal hydraulics (TH) system codes and three-dimensional computational fluid dynamics (3D CFD) codes. The CFD result was used as the reference where experimental data is not available. Then the results are compared components by components. Finally, the optimised correlations and recommendations on the pressure loss prediction method will be suggested as the "best practice guide".

Figure 5.1: Overall procedures of LACANES benchmark

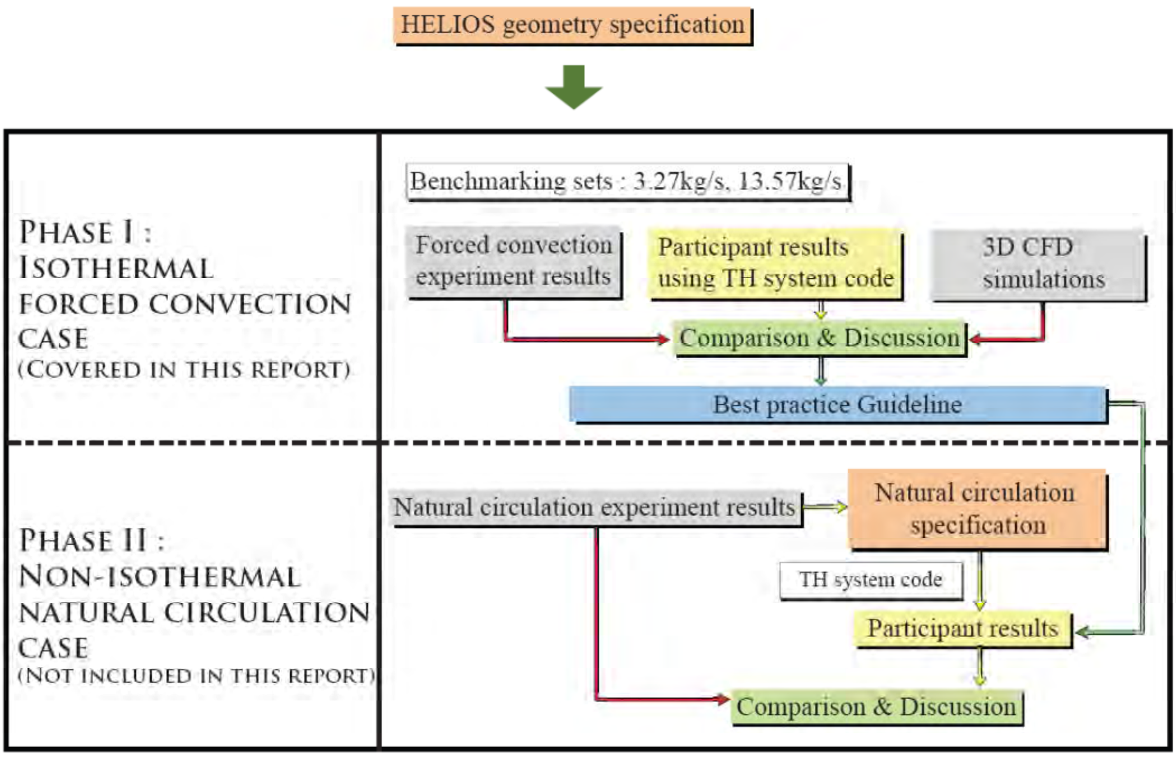

Table 5.1 describes the characteristics and available result of the 11 components which comprise the HELIOS forced convection flow path.

5.2 Result of system code simulation

Figure 5.2 shows comparison of total and partial pressure loss at high mass flow rate (13.57 kg/s). All data are obtained by the system code simulation except the "Measured+CFX®". The "Measured+CFX®" presents pressure loss data by experiment for core, orifice, gate valve, expansion tank, and heat exchanger and by CFX®, the CFD code, simulation for pipe, 45° elbow, 90° elbow, gasket, tee-straight and tee-branch. The ENEA and KIT/IKET calibrated case used core, orifice, and gate valve result of “Measured+CFX®” in order to adjust blind test results.

The total pressure of “Measured+CFX®” is 117 kPa and 85% of total pressure is contributed by the core, orifice, gate valve, expansion tank, and heat exchanger, the data are obtained by the experiment. The total pressure loss shows wide variation from 98 kPa to 153 kPa between the participants. Though the values between the participants showed large discrepancies, the main contribution to the pressure loss was found in the core, orifice, gate valve, gasket, and tee junctions.

Figure 5.3 shows comparison of the accumulated pressure loss versus the length of the loop. The largest pressure drop was found at core and followed by orifice, expansion tank (E/T), heat exchanger (H/X). The sum of pressure losses at five gate valves is also large though that of each gate valve is relatively small.

Table 5.1: Description on 11 main components and available data

Components	Number of components in HELIOS	Function	Flow characteristics	Available data		
				Correlation of codes and handbooks	CFD	Experiment
Core	1 ea	Heat source	Small flow area in rods bundle Barriers over the cross-section Discharge into a vessel Entrance in pipe	Y	Y	Y
Orifice	1 ea	Measuring flow rate	Sudden area changes	Y	Y	Y
Gate valve	5 ea	Regulation flow path	Sudden area changes	Y	Y	Y
Expansion tank	1 ea	Level buffer	Discharge into a vessel Entrance in pipe	Y	Y	Y
Heat exchanger	1 ea	Heat removal	Large flow area Barriers over the cross-section Discharge into a vessel Entrance in pipe	Y	Y	Y
45º elbow	9 ea		Changes of the stream direction	Y	Y	N
90º elbow	4 ea		Changes of the stream direction	Y	Y	N
Straight pipe	Many (14.9m)		Friction loss Effect on roughness	Y	Y	N
Tee-straight[4]	8 ea		Tee-branch with straight flow	Y	Y	N
Tee-branch	1 ea		Tee-branch with elbow flow	Y	Y	N
Gasket	17 ea		Recess	Y	Y	N

[4] In the Tee component, straight means that inlet flow and outlet flow are in the same direction and branch means that inlet flow and outlet flow are in the vertical.

Figure 5.2: Comparison of the total and partial pressure loss at high-mass flow rate case (13.57kg/s)

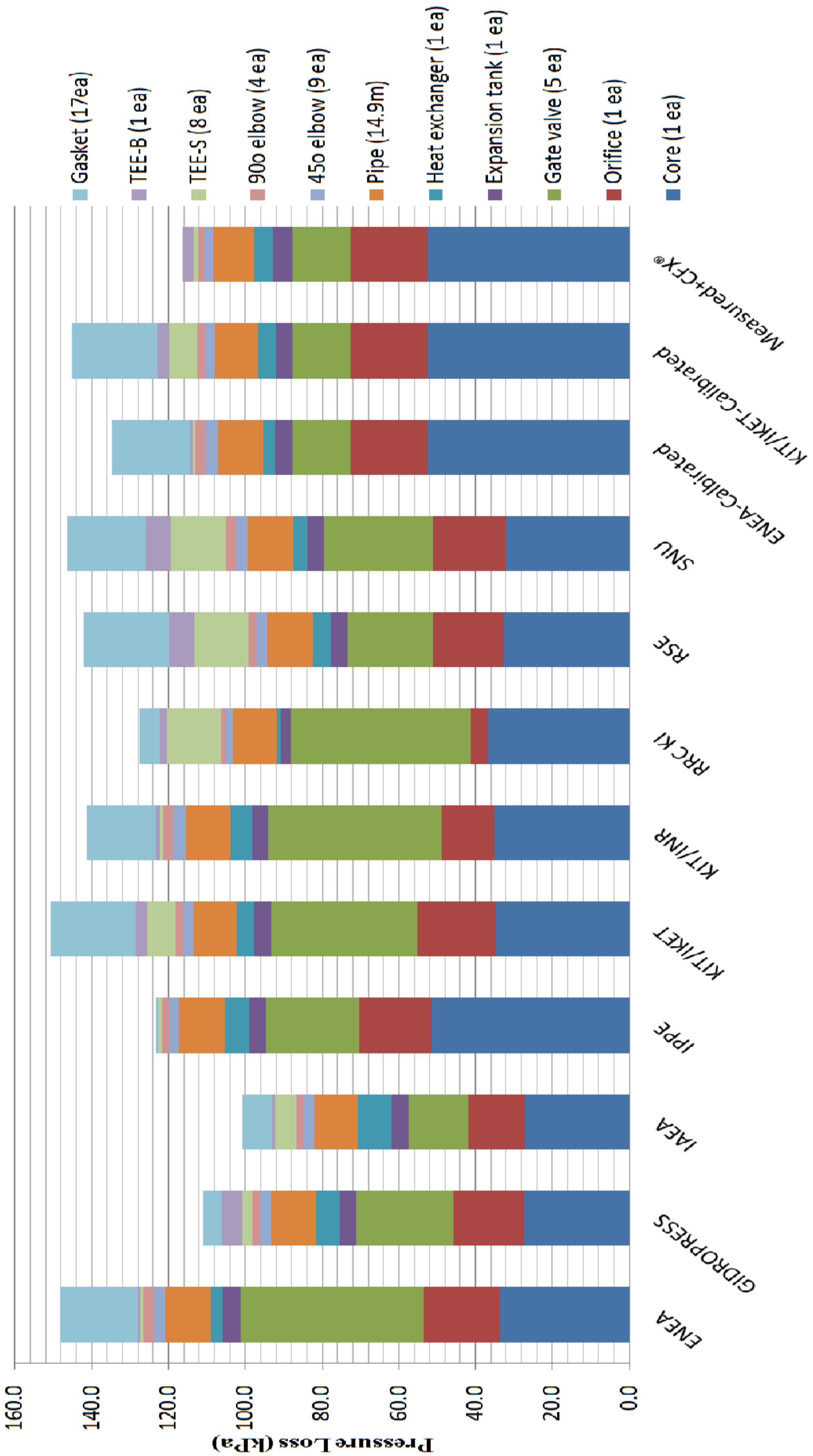

Figure 5.3: Comparison of the accumulated pressure loss at high-flow rate case (G/V: Gate Valve, E/T: Expansion Tank, H/X: Heat Exchanger)

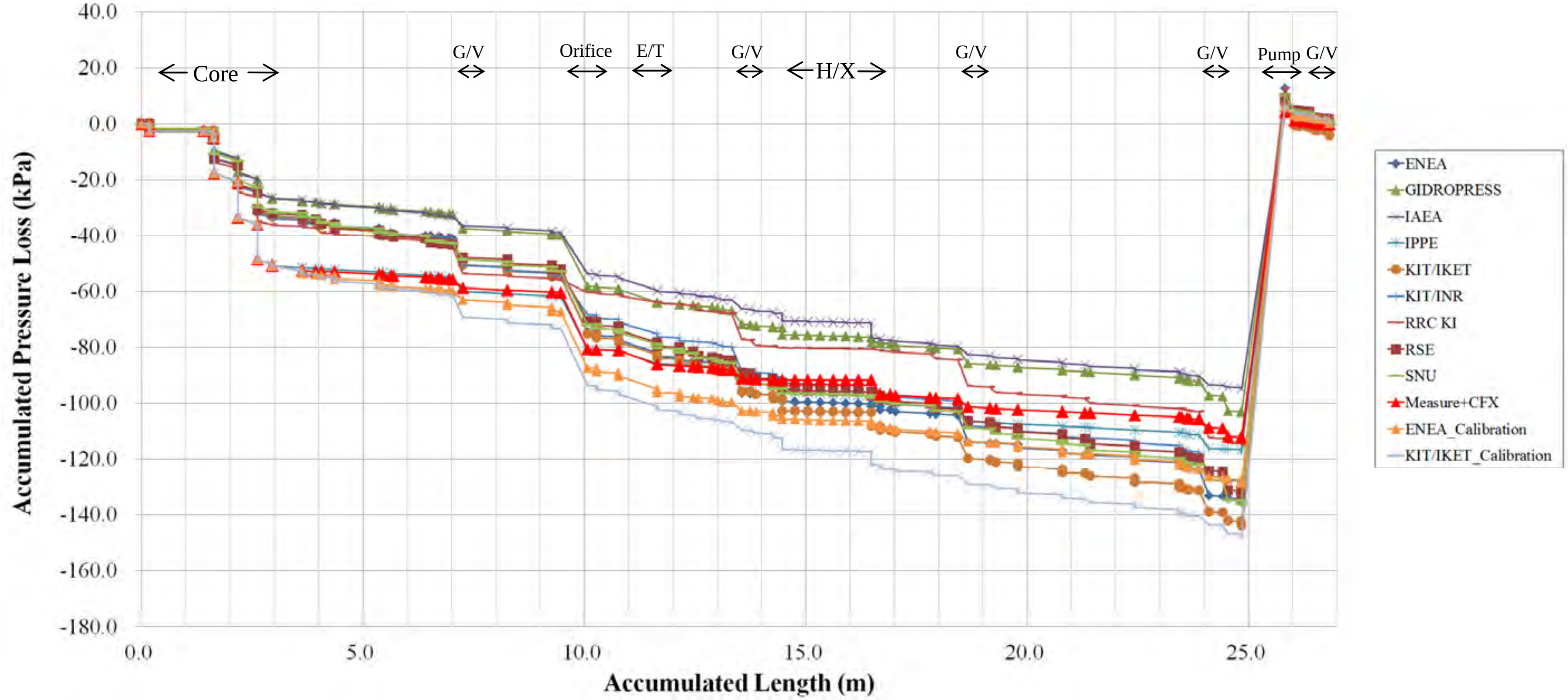

5.3 Result of CFD simulation

The pressure drop of core, orifice, gate valve, expansion tank and heat exchanger were calculated by the CFD codes: CFX® and Star-CD®. Figure 5.4 shows comparison between CFD and experiment result. All CFD results are in good agreement with experiment result within ±15% of discrepancy.

Figure 5.4: Comparison between CFD and experiment result

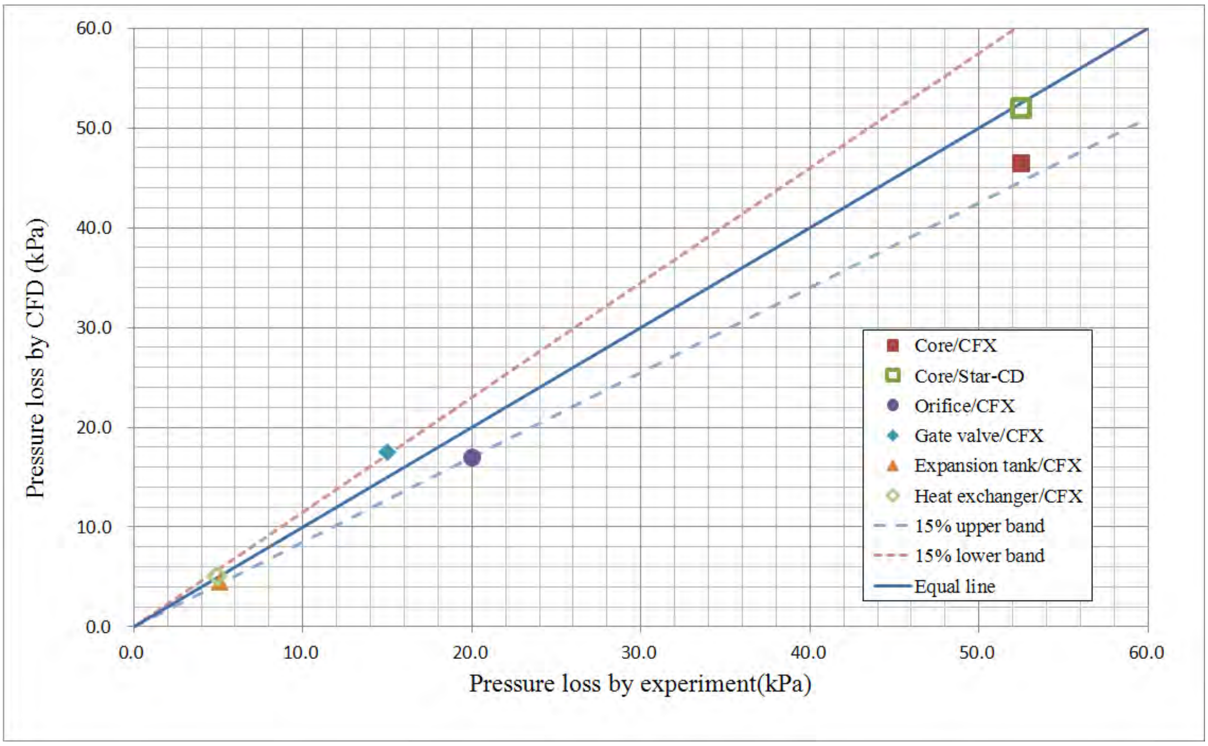

5.3.1 Core

The core was designed based on the core of PEACER-300. Figure 5.5 shows the schematic diagram of core area and LBE flow path. Similar to the conventional nuclear reactor, the LBE coolant flows downward from the inlet (down-comer) and flows upward from the bottom, then the LBE coolant passes through the circular flow channel core where circular heat rod bundle and spacers are installed. The core has the most complicate geometry in the HELIOS facility.

The core is cylindrical in shape and inner diameter of core is 127 mm. The inlet and outlet pipe inner diameter is 49.5 mm. Four heat rods are installed in the square lattice with three spacers. The lower plenum of the core was designed to provide the drain port and space to maintain instruments. The heat rods are fixed at 12.7 mm fittings. The fittings are bent at lower plenum area in order to provide space.

Figure 5.5: Schematic diagram of HELIOS core and flow path

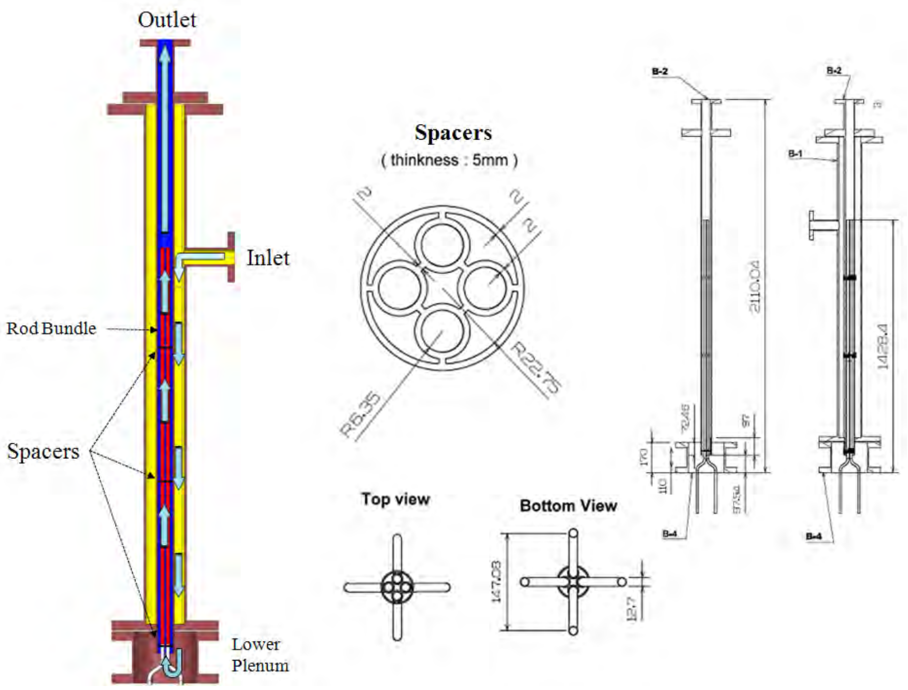

Two CFD simulations were performed: KIT/IKET by Star-CD®; and SNU by CFX®. Both participants used k-ε turbulence model. Figure 5.6 shows the pressure distribution at the centre plane. Both results show large pressure losses in three spacer areas which govern pressure loss in the core.

Table 5.2 shows the details of pressure loss distribution in the core, analysed by CFX® code simulation. The largest pressure loss was found at the bottom spacer (between point 1 and 2) because the entrance of the core in bottom spacer induces additional pressure drop. The pressure loss at the other spacers was about 11kPa. The pressure loss of the three spacers is about 70% of entire pressure loss of the core. Combined effect refers to both friction loss (inlet pipe, down-comer) and form loss (from inlet to down-comer, from down-comer to lower plenum).

Comparing both codes, the pressure loss by Star-CD® is 52 kPa and that of CFX® is 46 kPa. The experiment showed 52.5 kPa in the core.

Figure 5.6: Pressure distribution at the centre plane of the core
(a) results of Star-CD® (b) results of CFX®

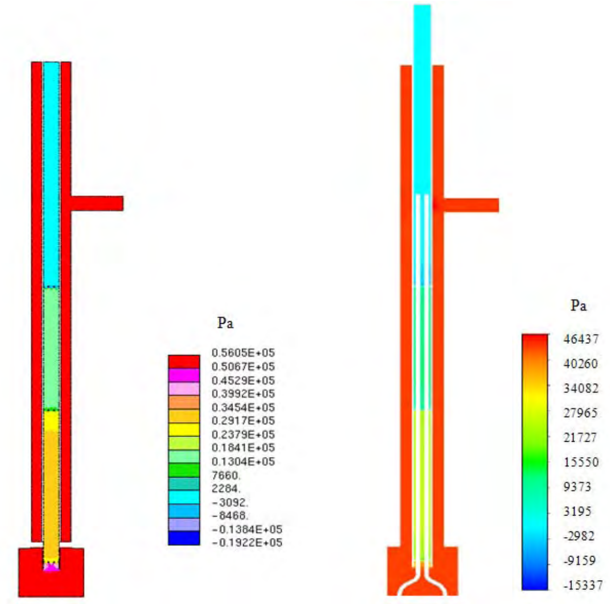

(a) (b)

Table 5.7: Pressure loss distribution in the core (from CFX® simulation)

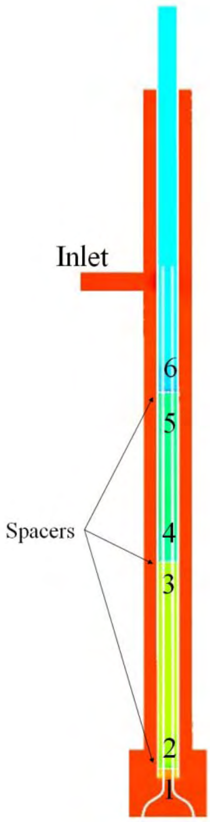

Point	Pressure (kPa)	Pressure loss effect	ΔP (kPa)
6	0		
		Spacer	10.8
5	10.8		
		Rod bundle	1.5
4	12.3		
		Spacer	11.2
3	23.5		
		Rod bundle	1.9
2	25.4		
		Sudden contraction and spacer	18.0
1	43.4		
		Combined effect*	3.0
Inlet	46.4		

5.3.2 Gate valve

Five gate valves were installed in the loop. All gate valves have sudden contraction and expansion in the valve seat area. Figure 5.8 shows two-dimensional schematic diagram of gate valve. Gate valves are designed to be fully opened in the normal operation condition. Sudden contraction and expansion is due to difference between A and B in Figure 5.8 (37 mm and 52 mm).

Figure 5.8: Schematic diagram of gate valve

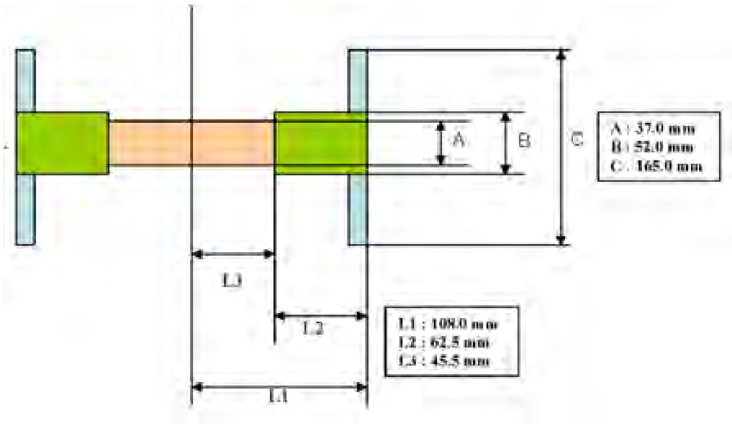

The CFX® code was used for the gate valve simulation. The initial condition was 13.57 kg/s flow rate (high-flow) at 250°C LBE and remained constant thus, the isothermal steady-state. The governing equation is the steady-state Reynolds-averaged Navier-Stokes equations (RANS) and the buoyancy effect is negligible. For the turbulence, k-ε model was used. In order to simulate under the fully developed flow condition, the virtual pipe (1 *m* and 0.8 *m*) was used before and after the valve (see Figure 5.10). Boundary conditions included the uniform flow rate of 13.57 kg/s at the inlet and the area averaged pressure of 0 Pa at the outlet. The smooth wall option was used with the given surface roughness and the no slip condition.

For the discretisation, finite element method with tetrahedral mesh was used. For the near wall meshes, the prismatic wedge mesh was used in order to obtain precise result, which may reproduce the transition of properties near the wall. The total number of elements was 1 697 767 including 1 378 590 tetrahedral meshes, 318 012 wedge meshes, and 1 165 pyramid meshes. Figure 5.9 shows the mesh structure with colour contour representing pressure distribution in the gate valve region.

Figure 5.10 shows the pressure change due to the gate valve. After a slight increase due to the wake, the pressure sharply decreases through the contraction area and then gradually increases after the expansion area. The calculated pressure loss at each gate valve by CFX® was ~3.5 kPa which is in good agreement with experiment data: 3 kPa.

Figure 5.9: Pressure distributions at gate valve

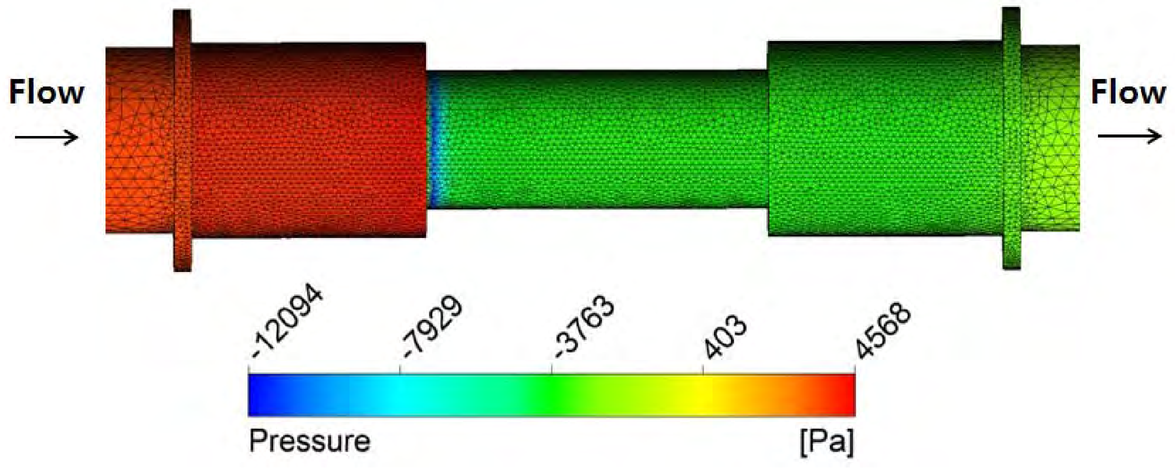

Figure 5.10: Pressure change due to the gate valve

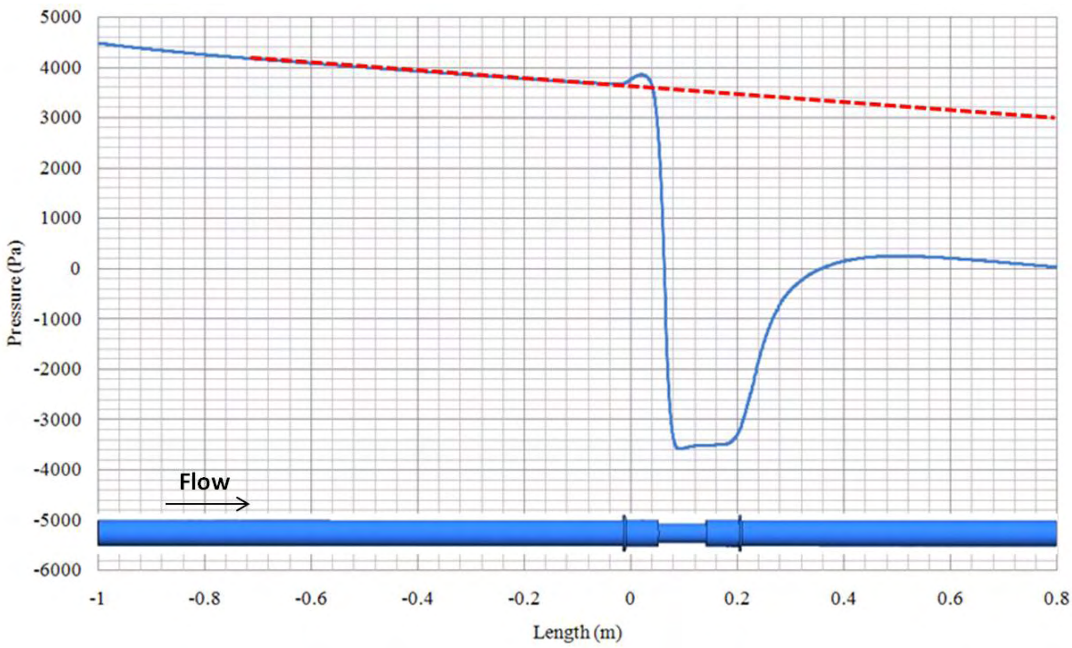

5.3.3 Orifice

The orifice is installed in the experimental facility in order to measure the flow rate and it causes the pressure drop. As shown in Figure 5.11, the orifice is a thin disc with 32.46 *mm* diameter hole. At the entrance to orifice, the sudden contraction (52.9 mm to 32.46 mm) occurrs, and then the orifice surface expands by 45 degree of inner disc surface. The pressure will decrease due to the sudden contraction and will gradually increase after the "vena-contracta point".

Figure 5.11: Schematic diagram of orifice

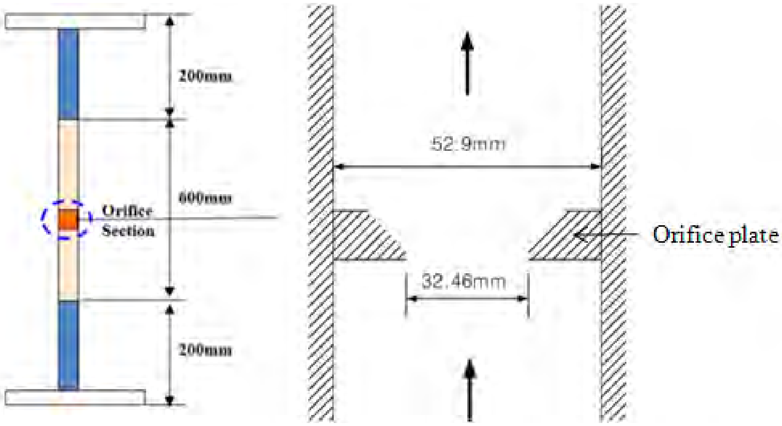

In order to obtain precise results, the actual geometrical data was used without any simplification. Similar to the gate valve 1 *m* of virtual pipe was installed before and after the orifice for the fully developed flow through the orifice. All other conditions were identical to the gate valve simulation case in Section 5.3.2: k-ε turbulence model; boundary conditions of the uniform flow rate (13.57 kg/s) inlet and 0 Pa at the outlet; smooth wall option with the given surface roughness; no slip condition; finite element method with tetrahedral mesh; and the prismatic wedge mesh for near wall meshes. The total number of elements was 1 567 036 including 1 247 859 tetrahedral meshes and 318 012 wedges meshes. Figure 5.12 shows the mesh structure with colour contour representing pressure distribution in the orifice region.

Figure 5.13 shows the pressure change due to the orifice. The pressure steeply decreases immediately through the orifice disc and then gradually increases after the expansion. The calculated pressure drop by CFX® was ~17 kPa which is similar to the experiment data: 20 kPa.

Figure 5.12: Pressure distribution at orifice

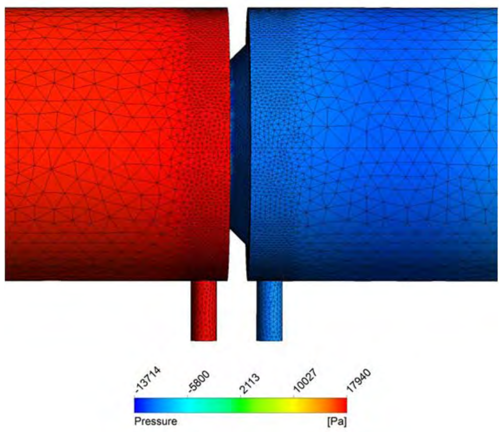

Figure 5.13: Pressure change due to the orifice

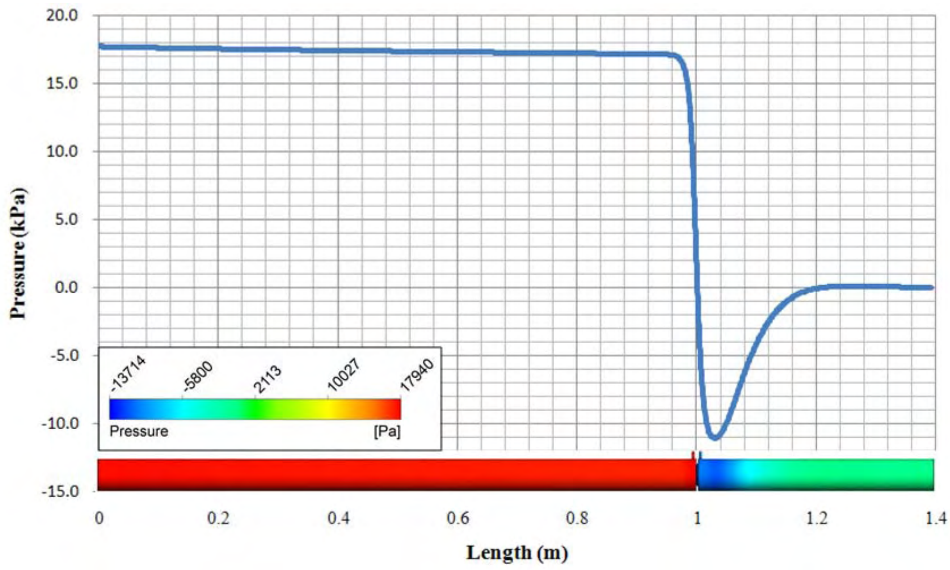

5.4 Comparison and discussion

5.4.1 *Core*

In the core, pressure could be dropped by the surface friction and by the form change. The pressure loss by the surface friction will occur in the inlet area, down-comer pipe, lower plenum, core and upper plenum. The pressure losses by the form change will occur at inlet to down-comer, down-comer to lower plenum, lower plenum to core, three spacers and core to upper plenum.

Figure 5.14: Pressure loss in the c ore at the high-mass flow rate case

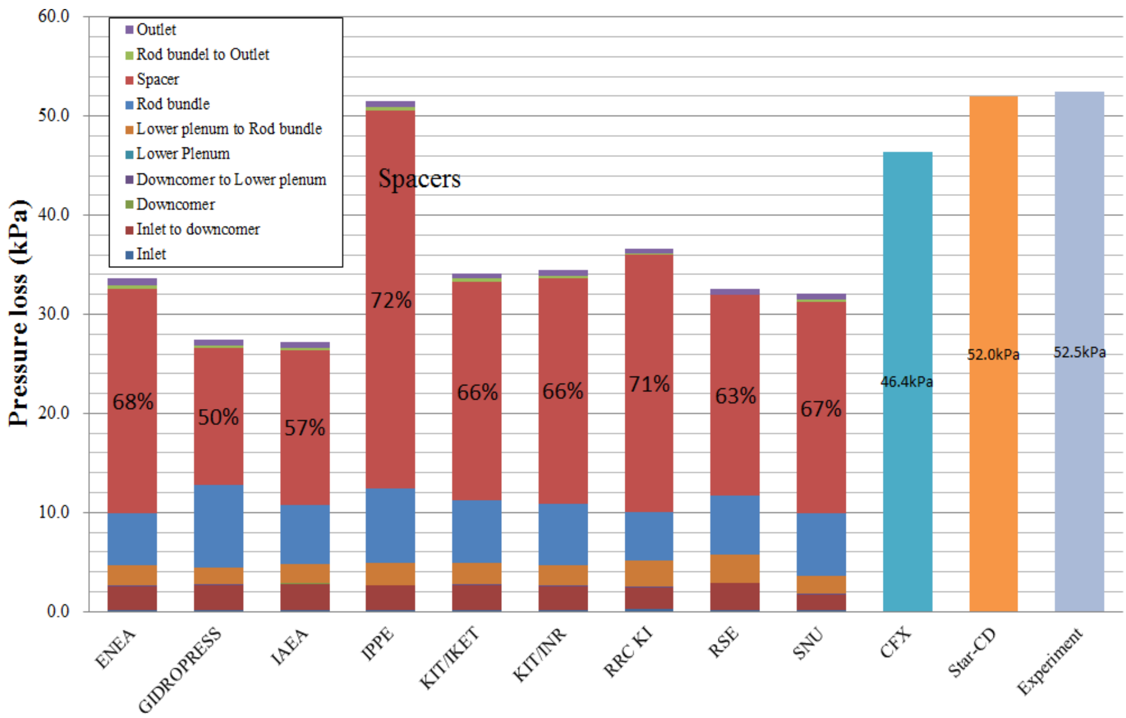

Figure 5.14 shows the comparison of the pressure loss in the core at the high-mass flow rate case. The CFD simulation results, CFX® and Star-CD®, showed 12% of difference. The result of Star-CD® is identical (1% of difference) to the measured data from the experiment.

The result of all participants showed that the pressure loss at the spacers is more than 50% of the total pressure loss. However, the pressure loss of the spacer varied 50-70% of total pressure loss between the participants. The main difference between the participants was the correlation for the spacer. All participants, except IPPE, used the Rehme correlations for the pressure loss calculation at the spacer. The IPPE employed empirical equation using the orifice geometry because fundamental flow behaviours of the spacer and the orifice are very similar. Both have sudden expansion and contraction. Equation and geometry for orifice used by IPPE are shown in Equation 1 and in Figure 5.15 [2]. In the Rehme correlation, the pressure loss coefficient is predicted by modified drag coefficient (C_v), average bundle fluid velocity (V_v) and area ratio. Modified drag coefficient is a function of the average bundle and the unrestricted area *Reynolds* number. Compared to experiment data and CFD simulation, the results using Rehme correlation showed maximum 40% of discrepancy. The main reason was that the Rehme correlation was developed for the large number of rod bundles while the HELIOS core had only four rods.

$$K = [0.5(1-\frac{F_1}{F_2})^{0.75} + \tau(1-\frac{F_0}{F_1})^{1.375} + (1-\frac{F_0}{F_1})^2 + \lambda\frac{l}{D_h}](\frac{F_1}{F_0})^2$$

$$\textit{Where } \tau = (2.4-l)\times 10^{-\varphi(l)}$$

$$\varphi(l) = 0.25 + \frac{0.535\times l^{-8}}{0.05 + l^{-8}} \qquad (5.1)$$

where K is form loss coefficient, F is flow area, W is flow rate, D_h is hydraulic resistance and l is thickness of orifice plate.

Figure 5.15: Schematic diagram of core spacer based on orifice shape

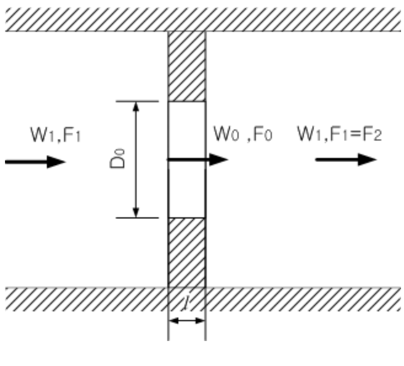

Concerning the two prediction methods based on handbook correlations, the orifice empirical correlation has a better agreement than Rehme correlation. However, the orifice empirical correlation cannot be recommended directly to calculate the pressure loss of spacers in other fluid system since this correlation was constructed for orifice, not for spacers. Thus, new correlations of C_v were recommended as shown in Equation 2, which were obtained by experimental measured data of HELIOS.

$$C_v = -7.65\log_{10}\mathrm{Re} + 49.0 \qquad (5.2)$$

All used C_v and new one which was modified by experimental data of HELIOS are shown in Figure 5.16.

Figure 5.16: Drag coefficient (C_v) of Rehme correlation for predicted pressure loss of grid spacer; modified new one based on measured data and four set used in benchmarking

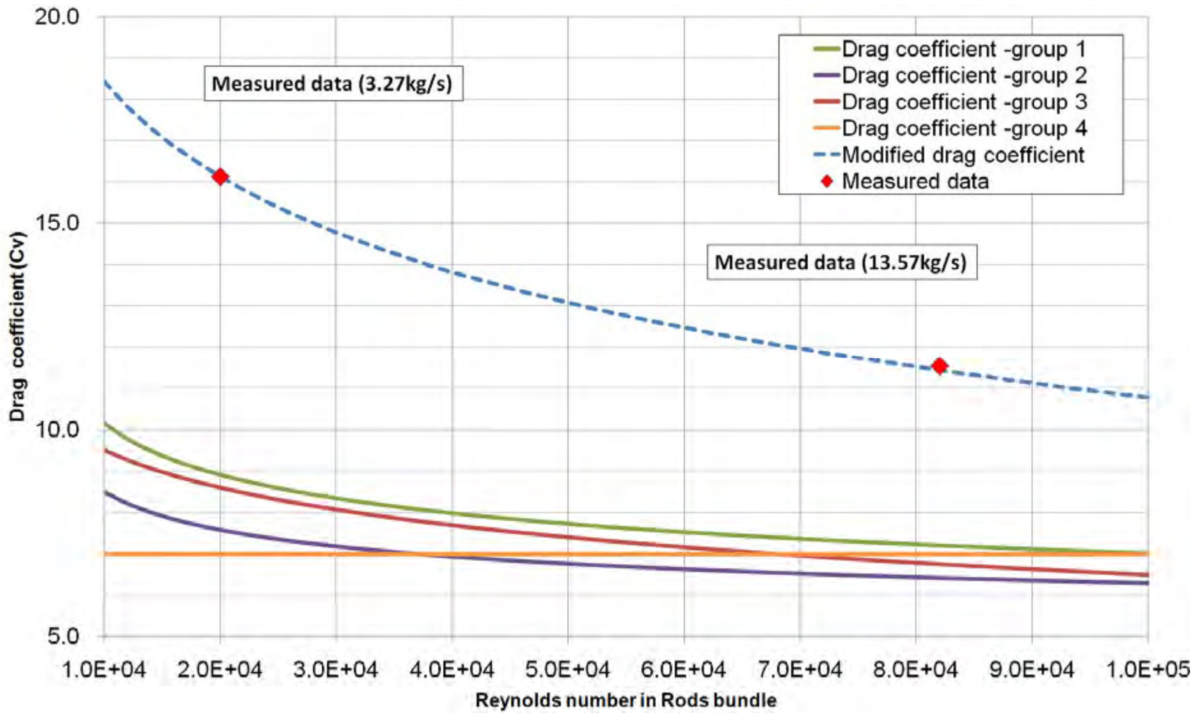

The pressure loss in the core was re-calculated using Equation 5.2. As shown in Figure 5.17, the results of participants are in good agreement with the experimental data.

Figure 5.17: Pressure loss in the core using equation 5.1

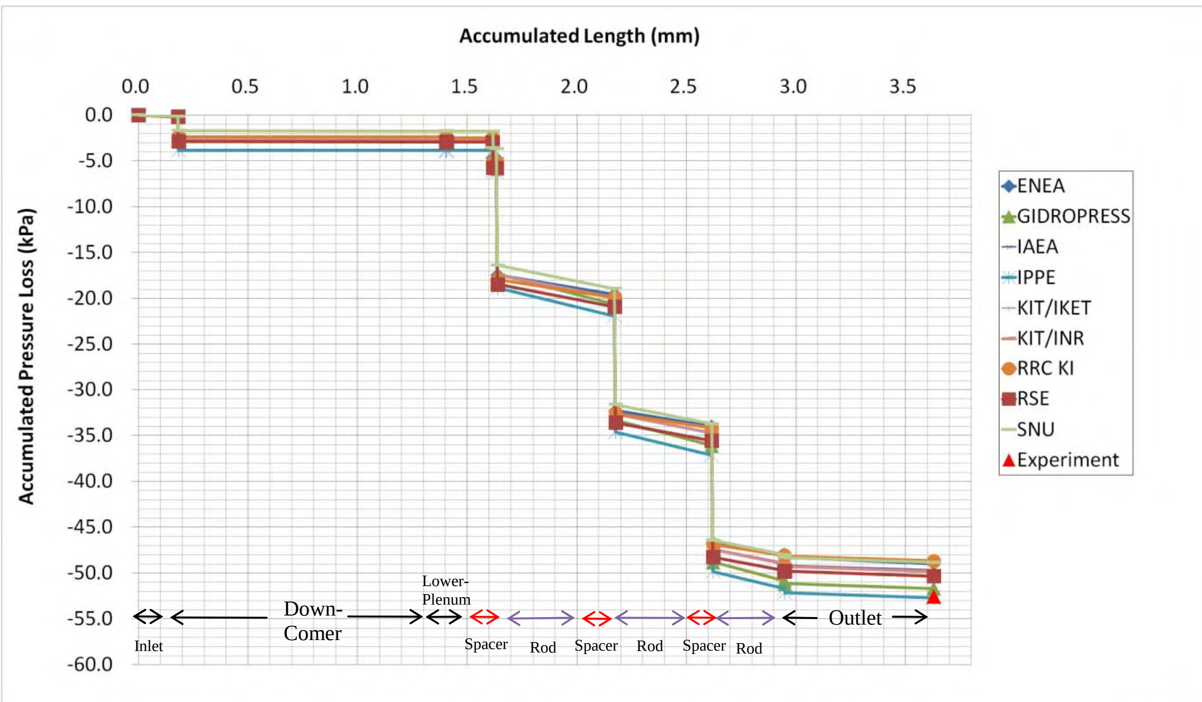

5.4.2 Orifice

Figure 5.18 shows comparison of the pressure loss in the orifice. The result of CFX® is in good agreement with the experiment and the result of participants is acceptable. The pressure drop correlation for the orifice used by ENEA, RSE, GIDROPRESS, IPPE, KIT/IKET and SNU, is recommended as follows [2-4]:

$$K = \left(1 + 0.707\sqrt{1 - \frac{F_0}{F_1}} - \frac{F_0}{F_1}\right)^2 \left(\frac{F_1}{F_0}\right)^2 \quad \text{for Re} \geq 10^5 \tag{5.3}$$

where, K is form loss coefficient, F is flow area, and Re is Reynolds number.

Figure 5.18: Pressure loss in the orifice at the high-mass flow rate

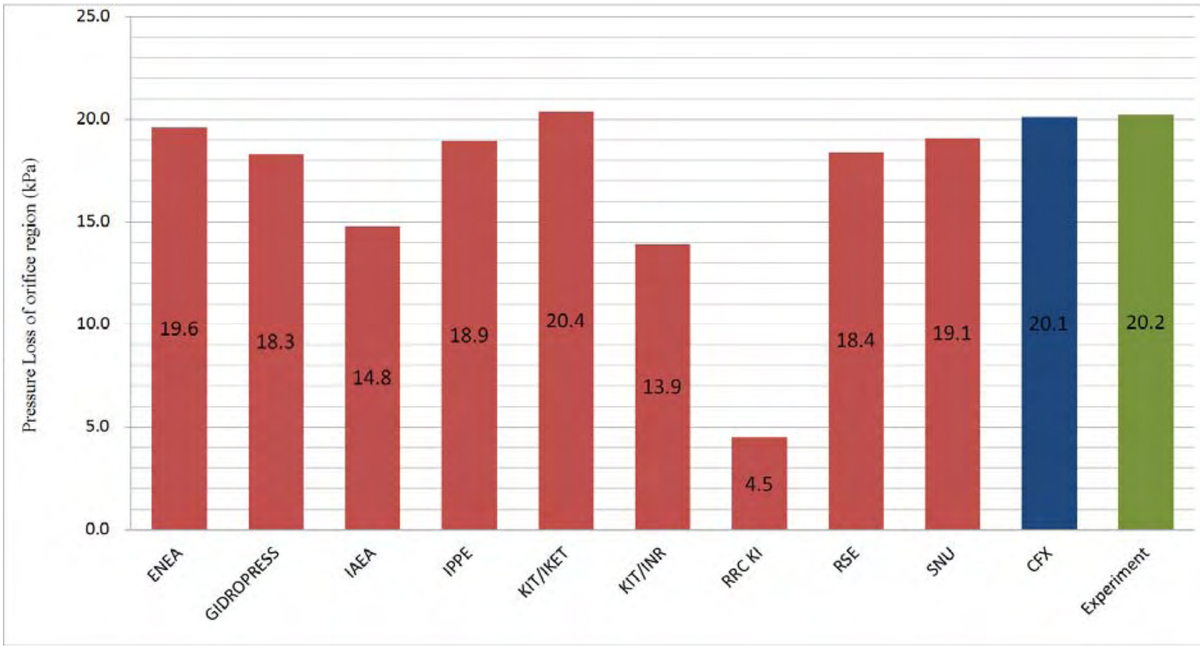

5.4.3 Gate valve

As shown in Figure 5.19, the pressure loss in the gate valve using CFX® is in good agreement with the experiment. The result of participants which uses Borda-Carnot correlation [5-8] is higher than the experiment. It has been found that the Borda-Carnot correlation over-estimates the pressure loss in the gate vale. Hence, for the gate valve, the CFD simulation or using provided manufacturer's data is recommended.

Figure 5.19: Pressure loss in the gate valve at the high-mass flow rate (other participants used manufacturer's data)

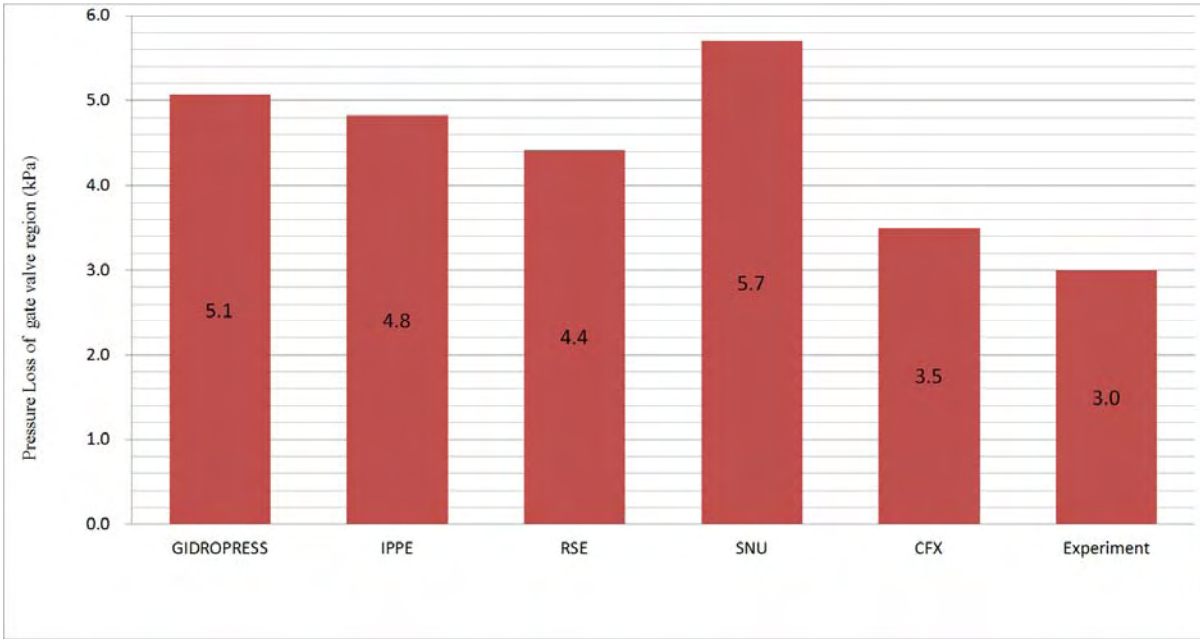

5.4.4 Heat exchanger

The pressure loss in the heat exchanger is mainly due to the shape change at the entrance and discharge as well as spacers for the pipe installation. As shown in Figure 5.20, the discrepancy of the pressure loss between the participants is large. In particular, the pressure loss at point 1 and 2 dominates the entire pressure loss in the heat exchanger. Since the result by the RSE is most comparable to the CFD and the experiment, the recommended pressure loss coefficients are shown in Figure 5.21.

Figure 5.20: Accumulated pressure loss in the heat exchanger at high-flow rate

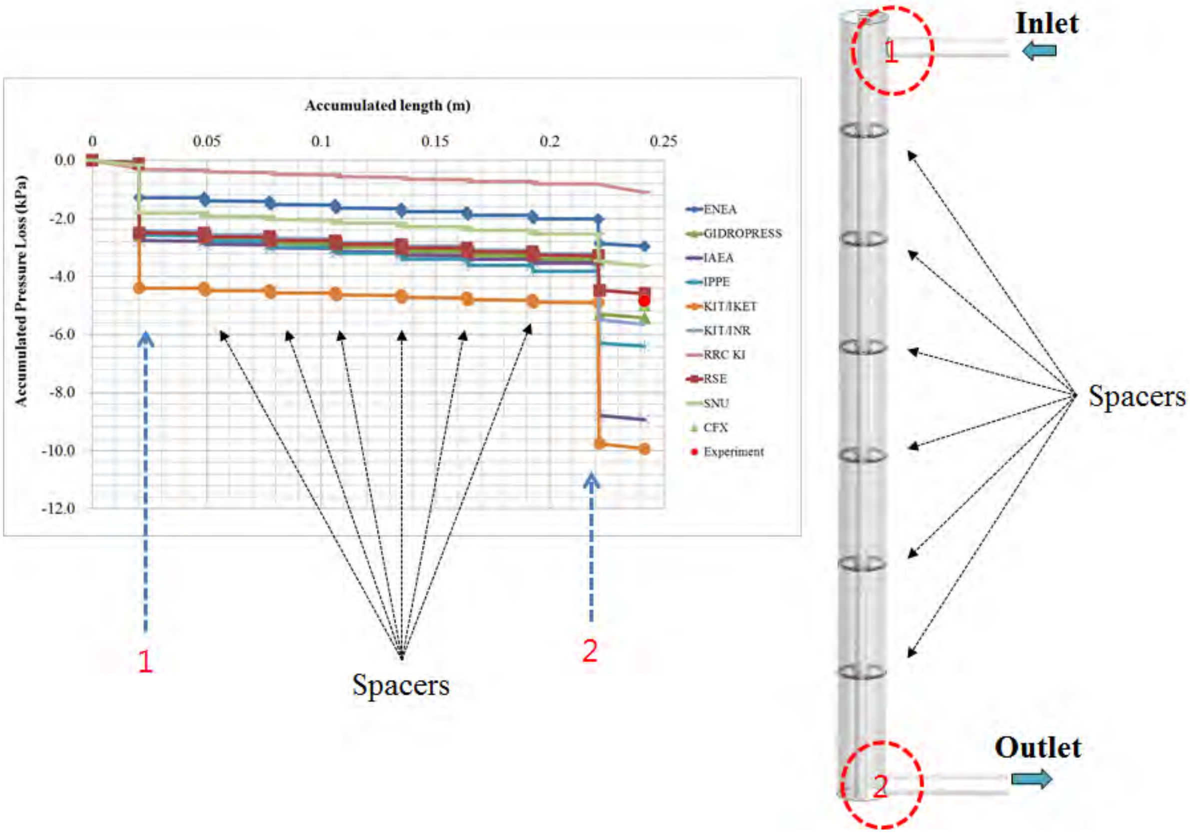

Figure 5.21: Geometry and pressure loss coefficients of entrance in a vessel and discharge into a pipe [2]

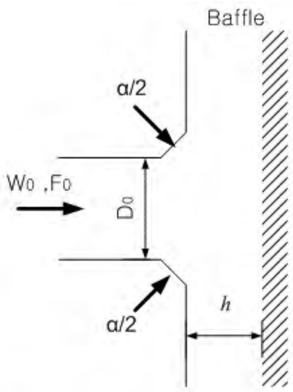

(a) Entrance in a vessel

α,deg	h/D_0									
	0.1	0.15	0.2	0.25	0.3	0.4	0.5	0.6	0.7	1
0							1.37	1.20	1.11	1.00
15				1.50	1.06	0.72	0.61	0.59	0.58	0.58
30			1.23	0.79	0.66	0.64	0.66	0.66	0.67	0.67
45		1.50	0.85	0.73	0.75	0.79	0.81	0.82	0.82	0.82
60		0.98	0.76	0.80	0.90	0.96	1.00	1.01	1.02	1.02
90	1.50	0.72	0.74	0.83	0.89	0.94	0.96	0.98	1.00	1.00

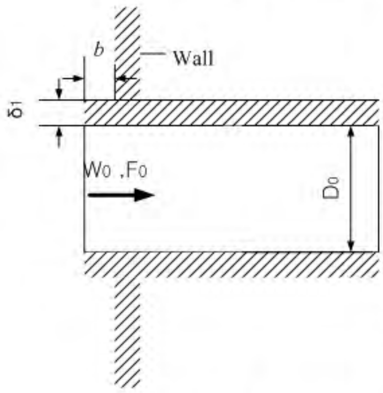

(b) Discharge into a pipe

δ_1/D_h	b/D_h										
	0	0.0002	0.005	0.01	0.02	0.05	0.1	0.2	0.3	0.5	∞
0	0.50	0.57	0.63	0.68	0.73	0.80	0.86	0.92	0.97	1.00	1.00
0.004	0.50	0.54	0.58	0.63	0.67	0.74	0.80	0.86	0.90	0.94	0.94
0.008	0.50	0.53	0.55	0.58	0.62	0.68	0.74	0.81	0.85	0.88	0.88
0.012	0.50	0.52	0.53	0.55	0.58	0.63	0.68	0.75	0.79	0.83	0.83
0.016	0.50	0.51	0.51	0.53	0.55	0.58	0.64	0.70	0.74	0.77	0.77
0.02	0.50	0.51	0.51	0.52	0.53	0.55	0.60	0.66	0.69	0.72	0.72
0.024	0.50	0.50	0.50	0.51	0.52	0.53	0.58	0.62	0.65	0.68	0.68
0.03	0.50	0.50	0.50	0.52	0.52	0.52	0.54	0.57	0.59	0.61	0.61
0.04	0.50	0.50	0.50	0.51	0.51	0.51	0.51	0.52	0.52	0.54	0.54
0.05	0.50	0.50	0.50	0.50	0.50	0.50	0.50	0.50	0.50	0.50	0.50
∞	0.50	0.50	0.50	0.50	0.50	0.50	0.50	0.50	0.50	0.50	0.50

The participants performed additional calculation using suggested form loss coefficient (Figure 5.21). As shown in Figure 5.22, the results are comparable to the experiment.

Figure 5.22: Accumulated pressure loss in the heat exchanger at high-flow rate using Figure 5.21

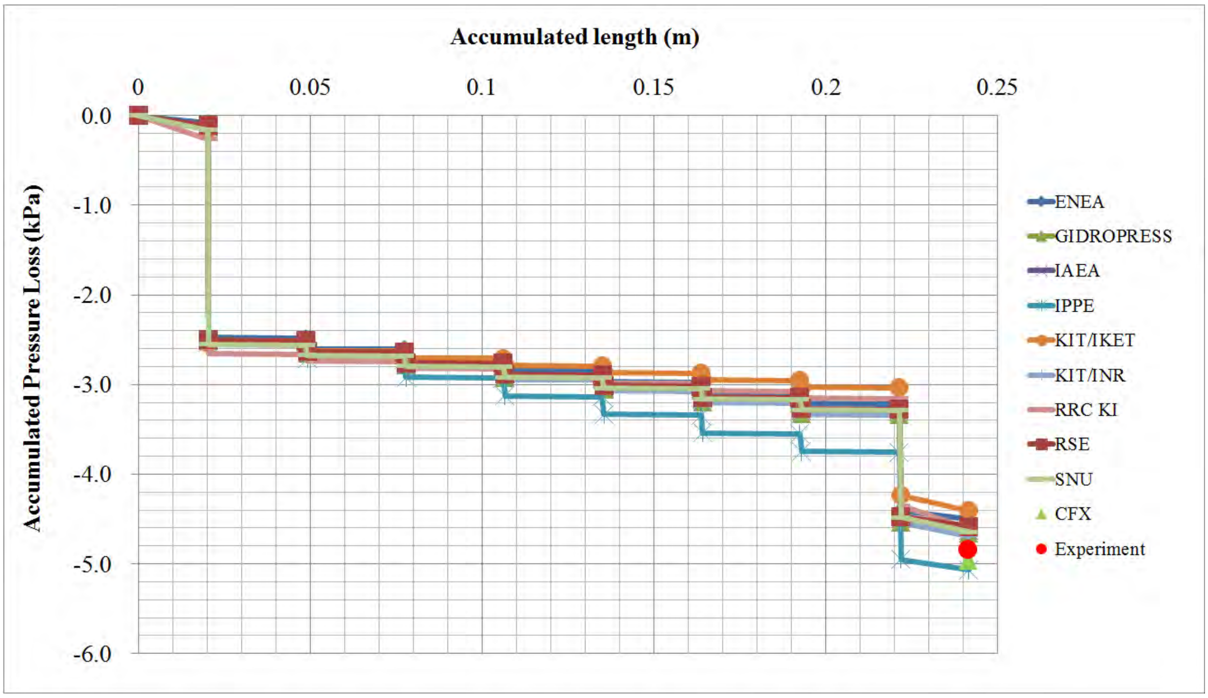

5.4.5 *Expansion tank*

As shown in Figure 5.23, the pressure loss in the expansion tank of the participants is in good agreement with CFX® and the experiment. As shown in the right of Figure 5.23, the expansion tank consists of straight pipe, 90° elbow pipe, form changes from straight pipe to expansion tank vessel and expansion tank vessel to straight pipe. Among these parts form changes are dominant for pressure loss. The recommended form loss coefficients for point 1 and 2 are shown in Figure 5.21, which are the same as the recommendations of heat exchanger.

Figure 5.23: Pressure loss in the expansion tank at the high-mass flow rate (left) and schematic diagram of expansion tank (right)

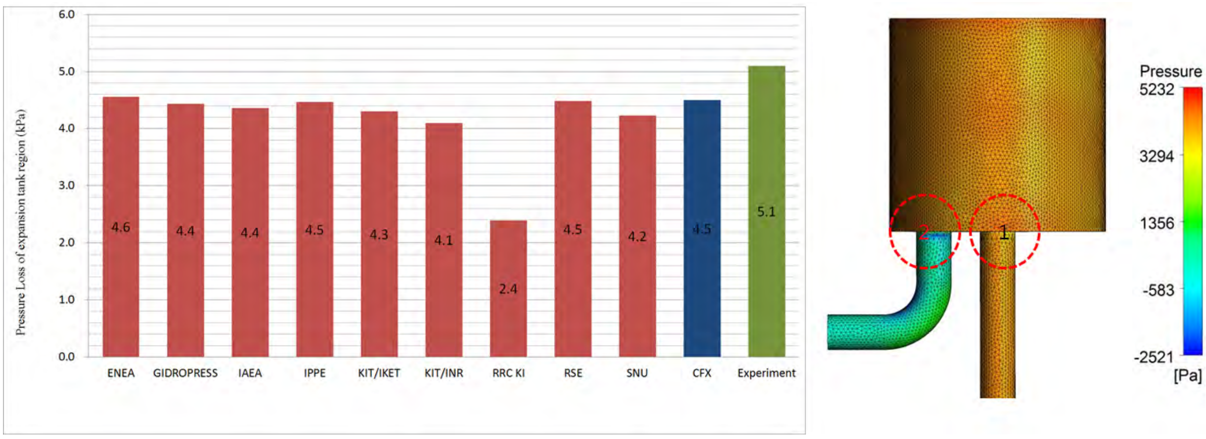

5.4.6 Straight and 45° and 90° elbow pipes

As shown in Figures 5.24, 5.25 and 5.26, the pressure loss due to the straight and 45° and 90° elbow pipes by participants is in good agreement with CFD simulation result. The recommended correlations are as follows:

Straight pipe [10]:

$$\frac{1}{\sqrt{f}} = -2\log_{10}\{\frac{\varepsilon}{3.7D} + \frac{2.51}{\mathrm{Re}}[1.14 - 2\log_{10}(\frac{\varepsilon}{D} - \frac{21.25}{\mathrm{Re}^{0.9}})]\} \tag{5.4}$$

45° and 90° elbow pipes [11]:

$$K = K_{\mathrm{Re}} \cdot K_{loc} + K_{fr}$$
$$K_{fr} = 0.0175 \cdot \frac{R_o}{D_o} \cdot \delta \cdot \lambda$$
$$K_{loc} = A_1 \cdot B_1 \tag{5.5}$$

where R_o is radius of curvature, D_o is diameter, δ is elbow angle, A_1, B_1, K_{Re}, K_{loc} are shown in the tables below:

Table 5.2: Value of A_1 for equation 5.4

δ	20.0	30.0	45.0	60.0	75.0
A_1	0.31	0.45	0.60	0.78	0.90
δ	90.0	110.0	130.0	150.0	180.0
A_1	1.00	1.13	1.20	1.28	1.40

where δ is elbow angle

Table 5.3: Value of B_1 for equation 5.4

R_0/D_0	0.50	0.60	0.70	0.80	0.90
B_1	1.18	0.77	0.51	0.37	0.28
R_0/D_0	1.00	1.25	0.50	2.00	4.00
B_1	0.21	0.19	0.17	0.15	0.11

where R_o is radius of curvature, D_o is diameter

Table 5.4: Value of k_{Re} for equation 5.4

Values of k_{Re}						
R_0/D_0	$Re \times 10^{-5}$					
	0.1	0.14	0.2	0.3	0.4	0.6
0.5-0.55	1.40	1.33	1.26	1.19	1.14	1.09
>0.55-0.70	1.67	1.58	1.49	1.40	1.34	1.26
>0.70	2.00	1.89	1.77	1.64	1.56	1.46
R_0/D_0	$Re \times 10^{-5}$					
	0.8	1.0	1.4	2.0	3.0	4.0
0.5-0.55	1.06	1.04	1.0	1.0	1.0	1.0
>0.55-0.70	1.21	1.19	1.17	1.14	1.06	1.0
>0.70	1.38	1.30	1.15	1.02	1.0	1.0

where R_o is radius of curvature, D_o is diameter, *Re* is Reynolds number

Table 5.5: Value of λ for equation 5.4

Value of λ									
$\bar{\Delta} = \frac{\Delta}{D_h}$	*Re*								
	3×10^3	4×10^3	6×10^3	10^4	2×10^4	4×10^4	6×10^4	10^5	2×10^5
0.0008	0.043	0.040	0.036	0.032	0.027	0.024	0.023	0.022	0.020
0.0006	0.046	0.040	0.036	0.032	0.027	0.023	0.022	0.021	0.018
0.0004	0.036	0.040	0.036	0.032	0.027	0.023	0.022	0.020	0.018
0.0002	0.036	0.040	0.036	0.032	0.027	0.022	0.021	0.019	0.017
0.0001	0.036	0.040	0.036	0.032	0.027	0.022	0.021	0.019	0.017
0.00005	0.036	0.040	0.036	0.032	0.027	0.022	0.021	0.019	0.016
0.00001	0.036	0.040	0.036	0.032	0.027	0.022	0.021	0.019	0.016
0.000005	0.036	0.040	0.036	0.032	0.027	0.022	0.021	0.019	0.016

where Δ is absolute roughness, D_h is hydraulic diameter, *Re* is Reynolds number

Figure 5.24: Sum of pressure loss in the straight pipe (15 m) at high-flow rate

Figure 5.25: Sum of pressure loss in the 45° elbow pipes (9ea) at high-flow rate

Figure 5.26: Sum of pressure losses in the 90° elbow pipes (4ea) at high-flow rate

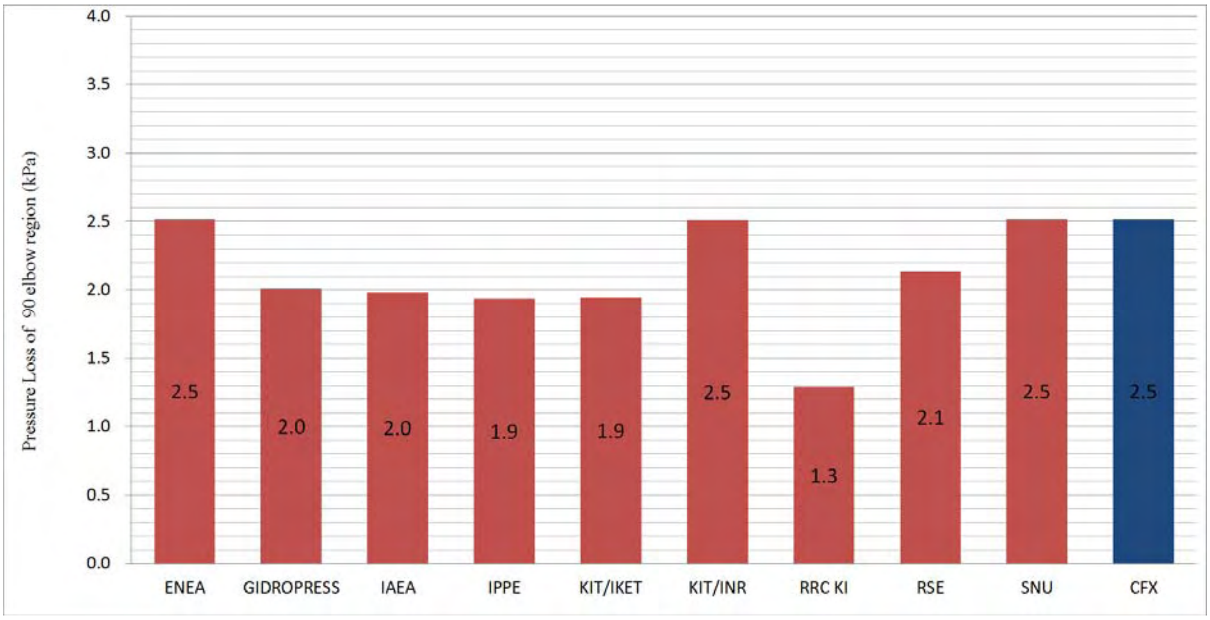

5.4.7 *Gasket*

While the experimental result is not available, the CFD result was used as reference. In order to increase reliability, two different CFD simulations were performed: CFX®; and Star-CD®. The CFD result showed that the pressure loss due to the gasket is negligible as shown in Figure 5.27. It is recommended that pressure loss of gasket should be neglected.

Figure 5.27: Pressure loss at gasket area at the high-flow rate

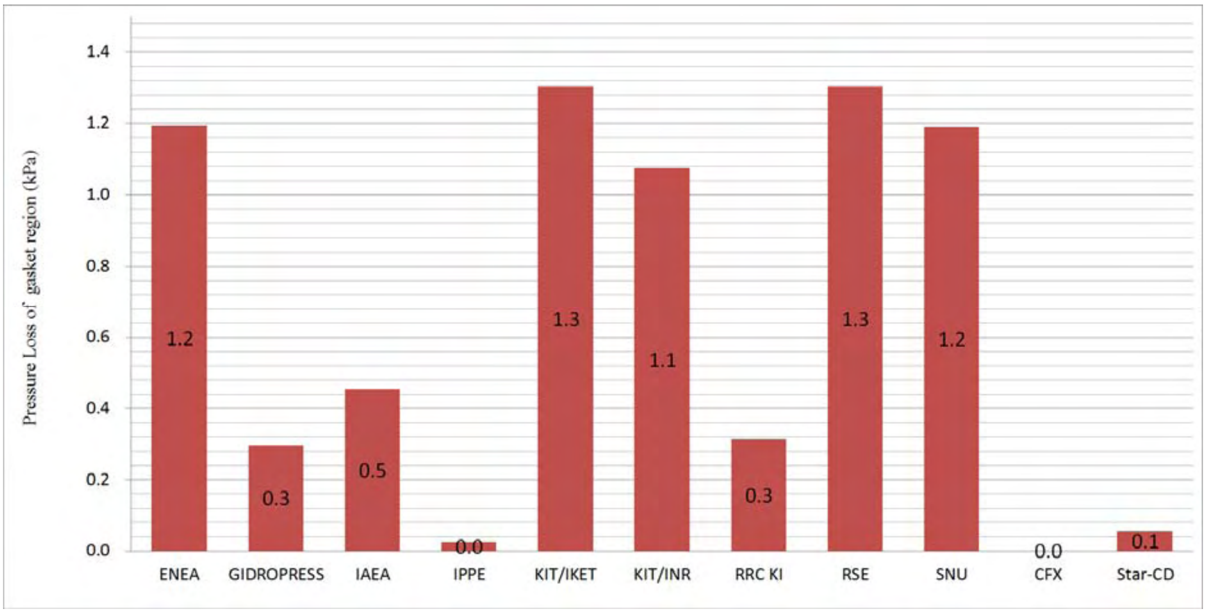

5.4.8 *Tee*

The CFD result was used as reference for pressure loss of the tee shape pipes: tee-straight and tee-branch (Figure 5.28). As shown in Figure 5.29, the pressure loss in the tee-straight was found small in CFD simulation. It is comparable to the ENEA, IPEE, IAEA and KIT/INR, who have considered only friction loss. Hence for the tee-straight it is recommended that form loss should be neglected.

For the tee-branch case shown in Figure 5.30, the result of KIT/IKET was in good agreement with the CFD. The recommended form loss coefficient is shown in Table 5.6 [9]:

Table 5.6: The recommended form loss coefficient for the tee-branch

Wa/Wz	0.0	0.2	0.4
K	0.98	0.87	0.90
Wa/Wz	0.6	0.8	1.0
K	0.98	1.12	1.29

where *Wz* is inlet flow, *Wa* is outlet flow, *K* is form loss coefficient

Figure 5.28: Schematic diagram of tee-straight (left) and tee-branch (right)

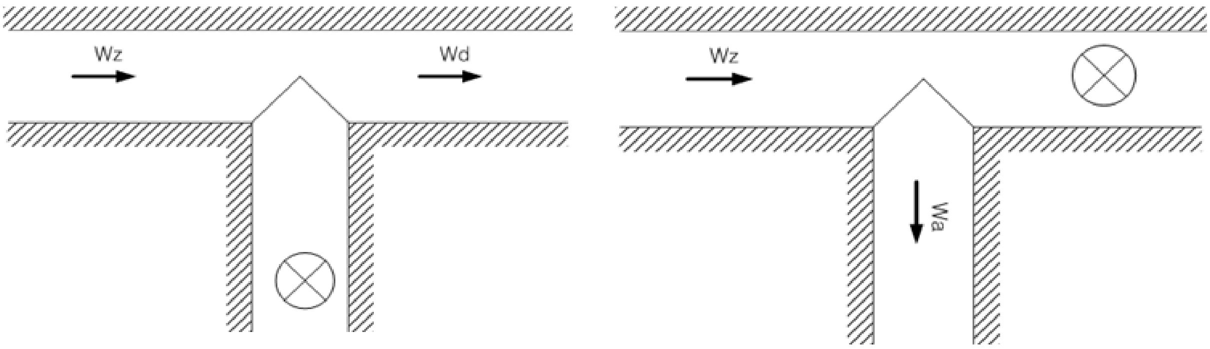

Figure 5.29: Sum of pressure loss in tee-straight (8ea) at high-flow rate

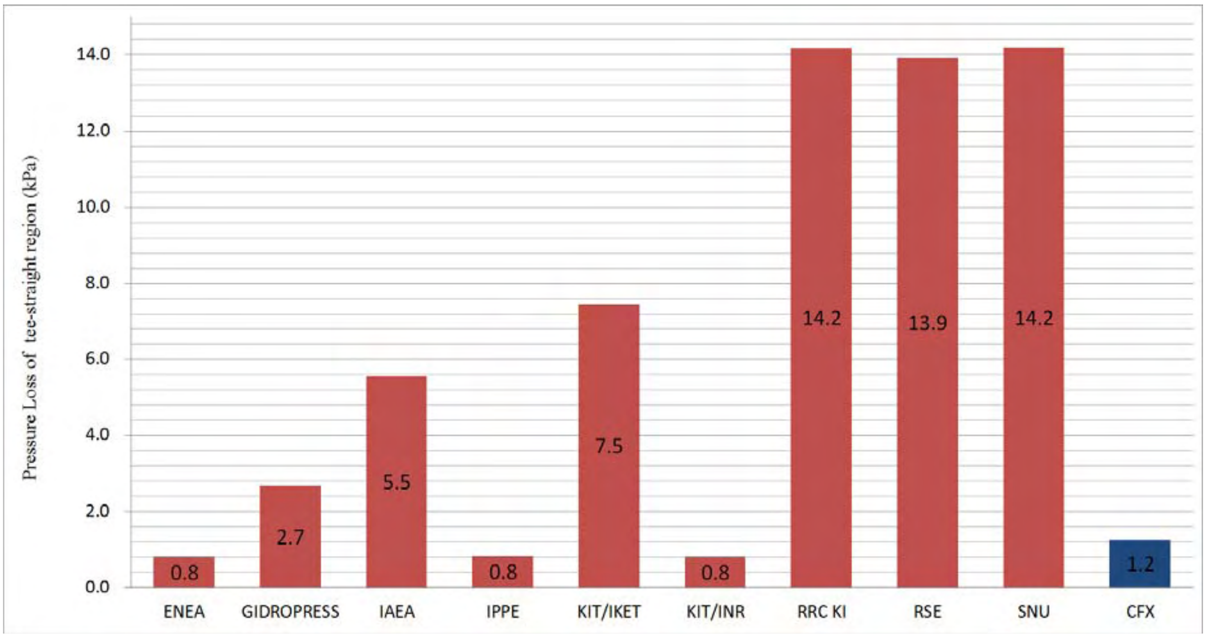

Figure 5.30: Pressure loss in tee-branch pipe at high-flow rate

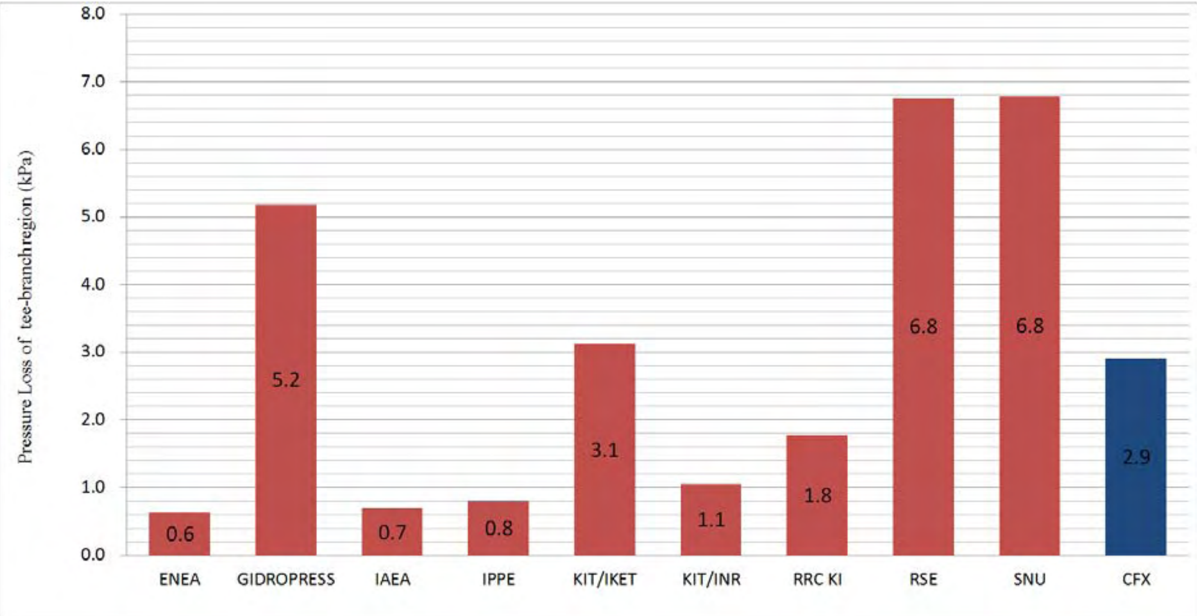

References

[1] OECD/NEA,"Benchmarking of thermal-hydraulic loop models for Lead-alloy-cooled advanced nuclear energy systems (LACANES) - Task Guideline for Phase 1: Characterisation of HELIOS".

[2] I.E. Idelchik (2000), Handbook of Hydraulic Resistance 3rd Edition, CRC.

[3] I.E. Idelchik (1948), Discharge Losses in Flow with Nonuniform Velocity Profile*, Proc. of ZAGI*. 1-24.

[4] I.E. Idelchik (1954), Hydraulic Resistance (physical mechanics foundations). M. Mashgiz.

[5] P.M. Slissky (1983), Methodical Recommendations to Calculation of Friction Factors in Tubes for Transition Zone, 31-34.

[6] Verein Deutscher Ingenieure (2006),VDI-Wärmeatlas 3.0, Springer Verlag, Berlin Heidelberg.

[7] B.S. Massey (1968), "Mechanics of Fluids", D Van Nostrand Co. New York, pp 217-219.

[8] J.K. Vennard (1961), "One-Dimensional Flow", In: V. L. Streeter (ed.), Handbook of Fluid Dynamics. 1st Edition. New York: McGraw Hill.

[9] Verein Deutscher Ingenieure (2006), VDI-Wärmeatlas 3.0, Springer Verlag, Berlin Heidelberg.

[10] I.E. Idelchik (1986), Handbook of Hydraulic Resistance, 2nd edition, Hemisphere Publishing Corporation.

[11] H. Nippert (1922), Uber den Stromungsverlust in gekrummten Kanalen, Forschungsarb. Geb. Ingenieurwes, no. 320, VDI, pp.85.

Chapter 6: Summary and conclusion

6.1 Summary

Utilising HELIOS facility, a thermal-hydraulic benchmark study has been conducted for the prediction of pressure loss in lead-alloy-cooled advanced nuclear energy systems (LACANES). The motivations of this benchmarking are to gain a better understanding about thermal-hydraulic behaviour of lead-alloy-cooled system and furthermore to construct the good guidelines for thermal-hydraulic modelling of it. Participants include representations of Germany, Italy, Republic of Korea, Russian Federation and IAEA. The LACANES benchmarking consists of forced convection (Phase-I) and natural circulation (Phase-II). This report describes the results of phase-I and recommendations for best practice for the pressure loss prediction for LACANES.

Through the LACANES benchmarking phase-I, best practice guidelines for pressure loss prediction are established. Experimental tests are conducted to obtain the pressure loss in the core, the gate valve, the orifice, the heat exchanger region, and the expansion tank region. Predictions are also performed by participants using correlations from handbooks. Furthermore, to improve the prediction for the complicated geometry and to solve the uncertainty of prediction from correlations, CFD simulations for all components are conducted.

Benchmarking regions consist of eleven components: core, orifice, gate valve, expansion tank, heat exchanger, 45° elbow, 90° elbow, tee-straight, tee-branch, gasket, and straight pipe. In the LACANES benchmarking phase-I, the following summary has been made:

1. In the core region, the predictions based on handbook correlations have uncertainty. The Rehme correlation was used for the prediction of a pressure loss on the spacers but it underestimated the results, while orifice empirical correlation for spacers has the highest agreement with measured data. Two CFD simulations using the Star-CD® and the CFX® have shown good agreement with the measured data.
2. The predictions based on handbook correlations have shown good agreement with the measured data in the orifice region. The empirical orifice correlation from the Idelchik handbook could be recommended for prediction of pressure loss in the orifice region.
3. The predictions of pressure losses on the gate valve obtained by the Borda-Carnot correlation overestimated the measured data. On the other hand, the CFD simulation has shown good agreement with the measured data.
4. In the expansion tank region, predictions by correlations and CFX® have shown good agreement with the measured data.
5. In the heat exchanger region, large discrepancies were caused by different correlations for the entrance and discharge region. As a best practice guideline for entrance and discharge region, Idelchik handbook correlations which showed good agreement with measured data were introduced.
6. Based on CFX® simulation in the gasket and tee-straight regions, the effect of gasket and tee-straight to pressure loss was low enough to neglect. In the gasket region, prediction by Idelchik recess correlation is recommended. On the other hand, it is recommended in the tee-straight region that tee-junction effect should be neglected.
7. In the tee-branch region, VDI handbook correlation was in good agreement with CFX® result.
8. In the 45° elbow, 90° elbow and the straight pipe region, all predictions including CFX® simulation are very similar.

9. For the benchmarking regions based on the measured data, CFD simulations provided more reliable results than any other correlations. CFD simulations could be recommended to obtain a high accuracy prediction of the pressure loss in LACANES. In the tee-straight, tee-branch, and the gasket, which have large discrepancies between predictions without measured data, CFD estimations are regarded as good guidelines to predict pressure losses.

Table 6.1 shows recommended correlations in the LACANES benchmarking phase-I. In this table, correlations having the good agreement with measured data or CFD results are introduced.

6.2 Conclusion

Lead-alloy has been highly investigated as coolant for new generation nuclear reactors owing to its many advantages consisting of low melting temperature, high boiling temperature, chemical stability and good neutron economy. Today, accelerator-driven transmutation systems and lead and lead-alloy-cooled fast reactors (LFR) have been developed worldwide such as SVBR 75/100 and BREST-300 in the Russian Federation, SSTAR in the USA, PEACER-300 and PASCAR in the Republic of Korea and MYRRHA project in Belgium.

Based on the world's efforts concerning lead-alloy-cooled system, LACANES benchmarking was launched in 2007. Now, understandable guidelines for prediction pressure loss were obtained based on comparison between many predictions calculated by handbook correlations or CFD simulations. From these activities, a better understanding of pressure loss modelling in lead-alloy-cooled system was obtained. The LACANES benchmark Phase-II in the case of natural circulation will be continued.

Table 6.1: Recommended correlations in the LACANES benchmarking phase-I

<table>
<tr><th>Components</th><th>Geometry</th><th>Recommended correlations</th><th>Reference</th></tr>
<tr><td>Spacer</td><td>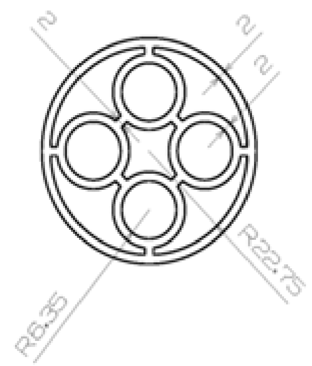
</td><td>$K = C_V\left(\frac{A_s}{A_v}\right)^2 \qquad C_V = -7.65\log_{10}\mathrm{Re} + 49.0$</td><td>Idelchik, I.E., Determination of the resistance coefficients during discharge through orifices, Gidrotekh. Stroit., no. 5, 31-36, 1953</td></tr>
<tr><td>Orifice</td><td>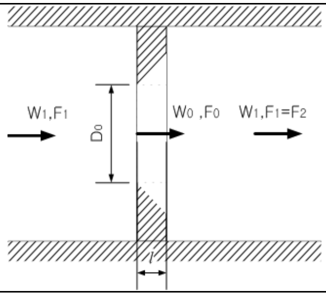
</td><td>$K = \left(1 + 0.707\sqrt{1-\frac{F_0}{F_1}} - \frac{F_0}{F_1}\right)^2\left(\frac{F_1}{F_0}\right)^2$
$\mathrm{Re} > 10^5$</td><td>Idelchik, I.E., Determination of the resistance coefficients during discharge through orifices, Gidrotekh. Stroit., no. 5, 31-36, 1953</td></tr>
<tr><td>Discharge into a vessel</td><td>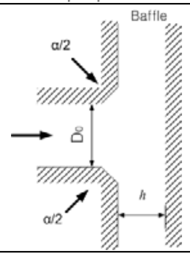
</td><td>
<table>
<tr><th></th><th colspan="10">h/D_0</th></tr>
<tr><td>α. deg</td><td>0.10</td><td>0.15</td><td>0.20</td><td>0.25</td><td>0.30</td><td>0.40</td><td>0.50</td><td>0.60</td><td>0.70</td><td>1.0</td></tr>
<tr><td>0</td><td>-</td><td>-</td><td>-</td><td>-</td><td>-</td><td>-</td><td>1.37</td><td>1.20</td><td>1.11</td><td>1.00</td></tr>
<tr><td>15</td><td>-</td><td>-</td><td>-</td><td>1.50</td><td>1.06</td><td>0.72</td><td>0.61</td><td>0.59</td><td>0.58</td><td>0.58</td></tr>
<tr><td>30</td><td>-</td><td>-</td><td>1.23</td><td>0.79</td><td>0.66</td><td>0.64</td><td>0.66</td><td>0.66</td><td>0.67</td><td>0.67</td></tr>
<tr><td>45</td><td>-</td><td>1.50</td><td>0.85</td><td>0.73</td><td>0.75</td><td>0.79</td><td>0.81</td><td>0.82</td><td>0.82</td><td>0.82</td></tr>
<tr><td>60</td><td>-</td><td>0.98</td><td>0.76</td><td>0.80</td><td>0.90</td><td>0.96</td><td>1.00</td><td>1.01</td><td>1.02</td><td>1.02</td></tr>
<tr><td>90</td><td>1.50</td><td>0.72</td><td>0.74</td><td>0.83</td><td>0.89</td><td>0.94</td><td>0.96</td><td>0.98</td><td>1.00</td><td>1.00</td></tr>
</table>
</td><td>Idelchik, I.E., Flow aerodynamics and pressure head losses in diffusers, Prom. Aerodin., no.3, 132-209, 1947</td></tr>
</table>

Entrance in tubes

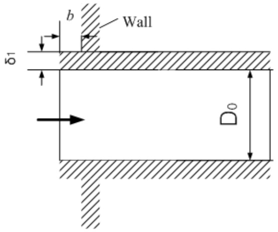

$\frac{\delta_1}{D_h}$	$\frac{b}{D_h}$										
	0	0.002	0.005	0.010	0.020	0.050	0.100	0.200	0.300	0.500	∞
0	0.50	0.57	0.63	0.68	0.73	0.80	0.86	0.92	0.97	1.00	1.00
0.004	0.50	0.54	0.58	0.63	0.67	0.74	0.80	0.86	0.90	0.94	0.94
0.008	0.50	0.53	0.55	0.58	0.62	0.68	0.74	0.81	0.85	0.88	0.88
0.012	0.50	0.52	0.53	0.55	0.58	0.63	0.68	0.75	0.79	0.83	0.83
0.016	0.50	0.51	0.51	0.53	0.55	0.58	0.64	0. 70	0.74	0.77	0.77
0.020	0.50	0.51	0.51	0.52	0.53	0.55	0.60	0.66	0.69	0.72	0.72
0.024	0.50	0.50	0.50	0.51	0.52	0.53	0.58	0.62	0.65	0.68	0.68
0.030	0.50	0.50	0.50	0.52	0.52	0.52	0.54	0.57	0.59	0.61	0.61
0.040	0.50	0.50	0.50	0.51	0.51	0.51	0.51	0.52	0.52	0.54	0.54
0.050	0.50	0.50	0.50	0.50	0.50	0.50	0.50	0.50	0.50	0.50	0.50
∞	0.50	0.50	0.50	0.50	0.50	0.50	0.50	0.50	0.50	0.50	0.50

Idelchik, I. E., Hydraulic resistance during flow entrance in channels and passage through orifices, Prom. Aerodin., no. 2, 27-57, BNT, NKAP, 1944

Straight pipe

$$\frac{1}{\sqrt{f}} = -2\log_{10}\{\frac{\varepsilon}{3.7D} + \frac{2.51}{\mathrm{Re}}[1.14 - 2\log_{10}(\frac{\varepsilon}{D} - \frac{21.25}{\mathrm{Re}^{0.9}})]\}$$

Idelchik I.E, - Handbook of Hydraulic Resistance, 2nd edition, Hemisphere Pub. Corp., -1986

Sudden changes

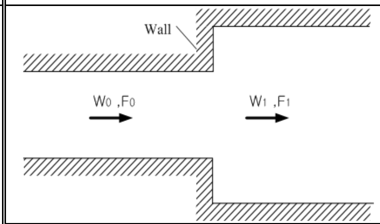

$$K_{SE} = \left(1 - \frac{F_0}{F_1}\right)^2$$

Idelchik I.E, - Handbook of Hydraulic Resistance, 2nd edition, Hemisphere Pub. Corp., -1986

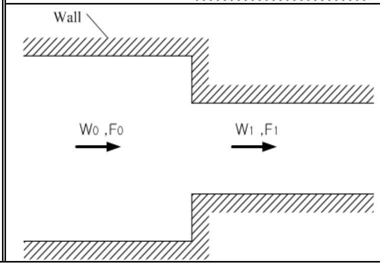

$$K_{SC} = 0.5 - 0.7\cdot\left(\frac{F_1}{F_0}\right) + 0.2\cdot\left(\frac{F_1}{F_0}\right)^2$$

B.S.Massey, Mechanics of Fluids, D.Van Nostrand Co., New York, 1968, pp.217-219

45°, 90° elbow

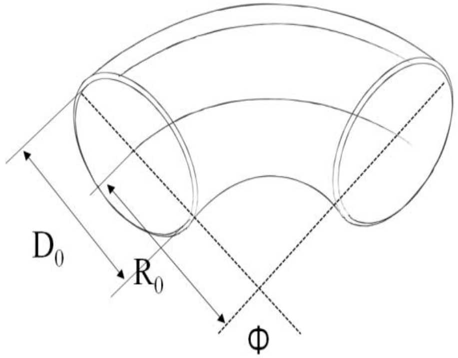

$$K = K_{\mathrm{Re}} \cdot K_{\mathrm{loc}} + K_{\mathrm{fr}}$$

$$K_{\mathrm{fr}} = 0.0175 \cdot \frac{R_o}{D_o} \cdot \phi \cdot \lambda$$

$$K_{\mathrm{loc}} = A_1 \cdot B_1$$

δ	20.0	30.0	45.0	60.0	75.0
A_1	0.31	0.45	0.60	0.78	0.90
δ	90.0	110.0	130.0	150.0	180.0
A_1	1.00	1.13	1.20	1.28	1.40

R_0/D_0	0.50	0.60	0.70	0.80	0.90
B_1	1.18	0.77	0.51	0.37	0.28
R_0/D_0	1.00	1.25	0.50	2.00	4.00
B_1	0.21	0.19	0.17	0.15	0.11

Values of k_{Re}						
R_0/D_0	$Re \times 10^{-5}$					
	0.1	0.14	0.2	0.3	0.4	0.6
0.5-0.55	1.40	1.33	1.26	1.19	1.14	1.09
>0.55-0.70	1.67	1.58	1.49	1.40	1.34	1.26
>0.70	2.00	1.89	1.77	1.64	1.56	1.46
R_0/D_0	$Re \times 10^{-5}$					
	0.8	1.0	1.4	2.0	3.0	4.0
0.5-0.55	1.06	1.04	1.0	1.0	1.0	1.0
>0.55-0.70	1.21	1.19	1.17	1.14	1.06	1.0
>0.70	1.38	1.30	1.15	1.02	1.0	1.0

Nippert, H., Uber den Stromungsverlust in gekrummten Kanalen, Forschungsarb. Geb. Ingenieurwes, no. 320, VDI, 1922, 85pp

Value of λ									
$\bar{\Delta}=\frac{\Delta}{D_h}$	*Re*								
	3×10^3	4×10^3	6×10^3	10^4	2×10^4	4×10^4	6×10^4	10^5	2×10^5
0.0008	0.043	0.040	0.036	0.032	0.027	0.024	0.023	0.022	0.020
0.0006	0.046	0.040	0.036	0.032	0.027	0.023	0.022	0.021	0.018
0.0004	0.036	0.040	0.036	0.032	0.027	0.023	0.022	0.020	0.018
0.0002	0.036	0.040	0.036	0.032	0.027	0.022	0.021	0.019	0.017
0.0001	0.036	0.040	0.036	0.032	0.027	0.022	0.021	0.019	0.017
0.00005	0.036	0.040	0.036	0.032	0.027	0.022	0.021	0.019	0.016
0.00001	0.036	0.040	0.036	0.032	0.027	0.022	0.021	0.019	0.016
0.000005	0.036	0.040	0.036	0.032	0.027	0.022	0.021	0.019	0.016

Gasket

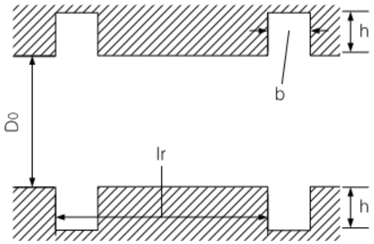

$$l_r / D_0 \geq 4, K = 0.046\frac{b}{D_0}$$

$$l_r / D_0 = 2, K = 0.059\frac{b}{D_0}$$

$$l_r / D_0 \leq 4, K = f\left(\frac{b}{D_o}, \frac{l_r}{D_o}\right)$$

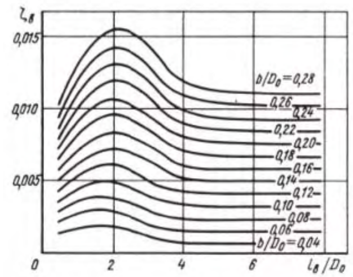

Trubenok, V.D., Determination of the coefficient of local resistances in tubes with rectangular annular recesses, in Applied Aerodynamics, pp.3-6, Kiev, 1980

<table>
<tr>
<td>Tee-straight</td>
<td>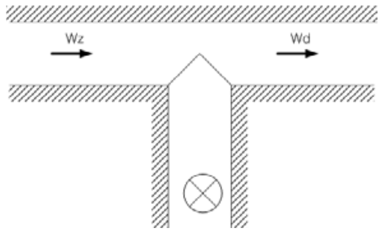
</td>
<td>Approximated as straight pipe</td>
<td></td>
</tr>
<tr>
<td>Tee-elbow</td>
<td>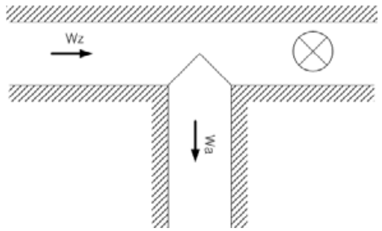
</td>
<td>
<table>
<tr><td>Wa/Wz</td><td>0.0</td><td>0.2</td><td>0.4</td></tr>
<tr><td>K</td><td>0.98</td><td>0.87</td><td>0.90</td></tr>
<tr><td>Wa/Wz</td><td>0.6</td><td>0.8</td><td>1.0</td></tr>
<tr><td>K</td><td>0.98</td><td>1.12</td><td>1.29</td></tr>
</table>
</td>
<td>Verein Deutscher Ingenieure, VDI-Wärmeatlas 3.0, Springer Verlag, Berlin Heidelberg, 2006</td>
</tr>
</table>

Where W is flow rate (m^3/s), F is flow area (m^2), D is diameter (m), R is radius (m), Φ is angle (degree), and Re is Reynolds number.

References

[1] N.E.Todreas, M.S. Kazimi (1990), eds. *Nuclear System I*. Hemisphere Publishing Corporation.

[2] OECD/NEA (2007), ed. Handbook on Lead-bismuth Eutectic Alloy and Lead Properties, Materials Compatibility, Thermal-hydraulics and Technolgies.

[3] H. Lee (2007), Analysis of Lead Bismuth Eutectic Loop (HELIOS) Flow Experiments using Analysis Method, MARS-LBE and CFX Codes, in Nuclear Engineering Department, Seoul National University.

[4] I.E. Idelchik (1994), ed. *Handbook of Hydraulic Resistance*. 3rd ed. CRC Press.

[5] OECD/NEA (2007), Handbook on Lead-bismuth Eutectic Alloy and Lead Properties, Materials Compatibility, Thermal-hydraulics and Technologies, No.6195.

[6] OECD/NEA (2007), Benchmarking of thermal-hydraulic loop models for Lead-alloy-cooled advanced nuclear energy systems (LACANES) - Task Guideline for Phase 1: Characterisation of HELIOS.

[7] I.S. Hwang *et al.* (2006), A Sustainable Regional Waste Transmutation System: P E A C E R, in ICAPP '06, Reno, NV, USA.

[8] I. S. Hwang, S.H. Jeong, B.G. Park, W. S. Yang, K.Y. Suh, C.H. Kim (2000), *Progress in Nuclear Energy*, 37(1-4).

[9] W.C. Nam, H.W. Lee, I.S. Hwang (2007), *Nucl. Eng. Des. 237*(3): pp. 316-324.

[10] F. M. White (1986), Fluid Mechanics 2nd edition, McGraw-Hill.

[11] S.H. Jeong (2006), Development of an Integral Test Loop, HELIOS and Investigation of Natural Circulation Ability for PEACER, in Nuclear Engineering Department, Seoul National University, Seoul.

[12] J. Lim, S.H. Jeong, Y. J. Oh, H. O. Nam, C. B. Bahn, S. H. Chang, W. C. Nam, K. H. Ryu, T. H. Lee, S. G. Lee, N. Y. Lee and I. S. Hwang (2007), Progresses in the Operation of Large Scale LBE Loop HELIOS, in *ICAPP,* Nice, France.

[13] S. H. Jeong, C.B. Bahn., S. H. Chang, Y. J. Oh, W. C. Nam, K. H. Ryu, H. O. Nam, J. Lim, N. Y. Lee and I. S. Hwang (2006), Operation Experience of LBE loop: HELIOS, in ICAPP '06.

[14] N.E.Todreas, M.S.Kazimi (1990), *Nuclear System I,* Thermal Hydraulics Fundamentals, Hemisphere Publishing Corporation.

[15] K. Rheme (1973), Pressure drop correlations for fuel element spacers, Nuclear Technology Review, Vol. 17 January 1973.

[16] I.E. Idelchik (1960), Account of Viscosity in Hydraulic Resistance of Baffles and Spacers. *J. Teploenergetika*. 75 – 80.

[17] I.E. Idelchik (2000), Handbook of hydraulic resistance 3rd *Edition*, CRC.

[18] A. Batta, J.H. Cho, A.G. Class, I.S. Hwang (2009), CFD Analysis Of Heavy Liquid Metal Flow In The Core of The HELIOS Loop, *HELIMERT2009*.

[19] STAR-CD User Guide Methodology Star-CD VERSION 4.06 © 2008 CD-Adap.

[20] CFX ANSYS CFX-Solver Modelling Guide ANSYS CFX Release 11.0 December 2006.

[21] I.E. Idelchik (1948), Discharge Losses in Flow with Nonuniform Velocity Profile, *Proc. of ZAGI*. 1-24.

[22] I.E. Idelchik (1954), Hydraulic Resistance (physical mechanics foundations), M.Mashgiz.

[23] P.M. Slissky (1983), Methodical Recommendations to Calculation of Friction Factors in Tubes for Transition Zone, 31-34.

[24] Verein Deutscher Ingenieure (2006), VDI-Wärmeatlas 3.0, Springer Verlag, Berlin Heidelberg.

[25] US Nuclear Regulatory Commission (2007), TRACE V5.0 User's Manual, US Washington, DC, 20555-0001.

[26] RELAP5/Mod.3.3. Code Manual, 2002.

Appendix A

(Component 3D Plan)

Figure A-1: 3D View of component #1 core vessel

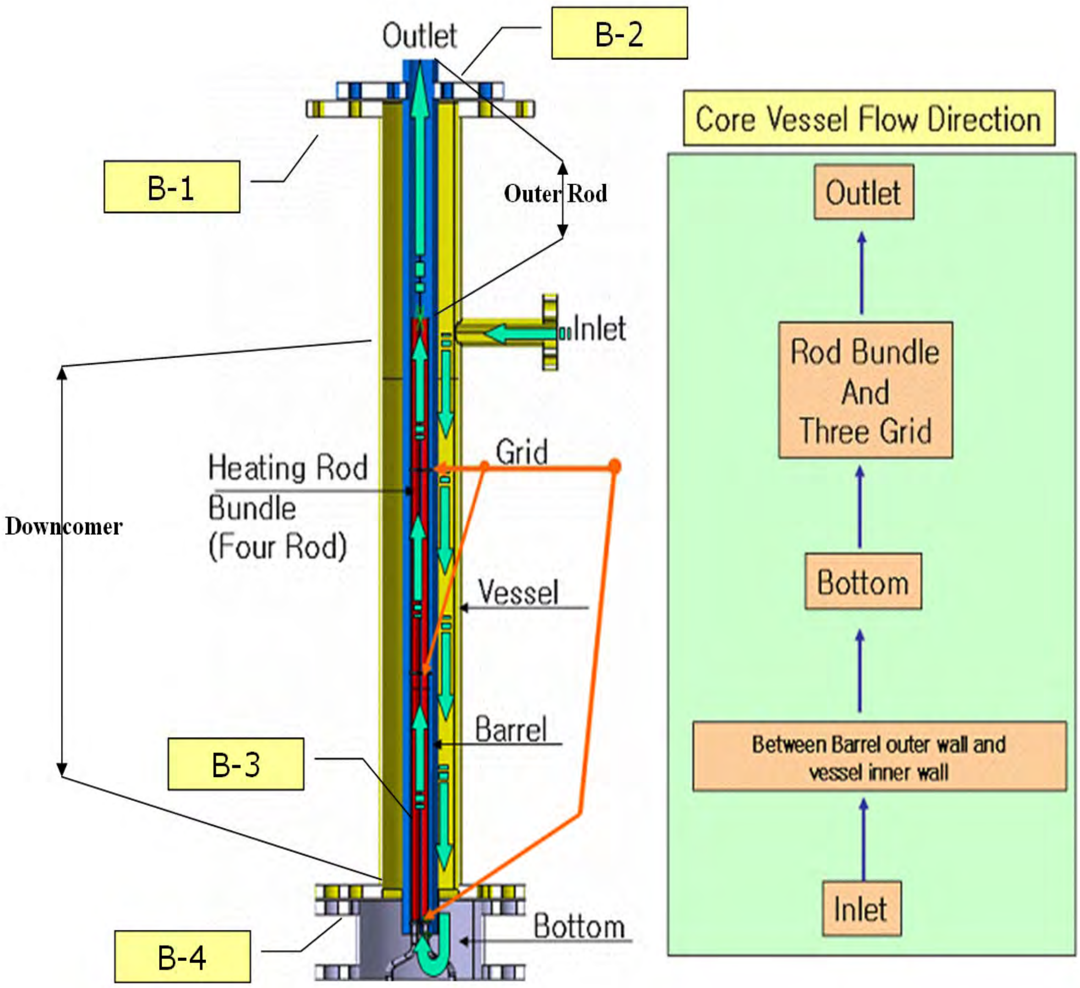

Figure A-2: 3D View of component #2 pipe with tee

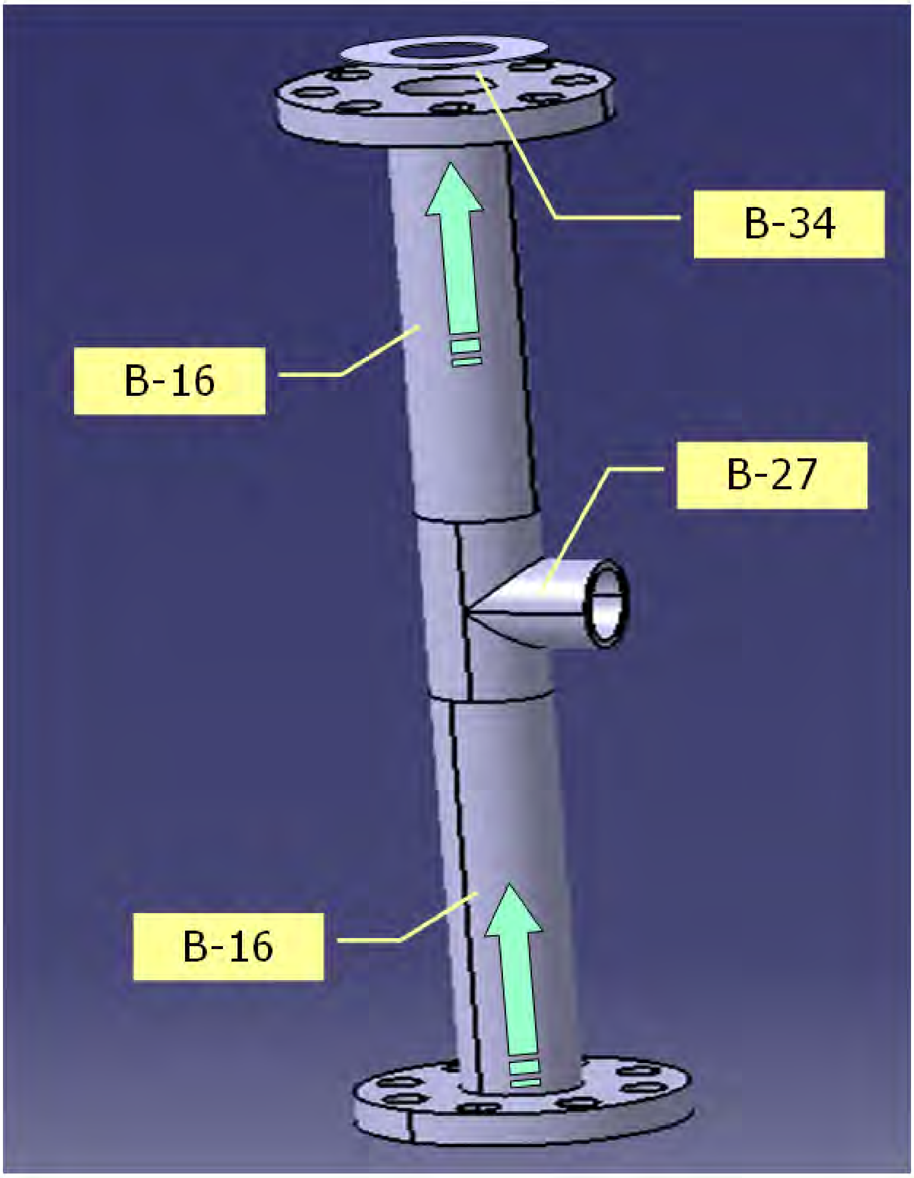

Figure A-4: 3D View of component #4 pipe with tee and elbows

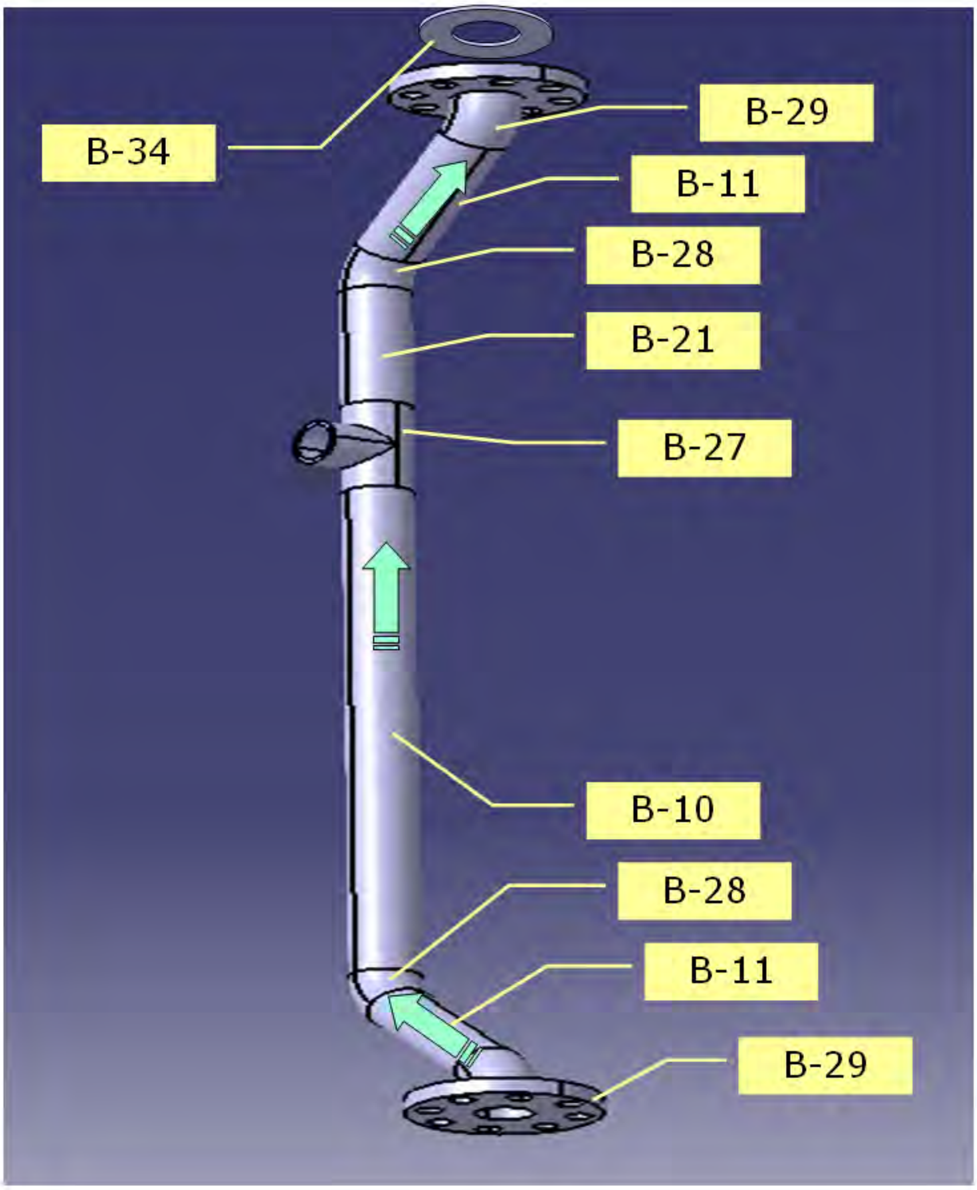

Figure A-10: 3D View of component #10 expansion tank

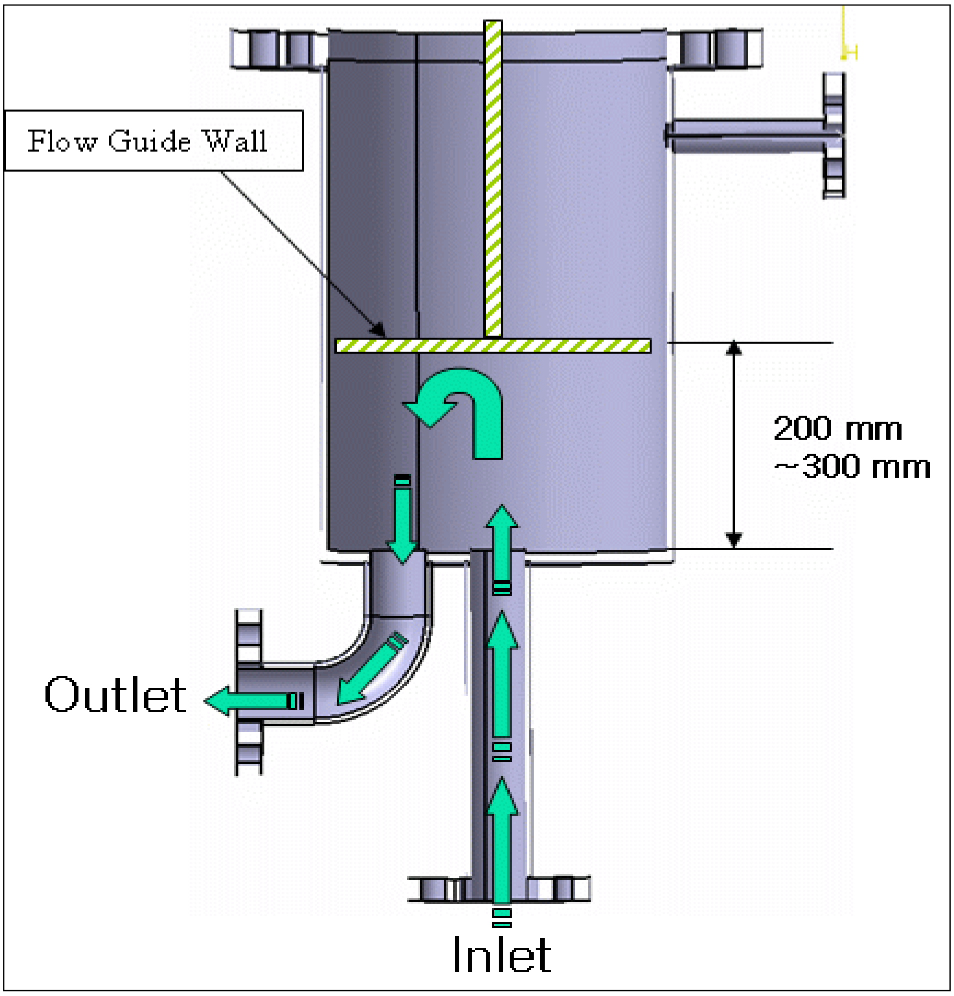

Figure A-12: 3D View of component #12 pipe with tee and elbow

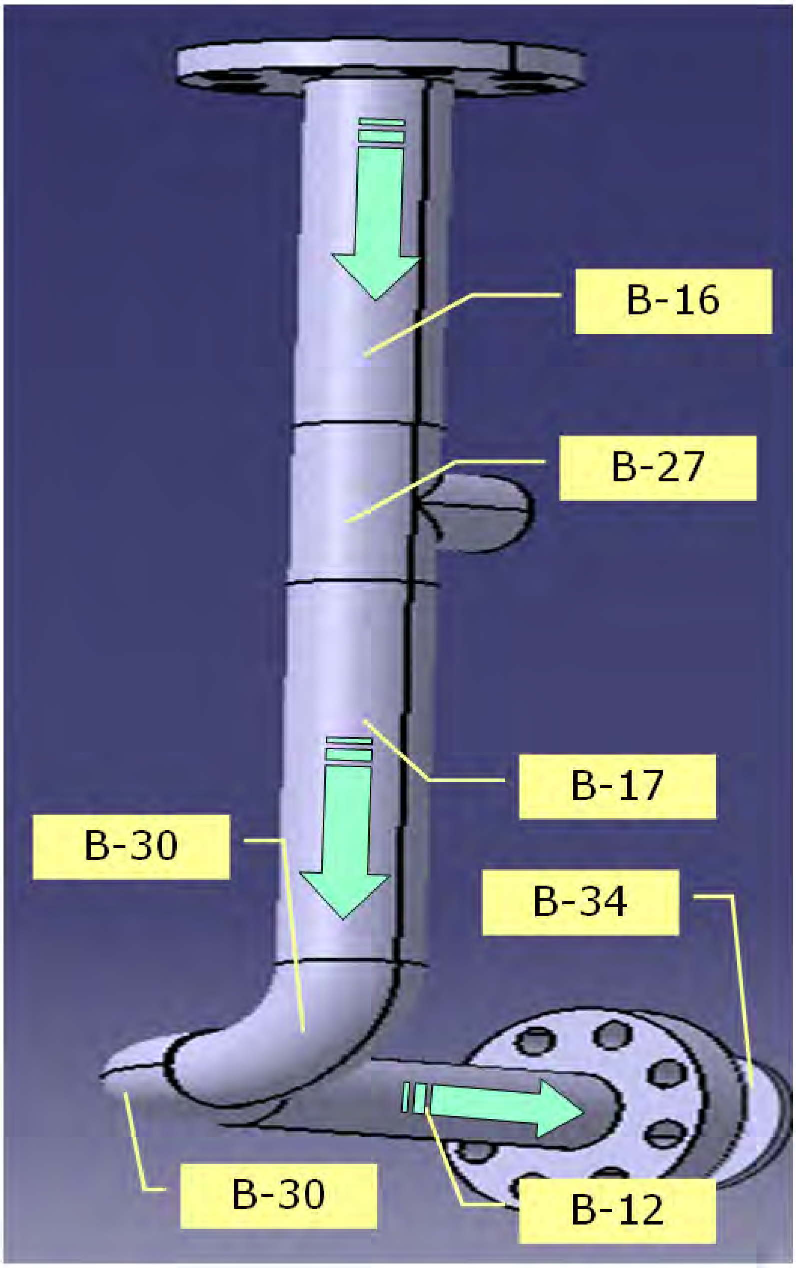

Figure A-14: 3D View of component #14 pipe with tee

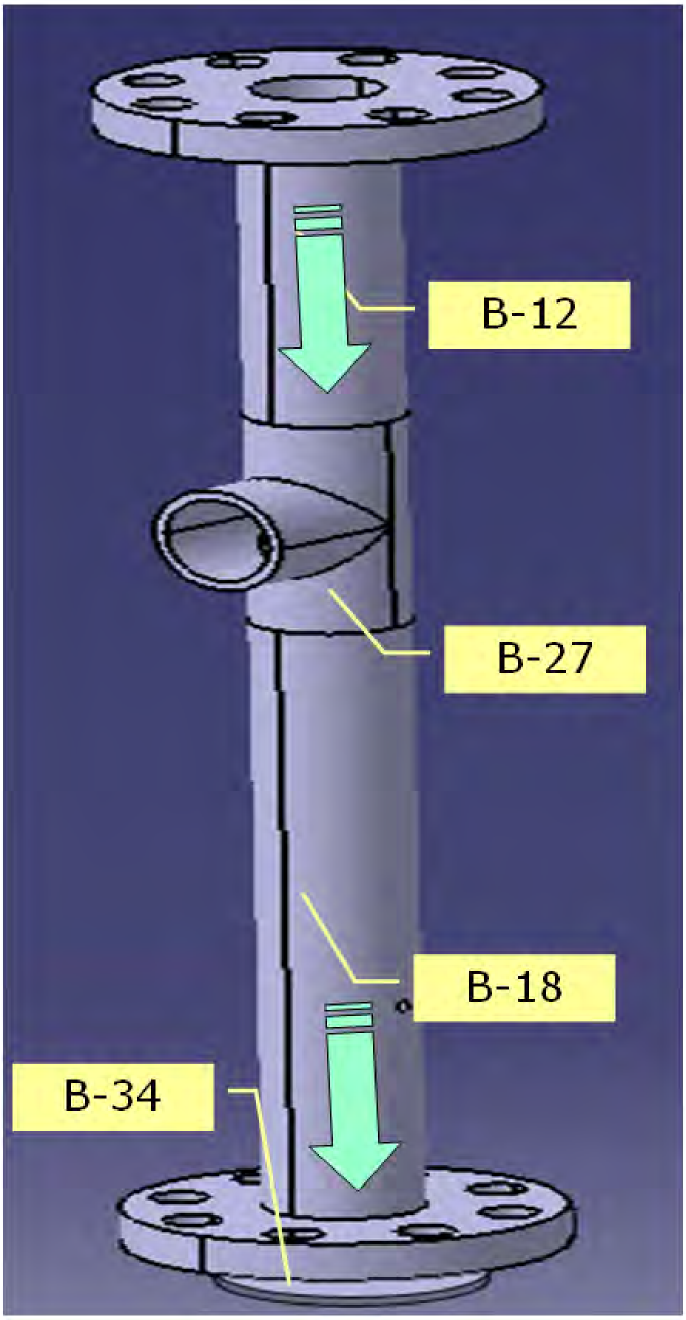

Figure A-15: 3D View of component #15 heat exchanger

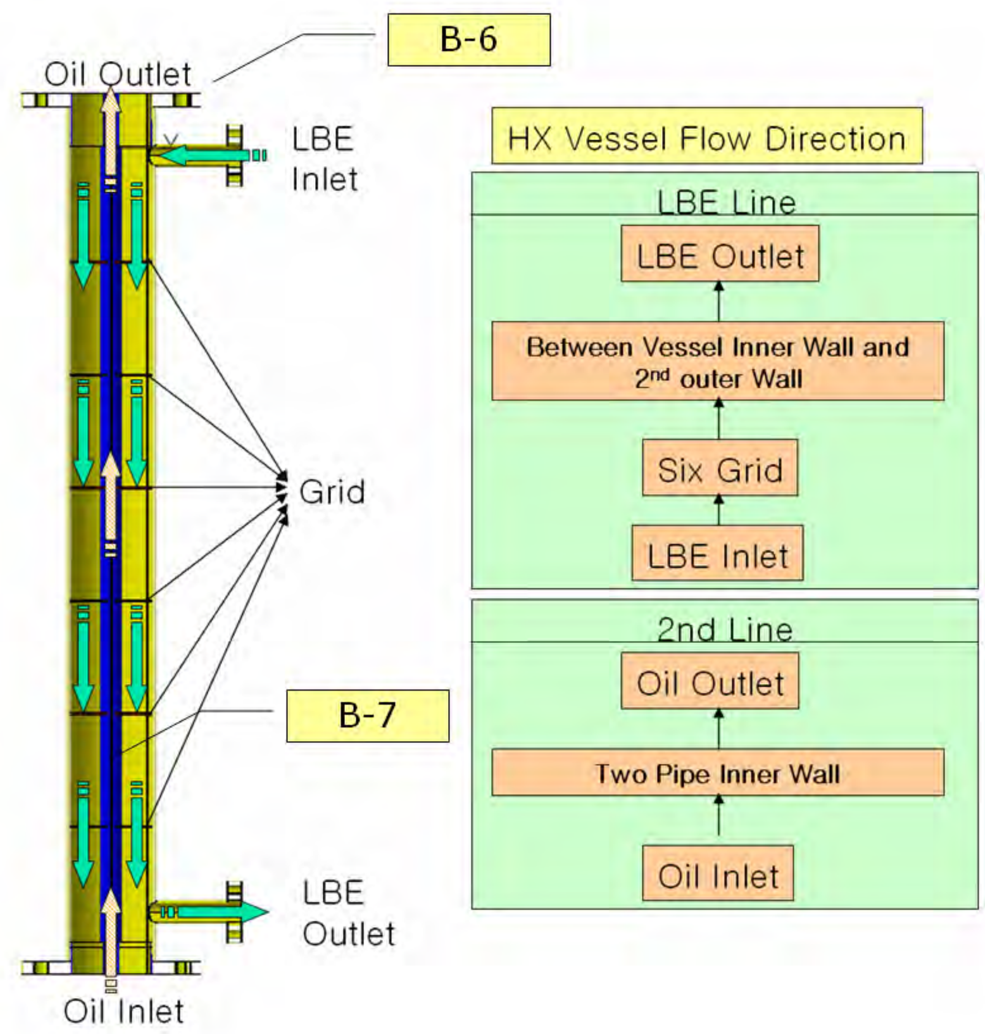

Figure A-16: 3D View of component #16 pipe with tee and elbow

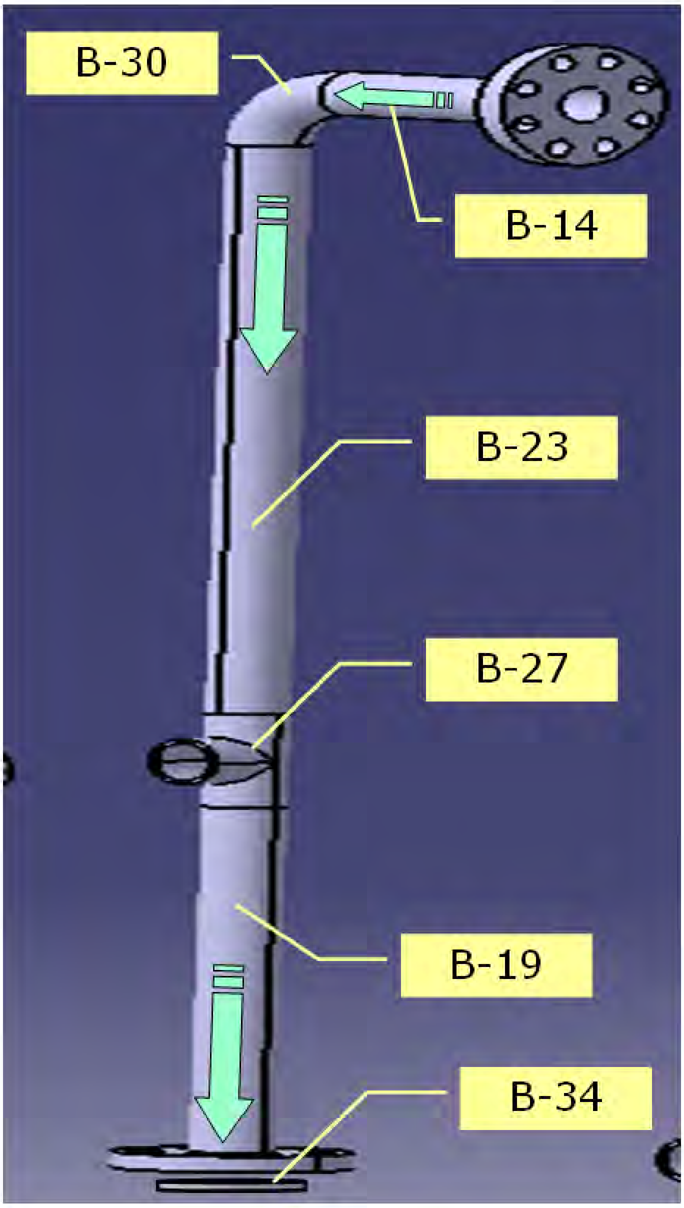

Figure A-18: 3D View of component #18 pipe with tee

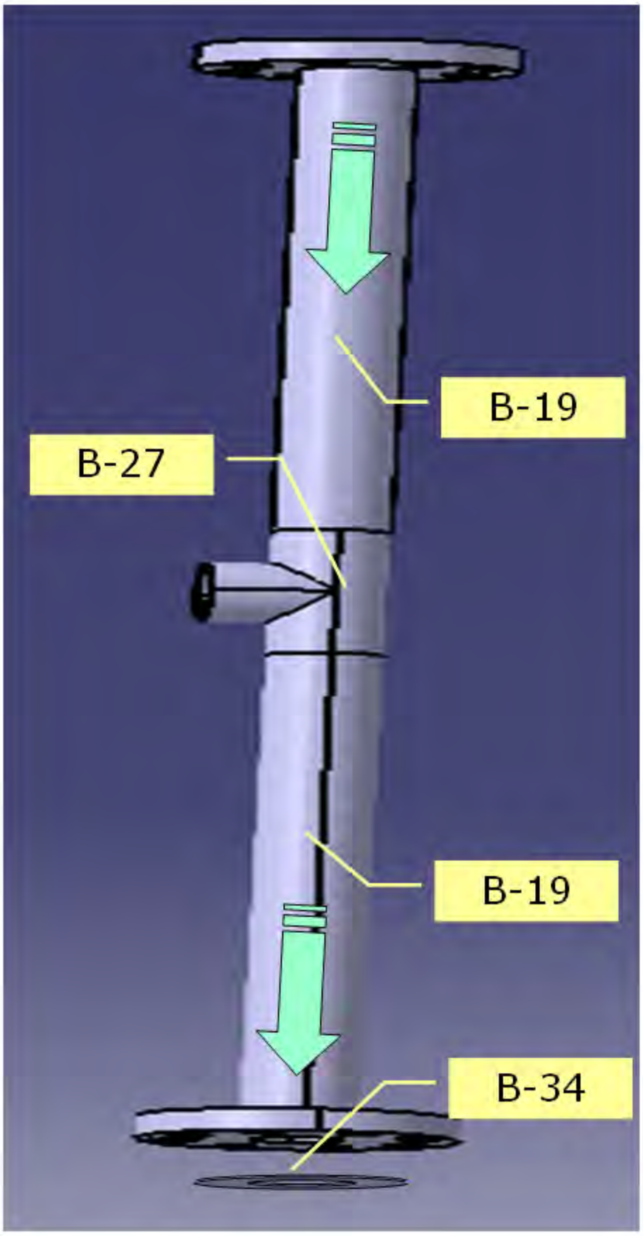

Figure A-20: 3D View of component #20 pipe with tee and elbow

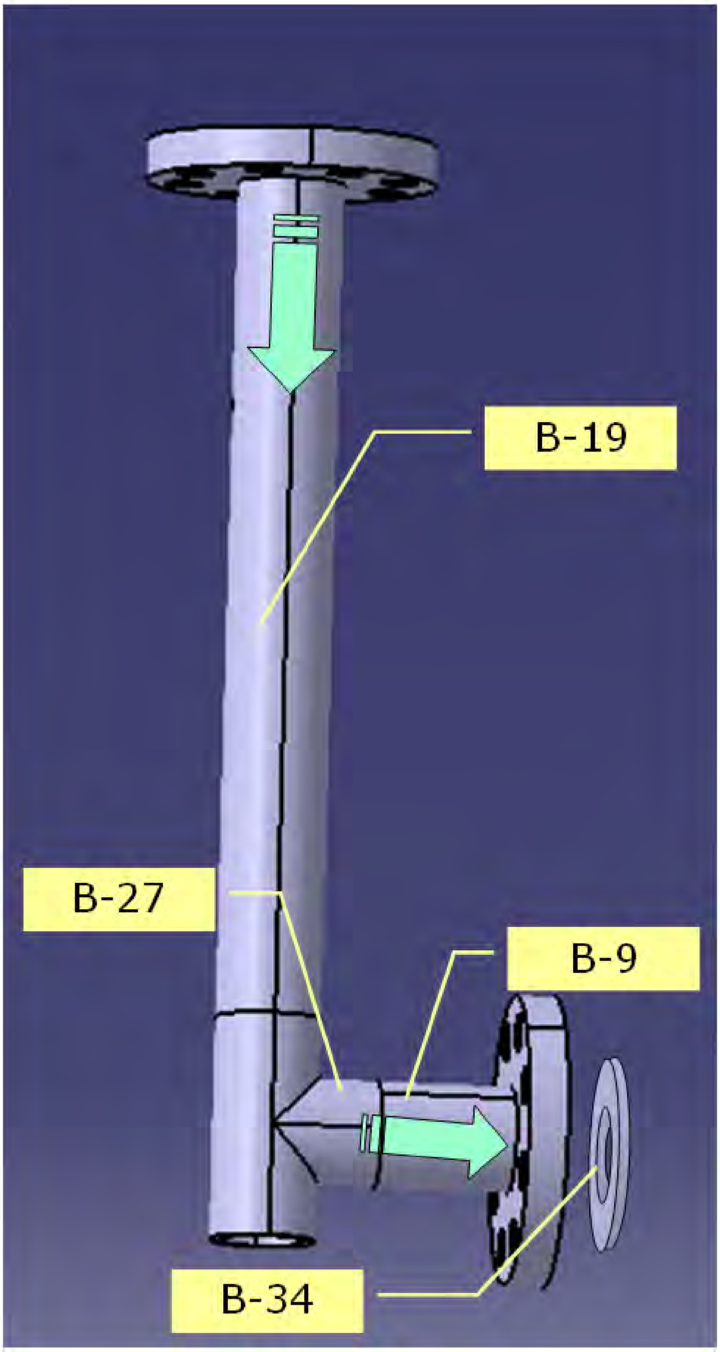

Figure A-21: 3D View of component #21 pipe with elbow

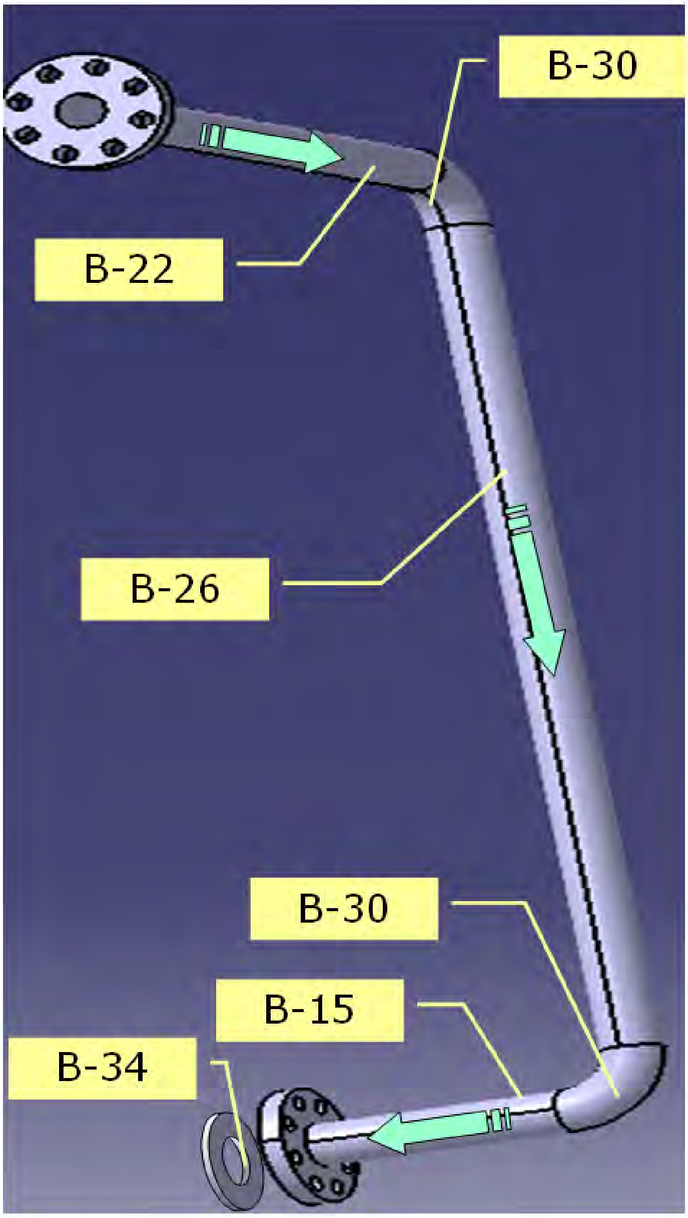

Figure A-23: 3D View of component #23 pipe with tee and elbow

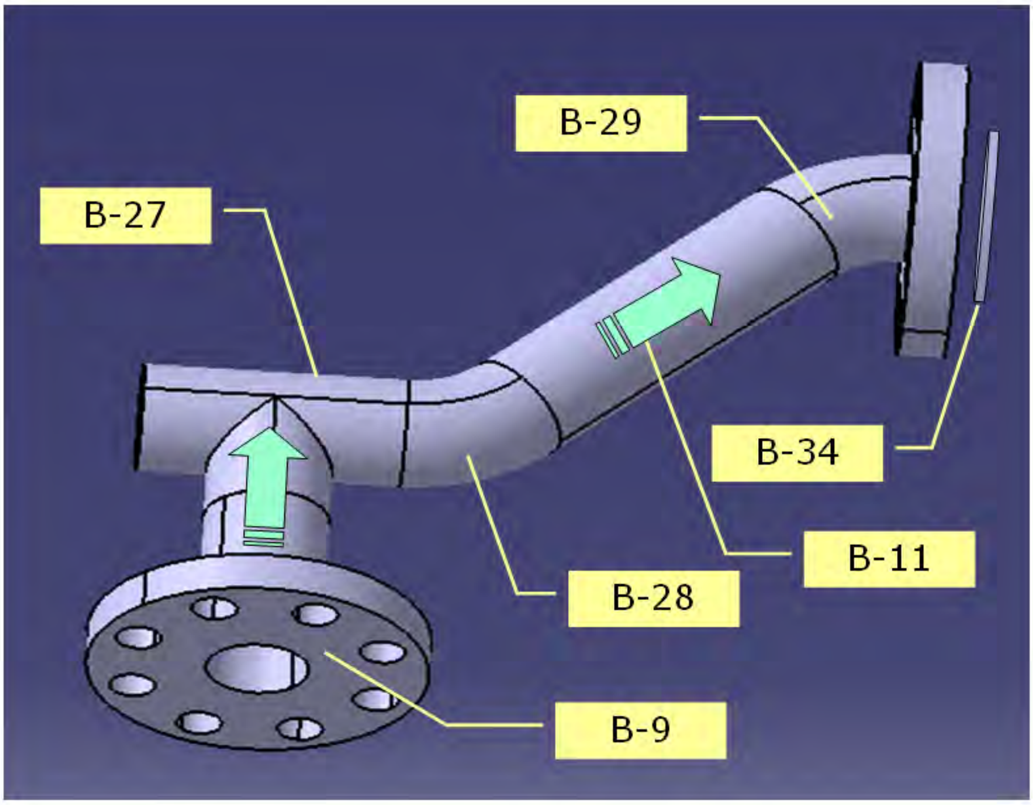

Figure A-24: 3D View of component #24 pipe with tee, elbow and valve

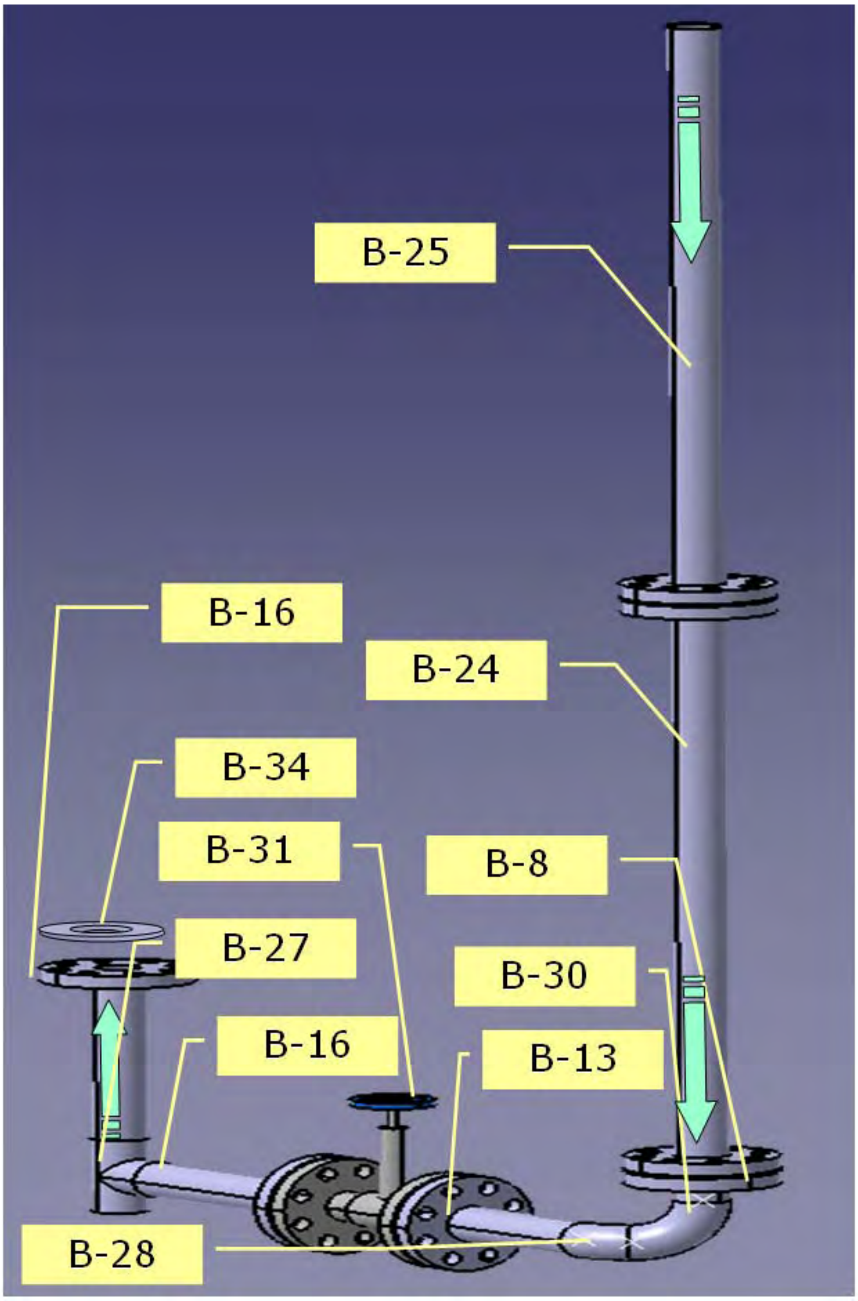

Figure A-25: 3D View of component #25 core

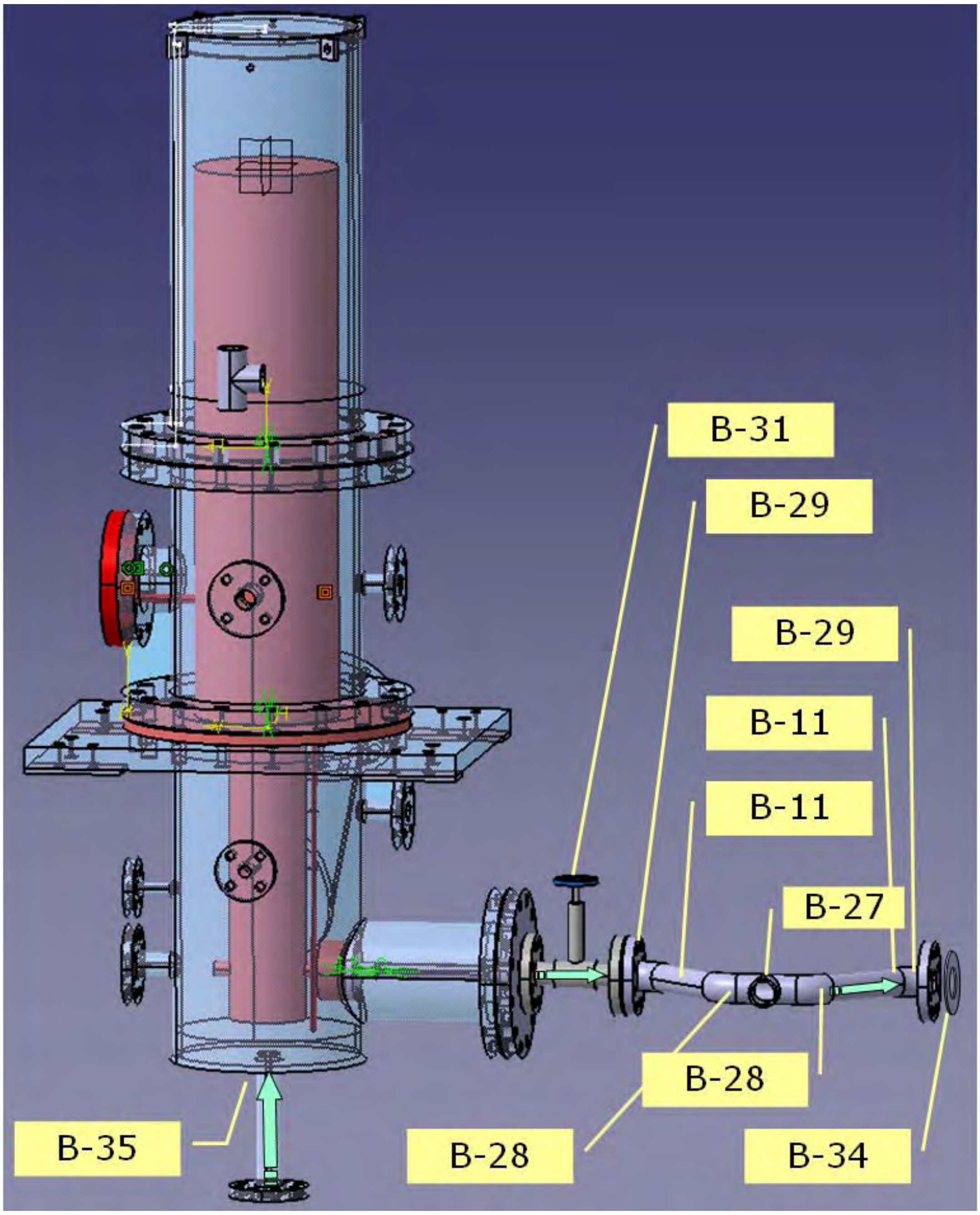

Appendix B

(Part Drawings and Data)

Figure B-1

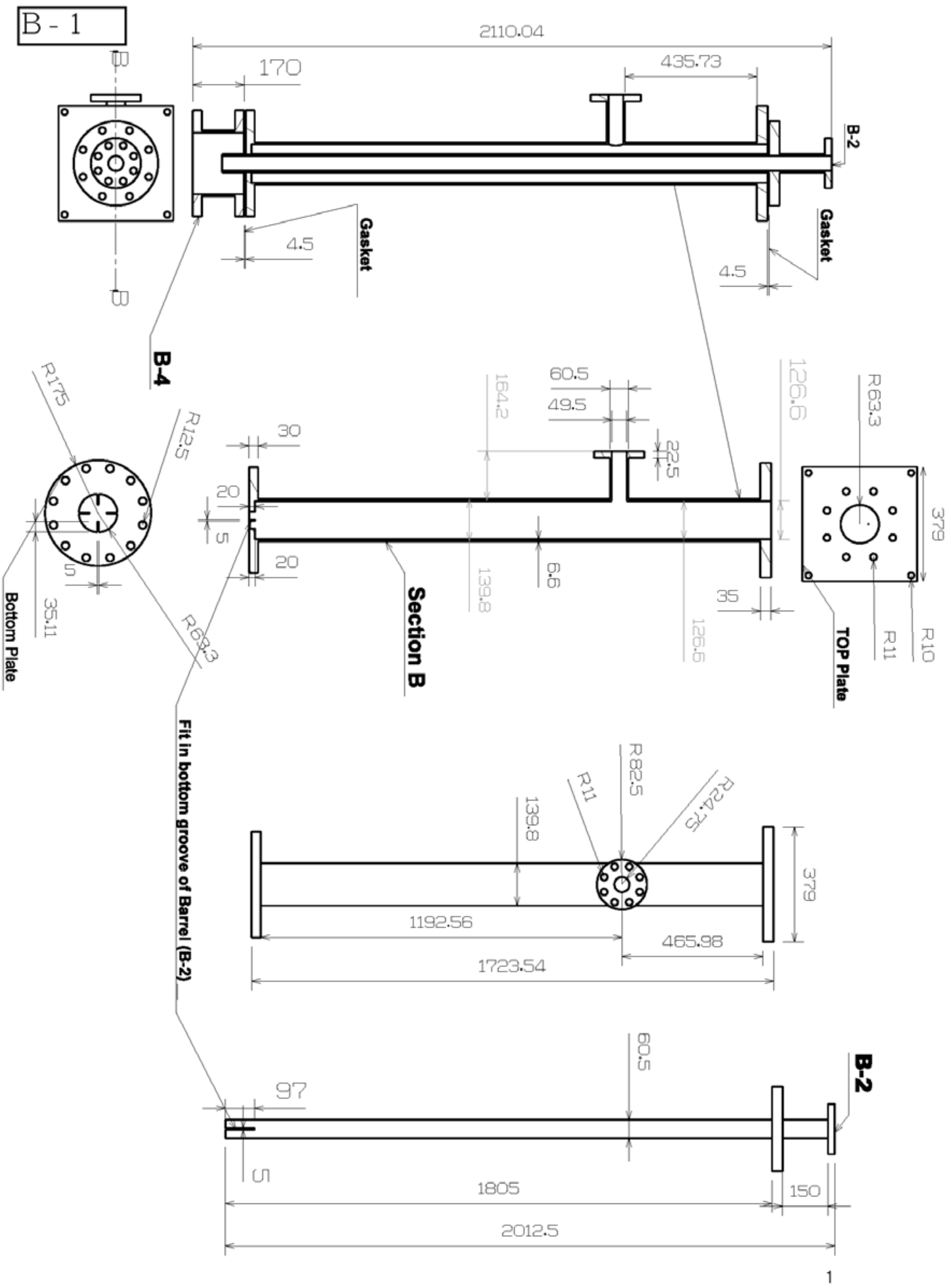
B - 1
2110.04
170
435.73
B-2
Gasket
4.5
Gasket
4.5
B-4
R175
R12.5
30
20
5
20
60.5
49.5
164.2
22.5
126.6
R63.3
379
139.8
6.6
Section B
35
126.6
R11
R10
TOP Plate
Bottom Plate
35.11
5
R63.3
Fit in bottom groove of Barrel (B-2)
R82.5
R11
R24.75
139.8
379
1192.56
465.98
1723.54
97
60.5
B-2
5
1805
150
2012.5
1

Figure B-2

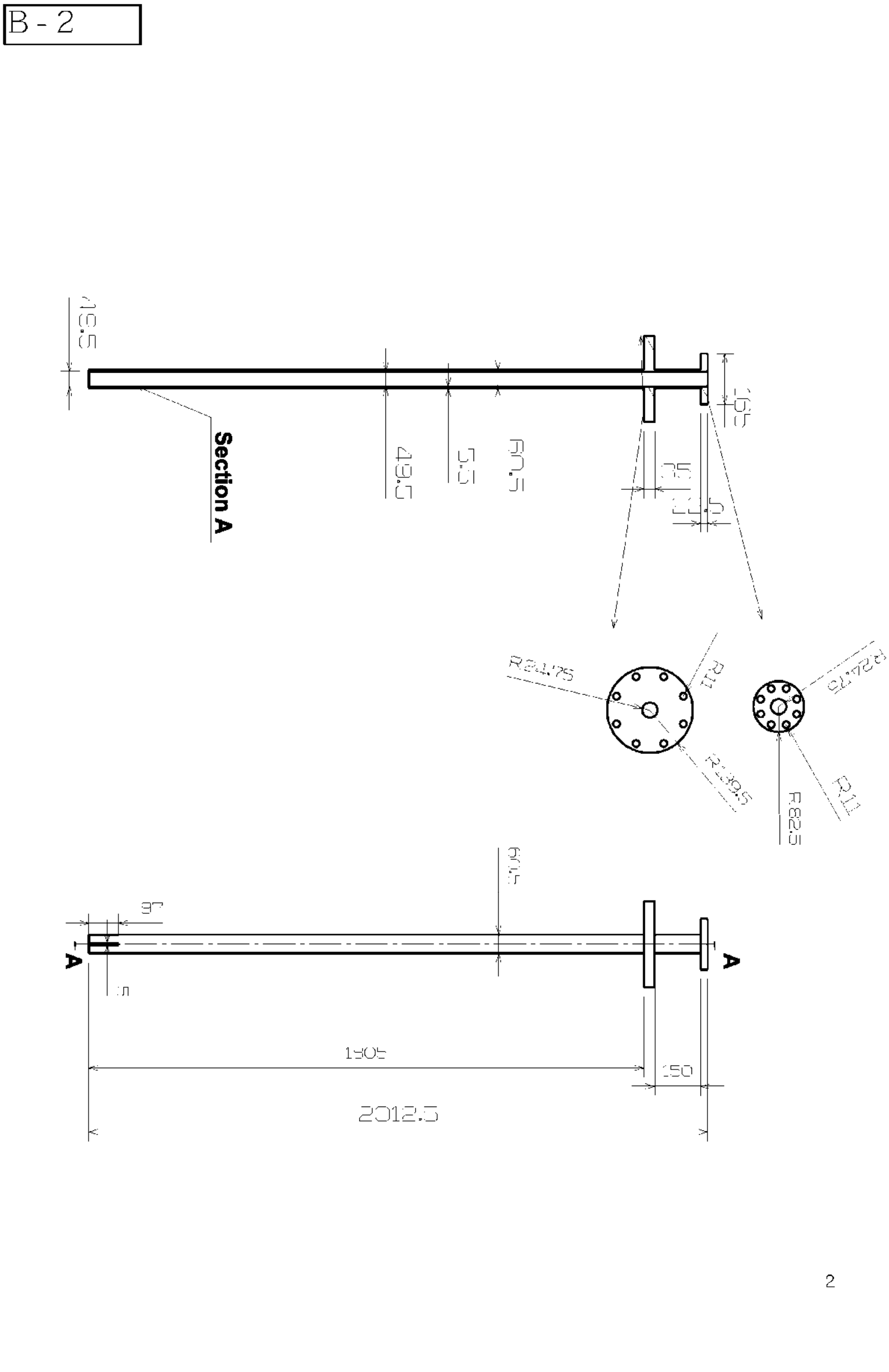

Figure B-3

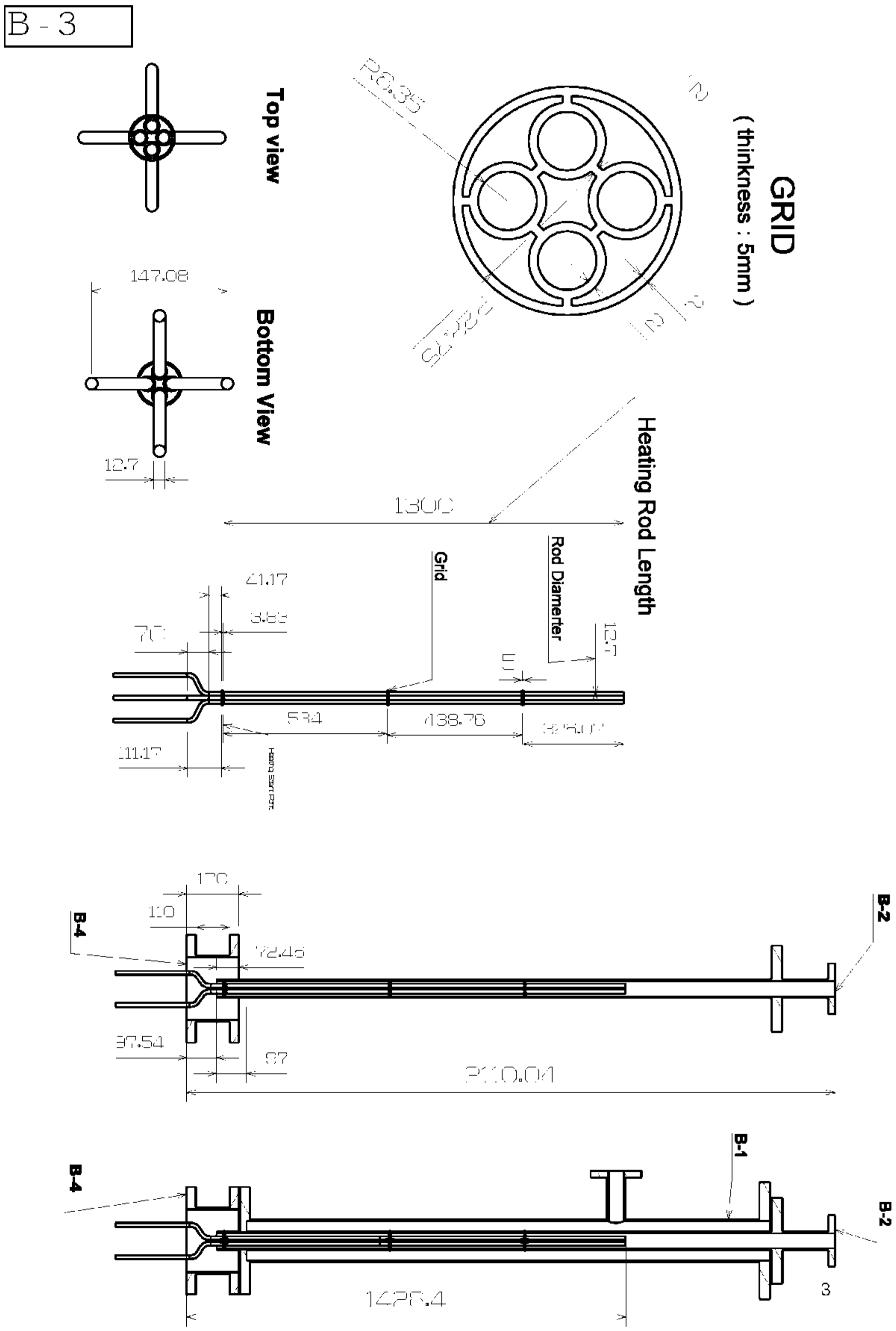
B - 3
Top view
Bottom View
GRID
(thinkness : 5mm)
R6.35
147.08
12.7
1300
Heating Rod Length
Rod Diamerter
Grid
41.17
70
534
438.76
111.17
170
110
72.46
37.54
87
2110.04
B-4
B-2
B-1
1426.4
3

Figure B-4

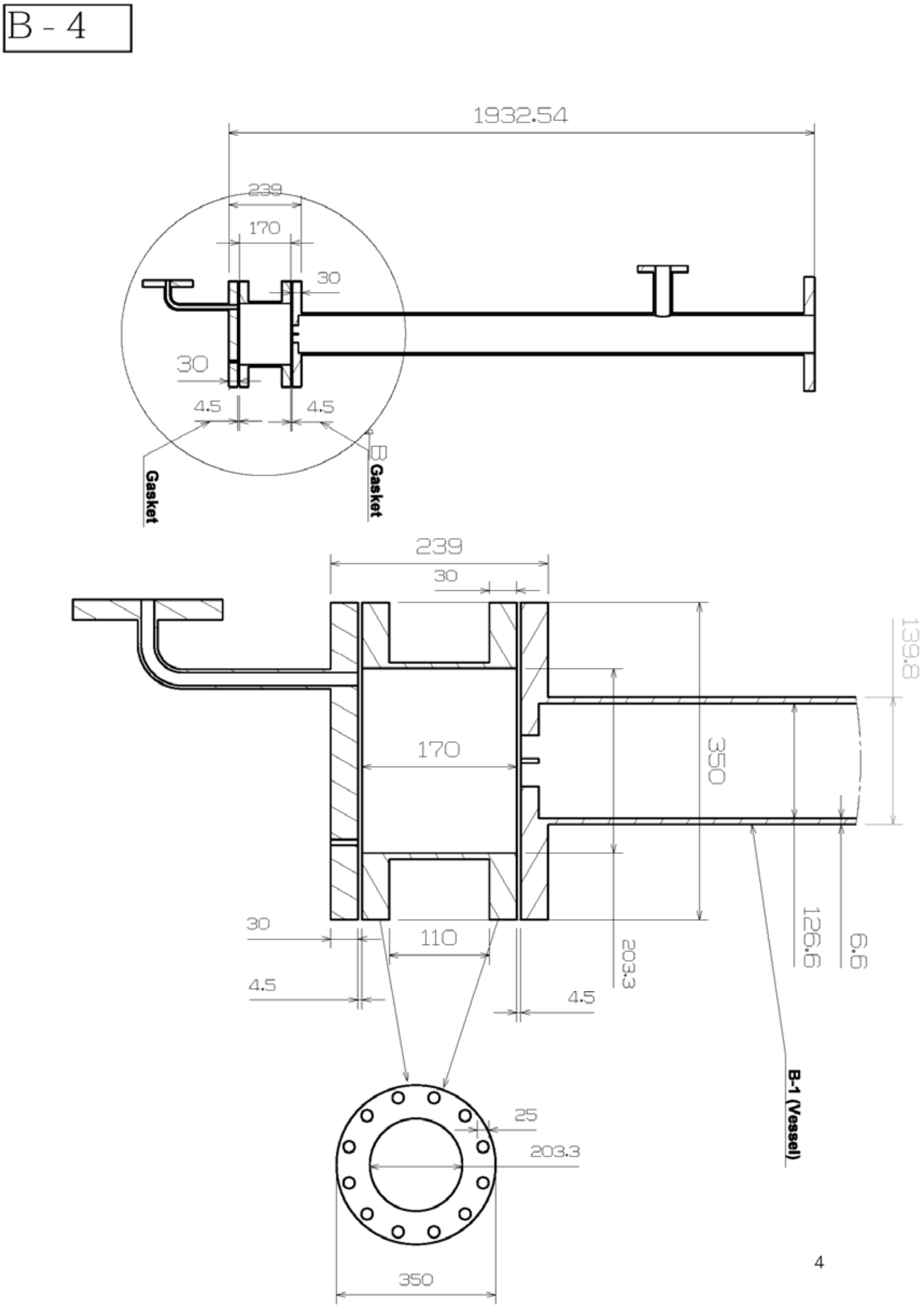
B - 4
1932.54
239
170
30
30
4.5
4.5
B
Gasket
Gasket
239
30
139.8
170
350
30
110
4.5
4.5
203.3
126.6
6.6
B-1 (Vessel)
25
203.3
350
4

Figure B-5

B - 5

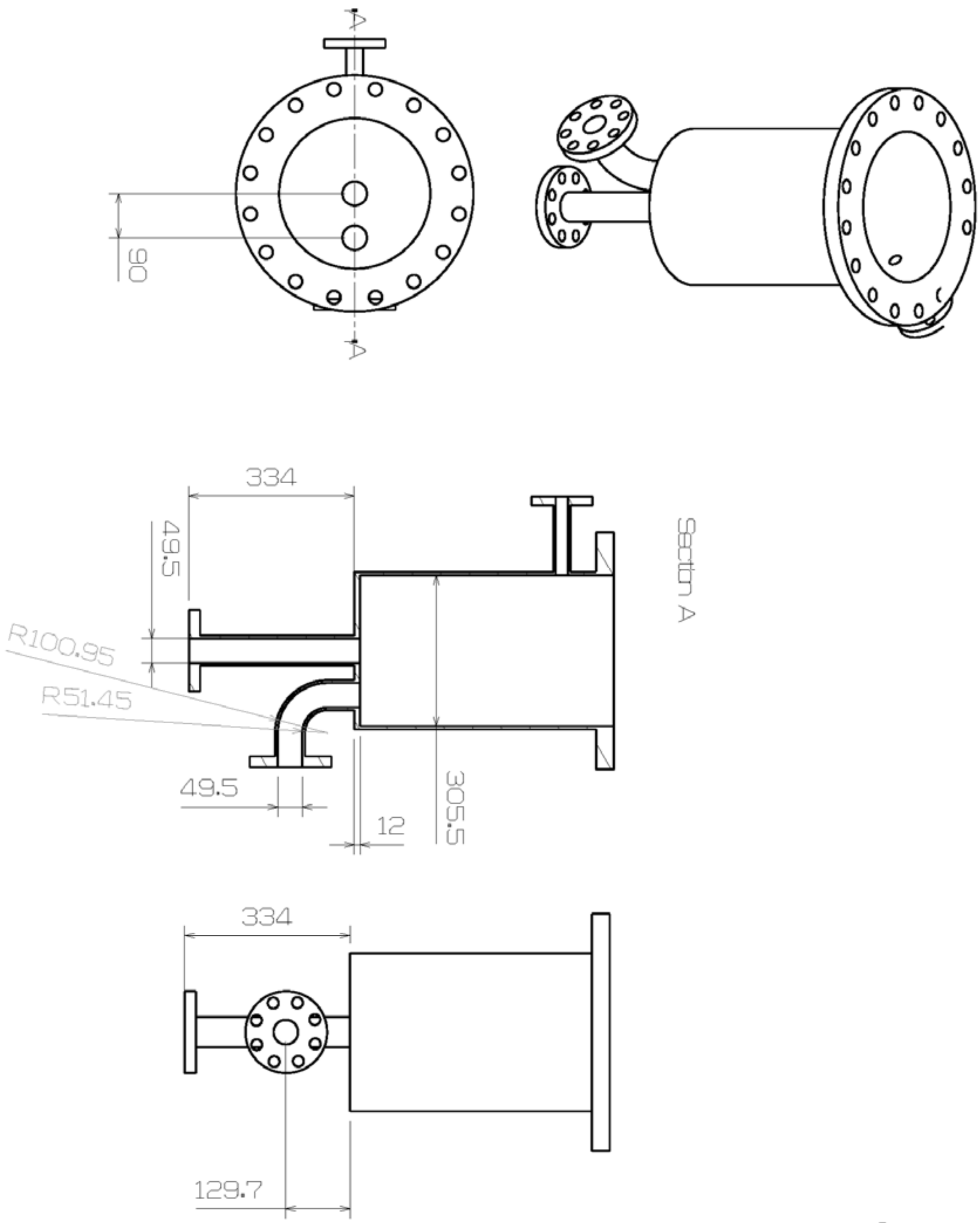

5

Figure B-6

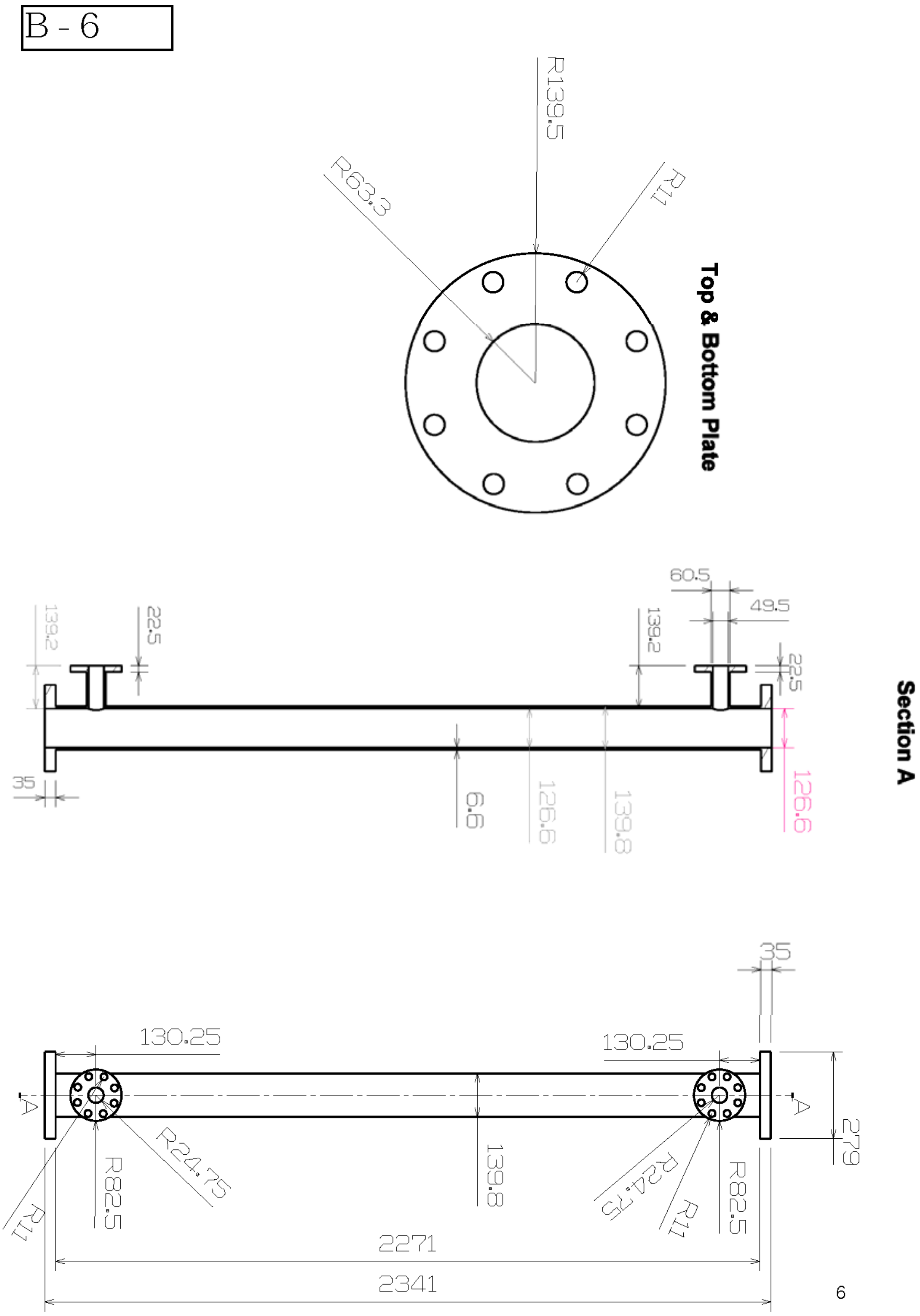
B - 6
R139.5
R63.3
R11
Top & Bottom Plate
60.5
49.5
139.2
22.5
139.2
22.5
35
6.6
126.6
139.8
126.6
Section A
35
130.25
130.25
A
A
279
R11
R82.5
R24.75
139.8
R24.75
R11
R82.5
2271
2341
6

Figure B-7

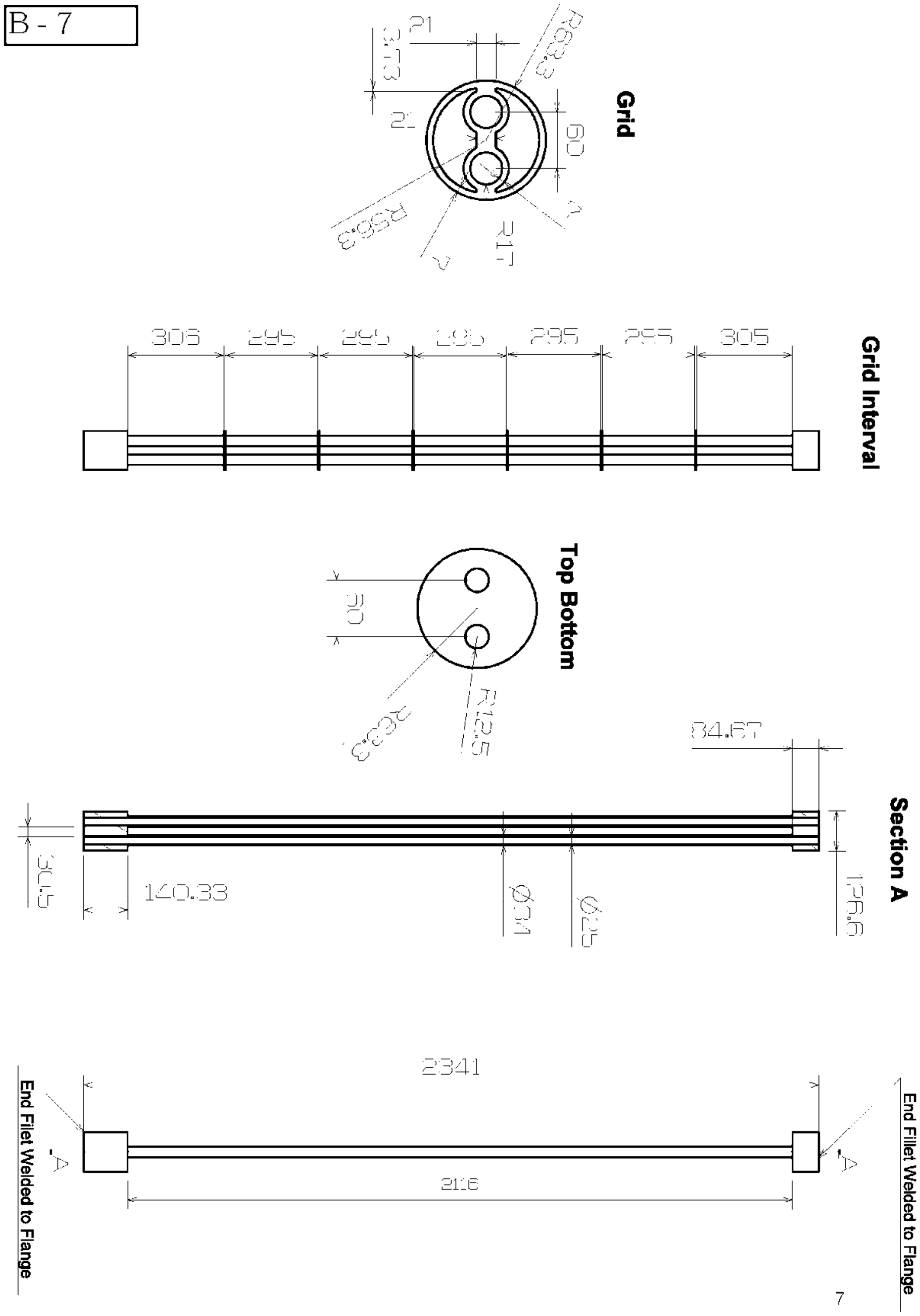
B - 7
Grid
Grid Interval
Top Bottom
Section A
End Filet Welded to Flange
End Fillet Welded to Flange
2341
7

Figure B-8

B - 8

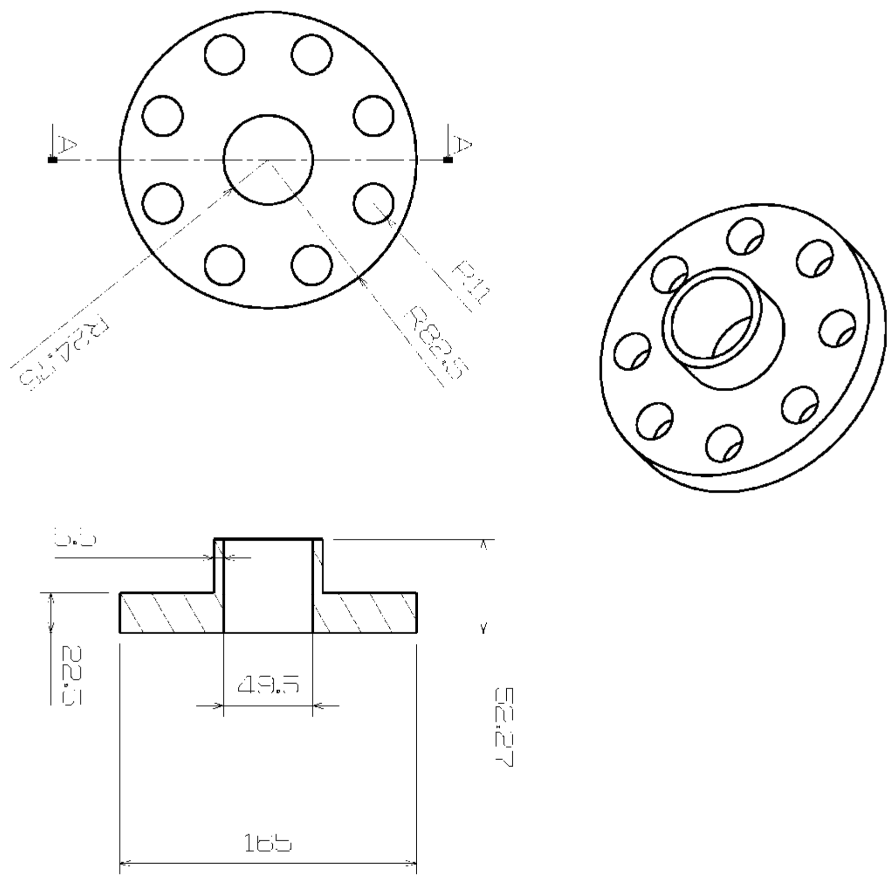

8

Figure B-9

B - 9

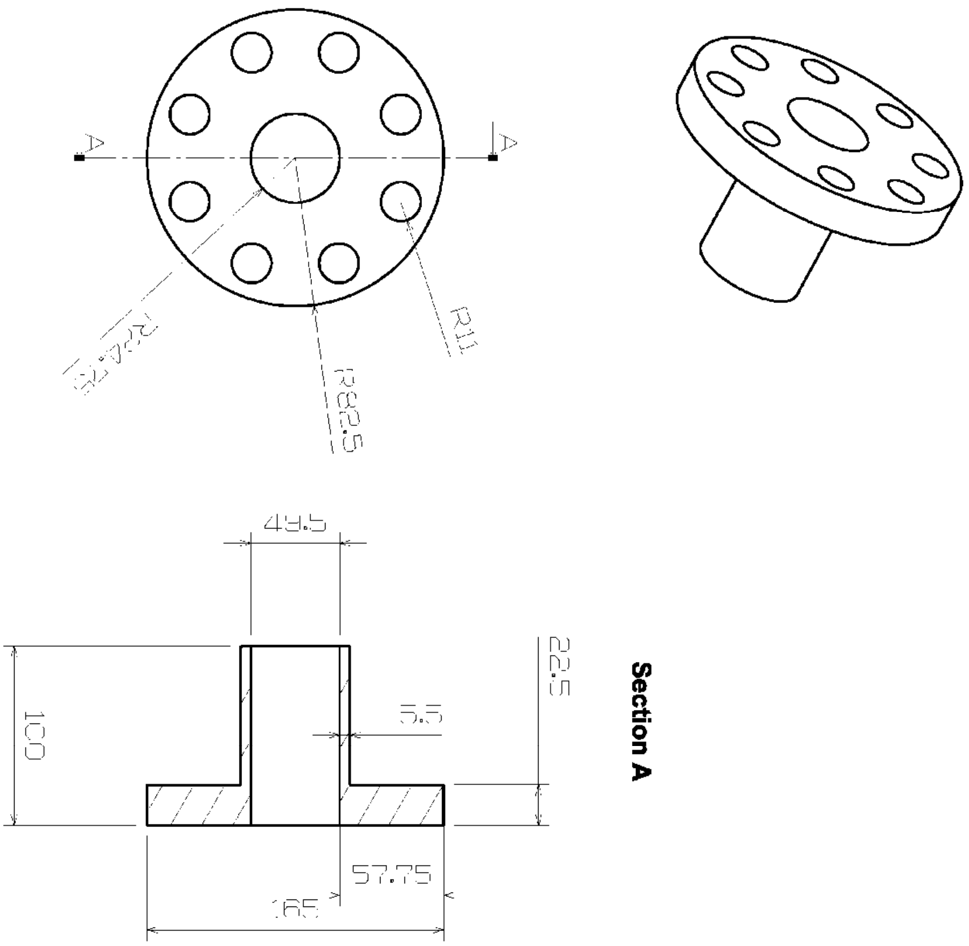

9

Figure B-10

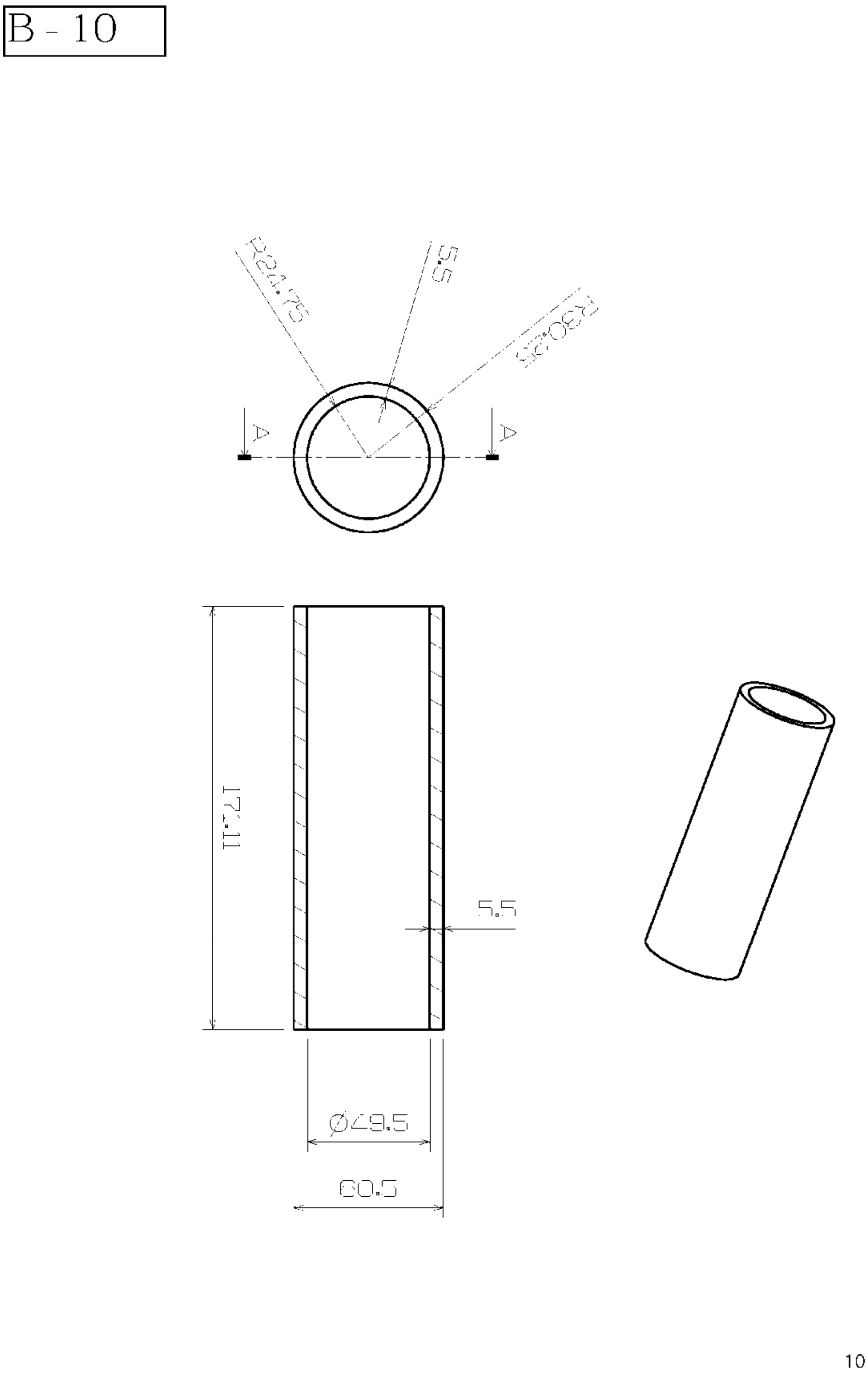

Figure B-11

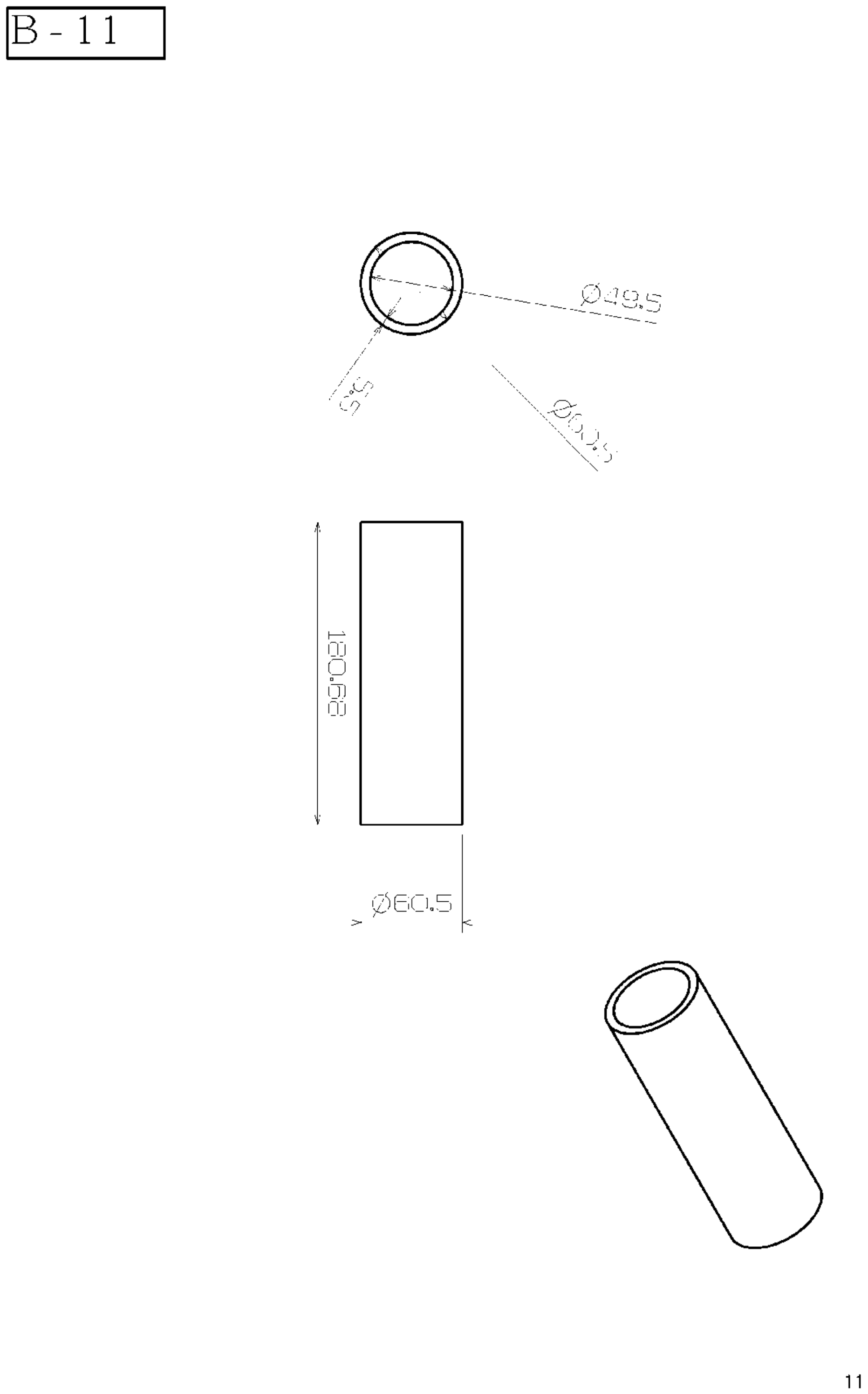

Figure B-12

B - 12

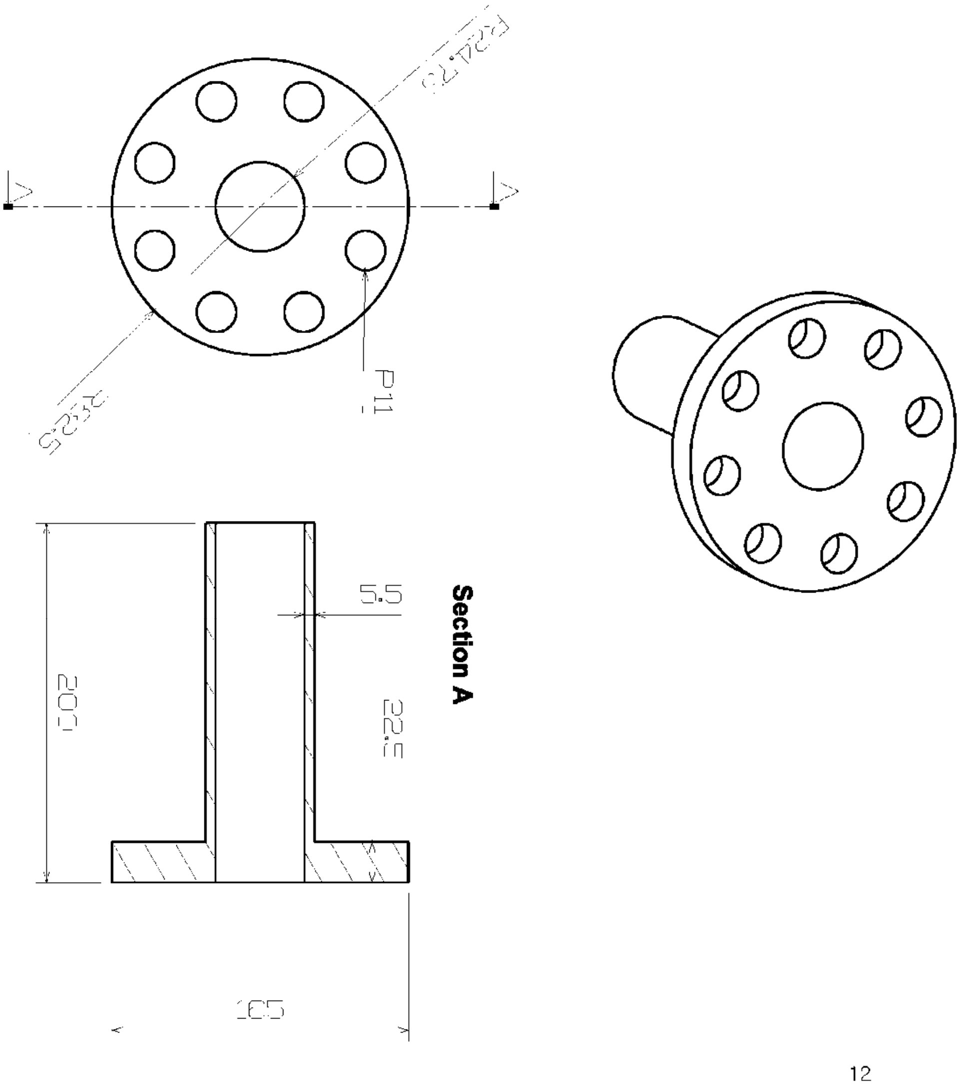

Figure B-13

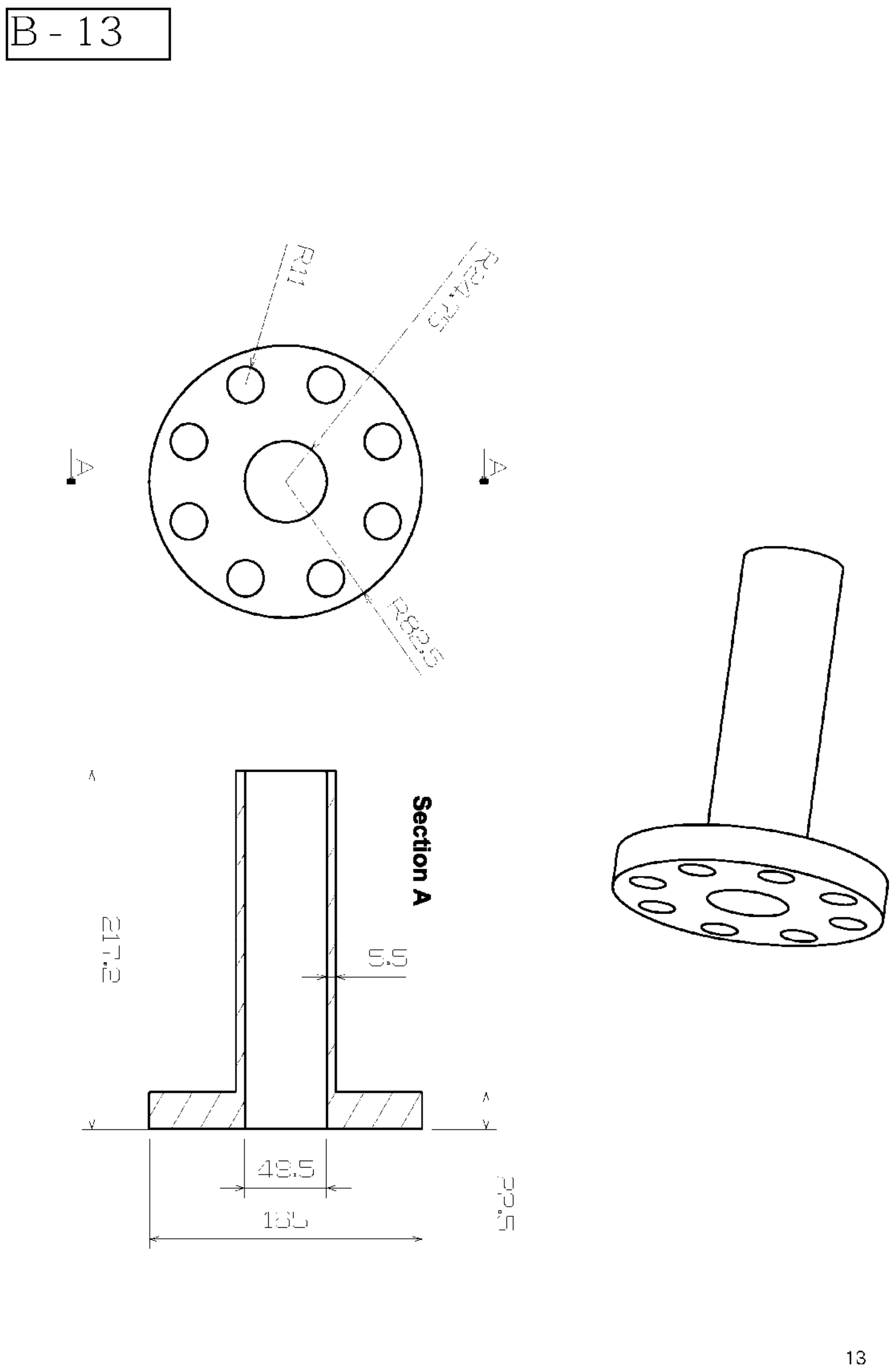

Figure B-14

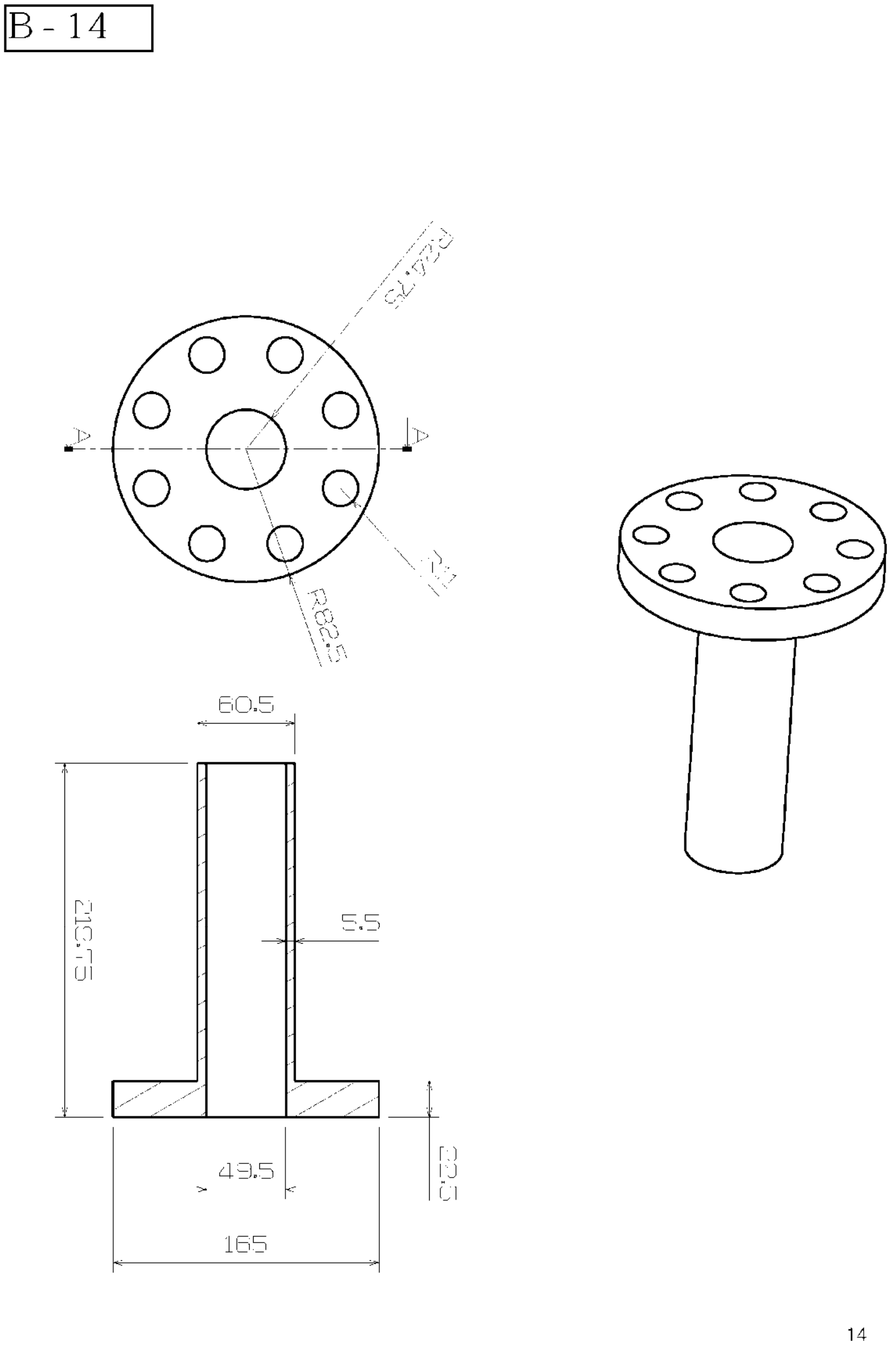

Figure B-15

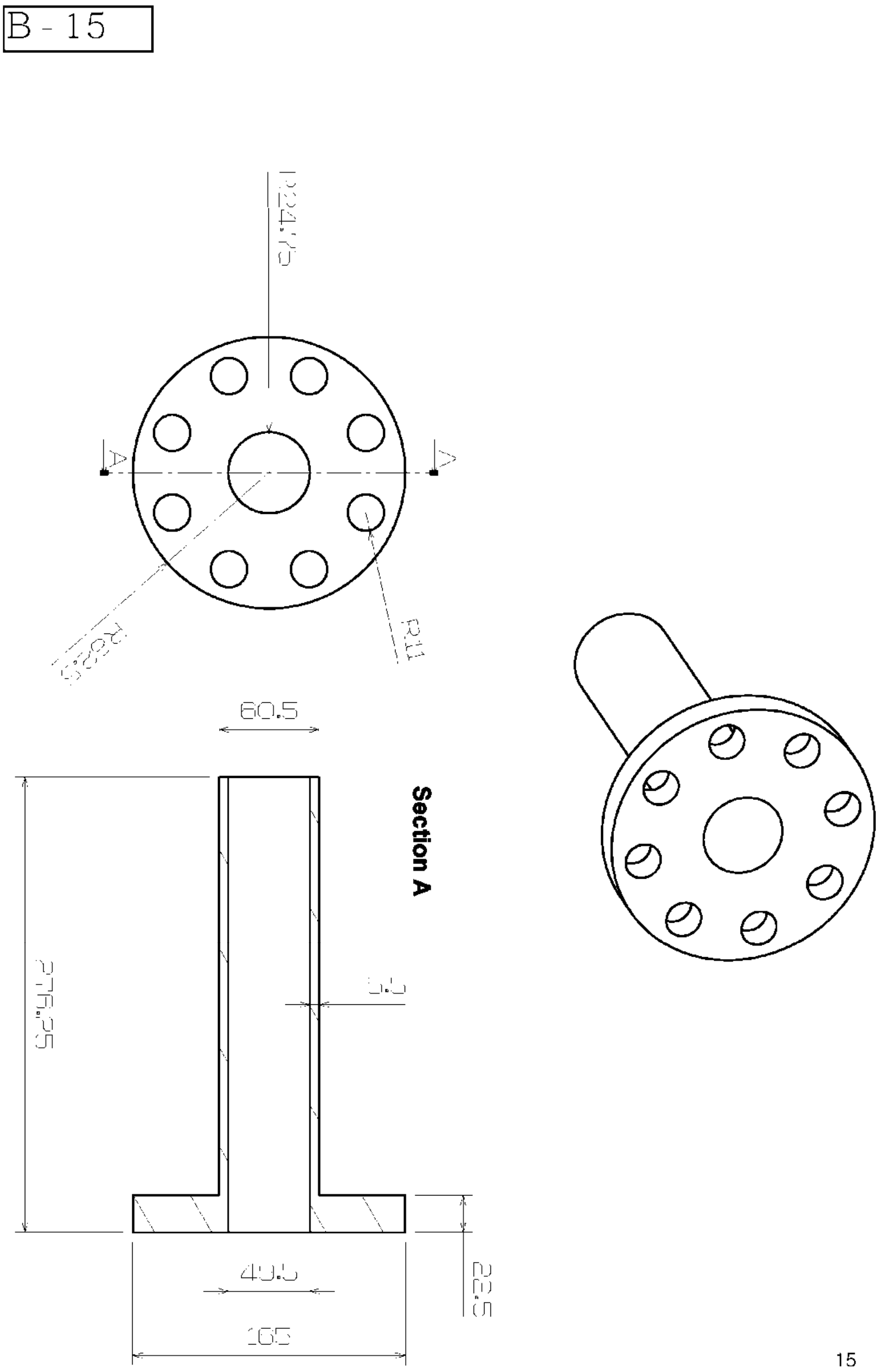

Figure B-16

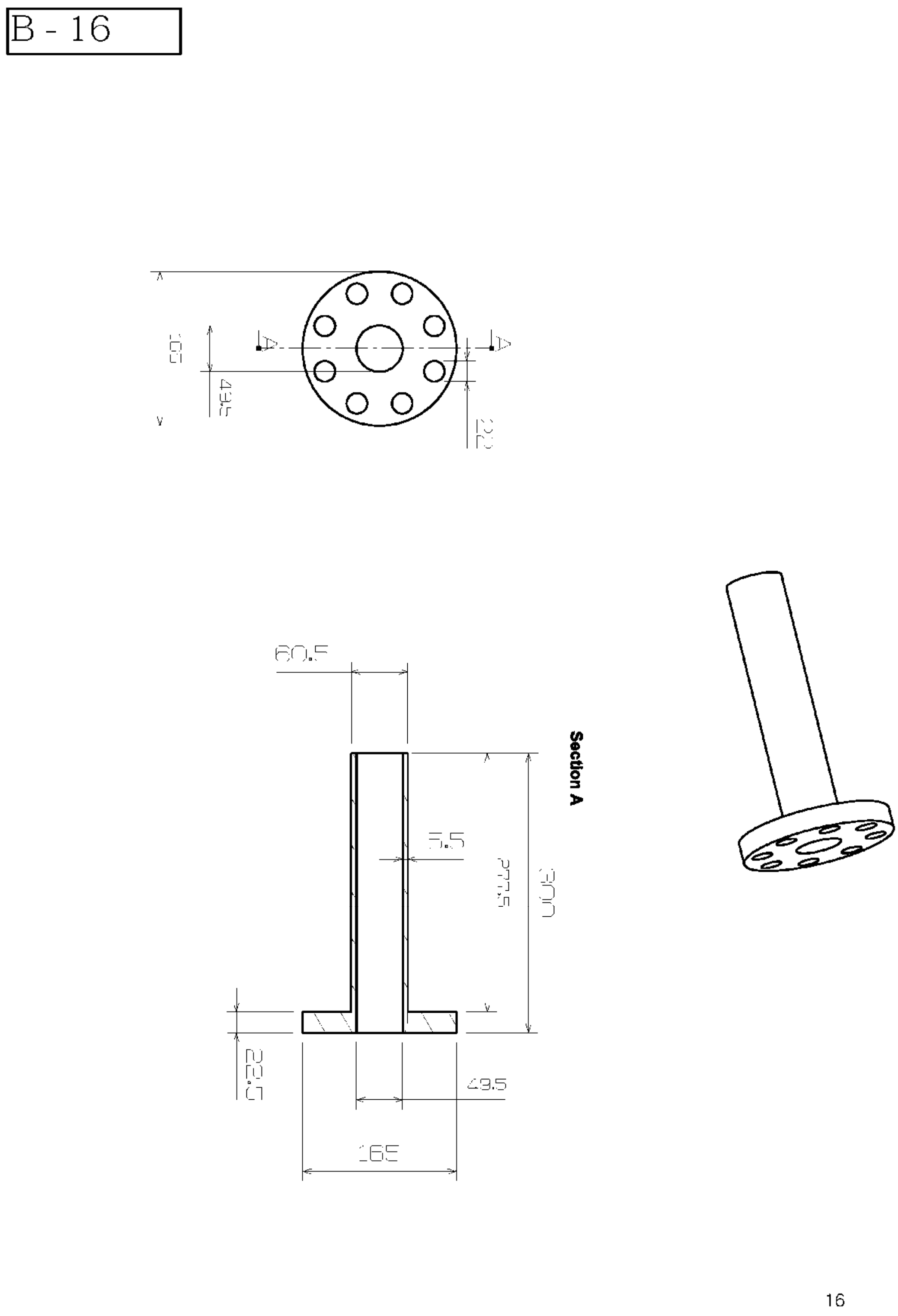

Figure B-17

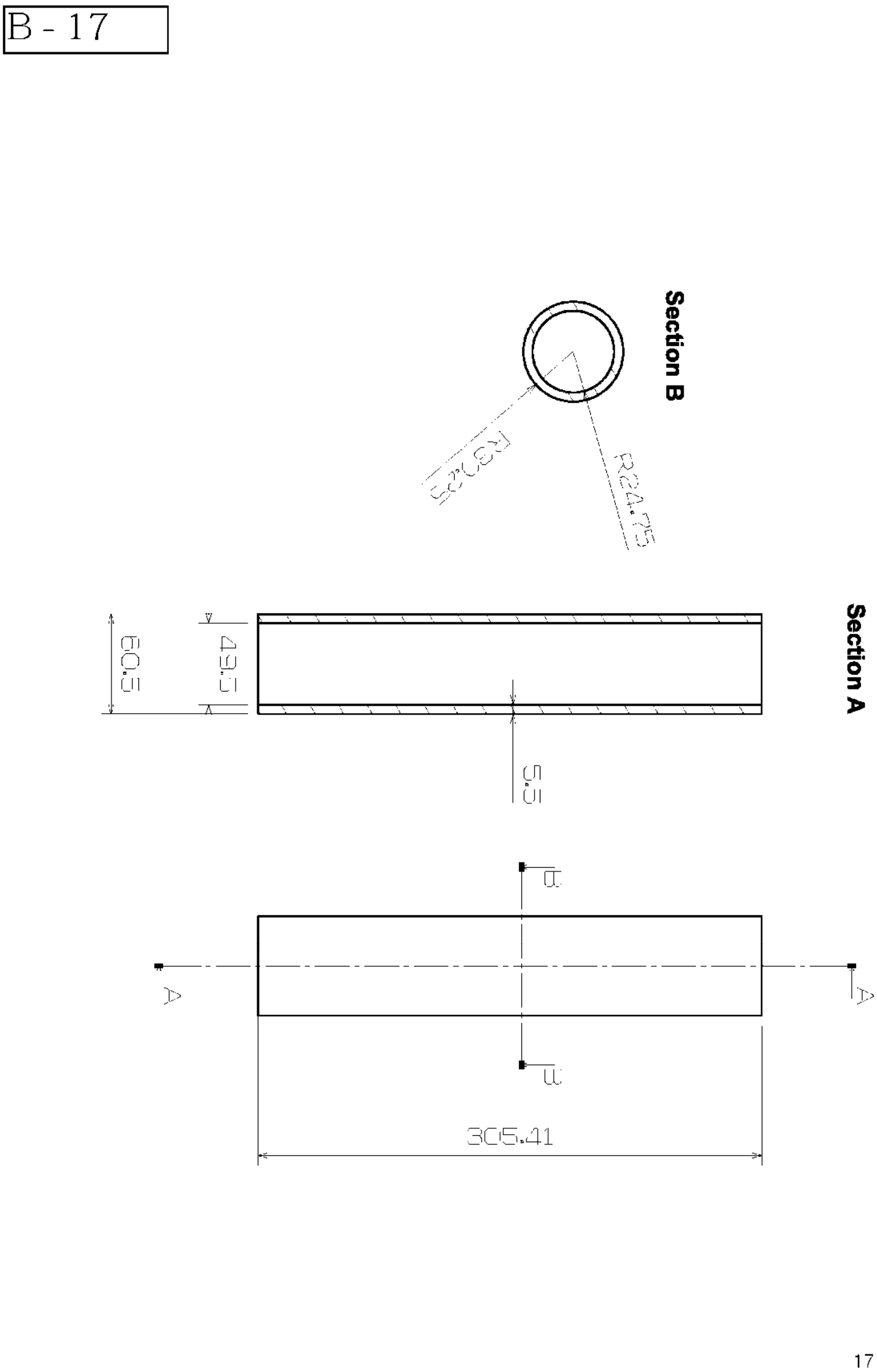

Figure B-18

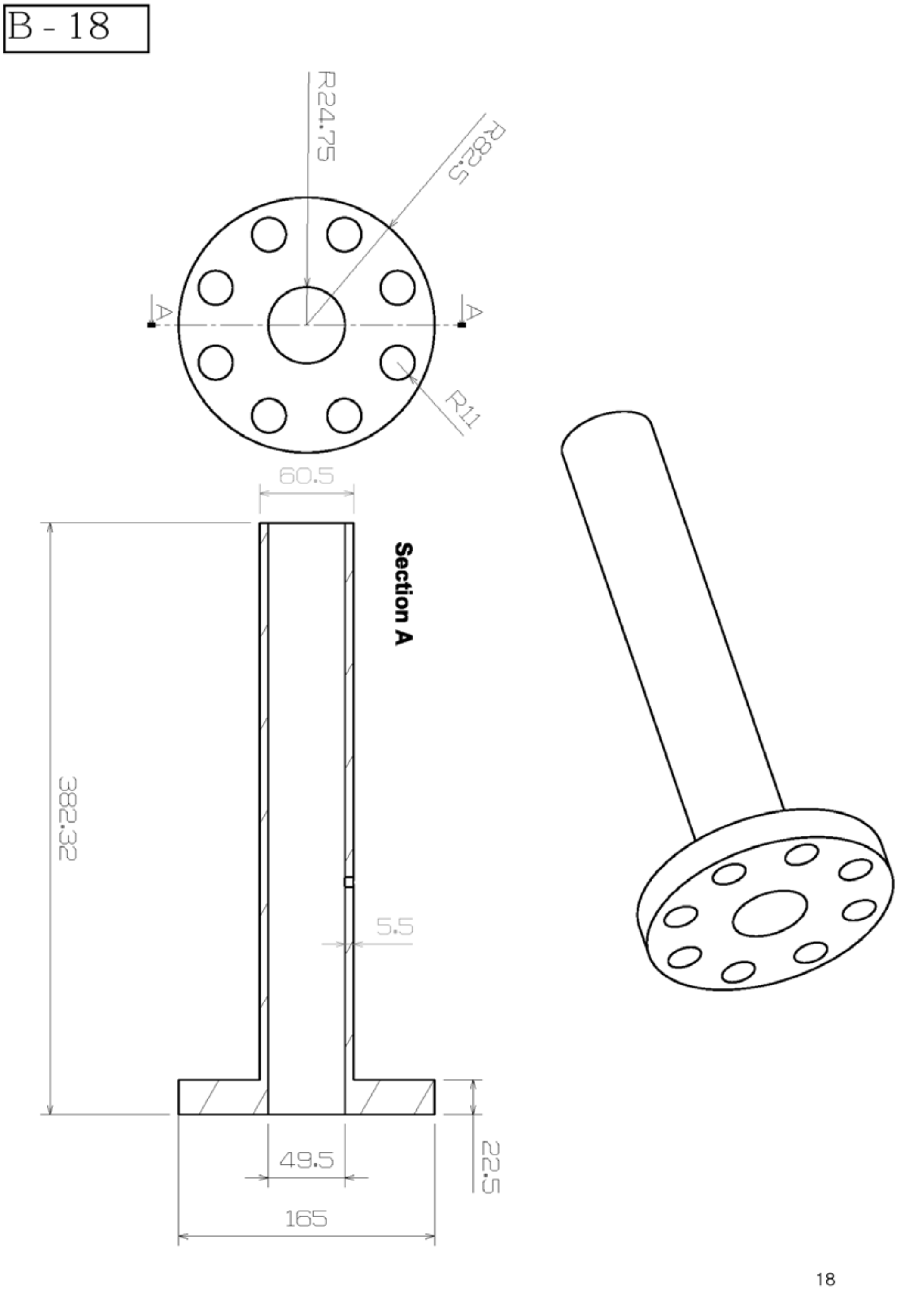

Figure B-19

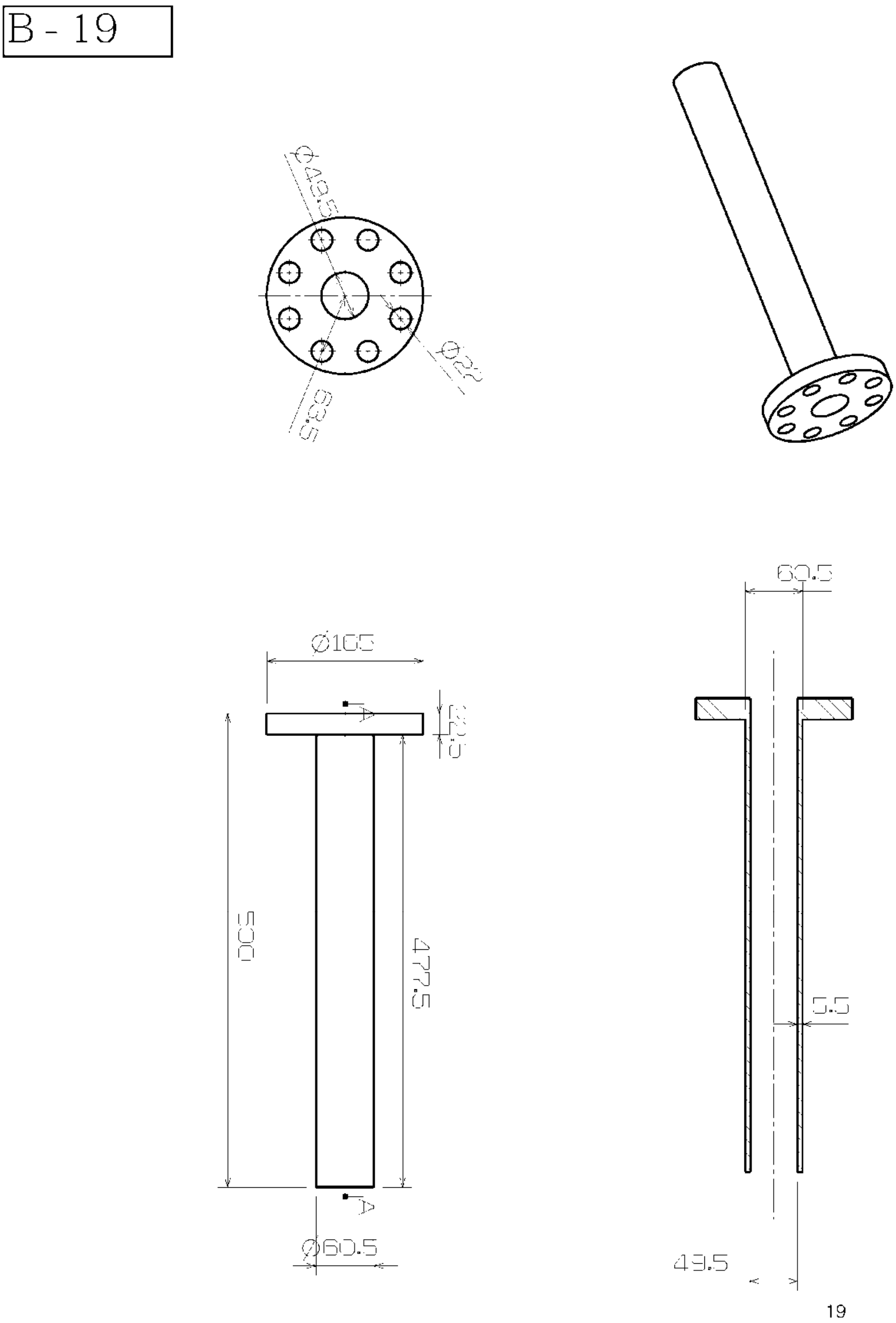

Figure B-20

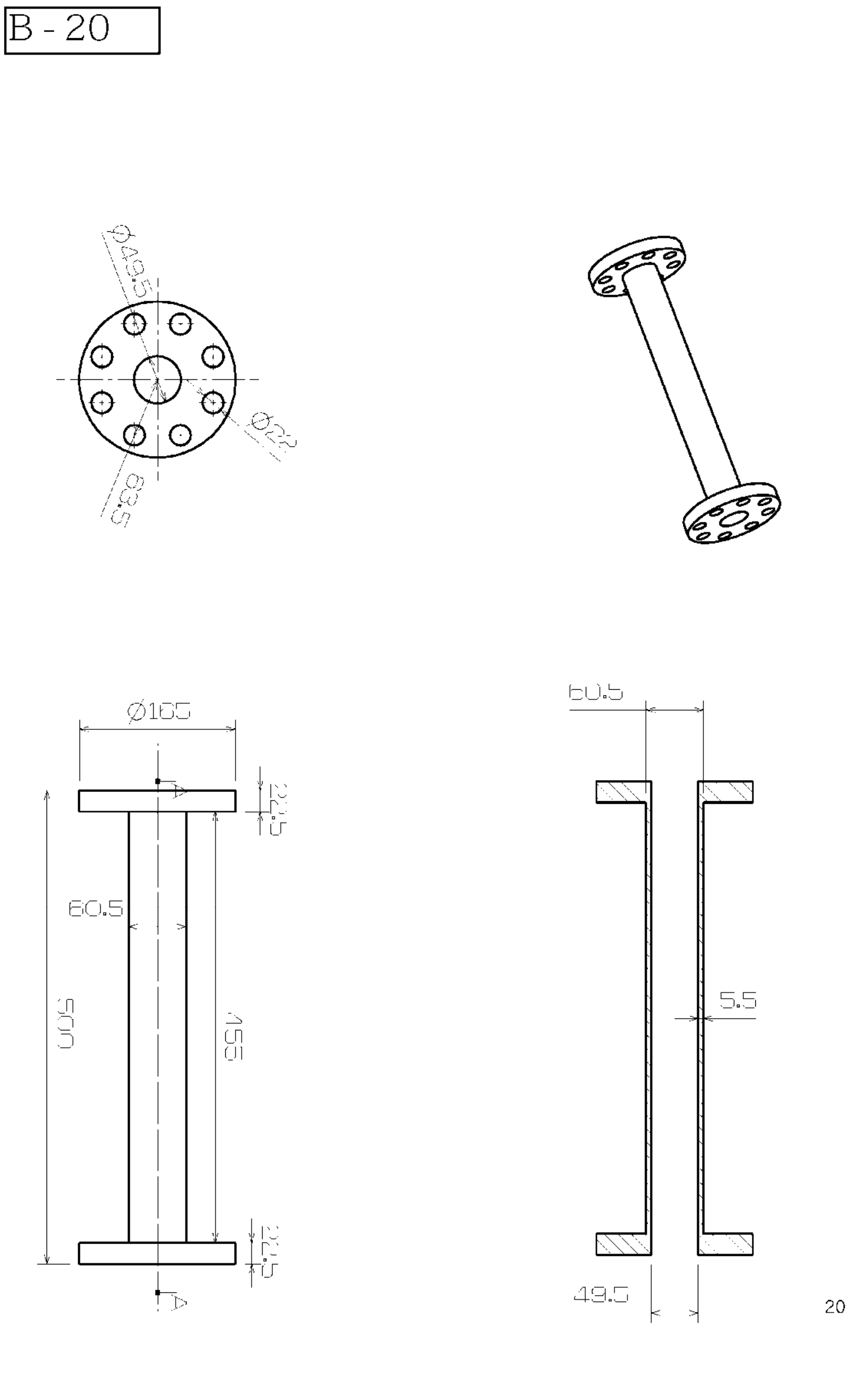

Figure B-21

B - 21

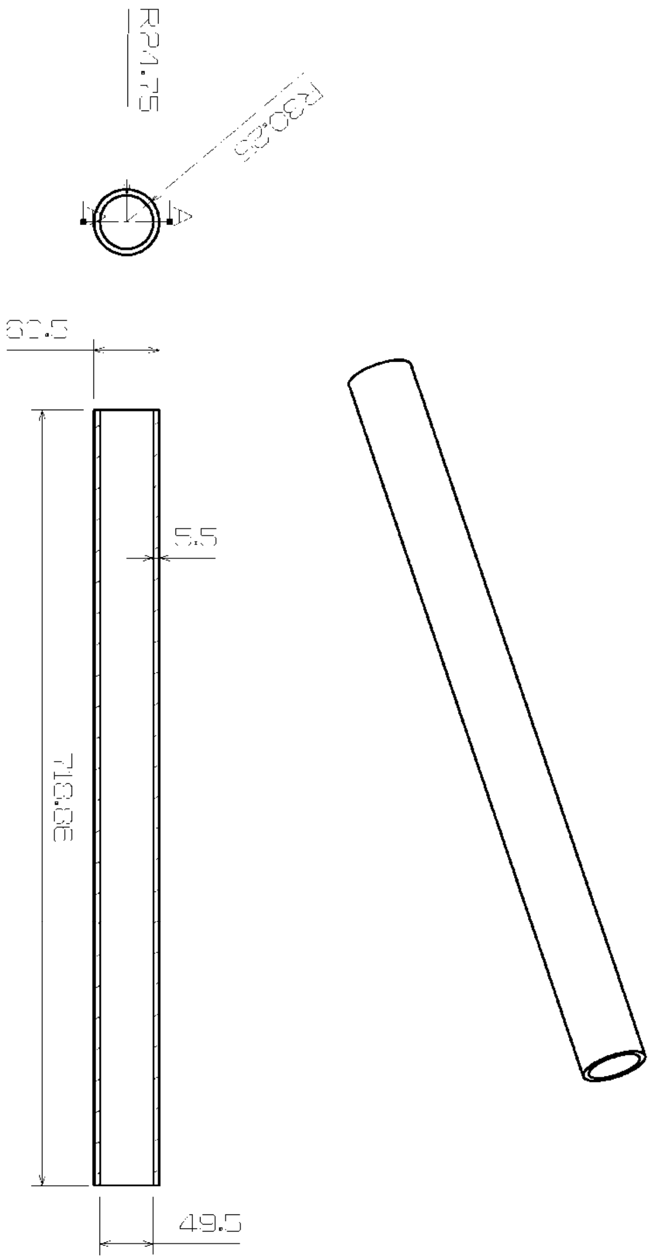

21

Figure B-22

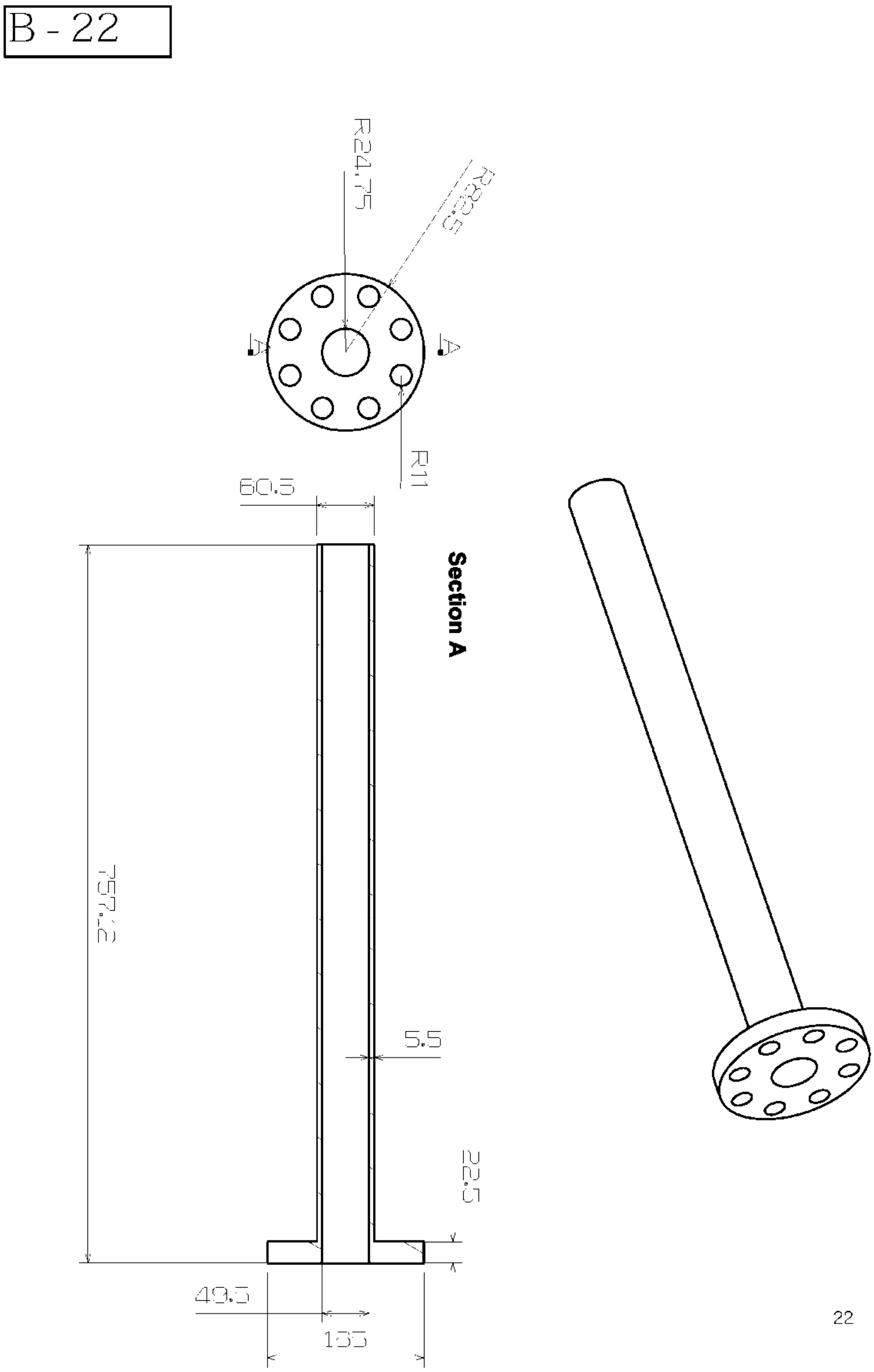

Figure B-23

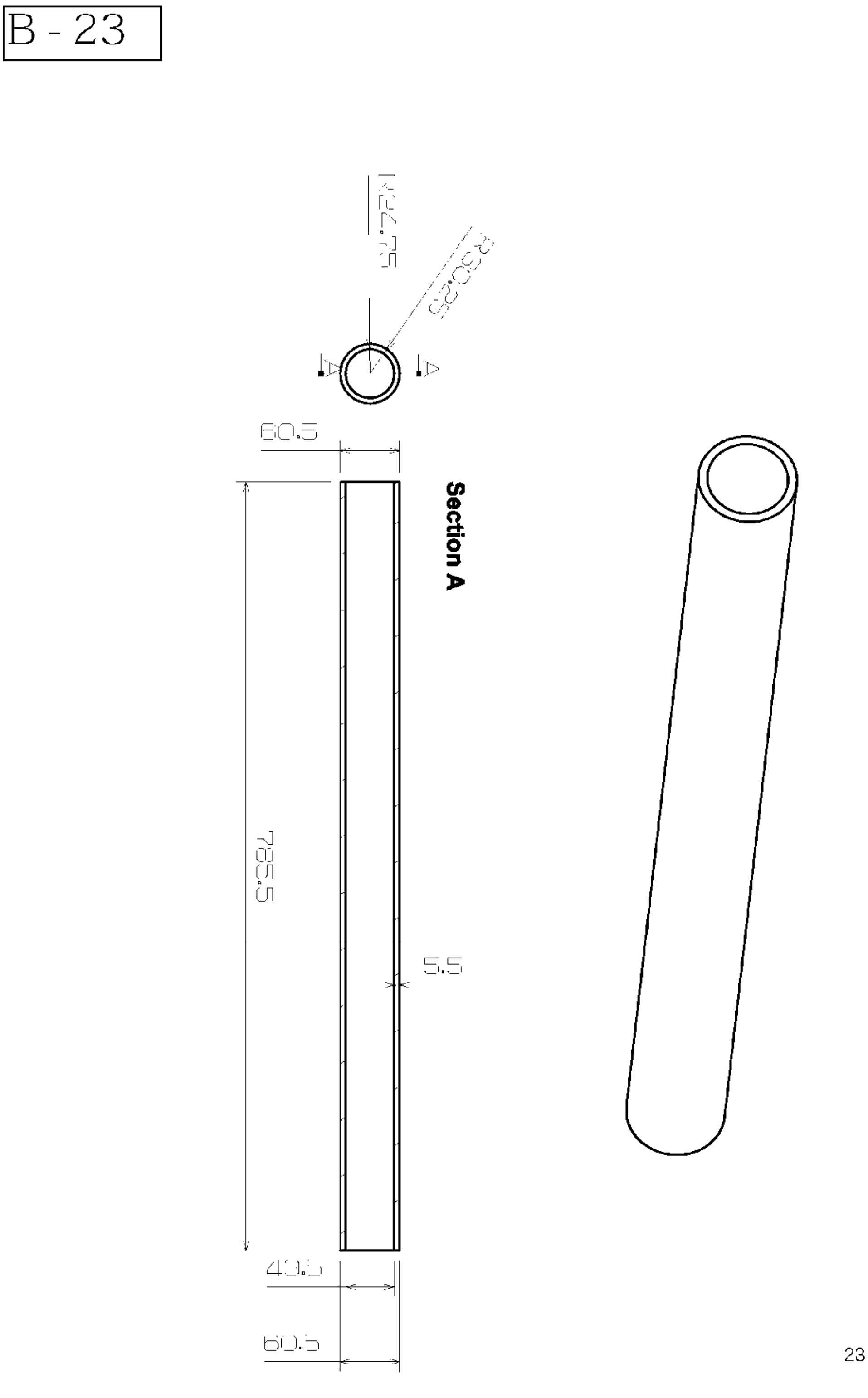

Figure B-24

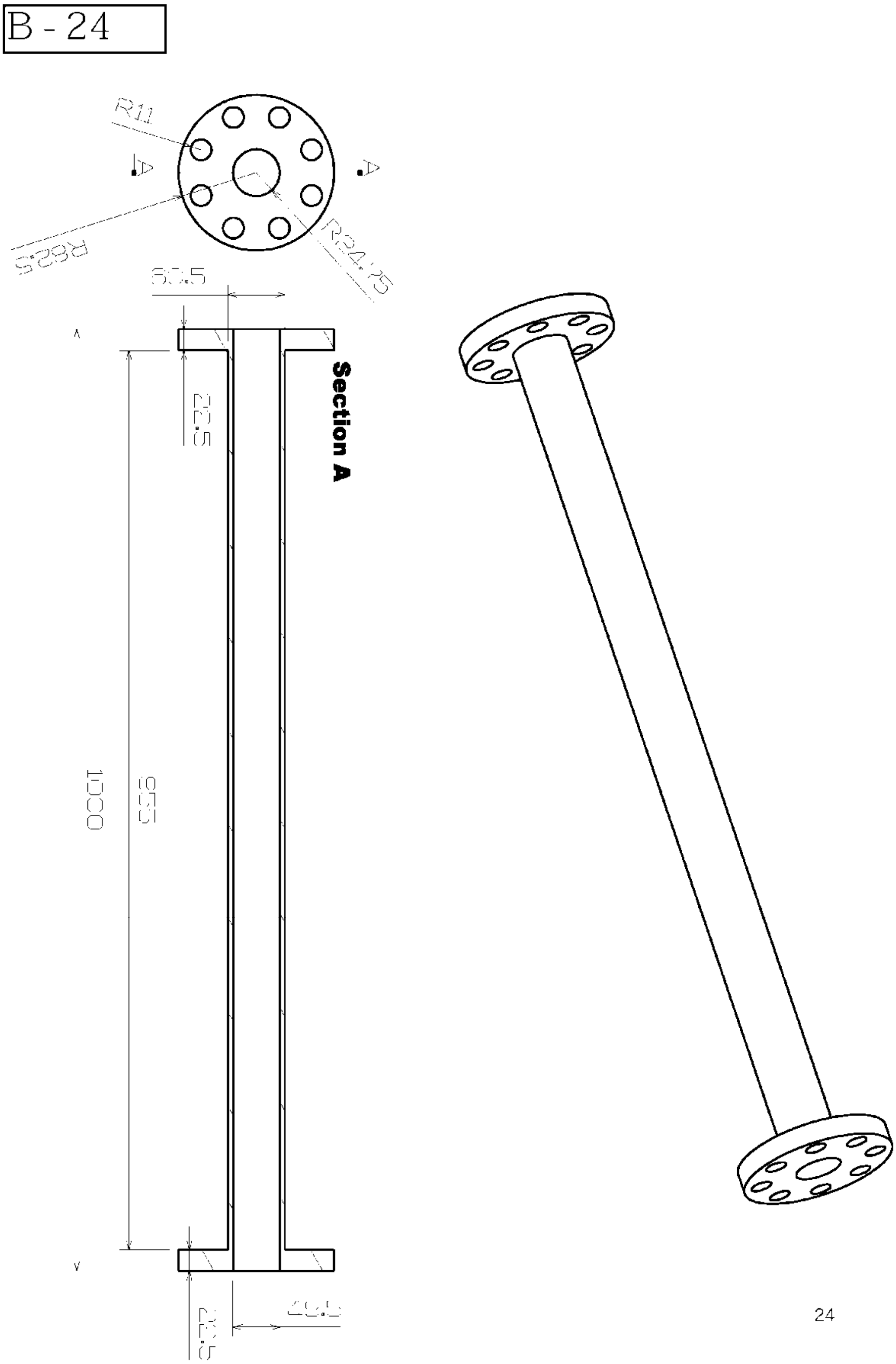

Figure B-25

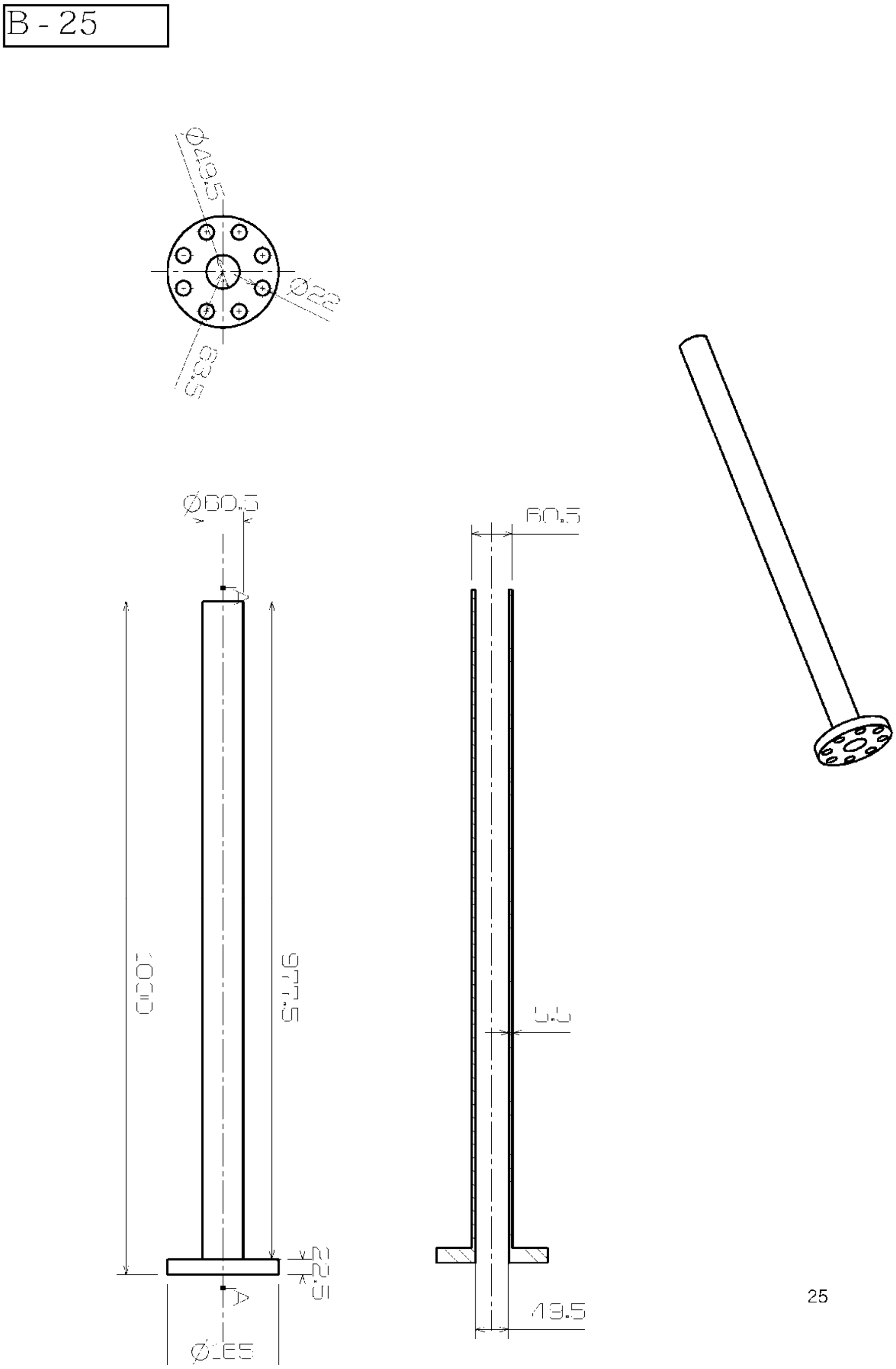

Figure B-26

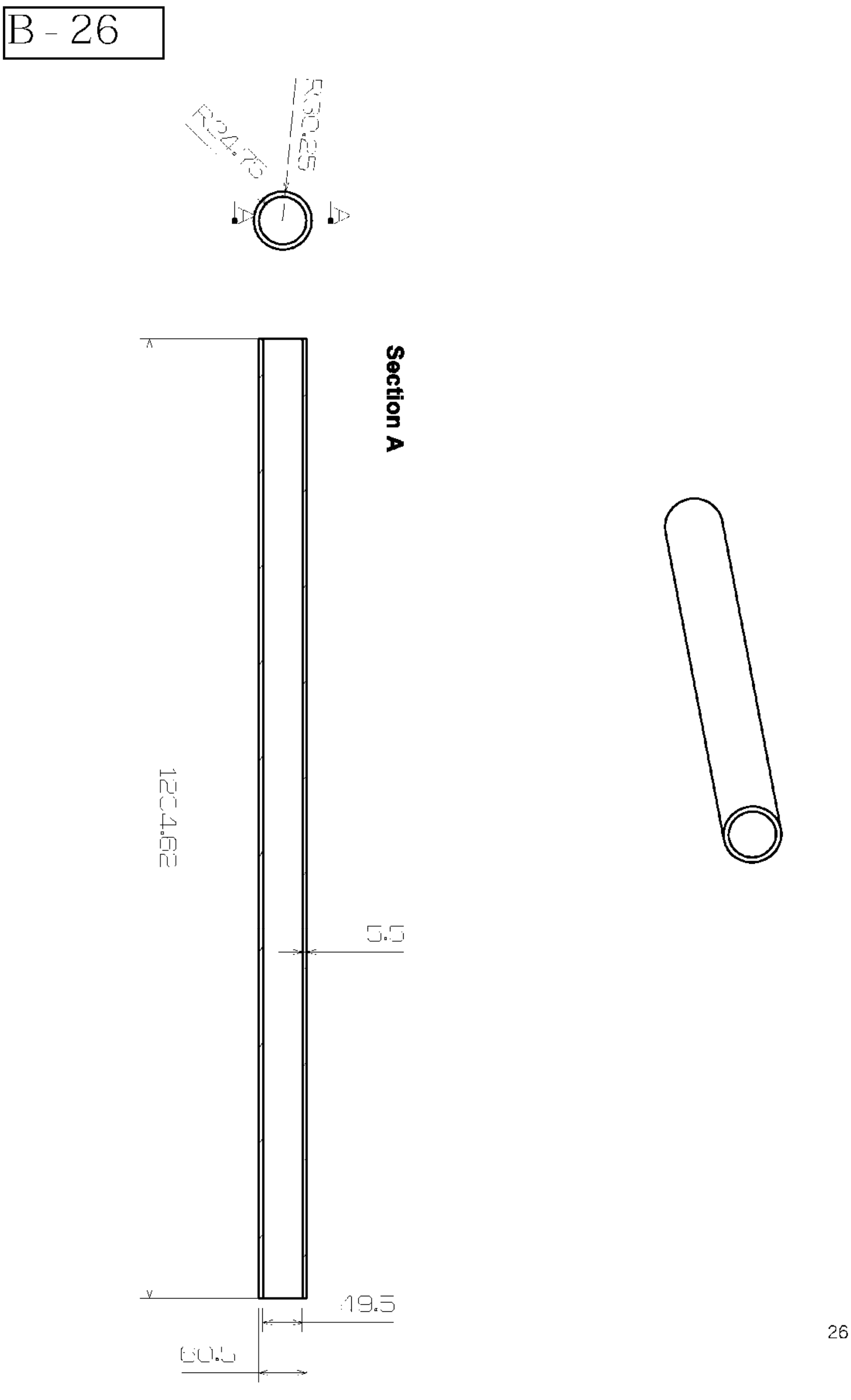

Figure B-27

B - 27

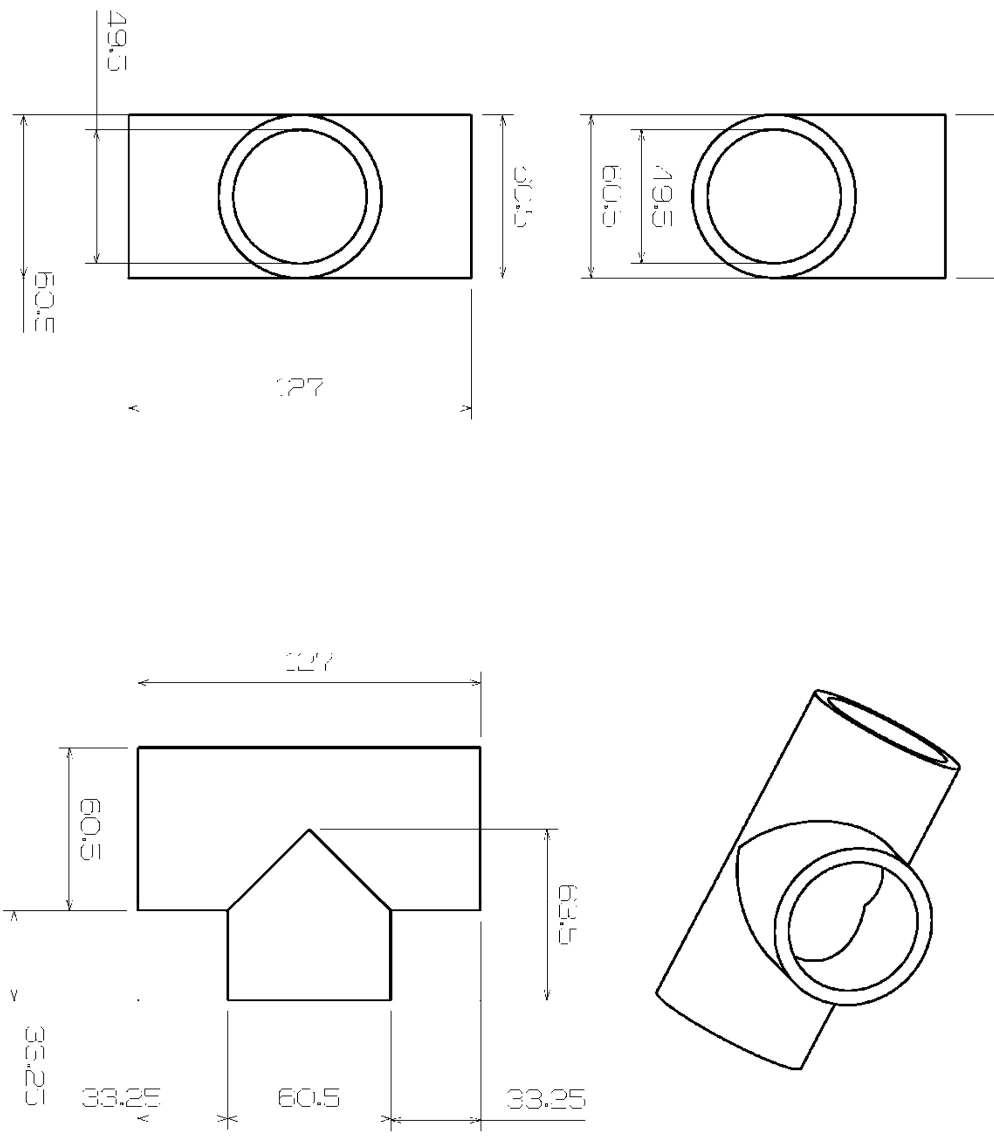

27

Figure B-28

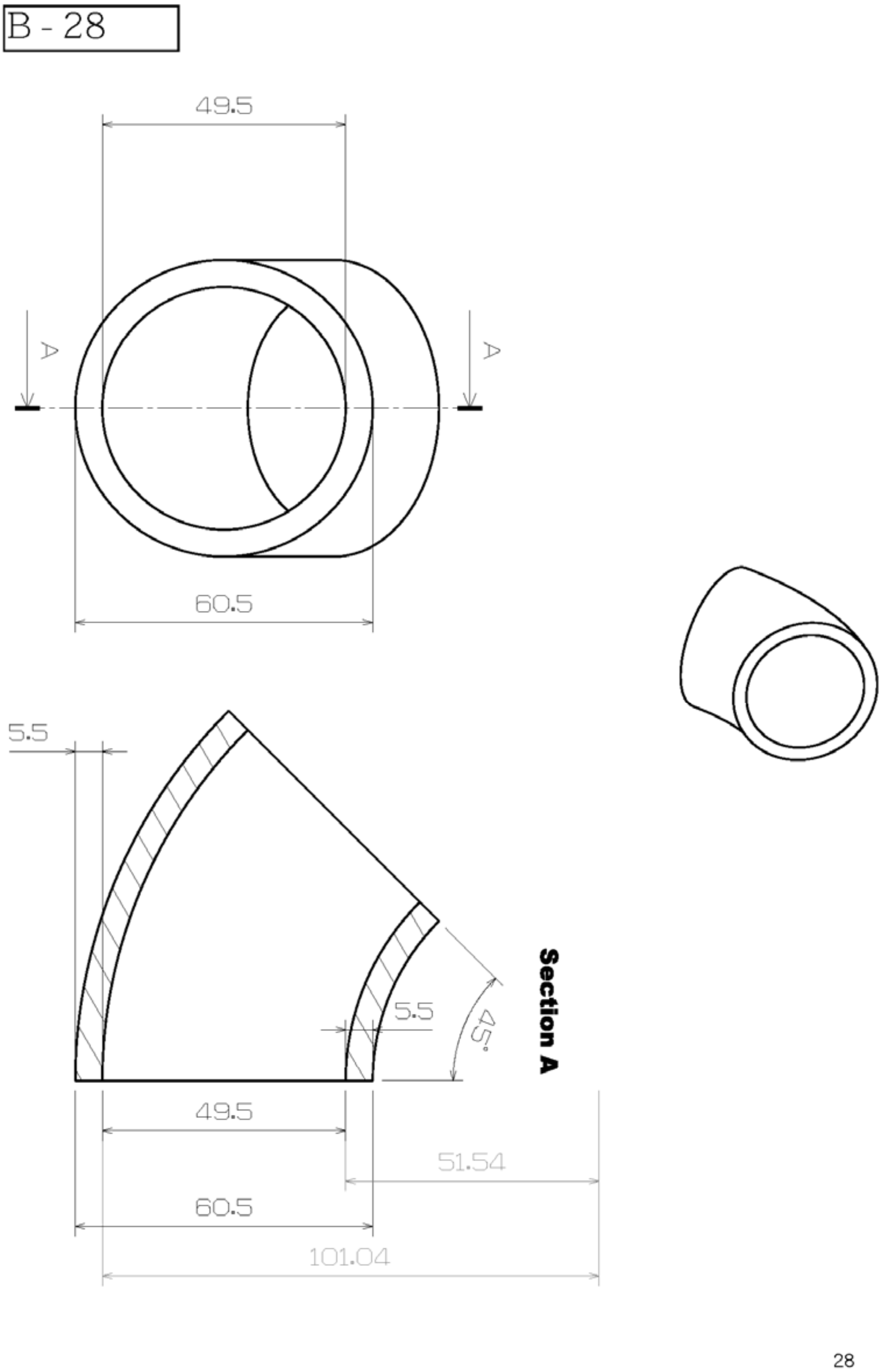

Figure B-29

B - 29

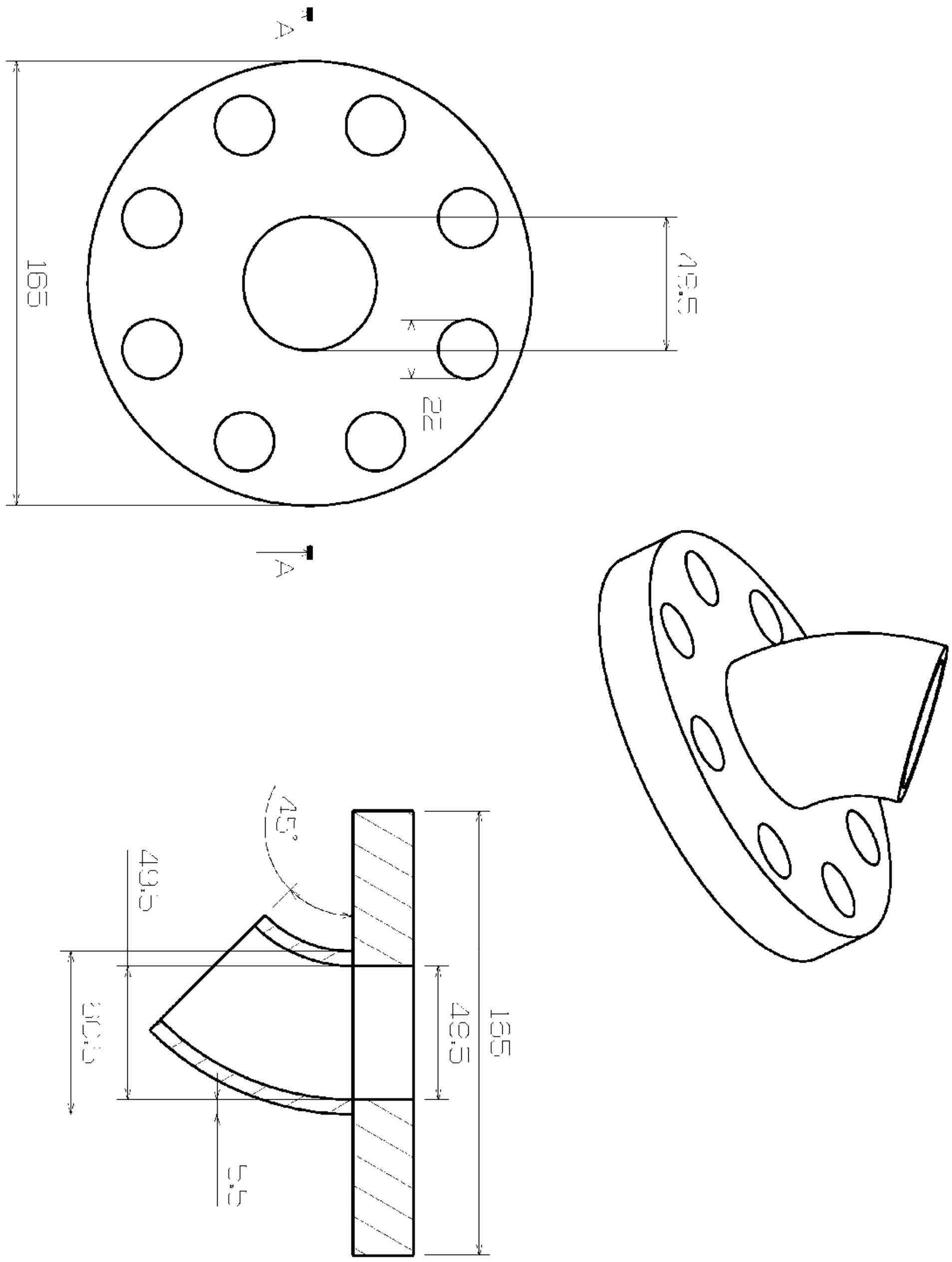

29

Figure B-30

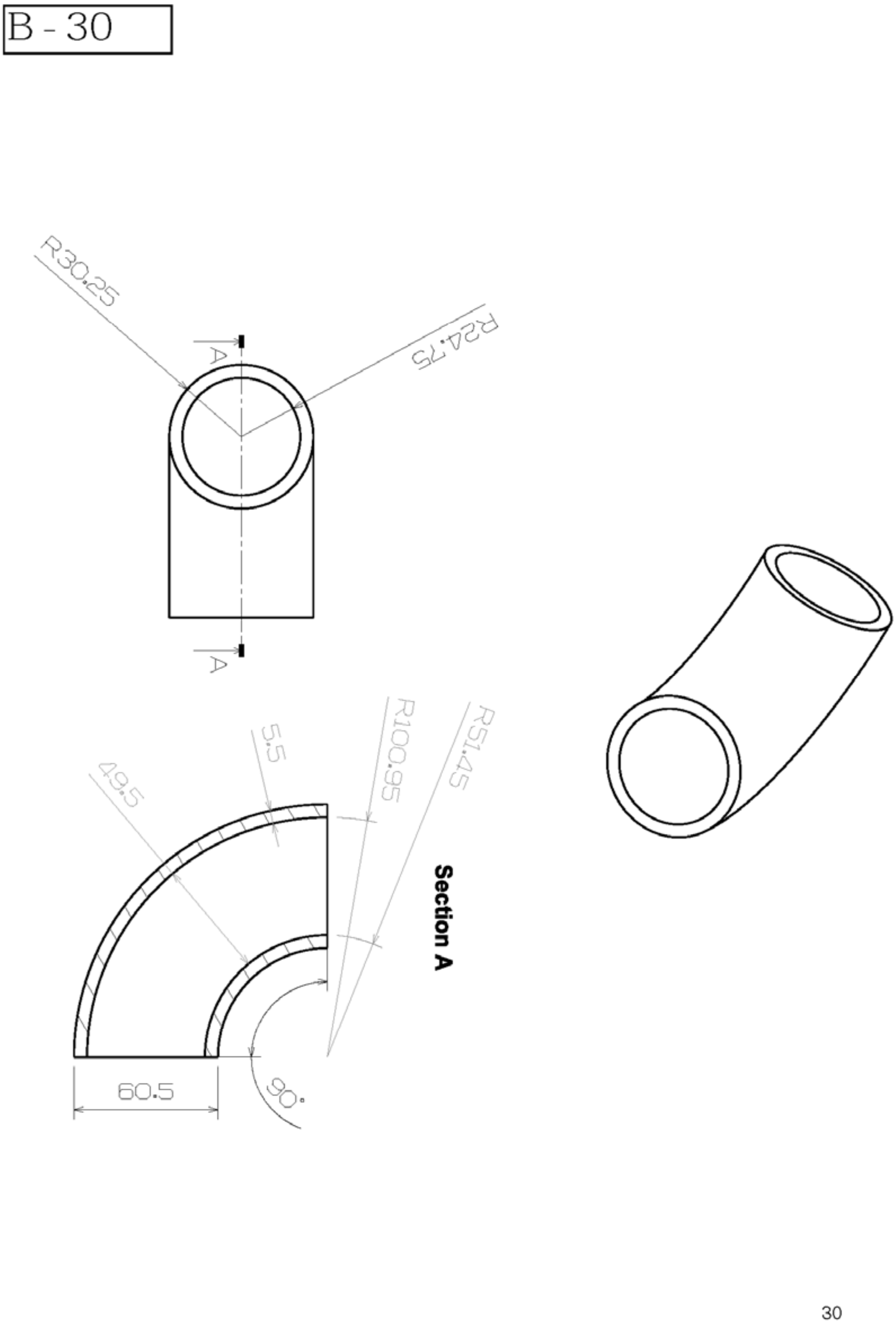

Figure B-31

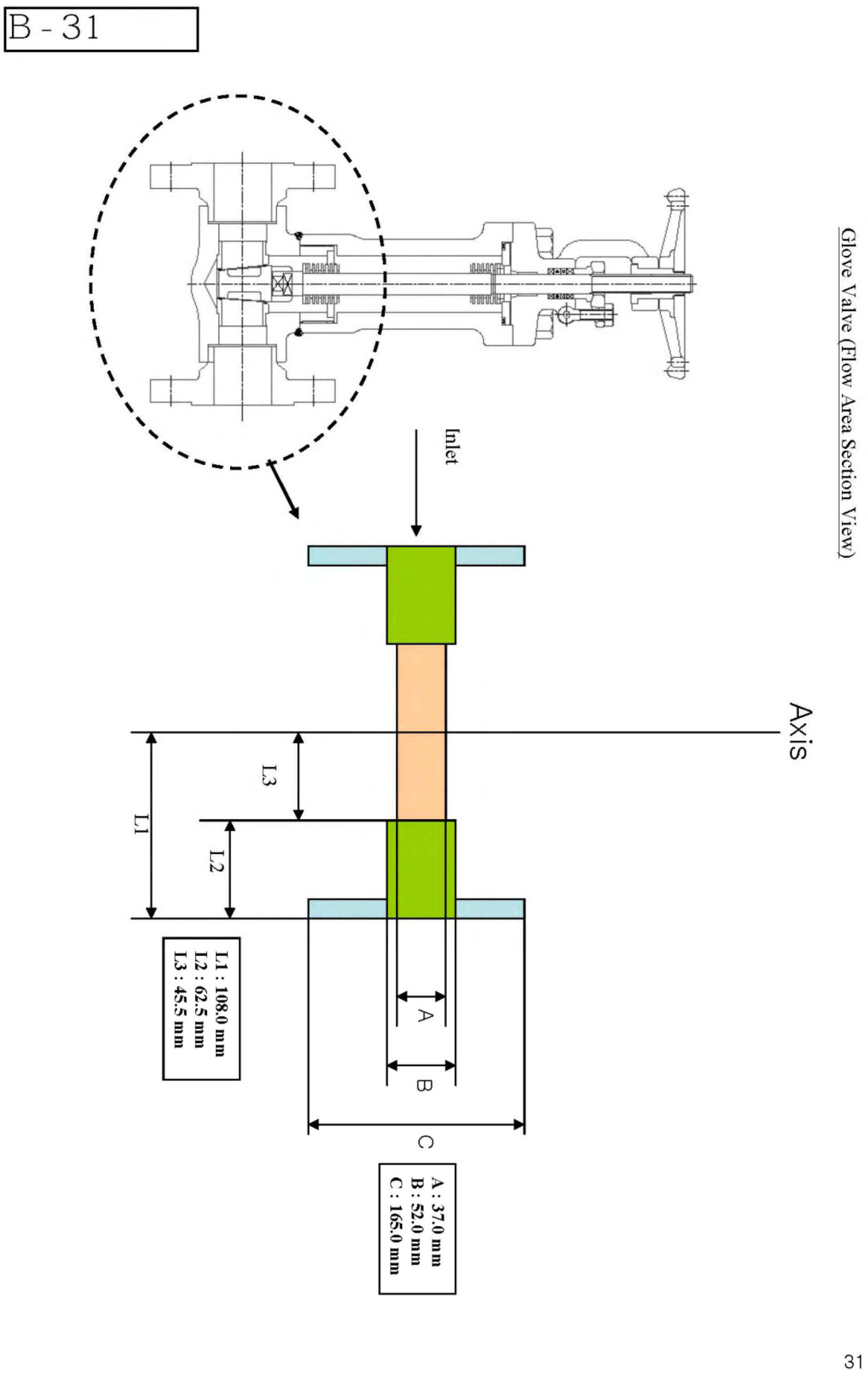

B - 31
Glove Valve (Flow Area Section View)
Inlet
Axis
L1
L2
L3
L1 : 108.0 mm
L2 : 62.5 mm
L3 : 45.5 mm
A
B
C
A : 37.0 mm
B : 52.0 mm
C : 165.0 mm
31

Figure B-32

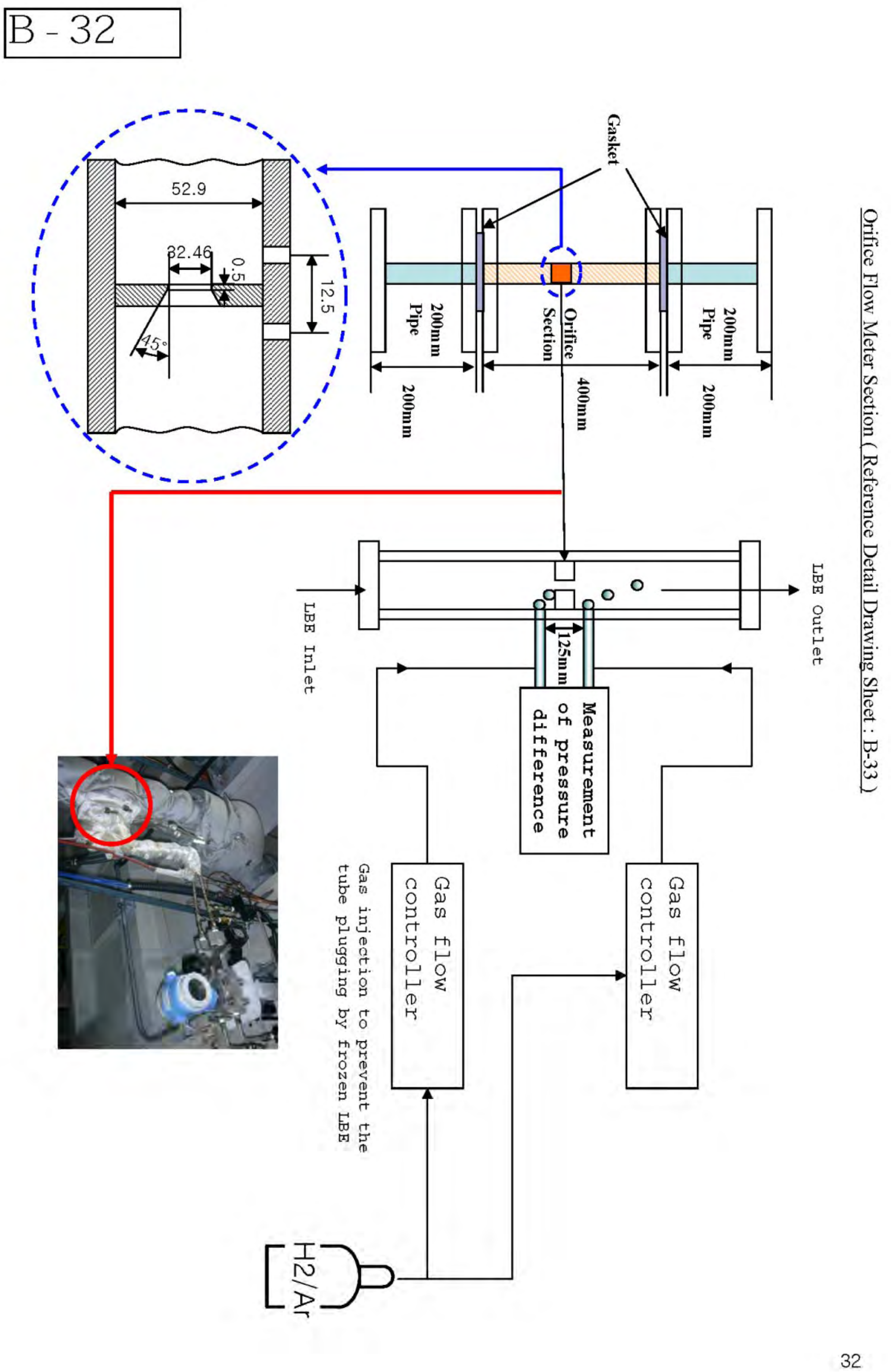
B - 32
Orifice Flow Meter Section (Reference Detail Drawing Sheet : B-33)
Gasket
200mm Pipe
Orifice Section
200mm Pipe
200mm
400mm
200mm
52.9
32.46
0.5
12.5
45°
LBE Inlet
LBE Outlet
125mm
Measurement of pressure difference
Gas flow controller
Gas flow controller
Gas injection to prevent the tube plugging by frozen LBE
H2/Ar
32

Figure B-33

B - 33

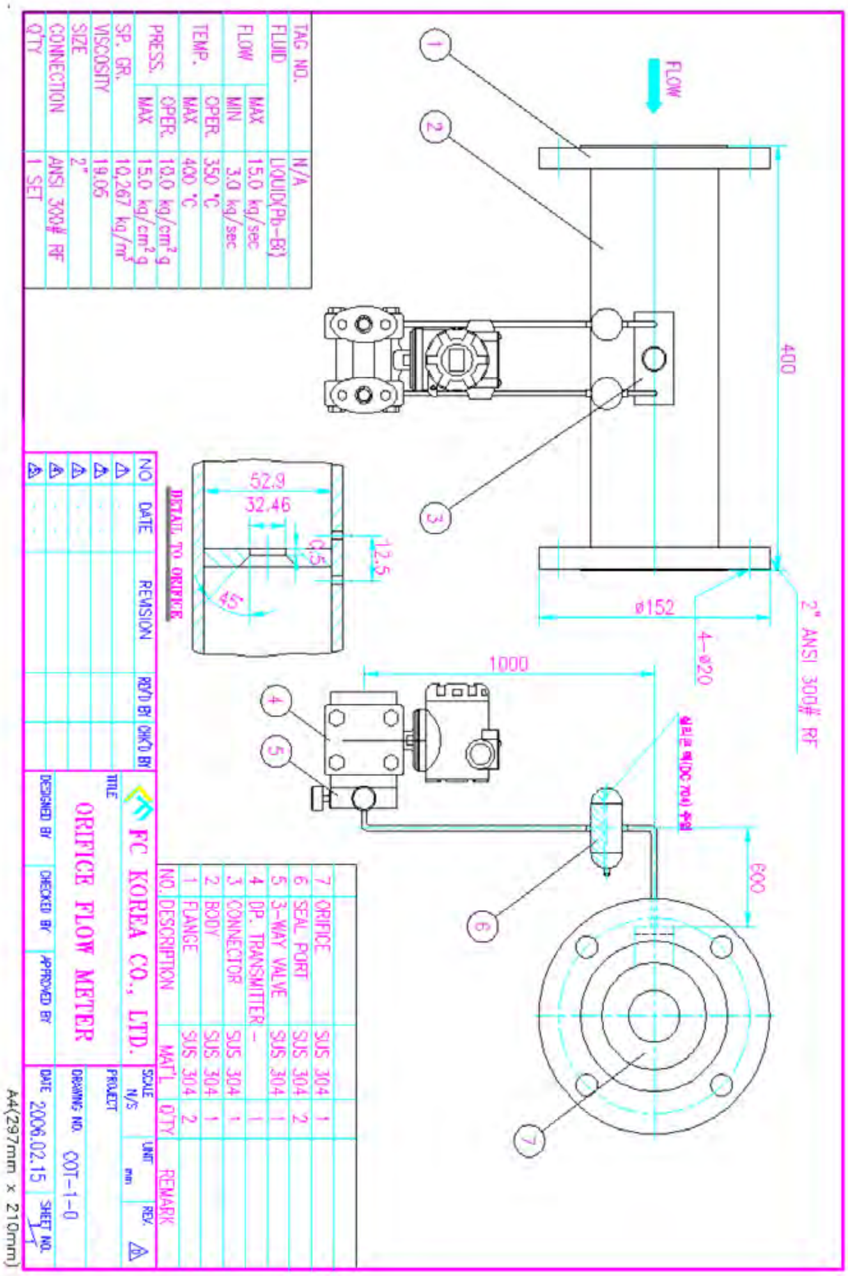

33

Figure B-34

B - 34

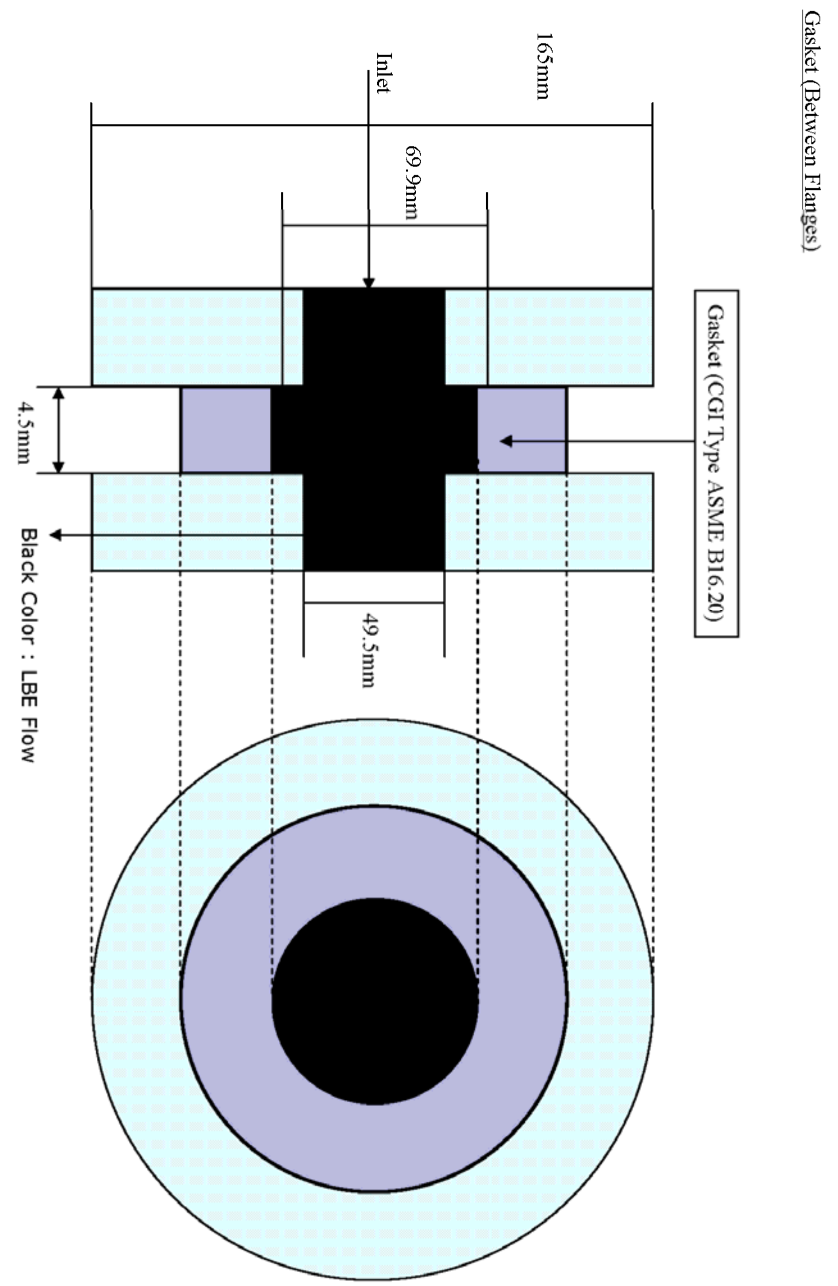

34

Figure B-35

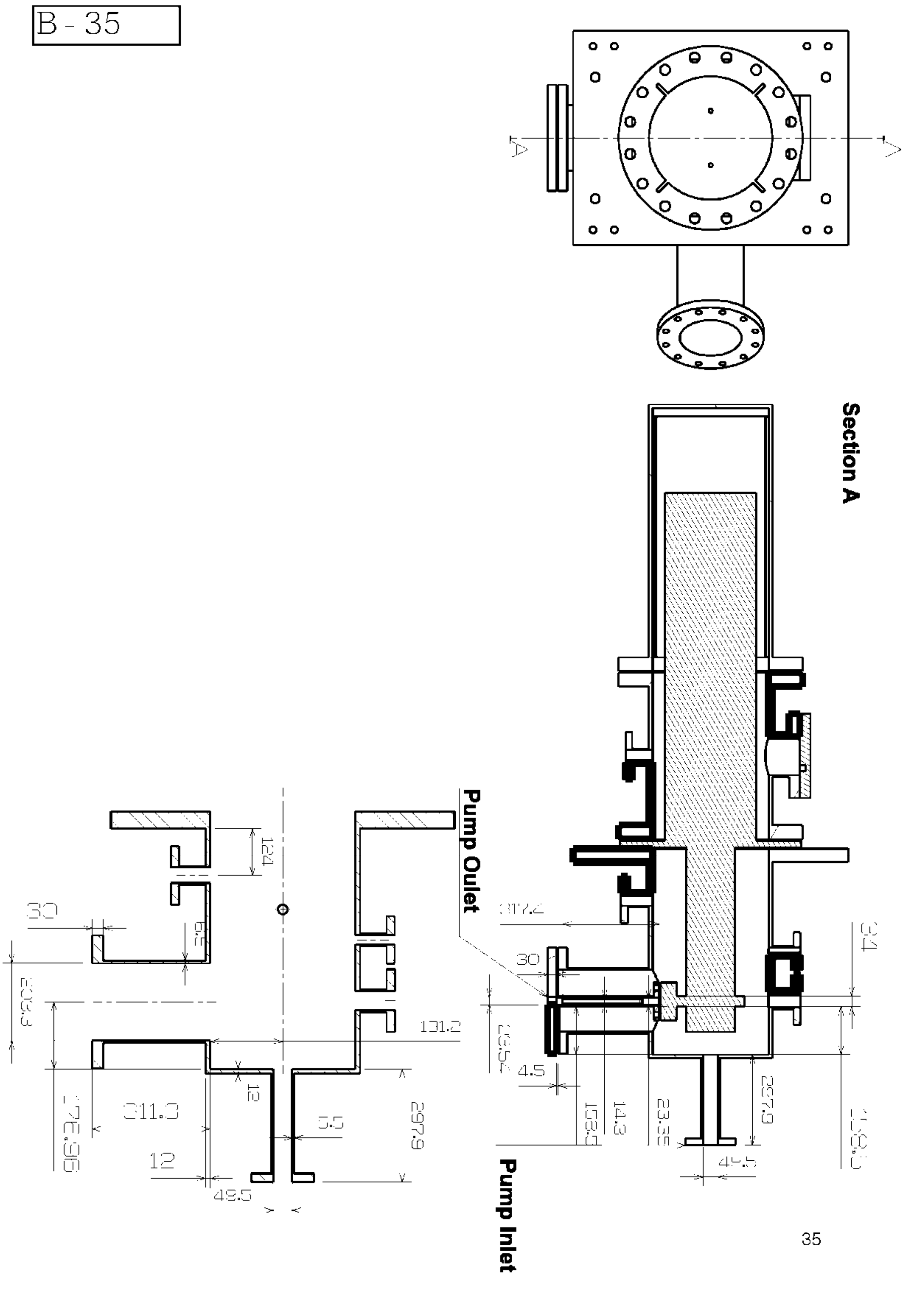

Figure B-36

B - 36

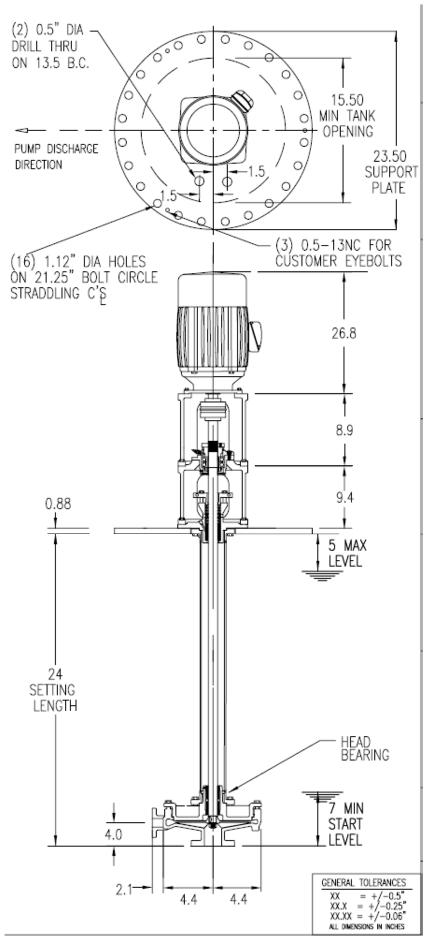

LaBour Taber 1001-30

36

Units are in British.

Figure B-37

B - 37

Type:	TABER 1000 - Vertical Process Sump Pump 1 Stage	Item :	1
Pump Model:	LaBour - 1001-30	Impeller No.:	
Nom. Speed:	1785 RPM, 60 Hz Electric	Fluid:	MOLTEN LEAD BISMUTH
Impeller Dia.:	6.25 inch	Temperature:	400 °C
Curve No.:	1001-17A	Viscosity:	
Market :	Process	Sp. Gravity:	11.3
		Your Ref. :	

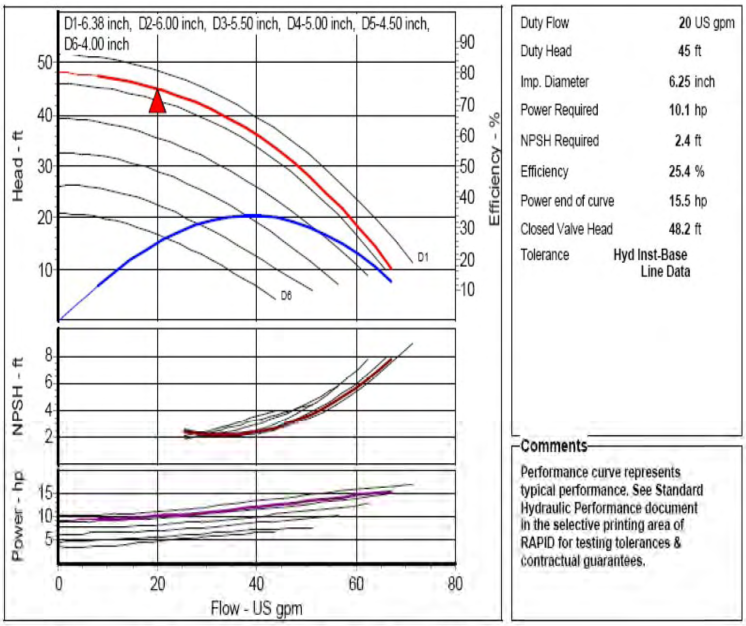

Flow (US gpm)	Head (ft)	Efficiency (%)	Power Required (hp)	NPSH Required (ft)
7.9	47.5	11.4	9.4	
15.3	46.2	20.6	9.8	
22.7	44.2	27.7	10.3	
30.1	41.4	32.3	11.0	2.2
37.5	37.6	34.2	11.8	2.3
44.9	32.7	33.2	12.6	2.9
52.3	26.6	29.3	13.5	4.0
59.7	19.1	22.4	14.5	5.6
67.1	10.1	12.5	15.5	7.8

Pump Characteristics curve

37

Units are in British.

Appendix C

Table C-1: Friction loss coefficient (1) at low-mass flow rate condition - ENEA, ERSE, GIDROPRESS

Sub Part No.	Sub Part Name	Accumulated Length (mm)	Accumulated Height (mm)	ENEA			ERSE			GIDROPRESS		
				Factor F(L/D)	Reference (Handbook or etc.)	Reference velocity (m/s)	Factor F(L/D)	Reference (Handbook or etc.)	Reference velocity (m/s)	Factor F(L/D)	Reference (Handbook or etc.)	Reference velocity (m/s)
1-1	Core Inlet	181	0	5.6281E-02	Colebrook-White correlation (calculated by Relap5 /Mod 3.3 code)	0.67904	0.0807	Frank M. White – Fluid Mechanics 2nd edition – Mc Graw-Hill	0.163	0.084		0.1634
1-2	Downcomer	1403	-1223	4.0142E-01	"	0.1345	0.6595	Moody chart – Colebrook interpolation formula	0.032	0.024		0.1634
1-3	Lower Plenum	1616	-1300	4.6404E-02	"	0.52792		“	0.021	0		0.1634
1-4	Core	2947	31	1.1820E+00	"	0.92135	1.8564	“	0.222	4.795		0.1634
1-5	Upper Plenum	3629	713	2.4929E-01	"	0.7275	0.3043	“	0.163	0.316		0.1634
1-6	Gasket [Between Flanges]	3633	717	1.0198E-01	"	0.67904		“		0.0015		0.1634
2-1	Pipe [One Side Flange]	3933	1017		"		0.1339	“	0.163	0.139		0.1634
2-2	Tee	4060	1144	4.2532E-02	"	0.67904	0.0485	“	0.109	0.059		0.1634
2-3	Pipe [One Side Flange]	4360	1444	1.0198E-01	"	0.67904	0.1339	“	0.163	0.139		0.1634
2-4	Gasket [Between Flanges]	4365	1449		"			“		0.0015		0.1634
3-1	Pipe [Both Side Flange]	5365	2449	3.1255E-01	"	0.67905	0.4464	“	0.163	0.464		0.1634

3-2	Gasket [Between Flanges]	5369	2453		"			“		0.0015		0.1634
4-1	45 Degree Elbow [One Side Flange]	5452	2530	7.4176E-02	"	0.67905	0.1542	“	0.163	0.038		0.1634
4-2	Pipe	5632	2658		"			“	0.163	0.084		0.1634
4-3	45 Degree Elbow	5692	2712	2.5399E-01	"	0.67905		“	0.163	0.028		0.1634
4-4	Pipe	6411	3431		"		0.3209	“	0.163	0.334		0.1634
4-5	Tee	6538	3558	4.2533E-02	"	0.67905	0.0567	“	0.163	0.059		0.1634
4-6	Pipe	6709	3729	7.0543E-02	"	0.67905	0.0764	“	0.163	0.079		0.1634
4-7	45 Degree Elbow	6769	3783		"		0.1442	“	0.163	0.028		0.1634
4-8	Pipe	6950	3910	9.5309E-02	"	0.67905		“	0.163	0.084		0.1634
4-9	45 Degree Elbow [One Side Flange]	7032	3987		"			“	0.163	0.038		0.1634
4-10	Gasket [Between Flanges]	7037	3991		"		0.1079	“		0.0015		0.1634
5-1	Gate valve	7253	4207	6.3226E-02	"	1.21535		“	0.292	0.215		0.1634
5-2	Gasket [Between Flanges]	7257	4212	3.3502E-01	"	0.67906		“		0.0015		0.1634
6-1	Pipe [Both Side Flange]	8257	5212		"		0.4464	“	0.163	0.464		0.1634
6-2	Gasket [Between Flanges]	8262	5216	3.3642E-01	"	0.67906		“		0.0015		0.1634
7-1	Pipe [Both Side Flange]	9262	6216		"		0.4464	“	0.163	0.464		0.1634

7-2	Gasket [Between Flanges]	9266	6221	6.5730E-02	"	0.67906		“		0.0015		0.1634
8-1	Pipe [One Side Flange]	9466	6421		"		0.3481	“	0.153	0.093		0.1634
8-2	Orifice	10066	7021	1.8452E-01	"	0.61578		“	0.380	0.0015		0.1634
8-3	Pipe [One Side Flange]	10266	7221	6.5731E-02	"	0.67907		“	0.153	0.202		0.1634
8-4	Gasket [Between Flanges]	10271	7225		"			“		0.0015		0.1634
9-1	Pipe[Both Side Flange]	10771	7725	1.6896E-01	"	0.67907	0.2232	“	0.163	0.093		0.1634
9-2	Gasket [Between Flanges]	10775	7730		"			“		0.0015		0.1634
10-1	Expansion Tank	11644	7934	2.1431E-01	"	0.70433	0.2591	“		0.232		0.1634
10-2	Gasket [Between Flanges]	11648	7934		"			“		0.0015		0.1634
11-1	Pipe [Both Side Flange]	12148	7934	1.6890E-01	"	0.67908	0.2232	“	0.163	0.342		0.1634
11-2	Gasket [Between Flanges]	12153	7934		"			“		0.0015		0.1634
12-1	Pipe [One Side Flange]	12453	7934	1.0044E-01	"	0.67908	0.1339	“	0.163	0.232		0.1634
12-2	Tee	12580	7934	4.2518E-02	"	0.67908	0.0567	“	0.163	0.0015		0.1634
12-3	Pipe	12885	7934	1.0224E-01	"	0.67908	0.1363	“	0.163	0.139		0.1634
12-4	90 Degree Elbow	13005	7858	4.0071E-02	"	0.67908	0.1069	“	0.163	0.059		0.1634
12-5	90 Degree	13125	7782	4.0071E-02	"	0.67908	0.1069	“	0.163	0.142		0.1634

	Elbow											
12-6	Pipe[One Side Flange]	13325	7782	6.7084E-02	"	0.67908	0.0893	“	0.163	0.056		0.1634
12-7	Gasket [Between Flanges]	13330	7782		"		0.1324	“		0.056		0.1634
13-1	Gate valve	13546	7782	6.3439E-02	"	1.08131		“	0.292	0.093		0.1634
13-2	Gasket [Between Flanges]	13550	7782	6.7072E-02	"	0.67908		“		0.0015		0.1634
14-1	Pipe [One Side Flange]	13750	7782		"		0.1116	“	0.163	0.215		0.1634
14-2	Tee	13877	7782	4.2518E-02	"	0.67908	0.0567	“	0.163	0.0015		0.1634
14-3	Pipe [One Side Flange]	14259	7782	1.2950E-01	"	0.67908	0.1707	“	0.163	0.093		0.1634
14-4	Gasket [Between Flanges]	14264	7782		"			“		0.059		0.1634
15-1	Heat Exchangner Vessel Inlet	14466	7782	3.6023E-02	"	0.67908	0.0621	“	0.163	0.177		0.1634
15-2	Heat Exchangner Internal	16477	5771	6.3975E-01	"	0.12129	1.0407	“	0.029	0.0015		0.1634
15-3	Heat Exchangner Outlet	16679	5771	4.5359E-02	"	0.67907	0.0621	“	0.163	0.065		0.1634
15-4	Gasket [Between Flanges]	16684	5771		"			“		0.036		0.1634
16-1	Pipe [One Side Flange]	16904	5771	7.3591E-02	"	0.67907	0.0981	“	0.163	0.065		0.1634
16-2	90 Degree Elbow	17024	5695	4.0073E-02	"	0.67907	0.0534	“	0.163	0.0015		0.1634

16-3	Pipe	17809	4909	2.6299E-01	"	0.67907	0.3506	“	0.163	0.102		0.1634
16-4	Tee	17936	4782	4.2521E-02	"	0.67906	0.0567	“	0.163	0.056		0.1634
16-5	Pipe [One Side Flange]	18436	4282	1.6741E-01	"	0.67906	0.2232	“	0.163	0.365		0.1634
16-6	Gasket [Between Flanges]	18441	4278		"		0.1148	“		0.059		0.1634
17-1	Gate valve	18657	4062	6.3671E-02	"	1.08129		“	0.292	0.232		0.1634
17-2	Gasket [Between Flanges]	18661	4057	1.6741E-01	"	0.67906		“		0.0015		0.1634
18-1	Pipe[One Side Flange]	19161	3557		"		0.2219	“	0.163	0.215		0.1634
18-2	Tee	19288	3430	4.2522E-02	"	0.67906	0.0567	“	0.163	0.0015		0.1634
18-3	Pipe [One Side Flange]	19788	2930	1.6892E-01	"	0.67906	0.2232	“	0.163	0.232		0.1634
18-4	Gasket [Between Flanges]	19793	2926		"			“		0.059		0.1634
19-1	Pipe [Both Side Flange]	20793	1926	3.3633E-01	"	0.67905	0.4464	“	0.163	0.232		0.1634
19-2	Gasket [Between Flanges]	20797	1921		"			“		0.0015		0.1634
20-1	Pipe[One Side Flange]	21297	1421	1.6741E-01	"	0.67905	0.2232	“	0.163	0.464		0.1634
20-2	Tee	21424	1294	4.2523E-02	"	0.67905	0.0567	“	0.163	0.0015		0.1634
24-1	Pipe [One Side Flange]	22424	294	3.3633E-01	"	0.67905	0.4901	“	0.163	0.464		0.1634
24-2	Gasket [Between Flanges]	22429	290		"			“		0.0015		0.1634

24-3	Pipe[Both Side Flange]	23429	-710	3.3483E-01	"	0.67904	0.4464	“	0.163	0.464		0.1634
24-4	Gasket [Between Flanges]	23433	-715	1.9008E-02	"	0.67904		“		0.0015		0.1634
24-5	Pipe [One Side Flange]	23485	-767		"		0.1035	“	0.163	0.024		0.1634
24-6	90 Degree Elbow	23605	-843	4.0076E-02	"	0.67904		“	0.163	0.056		0.1634
24-7	45 Degree Elbow	23665	-843	2.5545E-02	"	0.67904		“	0.163	0.028		0.1634
24-8	Pipe [One Side Flange]	23883	-843	7.2811E-02	"	0.67904	0.0970	“	0.163	0.1		0.1634
24-9	Gasket [Between Flanges]	23887	-843		"		0.1079	“		0.0015		0.1634
24-10	Gate valve	24103	-843	6.3492E-02	"	1.08125		“	0.292	0.215		0.1634
24-11	Gasket [Between Flanges]	24108	-843	1.0058E-01	"	0.67904				0.0015		0.1634
24-12	Pipe [One Side Flange]	24408	-843		"		0.1339	“	0.163	0.139		0.1634
24-13	Tee	24535	-779	4.2525E-02	"	0.67904	0.0567	“	0.163	0.059		0.1634
24-14	Pipe [One Side Flange]	24835	-479	1.0196E-01	"	0.67904	0.1339	“	0.163	0.139		0.1634
25-1	Gasket [Between Flanges]	24839	-475		"			“		0.0015		0.1634
25-2	Sump Tank	25816	0	3.5616E-01	"	3.66116	0.5454	“	1.957	0.138		0.1634
25-3	Gasket [Between Flanges]	25821	0		"		0.1079	“		0.0015		0.1634

25-4	Gate valve	26037	0	7.4582E-02	"	1.21533		“	0.292	0.215		0.1634
25-5	Gasket [Between Flanges]	26041	0	2.9414E-02	"	0.67904		“		0.0015		0.1634
25-6	45 Degree Elbow [One Side Flange]	26124	0		"		0.1442	“	0.163	0.038		0.1634
25-7	Pipe	26305	0	6.0501E-02	"	0.67904		“	0.163	0.084		0.1634
25-8	45 Degree Elbow	26365	0	1.8364E-02	"	0.67904		“	0.163	0.028		0.1634
25-9	Tee	26492	0	1.8616E-02	"	0.67904	0.0567	“	0.163	0.059		0.1634
25-10	45 Degree Elbow	26552	0	1.8364E-02	"	0.67904	0.1442	“	0.163	0.028		0.1634
25-11	Pipe	26732	0	6.0501E-02	"	0.67904		“	0.163	0.084		0.1634
25-12	45 Degree Elbow [One Side Flange]	26815	0	2.7625E-02	"	0.67904		“	0.163	0.038		0.1634
25-13	Gasket [Between Flanges]	26819	0					“	0.163	0.0015		0.1634

Table C-2: Friction loss coefficient (II) at low-mass flow rate condition - IAEA, IPPE, KIT/INR

Sub Part No.	Sub Part Name	Accumulated Length (mm)	Accumulated Height (mm)	IAEA			IPPE			KIT/INR		
				Factor F(L/D)	Reference (Handbook or etc.)	Reference velocity (m/s)	Factor F(L/D)	Reference (Handbook or etc.)	Reference velocity (m/s)	Factor F(L/D)	Reference (Handbook or etc.)	Reference velocity (m/s)
1-1	Core Inlet	181	0	0.0805	Ref [5]	0.163	7.48E-02	[1], page 65, paragraph 30	1.63E-01	0.0797	TRACE Theory Manual	0.1632
1-2	Downcomer	1403	-1223	0.4769	Ref [5]	0.032	5.77E-01	[1], Diagram 2-7	3.24E-02	0.5607	"	0.0323
1-3	Lower Plenum	1616	-1300				3.60E-02	[1], Diagram 2-7	3.24E-02	0.0317	"	0.0091
1-4	Core	2947	31	1.9459	Ref [5]	0.222	2.31E+00	[1], page 65, paragraph 30; [2], formula (1.18)	2.22E-01	1.9080	"	0.2216
1-5	Upper Plenum	3629	713	0.3038	Ref [5]	0.163	3.11E-01	[1], page 65, paragraph 30	1.63E-01	0.3001	"	0.1632
1-6	Gasket [Between Flanges]	3633	717			0.000	0.00E+00	[1], page 65, paragraph 30	1.63E-01	0.0015	"	0.0819
2-1	Pipe [One Side Flange]	3933	1017	0.1337	Ref [5]	0.163	1.37E-01	[1], page 65, paragraph 30	1.63E-01	0.1323	"	0.1632
2-2	Tee	4060	1144	0.0566	Ref [5]	0.163	5.79E-02	[1], page 65, paragraph 30	1.63E-01	0.0560	"	0.1632
2-3	Pipe [One Side Flange]	4360	1444	0.1337	Ref [5]	0.163	1.37E-01	[1], page 65, paragraph 30	1.63E-01	0.1323	"	0.1632
2-4	Gasket [Between Flanges]	4365	1449			0.000	0.00E+00	[1], page 65, paragraph 30	1.63E-01	0.0015	"	0.0819
3-1	Pipe [Both Side Flange]	5365	2449	0.4458	Ref [5]	0.163	4.56E-01	[1], page 65, paragraph 30	1.63E-01	0.4409	"	0.1632
3-2	Gasket [Between Flanges]	5369	2453				0.00E+00	[1], page 65, paragraph 30	1.63E-01	0.0015	"	0.0819

4-1	45 Degree Elbow [One Side Flange]	5452	2530	0.04	Ref [5]	0.163	3.76E-02	[1], Diagrams 6-1, 6-2, 2-1	1.63E-01	0.0364	"	0.1632
4-2	Pipe	5632	2658	0.0802	Ref [5]	0.163	8.23E-02	[1], page 65, paragraph 30	1.63E-01	0.0797	"	0.1632
4-3	45 Degree Elbow	5692	2712	0.03	Ref [5]	0.163	2.73E-02	[1], Diagrams 6-1, 6-2, 2-1	1.63E-01	0.0265	"	0.1632
4-4	Pipe	6411	3431	0.3205	Ref [5]	0.163	3.28E-01	[1], page 65, paragraph 30	1.63E-01	0.3170	"	0.1632
4-5	Tee	6538	3558	0.0566	Ref [5]	0.163	5.79E-02	[1], page 65, paragraph 30	1.63E-01	0.0560	"	0.1632
4-6	Pipe	6709	3729	0.0762	Ref [5]	0.163	7.80E-02	[1], page 65, paragraph 30	1.63E-01	0.0754	"	0.1632
4-7	45 Degree Elbow	6769	3783	0.03	Ref [5]	0.163	2.73E-02	[1], Diagrams 6-1, 6-2, 2-1	1.63E-01	0.0265	"	0.1632
4-8	Pipe	6950	3910	0.0807	Ref [5]	0.163	8.23E-02	[1], page 65, paragraph 30	1.63E-01	0.0797	"	0.1632
4-9	45 Degree Elbow [One Side Flange]	7032	3987	0.0374	Ref [5]	0.163	3.76E-02	[1], Diagrams 6-1, 6-2, 2-1	1.63E-01	0.0364	"	0.1632
4-10	Gasket [Between Flanges]	7037	3991				0.00E+00	[1], page 65, paragraph 30	1.63E-01	0.0015	"	0.0819
5-1	Gate valve	7253	4207	0.265	Ref [5]	0.147	2.58E-01	[1], page 65, paragraph 30	1.48E-01	0.1000	"	0.2339
5-2	Gasket [Between Flanges]	7257	4212				0.00E+00	[1], page 65, paragraph 30	1.63E-01	0.0015	"	0.0819
6-1	Pipe [Both Side Flange]	8257	5212	0.4458	Ref [5]	0.163	4.56E-01	[1], page 65, paragraph 30	1.63E-01	0.4409	"	0.1632
6-2	Gasket [Between Flanges]	8262	5216				0.00E+00	[1], page 65, paragraph 30	1.63E-01	0.0015	"	0.0819
7-1	Pipe [Both	9262	6216	0.4458	Ref [5]	0.163	4.56E-01	[1], page 65,	1.63E-01	0.4409	"	0.1632

	Side Flange]							paragraph 30				
7-2	Gasket [Between Flanges]	9266	6221				0.00E+00	[1], page 65, paragraph 30	1.63E-01	0.0015	"	0.0819
8-1	Pipe [One Side Flange]	9466	6421	0.0892	Ref [5]	0.163	9.11E-02	[1], page 65, paragraph 30	1.63E-01	0.0882	"	0.1632
8-2	Orifice	10066	7021	0.1702	Ref [5]	0.141	1.73E-01	[1], page 65, paragraph 30	1.43E-01	0.2512	"	0.1429
8-3	Pipe [One Side Flange]	10266	7221	0.0892	Ref [5]	0.163	9.11E-02	[1], page 65, paragraph 30	1.63E-01	0.0882	"	0.1632
8-4	Gasket [Between Flanges]	10271	7225				0.00E+00	[1], page 65, paragraph 30	1.63E-01	0.0015	"	0.0819
9-1	Pipe[Both Side Flange]	10771	7725	0.2229	Ref [5]	0.163	2.28E-01	[1], page 65, paragraph 30	1.63E-01	0.2205	"	0.1632
9-2	Gasket [Between Flanges]	10775	7730				0.00E+00	[1], page 65, paragraph 30	1.63E-01	0.0015	"	0.0819
10-1	Expansion Tank	11644	7934	0.3049	Ref [5]	0.163	2.74E-01	[1], page 65, paragraph 30	1.63E-01	0.7000	"	0.1059
10-2	Gasket [Between Flanges]	11648	7934				0.00E+00	[1], page 65, paragraph 30	1.63E-01	0.0015	"	0.0819
11-1	Pipe [Both Side Flange]	12148	7934	0.2229	Ref [5]	0.163	2.28E-01	[1], page 65, paragraph 30	1.63E-01	0.2205	"	0.1632
11-2	Gasket [Between Flanges]	12153	7934				0.00E+00	[1], page 65, paragraph 30	1.63E-01	0.0015	"	0.0819
12-1	Pipe [One Side Flange]	12453	7934	0.1337	Ref [5]	0.163	1.37E-01	[1], page 65, paragraph 30	1.63E-01	0.1323	"	0.1632
12-2	Tee	12580	7934	0.0566	Ref [5]	0.163	5.79E-02	[1], page 65, paragraph 30	1.63E-01	0.0560	"	0.1632
12-3	Pipe	12885	7934	0.1361	Ref [5]	0.163	1.39E-01	[1], page 65, paragraph 30	1.63E-01	0.1347	"	0.1632

12-4	90 Degree Elbow	13005	7858	0.05	Ref [5]	0.163	1.09E-01	[1], Diagram 6-19	1.63E-01	0.0529	"	0.1632
12-5	90 Degree Elbow	13125	7782	0.05	Ref [5]	0.163	0.00E+00	[1], Diagram 6-19	0.00E+00	0.0529	"	0.1632
12-6	Pipe[One Side Flange]	13325	7782	0.0892	Ref [5]	0.163	9.11E-02	[1], page 65, paragraph 30	1.63E-01	0.0882	"	0.1632
12-7	Gasket [Between Flanges]	13330	7782				0.00E+00	[1], page 65, paragraph 30	1.63E-01	0.0015	"	0.0819
13-1	Gate valve	13546	7782	0.265	Ref [5]	0.147	6.62E-02	[1], page 65, paragraph 30	2.93E-01	0.1000	"	0.2339
13-2	Gasket [Between Flanges]	13550	7782				0.00E+00	[1], page 65, paragraph 30	1.63E-01	0.0015	"	0.0819
14-1	Pipe [One Side Flange]	13750	7782	0.0892	Ref [5]	0.163	9.11E-02	[1], page 65, paragraph 30	1.63E-01	0.0882	"	0.1632
14-2	Tee	13877	7782	0.0566	Ref [5]	0.163	5.79E-02	[1], page 65, paragraph 30	1.63E-01	0.0560	"	0.1632
14-3	Pipe [One Side Flange]	14259	7782	0.1703	Ref [5]	0.163	1.74E-01	[1], page 65, paragraph 30	1.63E-01	0.1686	"	0.1632
14-4	Gasket [Between Flanges]	14264	7782				0.00E+00	[1], page 65, paragraph 30	1.63E-01	0.0015	"	0.0819
15-1	Heat Exchangner Vessel Inlet	14466	7782	0.0805	Ref [5]	0.016	6.34E-02	[1], page 65, paragraph 30	1.63E-01	0.0893	"	0.1632
15-2	Heat Exchangner Internal	16477	5771	0.9958	Ref [5]	0.029	1.16E+00	[1], page 65, paragraph 30; [2], formula (1.18)	2.92E-02	0.8740	"	0.0292
15-3	Heat Exchangner Outlet	16679	5771	0.0805	Ref [5]	0.163	6.34E-02	[1], page 65, paragraph 30	1.63E-01	0.0893	"	0.1632
15-4	Gasket [Between Flanges]	16684	5771				0.00E+00	[1], page 65, paragraph 30	1.63E-01	0.0015	"	0.0818

16-1	Pipe [One Side Flange]	16904	5771	0.0981	Ref [5]	0.163	1.00E-01	[1], page 65, paragraph 30	1.63E-01	0.0969	"	0.1632
16-2	90 Degree Elbow	17024	5695	0.0535	Ref [5]	0.163	5.45E-02	[1], Diagrams 6-1, 6-2, 2-1	1.63E-01	0.0529	"	0.1632
16-3	Pipe	17809	4909	0.3501	Ref [5]	0.163	3.58E-01	[1], page 65, paragraph 30	1.63E-01	0.3464	"	0.1632
16-4	Tee	17936	4782	0.0566	Ref [5]	0.163	5.79E-02	[1], page 65, paragraph 30	1.63E-01	0.0560	"	0.1632
16-5	Pipe [One Side Flange]	18436	4282	0.2229	Ref [5]	0.163	2.28E-01	[1], page 65, paragraph 30	1.63E-01	0.2205	"	0.1632
16-6	Gasket [Between Flanges]	18441	4278				0.00E+00	[1], page 65, paragraph 30	1.63E-01	0.0015	"	0.0818
17-1	Gate valve	18657	4062	0.27	Ref [5]	0.147	6.62E-02	[1], page 65, paragraph 30	2.93E-01	0.1000	"	0.2339
17-2	Gasket [Between Flanges]	18661	4057				0.00E+00	[1], page 65, paragraph 30	1.63E-01	0.0015	"	0.0819
18-1	Pipe[One Side Flange]	19161	3557	0.2229	Ref [5]	0.163	2.28E-01	[1], page 65, paragraph 30	1.63E-01	0.2205	"	0.1632
18-2	Tee	19288	3430	0.0566	Ref [5]	0.163	5.79E-02	[1], page 65, paragraph 30	1.63E-01	0.0560	"	0.1632
18-3	Pipe [One Side Flange]	19788	2930	0.2229	Ref [5]	0.163	2.28E-01	[1], page 65, paragraph 30	1.63E-01	0.2205	"	0.1632
18-4	Gasket [Between Flanges]	19793	2926				0.00E+00	[1], page 65, paragraph 30	1.63E-01	0.0015	"	0.0819
19-1	Pipe [Both Side Flange]	20793	1926	0.4458	Ref [5]	0.163	4.56E-01	[1], page 65, paragraph 30	1.63E-01	0.4409	"	0.1632
19-2	Gasket [Between Flanges]	20797	1921				0.00E+00	[1], page 65, paragraph 30	1.63E-01	0.0015	"	0.0819
20-1	Pipe[One Side Flange]	21297	1421	0.2229	Ref [5]	0.163	2.28E-01	[1], page 65, paragraph 30	1.63E-01	0.2205	"	0.1632

20-2	Tee	21424	1294	0.0566	Ref [5]	0.163	5.79E-02	[1], page 65, paragraph 30	1.63E-01	0.0560	"	0.1632
24-1	Pipe [One Side Flange]	22424	294	0.4458	Ref [5]	0.163	4.56E-01	[1], page 65, paragraph 30	1.63E-01	0.4409	"	0.1632
24-2	Gasket [Between Flanges]	22429	290		Ref [5]		0.00E+00	[1], page 65, paragraph 30	1.63E-01	0.0015	"	0.0819
24-3	Pipe[Both Side Flange]	23429	-710	0.4458	Ref [5]	0.163	4.56E-01	[1], page 65, paragraph 30	1.63E-01	0.4409	"	0.1632
24-4	Gasket [Between Flanges]	23433	-715		Ref [5]		0.00E+00	[1], page 65, paragraph 30	1.63E-01	0.0015	"	0.0819
24-5	Pipe [One Side Flange]	23485	-767	0.0232	Ref [5]	0.163	2.38E-02	[1], page 65, paragraph 30	1.63E-01	0.0231	"	0.1632
24-6	90 Degree Elbow	23605	-843	0.0535	Ref [5]	0.163	5.45E-02	[1], Diagrams 6-1, 6-2, 2-1	1.63E-01	0.0529	"	0.1632
24-7	45 Degree Elbow	23665	-843	0.03	Ref [5]	0.163	2.73E-02	[1], Diagrams 6-1, 6-2, 2-1	1.63E-01	0.0265	"	0.1632
24-8	Pipe [One Side Flange]	23883	-843	0.0967	Ref [5]	0.163	9.90E-02	[1], page 65, paragraph 30	1.63E-01	0.0958	"	0.1632
24-9	Gasket [Between Flanges]	23887	-843		Ref [5]		0.00E+00	[1], page 65, paragraph 30	1.63E-01	0.0015	"	0.0819
24-10	Gate valve	24103	-843	0.27	Ref [5]	0.147	6.62E-02	[1], page 65, paragraph 30	2.93E-01	0.1000	"	0.2339
24-11	Gasket [Between Flanges]	24108	-843		Ref [5]		0.00E+00	[1], page 65, paragraph 30	1.63E-01	0.0015	"	0.0819
24-12	Pipe [One Side Flange]	24408	-843	0.1337	Ref [5]	0.163	1.37E-01	[1], page 65, paragraph 30	1.63E-01	0.1323	"	0.1632
24-13	Tee	24535	-779	0.0566	Ref [5]	0.163	1.52E-02	[1], page 65, paragraph 30	1.63E-01	0.0280	"	0.1632
24-14	Pipe [One Side Flange]	24835	-479	0.1337	Ref [5]	0.163	1.66E-01	[1], page 65, paragraph 30	1.63E-01	0.1323	"	0.1632

25-1	Gasket [Between Flanges]	24839	-475		Ref [5]		0.00E+00	[1], page 65, paragraph 30	1.63E-01	0.0015	"	0.0819
25-2	Sump Tank	25816	0		Ref [5]	0.163	0.00E+00		0.00E+00	0.1176	"	0.005
25-3	Gasket [Between Flanges]	25821	0		Ref [5]		0.00E+00	[1], page 65, paragraph 30	1.63E-01	0.0015	"	0.0819
25-4	Gate valve	26037	0	0.27	Ref [5]	0.147	6.62E-02	[1], page 65, paragraph 30	2.93E-01	0.1000	"	0.2339
25-5	Gasket [Between Flanges]	26041	0		Ref [5]		0.00E+00	[1], page 65, paragraph 30	1.63E-01	0.0015	"	0.0819
25-6	45 Degree Elbow [One Side Flange]	26124	0	0.0374	Ref [5]	0.163	3.76E-02	[1], Diagrams 6-1, 6-2, 2-1	1.63E-01	0.0364	"	0.1632
25-7	Pipe	26305	0	0.0807	Ref [5]	0.163	8.23E-02	[1], page 65, paragraph 30	1.63E-01	0.0797	"	0.1632
25-8	45 Degree Elbow	26365	0	0.03	Ref [5]	0.163	2.73E-02	[1], Diagrams 6-1, 6-2, 2-1	1.63E-01	0.0265	"	0.1632
25-9	Tee	26492	0	0.0566	Ref [5]	0.163	5.79E-02	[1], page 65, paragraph 30	1.63E-01	0.0560	"	0.1632
25-10	45 Degree Elbow	26552	0	0.03	Ref [5]	0.163	2.73E-02	[1], Diagrams 6-1, 6-2, 2-1	1.63E-01	0.0265	"	0.1632
25-11	Pipe	26732	0	0.0807	Ref [5]	0.163	8.23E-02	[1], page 65, paragraph 30	1.63E-01	0.0797	"	0.1632
25-12	45 Degree Elbow [One Side Flange]	26815	0	0.0374	Ref [5]	0.163	3.76E-02	[1], Diagrams 6-1, 6-2, 2-1	1.63E-01	0.0364	"	0.1632
25-13	Gasket [Between Flanges]	26819	0		Ref [5]		0.00E+00	[1], page 65, paragraph 30	1.63E-01	0.0015	"	0.0819

Table C-3: Friction loss coefficient (III) at low-mass flow rate condition - RRC KI, SNU

Sub Part No.	Sub Part Name	Accumulated Length (mm)	Accumulated Height (mm)	RRC KI			SNU		
				Factor F(L/D)	Reference (Handbook or etc.)	Reference velocity (m/s)	Factor F(L/D)	Reference (Handbook or etc.)	Reference velocity (m/s)
1-1	Core Inlet	181	0	0.100	Slissky P.M. Methodical Recommendations to Calculation of Friction Factors in Tubes for Transition Zone // Proc. of Sc.-Tech. Hydraulics, M. 1983, pp. 31-44	0.163	0.0808	Colebrook-White correlation, calculated by MARS-LBE 3.11	0.1633
1-2	Downcomer	1403	-1223	0.460	Gynevsky A.S. Solodkin E.E., Hydraulic Resistance of Ring Channels // Industrial Aerodynamics, M. 1961,Iss. 20, pp. 202-215	0.032	0.5632	〃	0.0324
1-3	Lower Plenum	1616	-1300	0.000					
1-4	Core	2947	31	1.270	Sheinina A.V. Hydraulic Resistance of Rod Bundles in Axial Liquid Flow // Liquid Metals, M. 1967, pp. 210-223	0.206	1.9415	〃	0.2217
1-5	Upper Plenum	3629	713	0.220	Slissky P.M. Methodical Recommendations to Calculation of Friction Factors in Tubes for Transition Zone // Proc. of Sc.-Tech. Hydraulics, M. 1983, pp. 31-44	0.163	0.3048	〃	0.1633
1-6	Gasket [Between Flanges]	3633	717	0.000		0.163			
2-1	Pipe [One Side Flange]	3933	1017	0.096	Slissky P.M. Methodical Recommendations to Calculation of Friction Factors in Tubes for Transition Zone // Proc. of Sc.-Tech. Hydraulics, M. 1983, pp. 31-44	0.163	0.1342	〃	0.1633
2-2	Tee	4060	1144	0.040	Slissky P.M. Methodical Recommendations to Calculation of Friction Factors in Tubes for Transition Zone // Proc. of Sc.-Tech. Hydraulics, M. 1983, pp. 31-44	0.163			
2-3	Pipe [One Side Flange]	4360	1444	0.096	Slissky P.M. Methodical Recommendations to Calculation of Friction Factors in Tubes for Transition Zone // Proc. of Sc.-Tech. Hydraulics,	0.163	0.1342	〃	0.1633

					M. 1983, pp. 31-44				
2-4	Gasket [Between Flanges]	4365	1449	0.000		0.163			
3-1	Pipe [Both Side Flange]	5365	2449	0.322	Slissky P.M. Methodical Recommendations to Calculation of Friction Factors in Tubes for Transition Zone // Proc. of Sc.-Tech. Hydraulics, M. 1983, pp. 31-44	0.163	0.4474	〃	0.1633
3-2	Gasket [Between Flanges]	5369	2453	0.000		0.163			
4-1	45 Degree Elbow [One Side Flange]	5452	2530	0.027	Abramovich G.N. Air Dynamics of Local Drags // Industrial AirDynamics, M. 1935, Iss. 21, pp. 65-150	0.163	0.0101	〃 for one side flange	0.1633
4-2	Pipe	5632	2658	0.058	Slissky P.M. Methodical Recommendations to Calculation of Friction Factors in Tubes for Transition Zone // Proc. of Sc.-Tech. Hydraulics, M. 1983, pp. 31-44	0.163	0.0808	〃	0.1633
4-3	45 Degree Elbow	5692	2712	0.019	Abramovich G.N. Air Dynamics of Local Drags // Industrial AirDynamics, M. 1935, Iss. 21, pp. 65-150	0.163			
4-4	Pipe	6411	3431	0.231	Slissky P.M. Methodical Recommendations to Calculation of Friction Factors in Tubes for Transition Zone // Proc. of Sc.-Tech. Hydraulics, M. 1983, pp. 31-44	0.163	0.3216	〃	0.1633
4-5	Tee	6538	3558	0.041	Slissky P.M. Methodical Recommendations to Calculation of Friction Factors in Tubes for Transition Zone // Proc. of Sc.-Tech. Hydraulics, M. 1983, pp. 31-44	0.163			
4-6	Pipe	6709	3729	0.055	Slissky P.M. Methodical Recommendations to Calculation of Friction Factors in Tubes for Transition Zone // Proc. of Sc.-Tech. Hydraulics, M. 1983, pp. 31-44	0.163	0.0765	〃	0.1633
4-7	45 Degree Elbow	6769	3783	0.019	Abramovich G.N. Air Dynamics of Local Drags // Industrial AirDynamics, M. 1935, Iss. 21, pp. 65-150	0.163			

4-8	Pipe	6950	3910	0.058	Slissky P.M. Methodical Recommendations to Calculation of Friction Factors in Tubes for Transition Zone // Proc. of Sc.-Tech. Hydraulics, M. 1983, pp. 31-44	0.163	0.0808	〃	0.1633
4-9	45 Degree Elbow [One Side Flange]	7032	3987	0.027	Abramovich G.N. Air Dynamics of Local Drags // Industrial AirDynamics, M. 1935, Iss. 21, pp. 65-150	0.163	0.0101	〃 for one side flange	0.1633
4-10	Gasket [Between Flanges]	7037	3991	0.000					
5-1	Gate valve	7253	4207	0.070	Slissky P.M. Methodical Recommendations to Calculation of Friction Factors in Tubes for Transition Zone // Proc. of Sc.-Tech. Hydraulics, M. 1983, pp. 31-44	0.292	0.0650	〃	0.2923
5-2	Gasket [Between Flanges]	7257	4212	0.000					
6-1	Pipe [Both Side Flange]	8257	5212	0.322	Slissky P.M. Methodical Recommendations to Calculation of Friction Factors in Tubes for Transition Zone // Proc. of Sc.-Tech. Hydraulics, M. 1983, pp. 31-44	0.163	0.4474	〃	0.1633
6-2	Gasket [Between Flanges]	8262	5216	0.000					
7-1	Pipe [Both Side Flange]	9262	6216	0.322	Slissky P.M. Methodical Recommendations to Calculation of Friction Factors in Tubes for Transition Zone // Proc. of Sc.-Tech. Hydraulics, M. 1983, pp. 31-44	0.163	0.4474	〃	0.1633
7-2	Gasket [Between Flanges]	9266	6221	0.000					
8-1	Pipe [One Side Flange]	9466	6421	0.064	Slissky P.M. Methodical Recommendations to Calculation of Friction Factors in Tubes for Transition Zone // Proc. of Sc.-Tech. Hydraulics, M. 1983, pp. 31-44	0.163	0.0895	〃	0.1633
8-2	Orifice	10066	7021	0.193	Slissky P.M. Methodical Recommendations to Calculation of Friction Factors in Tubes for	0.138			

					Transition Zone // Proc. of Sc.-Tech. Hydraulics, M. 1983, pp. 31-44				
8-3	Pipe [One Side Flange]	10266	7221	0.064	Slissky P.M. Methodical Recommendations to Calculation of Friction Factors in Tubes for Transition Zone // Proc. of Sc.-Tech. Hydraulics, M. 1983, pp. 31-44	0.163	0.0895	〃	0.1633
8-4	Gasket [Between Flanges]	10271	7225	0.000					
9-1	Pipe[Both Side Flange]	10771	7725	0.161	Slissky P.M. Methodical Recommendations to Calculation of Friction Factors in Tubes for Transition Zone // Proc. of Sc.-Tech. Hydraulics, M. 1983, pp. 31-44	0.163	0.2237	〃	0.1633
9-2	Gasket [Between Flanges]	10775	7730	0.000					
10-1	Expansion Tank	11644	7934	0.000			0.1493	〃	0.1633
10-2	Gasket [Between Flanges]	11648	7934	0.000					
11-1	Pipe [Both Side Flange]	12148	7934	0.161	Slissky P.M. Methodical Recommendations to Calculation of Friction Factors in Tubes for Transition Zone // Proc. of Sc.-Tech. Hydraulics, M. 1983, pp. 31-44	0.163	0.2237	〃	0.1633
11-2	Gasket [Between Flanges]	12153	7934	0.000					
12-1	Pipe [One Side Flange]	12453	7934	0.097	Slissky P.M. Methodical Recommendations to Calculation of Friction Factors in Tubes for Transition Zone // Proc. of Sc.-Tech. Hydraulics, M. 1983, pp. 31-44	0.163	0.1342	〃	0.1633
12-2	Tee	12580	7934	0.041	Slissky P.M. Methodical Recommendations to Calculation of Friction Factors in Tubes for Transition Zone // Proc. of Sc.-Tech. Hydraulics, M. 1983, pp. 31-44	0.163			

12-3	Pipe	12885	7934	0.098	Slissky P.M. Methodical Recommendations to Calculation of Friction Factors in Tubes for Transition Zone // Proc. of Sc.-Tech. Hydraulics, M. 1983, pp. 31-44	0.163	0.1366	″	0.1633
12-4	90 Degree Elbow	13005	7858	0.039	Abramovich G.N. Air Dynamics of Local Drags // Industrial AirDynamics, M. 1935, Iss. 21, pp. 65-150	0.163			
12-5	90 Degree Elbow	13125	7782	0.039	Abramovich G.N. Air Dynamics of Local Drags // Industrial AirDynamics, M. 1935, Iss. 21, pp. 65-150	0.163			
12-6	Pipe[One Side Flange]	13325	7782	0.064	Slissky P.M. Methodical Recommendations to Calculation of Friction Factors in Tubes for Transition Zone // Proc. of Sc.-Tech. Hydraulics, M. 1983, pp. 31-44	0.163	0.0895	″	0.1633
12-7	Gasket [Between Flanges]	13330	7782	0.000					
13-1	Gate valve	13546	7782	0.070	Slissky P.M. Methodical Recommendations to Calculation of Friction Factors in Tubes for Transition Zone // Proc. of Sc.-Tech. Hydraulics, M. 1983, pp. 31-44	0.292	0.0650	″	0.2923
13-2	Gasket [Between Flanges]	13550	7782	0.000					
14-1	Pipe [One Side Flange]	13750	7782	0.064	Slissky P.M. Methodical Recommendations to Calculation of Friction Factors in Tubes for Transition Zone // Proc. of Sc.-Tech. Hydraulics, M. 1983, pp. 31-44	0.163	0.0895	″	0.1633
14-2	Tee	13877	7782	0.041	Slissky P.M. Methodical Recommendations to Calculation of Friction Factors in Tubes for Transition Zone // Proc. of Sc.-Tech. Hydraulics, M. 1983, pp. 31-44	0.163			
14-3	Pipe [One Side Flange]	14259	7782	0.123	Slissky P.M. Methodical Recommendations to Calculation of Friction Factors in Tubes for Transition Zone // Proc. of Sc.-Tech. Hydraulics, M. 1983, pp. 31-44	0.163	0.1709	″	0.1633
14-4	Gasket	14264	7782	0.000					

	[Between Flanges]								
15-1	Heat Exchangner Vessel Inlet	14466	7782	0.110	Slissky P.M. Methodical Recommendations to Calculation of Friction Factors in Tubes for Transition Zone // Proc. of Sc.-Tech. Hydraulics, M. 1983, pp. 31-44	0.163	0.0906	″	0.1633
15-2	Heat Exchangner Internal	16477	5771	0.650	Sheinina A.V. Hydraulic Resistance of Rod Bundles in Axial Liquid Flow // Liquid Metals, M. 1967, pp. 210-223	0.029	0.8139	″	0.0292
15-3	Heat Exchangner Outlet	16679	5771	0.110	Slissky P.M. Methodical Recommendations to Calculation of Friction Factors in Tubes for Transition Zone // Proc. of Sc.-Tech. Hydraulics, M. 1983, pp. 31-44	0.163	0.0906	″	0.1633
15-4	Gasket [Between Flanges]	16684	5771	0.000					
16-1	Pipe [One Side Flange]	16904	5771	0.071	Slissky P.M. Methodical Recommendations to Calculation of Friction Factors in Tubes for Transition Zone // Proc. of Sc.-Tech. Hydraulics, M. 1983, pp. 31-44	0.163	0.0983	″	0.1633
16-2	90 Degree Elbow	17024	5695	0.039	Abramovich G.N. Air Dynamics of Local Drags // Industrial AirDynamics, M. 1935, Iss. 21, pp. 65-150	0.163			
16-3	Pipe	17809	4909	0.253	Slissky P.M. Methodical Recommendations to Calculation of Friction Factors in Tubes for Transition Zone // Proc. of Sc.-Tech. Hydraulics, M. 1983, pp. 31-44	0.163	0.3514	″	0.1633
16-4	Tee	17936	4782	0.041	Slissky P.M. Methodical Recommendations to Calculation of Friction Factors in Tubes for Transition Zone // Proc. of Sc.-Tech. Hydraulics, M. 1983, pp. 31-44	0.163			
16-5	Pipe [One Side Flange]	18436	4282	0.161	Slissky P.M. Methodical Recommendations to Calculation of Friction Factors in Tubes for Transition Zone // Proc. of Sc.-Tech. Hydraulics, M. 1983, pp. 31-44	0.163	0.2237	″	0.1633
16-6	Gasket [Between	18441	4278	0.000					

	Flanges]								
17-1	Gate valve	18657	4062	0.070	Slissky P.M. Methodical Recommendations to Calculation of Friction Factors in Tubes for Transition Zone // Proc. of Sc.-Tech. Hydraulics, M. 1983, pp. 31-44	0.292	0.0650	〃	0.2923
17-2	Gasket [Between Flanges]	18661	4057	0.000					
18-1	Pipe[One Side Flange]	19161	3557	0.161	Slissky P.M. Methodical Recommendations to Calculation of Friction Factors in Tubes for Transition Zone // Proc. of Sc.-Tech. Hydraulics, M. 1983, pp. 31-44	0.163	0.2237	〃	0.1633
18-2	Tee	19288	3430	0.041	Slissky P.M. Methodical Recommendations to Calculation of Friction Factors in Tubes for Transition Zone // Proc. of Sc.-Tech. Hydraulics, M. 1983, pp. 31-44	0.163			
18-3	Pipe [One Side Flange]	19788	2930	0.161	Slissky P.M. Methodical Recommendations to Calculation of Friction Factors in Tubes for Transition Zone // Proc. of Sc.-Tech. Hydraulics, M. 1983, pp. 31-44	0.163	0.2237	〃	0.1633
18-4	Gasket [Between Flanges]	19793	2926	0.000					
19-1	Pipe [Both Side Flange]	20793	1926	0.322	Slissky P.M. Methodical Recommendations to Calculation of Friction Factors in Tubes for Transition Zone // Proc. of Sc.-Tech. Hydraulics, M. 1983, pp. 31-44	0.163	0.4474	〃	0.1633
19-2	Gasket [Between Flanges]	20797	1921	0.000					
20-1	Pipe[One Side Flange]	21297	1421	0.161	Slissky P.M. Methodical Recommendations to Calculation of Friction Factors in Tubes for Transition Zone // Proc. of Sc.-Tech. Hydraulics, M. 1983, pp. 31-44	0.163	0.2237	〃	0.1633
20-2	Tee	21424	1294	0.041	Slissky P.M. Methodical Recommendations to Calculation of Friction Factors in Tubes for Transition Zone // Proc. of Sc.-Tech. Hydraulics,	0.163			

					M. 1983, pp. 31-44				
24-1	Pipe [One Side Flange]	22424	294	0.322	Slissky P.M. Methodical Recommendations to Calculation of Friction Factors in Tubes for Transition Zone // Proc. of Sc.-Tech. Hydraulics, M. 1983, pp. 31-44	0.163	0.4474	″	0.1633
24-2	Gasket [Between Flanges]	22429	290	0.000					
24-3	Pipe[Both Side Flange]	23429	-710	0.322	Slissky P.M. Methodical Recommendations to Calculation of Friction Factors in Tubes for Transition Zone // Proc. of Sc.-Tech. Hydraulics, M. 1983, pp. 31-44	0.163	0.4474	″	0.1633
24-4	Gasket [Between Flanges]	23433	-715	0.000					
24-5	Pipe [One Side Flange]	23485	-767	0.017	Slissky P.M. Methodical Recommendations to Calculation of Friction Factors in Tubes for Transition Zone // Proc. of Sc.-Tech. Hydraulics, M. 1983, pp. 31-44	0.163	0.0234	″	0.1633
24-6	90 Degree Elbow	23605	-843	0.039	Abramovich G.N. Air Dynamics of Local Drags // Industrial AirDynamics, M. 1935, Iss. 21, pp. 65-150	0.163			
24-7	45 Degree Elbow	23665	-843	0.019	Abramovich G.N. Air Dynamics of Local Drags // Industrial AirDynamics, M. 1935, Iss. 21, pp. 65-150	0.163			
24-8	Pipe [One Side Flange]	23883	-843	0.070	Slissky P.M. Methodical Recommendations to Calculation of Friction Factors in Tubes for Transition Zone // Proc. of Sc.-Tech. Hydraulics, M. 1983, pp. 31-44	0.163	0.0972	″	0.1633
24-9	Gasket [Between Flanges]	23887	-843	0.000					
24-10	Gate valve	24103	-843	0.070	Slissky P.M. Methodical Recommendations to Calculation of Friction Factors in Tubes for Transition Zone // Proc. of Sc.-Tech. Hydraulics, M. 1983, pp. 31-44	0.292	0.0650	″	0.2923

24-11	Gasket [Between Flanges]	24108	-843	0.097	Slissky P.M. Methodical Recommendations to Calculation of Friction Factors in Tubes for Transition Zone // Proc. of Sc.-Tech. Hydraulics, M. 1983, pp. 31-44	0.163			
24-12	Pipe [One Side Flange]	24408	-843	0.041	Slissky P.M. Methodical Recommendations to Calculation of Friction Factors in Tubes for Transition Zone // Proc. of Sc.-Tech. Hydraulics, M. 1983, pp. 31-44	0.163	0.1342	〃	0.1633
24-13	Tee	24535	-779	0.097	Slissky P.M. Methodical Recommendations to Calculation of Friction Factors in Tubes for Transition Zone // Proc. of Sc.-Tech. Hydraulics, M. 1983, pp. 31-44	0.163			
24-14	Pipe [One Side Flange]	24835	-479	0.000			0.1342	〃	0.1633
25-1	Gasket [Between Flanges]	24839	-475	0.322	Slissky P.M. Methodical Recommendations to Calculation of Friction Factors in Tubes for Transition Zone // Proc. of Sc.-Tech. Hydraulics, M. 1983, pp. 31-44	0.163			
25-2	Sump Tank	25816	0						
25-3	Gasket [Between Flanges]	25821	0						
25-4	Gate valve	26037	0	0.070	Slissky P.M. Methodical Recommendations to Calculation of Friction Factors in Tubes for Transition Zone // Proc. of Sc.-Tech. Hydraulics, M. 1983, pp. 31-44	0.292	0.0650	〃	0.2923
25-5	Gasket [Between Flanges]	26041	0	0.000					
25-6	45 Degree Elbow [One Side Flange]	26124	0	0.027	Abramovich G.N. Air Dynamics of Local Drags // Industrial AirDynamics, M. 1935, Iss. 21, pp. 65-150	0.163	0.0101	〃 for one side flange	0.1633
25-7	Pipe	26305	0	0.058	Slissky P.M. Methodical Recommendations to Calculation of Friction Factors in Tubes for Transition Zone // Proc. of Sc.-Tech. Hydraulics, M. 1983, pp. 31-44	0.163	0.0808	〃	0.1633

25-8	45 Degree Elbow	26365	0	0.019	Abramovich G.N. Air Dynamics of Local Drags // Industrial AirDynamics, M. 1935, Iss. 21, pp. 65-150	0.163			
25-9	Tee	26492	0	0.041	Slissky P.M. Methodical Recommendations to Calculation of Friction Factors in Tubes for Transition Zone // Proc. of Sc.-Tech. Hydraulics, M. 1983, pp. 31-44	0.163			
25-10	45 Degree Elbow	26552	0	0.019	Abramovich G.N. Air Dynamics of Local Drags // Industrial AirDynamics, M. 1935, Iss. 21, pp. 65-150	0.163			
25-11	Pipe	26732	0	0.058	Slissky P.M. Methodical Recommendations to Calculation of Friction Factors in Tubes for Transition Zone // Proc. of Sc.-Tech. Hydraulics, M. 1983, pp. 31-44	0.163	0.0808	〃	0.1633
25-12	45 Degree Elbow [One Side Flange]	26815	0	0.027	Abramovich G.N. Air Dynamics of Local Drags // Industrial AirDynamics, M. 1935, Iss. 21, pp. 65-150	0.163	0.0101	〃 for one side flange	0.1633
25-13	Gasket [Between Flanges]	26819	0	0.000					

Table C-4: Form loss coefficient (I) at low-mass flow rate condition - ENEA, ERSE, GIDROPRESS, IPPE

Sub Part	ENEA			ERSE			GIDROPRESS			IPPE		
	Factor (K)	Reference (HandBook or etc.)	Reference Velocity (m/s)	Factor (K)	Reference (HandBook or etc.)	Reference Velocity (m/s)	Factor (K)	Reference (HandBook or etc.)	Reference Velocity (m/s)	Factor (K)	Reference (HandBook or etc.)	Reference Velocity (m/s)
25-13 → 1-1	0.24852	Borda-Carnot correlation by Idelchik	0.67904	1.689	(1)		0.11		0.1634	0.00E+00	[1], Diagram 2-12	0.00E+00
1-1 → 1-2	0.99423	"	0.67904				1.04		0.1634	1.04E+00	[1], Diagram 7-4	1.63E-01
1-2 → 1-3	0.40641	"	0.13450	1.118	"		0.018		0.1634	2.50E-02	[1], Diagrams 4-2, 4-6, 4-1	3.47E-02
1-3 → 1-4	0.45568	"	0.92134				0.755		0.1634	5.00E-01	[1], Diagram 3-1	2.22E-01
in 1-4	5.17890	Rehme correlation for grids	0.92134	5.556	(2)	0.222	17.3		0.1634	1.94E+00	[1], Diagrams 4-14, 4-15, 4-19	4.34E-01
1-4 → 1-5	0.06917	Borda-Carnot correlation by Idelchik	0.92135				0.13		0.1634	9.76E-02	[1], Diagrams 4-2, 4-6, 4-1	2.22E-01
1-5 → 1-6	0.24852	"	0.67904	0.550	(1)		0.016		0.1634	1.04E-02	[1], Diagram 2-12	1.63E-01
1-6 → 2.1	0.24926	"	0.67904				0.107		0.1634	0.00E+00	[1], Diagram 2-12	0.00E+00
in 2-2	0.00000			0.700	"	0.109	0.1		0.1634	0.00E+00		0.00E+00
2-3 → 2-4	0.24852	Borda-Carnot correlation by Idelchik	0.67904	0.550	"		0.016		0.1634	1.04E-02	[1], Diagram 2-12	1.63E-01
2-4 → 3-1	0.24926	"	0.67904				0.107		0.1634	0.00E+00	[1], Diagram 2-12	0.00E+00
3-1 → 3-2	0.24852	"	0.67904	0.550	"		0.016		0.1634	1.04E-02	[1], Diagram 2-12	1.63E-01
3-2 → 4-1	0.24926	"	0.67904				0.107		0.1634	0.00E+00	[1], Diagram 2-12	0.00E+00
in 4-1	0.13593	45° Elbow correlation by Idelchik	0.67905	0.095	"	0.163	0.11		0.1634	1.17E-01	[1], Diagrams 6-1, 6-2, 2-1	1.63E-01
in 4-3	0.13593	"	0.67905	0.095	"	0.163	0.11		0.1634	1.17E-01	[1], Diagrams 6-1, 6-2, 2-1	1.63E-01

in 4-5	0.00000			0.700	“	0.163	0.1		0.1634	0.00E+00		1.63E-01
in 4-7	0.13593	45° Elbow correlation by Idelchik	0.67905	0.095	“	0.163	0.11		0.1634	1.17E-01	[1], Diagrams 6-1, 6-2, 2-1	1.63E-01
in 4-9	0.13593	"	0.67905	0.095	“	0.163	0.11		0.1634	1.17E-01	[1], Diagrams 6-1, 6-2, 2-1	1.63E-01
4-9 → 4-10	0.24852	Borda-Carnot correlation by Idelchik	0.67906	1.692			0.016		0.1634	1.04E-02	[1], Diagram 2-12	1.63E-01
4-10 → 5-1	0.22329	"	0.67906				0.107		0.1634	0.00E+00	[1], Diagram 2-12	0.00E+00
in 5-1	0.89700	Valve coefficient supplied by manufacturer	1.21535		“	0.292	1.72		0.1634	5.76E-01	[1], Diagrams 4-9, 4-10, 4-2, 4-6, 4-1	2.93E-01
5-1 → 5-2	0.19943	Borda-Carnot correlation by Idelchik	0.67906				0.016		0.1634	1.04E-02	[1], Diagram 2-12	1.63E-01
5-2 → 6-1	0.24926	"	0.67906				0.107		0.1634	0.00E+00	[1], Diagram 2-12	0.00E+00
6-1 → 6-2	0.24852	"	0.67906	0.550	“		0.016		0.1634	1.04E-02	[1], Diagram 2-12	1.63E-01
6-2 → 7-1	0.24926	"	0.67906				0.107		0.1634	0.00E+00	[1], Diagram 2-12	0.00E+00
7-1 → 7-2	0.24852	"	0.67906	0.550	“		0.016		0.1634	1.04E-02	[1], Diagram 2-12	1.63E-01
7-2 → 8-1	0.24926	"	0.67906	0.015	“		0.107		0.1634	0.00E+00	[1], Diagram 2-12	0.00E+00
in 8-2	0.46481(*) 9.8507 0.43181(*)	Orifice correlation by Idelchik	0.67906 0.59468 0.67907	2.260	(3)	0.380	7.796		0.1634	1.30E+00	[1], Diagrams 4-14, 4-15, 4-19	3.80E-01
8-3 → 8-4	0.24852	Borda-Carnot correlation by Idelchik	0.67907	0.105	(1)		0.016		0.1634	1.04E-02	[1], Diagram 2-12	1.63E-01
8-4 → 9-1	0.24926	"	0.67907	0.550	“		0.107		0.1634	0.00E+00	[1], Diagram 2-12	0.00E+00
9-1 → 9-2	0.24852	"	0.67907	0.550	“		0.016		0.1634	1.04E-02	[1], Diagram 2-12	1.63E-01
9-2 → 10-1	0.24926	"	0.67907				0.107		0.1634	0.00E+00	[1], Diagram 2-12	0.00E+00
in 10-1	0.9418(*)	"	0.679	1.700	“		1.61		0.1634	1.69E+00	[1], Diagrams 6-1,	1.63E-01

	0.48687 (**)		0.831								6-2, 2-1	
10-1 → 10-2	0.22218 (*) 0.24852	90° Elbow correlation by Idelchik	0.67908 0.67908	0.550	“		0.016		0.1634	1.04E-02	[1], Diagram 2-12	1.63E-01
10-2 → 11-1	0.24926	Borda-Carnot correlation by Idelchik	0.67908				0.107		0.1634	0.00E+00	[1], Diagram 2-12	0.00E+00
11-1 → 11-2	0.24852	"	0.67908	0.550	“		0.016		0.1634	1.04E-02	[1], Diagram 2-12	1.63E-01
11-2 → 12-1	0.24926	"	0.67908				0.107		0.1634	0.00E+00	[1], Diagram 2-12	0.00E+00
in 12-2	0.00000			0.700	“	0.163	0.1		0.1634	0.00E+00		1.63E-01
in 12-4	0.22218	90° Elbow correlation by Idelchik	0.67908	0.263	“	0.163	0.17		0.1634	3.89E-01	[1], Diagram 2-12	1.63E-01
in 12-5	0.22218	"	0.67908	0.263	“	0.163	0.17		0.1634	0.00E+00	[1], Diagram 2-12	0.00E+00
12-6 → 12-7	0.24852	Borda-Carnot correlation by Idelchik	0.67908	1.692			0.016		0.1634	1.04E-02	[1], Diagram 2-12	1.63E-01
12-7 → 13-1	0.22329	"	0.67908				0.107		0.1634	0.00E+00	[1], Diagram 2-12	0.00E+00
in 13-1	0.89700	Valve coefficient supplied by manufacturer	1.21539		“	0.292	1.72		0.1634	5.76E-01	[1], Diagrams 4-9, 4-10, 4-2, 4-6, 4-1	2.93E-01
13-1 → 13-2	0.19943	Borda-Carnot correlation by Idelchik	0.67906				0.016		0.1634	1.04E-02	[1], Diagram 2-12	1.63E-01
13-2 → 14-1	0.24926	"	0.67906				0.107		0.1634	0.00E+00	[1], Diagram 2-12	0.00E+00
in 14-2	0.00000			0.700	“	0.163	0.1		0.1634	0.00E+00		1.63E-01
14-3 → 14-4	0.24852	Borda-Carnot correlation by Idelchik	0.67908	1.550			0.016		0.1634	1.04E-02	[1], Diagram 2-12	1.63E-01
14-4 → 15-1	0.24926	"	0.67908		“		0.107		0.1634	0.00E+00	[1], Diagram 2-12	0.00E+00
15-1 → 15-	0.49723	"	0.67908				1.03		0.1634	1.03E+00	[1], Diagram 7-4	1.63E-01

2												
in 15-2	9.03600	Rehme correlation for grids	0.12129	11.576	(2)	0.029	0.54		0.1634	3.97E+00	[1], Diagrams 4-14, 4-15, 4-19	5.30E-02
15-2 → 15-3	0.35257	Borda-Carnot correlation by Idelchik	0.67907	1.050	(1)		0.79		0.1634	1.03E+00	[1], Diagram 7-18	1.63E-01
15-3 → 15-4	0.24852	"	0.67907				0.016		0.1634	1.04E-02	[1], Diagram 2-12	1.63E-01
15-4 → 16-1	0.24926	"	0.67907				0.107		0.1634	0.00E+00	[1], Diagram 2-12	0.00E+00
in 16-2	0.22218	90° Elbow correlation by Idelchik	0.67907	0.263	“	0.163	0.17		0.1634	1.95E-01	[1], Diagrams 6-1, 6-2, 2-1	1.63E-01
in 16-4	0.00000			0.700	“	0.163	0.1		0.1634	0.00E+00		1.63E-01
16-5 → 16-6	0.24852	Borda-Carnot correlation by Idelchik	0.67906	1.692			0.016		0.1634	1.04E-02	[1], Diagram 2-12	1.63E-01
16-6 → 17-1	0.22329	"	0.67908				0.107		0.1634	0.00E+00	[1], Diagram 2-12	0.00E+00
in 17-1	0.89700	Valve coefficient supplied by manufacturer	1.21536		“	0.292	1.72		0.1634	5.76E-01	[1], Diagrams 4-9, 4-10, 4-2, 4-6, 4-1	2.93E-01
17-1 → 17-2	0.19943	Borda-Carnot correlation by Idelchik	0.67906				0.016		0.1634	1.04E-02	[1], Diagram 2-12	1.63E-01
17-2 → 18-1	0.24926	"	0.67906				0.107		0.1634	0.00E+00	[1], Diagram 2-12	0.00E+00
in 18-2	0.00000			0.700	“	0.163	0.1		0.1634	0.00E+00		1.63E-01
18-3 → 18-4	0.24852	Borda-Carnot correlation by Idelchik	0.67908	0.550	“		0.016		0.1634	1.04E-02	[1], Diagram 2-12	1.63E-01
18-4 → 19-1	0.24926	"	0.67908				0.107		0.1634	0.00E+00	[1], Diagram 2-12	0.00E+00
19-1 → 19-2	0.24852	"	0.67908	0.550	“		0.016		0.1634	1.04E-02	[1], Diagram 2-12	1.63E-01
19-2 → 20-1	0.24926	"	0.67908				0.107		0.1634	0.00E+00	[1], Diagram 2-12	0.00E+00

in 20-2	0.00000			0.700	“	0.163	0.1		0.1634	0.00E+00		1.63E-01
24-1 → 24-2	0.24852	Borda-Carnot correlation by Idelchik	0.67908	0.570	“		0.016		0.1634	1.04E-02	[1], Diagram 2-12	1.63E-01
24-2 → 24-3	0.24926	"	0.67908				0.107		0.1634	0.00E+00	[1], Diagram 2-12	0.00E+00
24-3 → 24-4	0.24852	"	0.67905	0.550	“		0.016		0.1634	1.04E-02	[1], Diagram 2-12	1.63E-01
24-4 → 24-5	0.24926	"	0.67904				0.107		0.1634	0.00E+00	[1], Diagram 2-12	0.00E+00
in 24-6	0.22218	90° Elbow correlation by Idelchik	0.67904	0.381	“	0.163	0.17		0.1634	1.95E-01	[1], Diagrams 6-1, 6-2, 2-1	1.63E-01
in 24-7	0.13593	45° Elbow correlation by Idelchik	0.67904			0.163	0.11		0.1634	1.17E-01	[1], Diagrams 6-1, 6-2, 2-1	1.63E-01
24-8 → 24-9	0.24852	Borda-Carnot correlation by Idelchik	0.67904	1.692			0.016		0.1634	1.04E-02	[1], Diagram 2-12	1.63E-01
24-9 → 24-10	0.22329	"	0.67904				0.107		0.1634	0.00E+00	[1], Diagram 2-12	0.00E+00
in 24-10	0.89700	Valve coefficient supplied by manufacturer	1.21532		“	0.292	1.72		0.1634	5.76E-01	[1], Diagrams 4-9, 4-10, 4-2, 4-6, 4-1	2.93E-01
24-10 → 24-11	0.19943	Borda-Carnot correlation by Idelchik	0.67904				0.016		0.1634	0.00E+00	[1], Diagram 2-12	0.00E+00
24-11 → 24-12	0.24926	"	0.67904				0.107		0.1634	1.04E-02	[1], Diagram 2-12	1.63E-01
in 24-13	0.22218		0.67904	0.700	“	0.163	1.43		0.1634	1.10E+00	[1], Diagram 7-4	1.63E-01
24-14 → 25-1	0.24852	Borda-Carnot correlation by Idelchik	0.67904	0.550	“		0.016		0.1634	1.04E-02	[1], Diagram 2-12	1.63E-01

25-1 → 25-2	0.24926	"	0.67904				0.107		0.1634	0.00E+00	[1], Diagram 2-12	0.00E+00
in 25-2	0.98324(*) 0.71059 (**)	"	0.679 8.13425			1.957	1.45		0.1634	0.00E+00		0.00E+00
25-2 → 25-3	0.78604	Borda-Carnot correlation by Idelchik	8.13445	1.692			0.016		0.1634	1.04E-02	[1], Diagram 2-12	1.63E-01
25-3 → 25-4	0.22329	"	8.13445				0.107		0.1634	0.00E+00	[1], Diagram 2-12	0.00E+00
in 25-4	0.89700	Valve coefficient supplied by manufacturer	1.21533		"	0.292	1.72		0.1634	5.76E-01	[1], Diagrams 4-9, 4-10, 4-2, 4-6, 4-1	2.93E-01
25-4 → 25-5	0.19943	Borda-Carnot correlation by Idelchik	0.67904				0.016		0.1634	1.04E-02	[1], Diagram 2-12	1.63E-01
25-5 → 25-6	0.24926	"	0.67904				0.107		0.1634	0.00E+00	[1], Diagram 2-12	0.00E+00
in 25-6	0.13593	45° Elbow correlation by Idelchik	0.67904	0.191	"	0.163	0.11		0.1634	1.17E-01	[1], Diagrams 6-1, 6-2, 2-1	1.63E-01
in 25-8	0.13593	"	0.67904			0.163	0.11		0.1634	1.17E-01	[1], Diagrams 6-1, 6-2, 2-1	1.63E-01
in 25-9	0.00000			0.700	"	0.163	0.1		0.1634	0.00E+00		1.63E-01
in 25-10	0.13593	45° Elbow correlation by Idelchik	0.67904	0.191	"	0.163	0.11		0.1634	1.17E-01	[1], Diagrams 6-1, 6-2, 2-1	1.63E-01
in 25-12	0.13593	"	0.67904			0.163	0.11		0.1634	1.17E-01	[1], Diagrams 6-1, 6-2, 2-1	1.63E-01
25-12 → 25-13	0.24926	Borda-Carnot correlation by Idelchik	0.67904				0.016		0.1634	1.04E-02	[1], Diagram 2-12	1.63E-01

Table C-5: Form loss coefficient (II) at low-mass flow rate condition - KIT/INR, RRC KI, SNU

Sub Part	KIT/INR			RRC KI			SNU		
	Factor (K)	Reference (HandBook or etc.)	Reference Velocity (m/s)	Factor (K)	Reference (HandBook or etc.)	Reference Velocity (m/s)	Factor (K)	Reference (HandBook or etc.)	Reference Velocity (m/s)
25-13 → 1-1	0.1993	TRACE Theory Manual	0.1632	0.13	Offengenden Yu.S., Hydraulic Calculation of Plastic Pipes // HydroTechnics and Melioration, 1972,#1, pp. 24-28	0.163	0.2623	(a)	0.1633
1-1 → 1-2	0.9936	"	0.1632	0.726	M.Taliev, Calculation of Drag Coefficients of Tee Connectors, M. Mashgiz, 1952, p. 52	0.163	0.6825	(a)	0.1633
1-2 → 1-3	0.3780	"	0.0323	0.93	Idelchik I.E., Discharge Losses in Flow with Nonuniform Velocity Profile // Proc. of ZAGI, 1948, Iss. 662, pp. 1-24	0.032	0.3888	(a)	0.1633
1-3 → 1-4	0.4690	"	0.2216	1.4	Idelchik I.E., Hinsburg Ia.L., Hydraulic Resistence of Ring Turns of 180° // Thermal Energy, 1968, #4, pp. 87-90	0.206	0.0911	(a)	0.2217
in 1-4	6.5490	Rehme	0.2216	3 x 0.235	Idelchik I.E., Hydraulic Resistance (physical mechanics foundations)// M., 1954, p. 316	0.206	5.3000	(b)	0.2217
1-4 → 1-5	0.0693	TRACE Theory Manual	0.2216	0.025	Idelchik I.E., Account of Viscosity in Hydraulic Resistance of Buffles and Spacers // J. Teploenergetika, 1960, # 9, pp. 75 - 80	0.199	0.0723	(a)	0.2217
1-5 → 1-6	0.2486	"	0.1632	0.115	Rapp R., Alperi R.W., Pressure Loss in Convolution Pipes // Building systems Design, 1970, April, pp. 26-28	0.163	0.2638	(a)	0.1633
1-6 → 2.1	0.1993	"	0.0819	0.13	Offengenden Yu.S., Hydraulic Calculation of Plastic Pipes // HydroTechnics and Melioration, 1972,#1, pp. 24-28	0.163	0.2623	(a)	0.1633
in 2-2	0.4000	VDI Waermeatlas	0.1632	0.7	Zusmanovich V.M., Resistance of Tees of Sink Gas- and Water- Pipes // Problems of Heat Supply and Ventilation, M., 1953, pp. 10 - 30	0.163	0.7000	(c)	0.1633
2-3 → 2-4	0.2486	TRACE Theory Manual	0.1632	0.115	Rapp R., Alperi R.W., Pressure Loss in Convolution Pipes // Building systems Design, 1970, April, pp. 26-28	0.163	0.2638	(a)	0.1633
2-4 → 3-1	0.1993	"	0.0819	0.13	Offengenden Yu.S., Hydraulic Calculation of	0.163	0.2623	(a)	0.1633

					Plastic Pipes // HydroTechnics and Melioration, 1972,#1, pp. 24-28				
3-1 → 3-2	0.2486	"	0.1632	0.115	Rapp R., Alperi R.W., Pressure Loss in Convolution Pipes // Building systems Design, 1970, April, pp. 26-28	0.163	0.2638	(a)	0.1633
3-2 → 4-1	0.1993	"	0.0819	0.13	Offengenden Yu.S., Hydraulic Calculation of Plastic Pipes // HydroTechnics and Melioration, 1972,#1, pp. 24-28	0.163	0.2623	(a)	0.1633
in 4-1	0.2289	Idelchik	0.1632	0.068	Abramovich G.N., Air Dynamics of Local Drags // Industrial AirDynamics, M. 1935, Iss. 21, pp. 65-150	0.163	0.2300	(a)	0.1633
in 4-3	0.2289	"	0.1632	0.068	Abramovich G.N., Air Dynamics of Local Drags // Industrial AirDynamics, M. 1935, Iss. 21, pp. 65-150	0.163	0.2300	(c)	0.1633
in 4-5	0.4000	VDI Waermeatlas	0.1632	0.7	Zusmanovich V.M., Resistance of Tees of Sink Gas- and Water- Pipes // Problems of Heat Supply and Ventilation, M., 1953, pp. 10 - 30	0.163	0.7000	(c)	0.1633
in 4-7	0.2289	Idelchik	0.1632	0.068	Abramovich G.N., Air Dynamics of Local Drags // Industrial AirDynamics, M. 1935, Iss. 21, pp. 65-150	0.163	0.2300	(c)	0.1633
in 4-9	0.2289	"	0.1632	0.068	Abramovich G.N., Air Dynamics of Local Drags // Industrial AirDynamics, M. 1935, Iss. 21, pp. 65-150	0.163	0.2300	(c)	0.1633
4-9 → 4-10	0.2486	TRACE Theory Manual	0.1632	0.115	Rapp R., Alperi R.W., Pressure Loss in Convolution Pipes // Building systems Design, 1970, April, pp. 26-28	0.163	0.2638	(a)	0.1633
4-10 → 5-1	0.1739	"	0.0819	0.13	Offengenden Yu.S., Hydraulic Calculation of Plastic Pipes // HydroTechnics and Melioration, 1972,#1, pp. 24-28	0.163	0.2270	(a)	0.1480
in 5-1	0.9730	Glove-Specification	0.2918	1	Ianshin B.I., HydroDynamic Characteristics of Valves and Pipes // Mashgiz, M., 1965, p. 260	0.292	0.5100	(a)	0.2923
5-1 → 5-2	0.1994	TRACE Theory Manual	0.1479	0.13	Offengenden Yu.S., Hydraulic Calculation of Plastic Pipes // HydroTechnics and Melioration, 1972,#1, pp. 24-28	0.163	0.2129	(a)	0.1480
5-2 → 6-1	0.1993	"	0.0819	0.13	Offengenden Yu.S., Hydraulic Calculation of	0.163	0.2623	(a)	0.1633

					Plastic Pipes // HydroTechnics and Melioration, 1972,#1, pp. 24-28				
6-1 → 6-2	0.2485	"	0.1632	0.115	Rapp R., Alperi R.W., Pressure Loss in Convolution Pipes // Building systems Design, 1970, April, pp. 26-28	0.163	0.2638	(a)	0.1633
6-2 → 7-1	0.1993	"	0.0819	0.13	Offengenden Yu.S., Hydraulic Calculation of Plastic Pipes // HydroTechnics and Melioration, 1972,#1, pp. 24-28	0.163	0.2623	(a)	0.1633
7-1 → 7-2	0.2485	"	0.1632	0.115	Rapp R., Alperi R.W., Pressure Loss in Convolution Pipes // Building systems Design, 1970, April, pp. 26-28	0.163	0.2638	(a)	0.1633
7-2 → 8-1	0.1993	"	0.0819	0.13	Offengenden Yu.S., Hydraulic Calculation of Plastic Pipes // HydroTechnics and Melioration, 1972,#1, pp. 24-28	0.163	0.2623	(a)	0.1633
in 8-2	7.4015	Idelchik	0.1429	2.43	Idelchik I.E., Account of Viscosity in Hydraulic Resistance of Buffles and Spacers // J. Teploenergetika, 1960, # 9, pp. 75 - 80	0.143	8.3900	(c)	0.1633
8-3 → 8-4	0.2485	TRACE Theory Manual	0.1632	0.115	Rapp R., Alperi R.W., Pressure Loss in Convolution Pipes // Building systems Design, 1970, April, pp. 26-28	0.163	0.2638	(a)	0.1633
8-4 → 9-1	0.1993	"	0.0819	0.13	Offengenden Yu.S., Hydraulic Calculation of Plastic Pipes // HydroTechnics and Melioration, 1972,#1, pp. 24-28	0.163	0.2623	(a)	0.1633
9-1 → 9-2	0.2485	"	0.1632	0.115	Rapp R., Alperi R.W., Pressure Loss in Convolution Pipes // Building systems Design, 1970, April, pp. 26-28	0.163	0.2638	(a)	0.1633
9-2 → 10-1	0.1993	"	0.0819	0.13	Offengenden Yu.S., Hydraulic Calculation of Plastic Pipes // HydroTechnics and Melioration, 1972,#1, pp. 24-28	0.163	0.2623	(a)	0.1633
in 10-1	1.4811	"	0.1632	1	Idelchik I.E., Discharge Losses in Flow with Nonuniform Velocity Profile // Proc. of ZAGI, 1948, Iss. 662, pp. 1-24	0.163	1.4047	(a)	0.1633
10-1 → 10-2	0.2485	"	0.1632	0.2	Karev V.N., Pressure Losses at Pipe Sudden Contraction and Influence of Local Drags for Flow Disturbance // Oil Economy, 1953, #8, pp. 3-7	0.163	0.2638	(a)	0.1633
10-2 → 11-1	0.1993	"	0.0819	0.13	Offengenden Yu.S., Hydraulic Calculation of	0.163	0.2623	(a)	0.1633

					Plastic Pipes // HydroTechnics and Melioration, 1972,#1, pp. 24-28				
11-1 → 11-2	0.2485	"	0.1632	0.115	Rapp R., Alperi R.W., Pressure Loss in Convolution Pipes // Building systems Design, 1970, April, pp. 26-28	0.163	0.2638	(a)	0.1633
11-2 → 12-1	0.1993	"	0.0819	0.13	Offengenden Yu.S., Hydraulic Calculation of Plastic Pipes // HydroTechnics and Melioration, 1972,#1, pp. 24-28	0.163	0.2623	(a)	0.1633
in 12-2	0.4000	VDI Waermeatlas	0.1632	0.7	Zusmanovich V.M., Resistance of Tees of Sink Gas- and Water- Pipes // Problems of Heat Supply and Ventilation, M., 1953, pp. 10 - 30	0.163	0.7000	(c)	0.1633
in 12-4	0.3174	Idelchik	0.1632	0.096	Abramovich G.N., Air Dynamics of Local Drags // Industrial AirDynamics, M. 1935, Iss. 21, pp. 65-150	0.163	0.2600	(c)	0.1633
in 12-5	0.3174	"	0.1632	0.096	Abramovich G.N., Air Dynamics of Local Drags // Industrial AirDynamics, M. 1935, Iss. 21, pp. 65-150	0.163	0.2600	(c)	0.1633
12-6 → 12-7	0.2485	TRACE Theory Manual	0.1632	0.115	Rapp R., Alperi R.W., Pressure Loss in Convolution Pipes // Building systems Design, 1970, April, pp. 26-28	0.163	0.2638	(a)	0.1633
12-7 → 13-1	0.1739	"	0.0819	0.13	Offengenden Yu.S., Hydraulic Calculation of Plastic Pipes // HydroTechnics and Melioration, 1972,#1, pp. 24-28	0.163	0.2270	(a)	0.1480
in 13-1	0.9730	Glove-Specification	0.2918	1	Ianshin B.I., HydroDynamic Characteristics of Valves and Pipes // Mashgiz, M., 1965, p. 260	0.292	0.5100	(a)	0.2923
13-1 → 13-2	0.1994	TRACE Theory Manual	0.1479	0.115	Rapp R., Alperi R.W., Pressure Loss in Convolution Pipes // Building systems Design, 1970, April, pp. 26-28	0.163	0.2129	(a)	0.1480
13-2 → 14-1	0.1993	"	0.0819	0.13	Offengenden Yu.S., Hydraulic Calculation of Plastic Pipes // HydroTechnics and Melioration, 1972,#1, pp. 24-28	0.163	0.2623	(a)	0.1633
in 14-2	0.4000	VDI Waermeatlas	0.1632	0.7	Zusmanovich V.M., Resistance of Tees of Sink Gas- and Water- Pipes // Problems of Heat Supply and Ventilation, M., 1953, pp. 10 - 30	0.163	0.7000	(c)	0.1633
14-3 → 14-4	0.2485	TRACE	0.1632	0.115	Rapp R., Alperi R.W., Pressure Loss in	0.163	0.2638	(a)	0.1633

		Theory Manual			Convolution Pipes // Building systems Design, 1970, April, pp. 26-28				
14-4 → 15-1	0.1993	"	0.0819	0.13	Offengenden Yu.S., Hydraulic Calculation of Plastic Pipes // HydroTechnics and Melioration, 1972,#1, pp. 24-28	0.163	0.2623	(a)	0.1633
15-1 → 15-2	0.9500	"	0.1632	0.726	M.Taliev, Calculation of Drag Coefficients of Tee Connectors, M. Mashgiz, 1952, p. 52	0.029	0.7163	(a)	0.1633
in 15-2	12.4800	Rehme	0.0292	6*0.99	Idelchik I.E., Hydraulic Resistance (physical mechanics foundations)// M., 1954, p. 316	0.029	11.3800	(b)	0.0290
15-2 → 15-3	0.9500	TRACE Theory Manual	0.1632	0.2	Karev V.N., Pressure Losses at Pipe Sudden Contraction and Influence of Local Drags for Flow Disturbance // Oil Economy, 1953, #8, pp. 3-7	0.029	0.3915	(a)	0.1633
15-3 → 15-4	0.2485	"	0.1632	0.115	Rapp R., Alperi R.W., Pressure Loss in Convolution Pipes // Building systems Design, 1970, April, pp. 26-28	0.163	0.2638	(a)	0.1633
15-4 → 16-1	0.1993	"	0.0819	0.13	Offengenden Yu.S., Hydraulic Calculation of Plastic Pipes // HydroTechnics and Melioration, 1972,#1, pp. 24-28	0.163	0.2623	(a)	0.1633
in 16-2	0.3174	Idelchik	0.1632	0.096	Abramovich G.N., Air Dynamics of Local Drags // Industrial AirDynamics, M. 1935, Iss. 21, pp. 65-150	0.163	0.2600	(c)	0.1633
in 16-4	0.4000	VDI Waermeatlas	0.1632	0.7	Zusmanovich V.M., Resistance of Tees of Sink Gas- and Water- Pipes // Problems of Heat Supply and Ventilation, M., 1953, pp. 10 - 30	0.163	0.7000	(c)	0.1633
16-5 → 16-6	0.2485	TRACE Theory Manual	0.1632	0.115	Rapp R., Alperi R.W., Pressure Loss in Convolution Pipes // Building systems Design, 1970, April, pp. 26-28	0.163	0.2638	(a)	0.1633
16-6 → 17-1	0.1739	"	0.0819	0.13	Offengenden Yu.S., Hydraulic Calculation of Plastic Pipes // HydroTechnics and Melioration, 1972,#1, pp. 24-28	0.163	0.2270	(a)	0.1480
in 17-1	0.9730	Glove-Specification	0.2918	1	Ianshin B.I., HydroDynamic Characteristics of Valves and Pipes // Mashgiz, M., 1965, p. 260	0.292	0.5100	(a)	0.2923
17-1 → 17-2	0.1994	TRACE Theory Manual	0.1479	0.115	Rapp R., Alperi R.W., Pressure Loss in Convolution Pipes // Building systems Design, 1970, April, pp. 26-28	0.163	0.2129	(a)	0.1480

17-2 → 18-1	0.1993	"	0.0819	0.13	Offengenden Yu.S., Hydraulic Calculation of Plastic Pipes // HydroTechnics and Melioration, 1972,#1, pp. 24-28	0.163	0.2623	(a)	0.1633
in 18-2	0.4000	VDI Waermeatlas	0.1632	0.7	Zusmanovich V.M., Resistance of Tees of Sink Gas- and Water- Pipes // Problems of Heat Supply and Ventilation, M., 1953, pp. 10 - 30	0.163	0.7000	(c)	0.1633
18-3 → 18-4	0.2485	TRACE Theory Manual	0.1632	0.115	Rapp R., Alperi R.W., Pressure Loss in Convolution Pipes // Building systems Design, 1970, April, pp. 26-28	0.163	0.2638	(a)	0.1633
18-4 → 19-1	0.1993	"	0.0819	0.13	Offengenden Yu.S., Hydraulic Calculation of Plastic Pipes // HydroTechnics and Melioration, 1972,#1, pp. 24-28	0.163	0.2623	(a)	0.1633
19-1 → 19-2	0.2485	"	0.1632	0.115	Rapp R., Alperi R.W., Pressure Loss in Convolution Pipes // Building systems Design, 1970, April, pp. 26-28	0.163	0.2638	(a)	0.1633
19-2 → 20-1	0.1993	"	0.0819	0.13	Offengenden Yu.S., Hydraulic Calculation of Plastic Pipes // HydroTechnics and Melioration, 1972,#1, pp. 24-28	0.163	0.2623	(a)	0.1633
in 20-2	0.4000	VDI Waermeatlas	0.1632	0.7	Zusmanovich V.M., Resistance of Tees of Sink Gas- and Water- Pipes // Problems of Heat Supply and Ventilation, M., 1953, pp. 10 - 30	0.163	0.7000	(c)	0.1633
24-1 → 24-2	0.2485	TRACE Theory Manual	0.1632	0.115	Rapp R., Alperi R.W., Pressure Loss in Convolution Pipes // Building systems Design, 1970, April, pp. 26-28	0.163	0.2638	(a)	0.1633
24-2 → 24-3	0.1993	"	0.0819	0.13	Offengenden Yu.S., Hydraulic Calculation of Plastic Pipes // HydroTechnics and Melioration, 1972,#1, pp. 24-28	0.163	0.2623	(a)	0.1633
24-3 → 24-4	0.2485	"	0.1632	0.115	Rapp R., Alperi R.W., Pressure Loss in Convolution Pipes // Building systems Design, 1970, April, pp. 26-28	0.163	0.2638	(a)	0.1633
24-4 → 24-5	0.1993	"	0.0819	0.13	Offengenden Yu.S., Hydraulic Calculation of Plastic Pipes // HydroTechnics and Melioration, 1972,#1, pp. 24-28	0.163	0.2623	(a)	0.1633
in 24-6	0.3174	Idelchik	0.1632	0.096	Abramovich G.N., Air Dynamics of Local Drags // Industrial AirDynamics, M. 1935, Iss. 21, pp. 65-150	0.163	0.2600	(c)	0.1633

in 24-7	0.2289	"	0.1632	0.068	Abramovich G.N., Air Dynamics of Local Drags // Industrial AirDynamics, M. 1935, Iss. 21, pp. 65-150	0.163	0.2300	(c)	0.1633
24-8 → 24-9	0.2485	TRACE Theory Manual	0.1632	0.115	Rapp R., Alperi R.W., Pressure Loss in Convolution Pipes // Building systems Design, 1970, April, pp. 26-28	0.163	0.2638	(a)	0.1633
24-9 → 24-10	0.1739	"	0.0819	0.13	Offengenden Yu.S., Hydraulic Calculation of Plastic Pipes // HydroTechnics and Melioration, 1972,#1, pp. 24-28	0.163	0.2270	(a)	0.1480
in 24-10	0.9730	Glove-Specification	0.2918	1	Ianshin B.I., HydroDynamic Characteristics of Valves and Pipes // Mashgiz, M., 1965, p. 260	0.292	0.5100	(a)	0.2923
24-10 → 24-11	0.1994	TRACE Theory Manual	0.1479	0.13	Offengenden Yu.S., Hydraulic Calculation of Plastic Pipes // HydroTechnics and Melioration, 1972,#1, pp. 24-28	0.163	0.2129	(a)	0.1480
24-11 → 24-12	0.1993	"	0.0819	0.13	Offengenden Yu.S., Hydraulic Calculation of Plastic Pipes // HydroTechnics and Melioration, 1972,#1, pp. 24-28	0.163	0.2623	(a)	0.1633
in 24-13	2.0000	VDI Waermeatlas	0.1632	0.7	Zusmanovich V.M., Resistance of Tees of Sink Gas- and Water- Pipes // Problems of Heat Supply and Ventilation, M., 1953, pp. 10 - 30	0.163	2.8000	(c)	0.1633
24-14 → 25-1	0.2485	TRACE Theory Manual	0.1632	0.115	Rapp R., Alperi R.W., Pressure Loss in Convolution Pipes // Building systems Design, 1970, April, pp. 26-28	0.163	0.2638	(a)	0.1633
25-1 → 25-2	0.8812	"	0.0819	0.13	Offengenden Yu.S., Hydraulic Calculation of Plastic Pipes // HydroTechnics and Melioration, 1972,#1, pp. 24-28	0.163	0.2623	(a)	0.1633
in 25-2	0.0000		0.005	1	Idelchik I.E., Discharge Losses in Flow with Nonuniform Velocity Profile // Proc. of ZAGI, 1948, Iss. 662, pp. 1-24	0.163			
25-2 → 25-3	0.9180	"	1.956	0.115	Rapp R., Alperi R.W., Pressure Loss in Convolution Pipes // Building systems Design, 1970, April, pp. 26-28	0.163	0.2638	(a)	0.1633
25-3 → 25-4	0.1739	"	0.0819	0.13	Offengenden Yu.S., Hydraulic Calculation of Plastic Pipes // HydroTechnics and Melioration, 1972,#1, pp. 24-28	0.163	0.2270	(a)	0.1480

in 25-4	0.9730	Glove-Specification	0.2918	1	Ianshin B.I., HydroDynamic Characteristics of Valves and Pipes // Mashgiz, M., 1965, p. 260	0.292	0.5100	(a)	0.1633
25-4 → 25-5	0.1994	TRACE Theory Manual	0.1479	0.115	Rapp R., Alperi R.W., Pressure Loss in Convolution Pipes // Building systems Design, 1970, April, pp. 26-28	0.163	0.2129	(a)	0.1480
25-5 → 25-6	0.1993	"	0.0819	0.13	Offengenden Yu.S., Hydraulic Calculation of Plastic Pipes // HydroTechnics and Melioration, 1972,#1, pp. 24-28	0.163	0.2623	(a)	0.1633
in 25-6	0.2289	Idelchik	0.1632	0.068	Abramovich G.N., Air Dynamics of Local Drags // Industrial AirDynamics, M. 1935, Iss. 21, pp. 65-150	0.163	0.2300	(c)	0.1633
in 25-8	0.2289	"	0.1632	0.068	Abramovich G.N., Air Dynamics of Local Drags // Industrial AirDynamics, M. 1935, Iss. 21, pp. 65-150	0.163	0.2300	(c)	0.1633
in 25-9	0.4000	VDI Waermeatlas	0.1632	0.7	Zusmanovich V.M., Resistance of Tees of Sink Gas- and Water- Pipes // Problems of Heat Supply and Ventilation, M., 1953, pp. 10 - 30	0.163	0.7000	(c)	0.1633
in 25-10	0.2289	Idelchik	0.1632	0.068	Abramovich G.N., Air Dynamics of Local Drags // Industrial AirDynamics, M. 1935, Iss. 21, pp. 65-150	0.163	0.2300	(c)	0.1633
in 25-12	0.2289	"	0.1632	0.068	Abramovich G.N., Air Dynamics of Local Drags // Industrial AirDynamics, M. 1935, Iss. 21, pp. 65-150	0.163	0.2300	(c)	0.1633
25-12 → 25-13	0.2485	TRACE Theory Manual	0.1632	0.115	Rapp R., Alperi R.W., Pressure Loss in Convolution Pipes // Building systems Design, 1970, April, pp. 26-28	0.163	0.2638	(a)	0.1633

Table C-6: Friction loss coefficient (1) at high-mass flow rate condition - ENEA, ERSE, GIDROPRESS

Sub Part No.	Sub Part Name	Accumulated Length (mm)	Accumulated Height (mm)	ENEA			ERSE			GIDROPRESS		
				Factor F(L/D)	Reference (Handbook or etc.)	Reference velocity (m/s)	Factor F(L/D)	Reference (Handbook or etc.)	Reference velocity (m/s)	Factor F(L/D)	Reference (Handbook or etc.)	Reference velocity (m/s)
1-1	Core Inlet	181	0	5.6281E-02	Colebrook-White correlation (calculated by Relap5 /Mod 3.3 code)	0.67904	0.0605	Frank M. White – Fluid Mechanics 2nd edition – Mc Graw-Hill	0.678	0.06	***	0.678
1-2	Downcomer	1403	-1223	4.0142E-01	"	0.1345	0.4629	Moody chart – Colebrook interpolation formula	0.134	0.016		0.678
1-3	Lower Plenum	1616	-1300	4.6404E-02	"	0.52792		“	0.089	0		0.678
1-4	Core	2947	31	1.1820E+00	"	0.92135	1.3531	“	0.920	3.457		0.678
1-5	Upper Plenum	3629	713	2.4929E-01	"	0.7275	0.2281	“	0.678	0.226		0.678
1-6	Gasket [Between Flanges]	3633	717	1.0198E-01	"	0.67904		“		0.0011		0.678
2-1	Pipe [One Side Flange]	3933	1017		"		0.1004	“	0.678	0.1		0.678
2-2	Tee	4060	1144	4.2532E-02	"	0.67904	0.0360	“	0.454	0.04		0.678
2-3	Pipe [One Side Flange]	4360	1444	1.0198E-01	"	0.67904	0.1004	“	0.678	0.1		0.678
2-4	Gasket [Between Flanges]	4365	1449		"			“		0.0011		0.678
3-1	Pipe [Both Side Flange]	5365	2449	3.1255E-01	"	0.67905	0.3347	“	0.678	0.332		0.678
3-2	Gasket	5369	2453		"			“		0.0011		0.678

	[Between Flanges]											
4-1	45 Degree Elbow [One Side Flange]	5452	2530	7.4176E-02	"	0.67905	0.1156	“	0.678	0.027		0.678
4-2	Pipe	5632	2658		"			“	0.678	0.06		0.678
4-3	45 Degree Elbow	5692	2712	2.5399E-01	"	0.67905		“	0.678	0.02		0.678
4-4	Pipe	6411	3431		"		0.2406	“	0.678	0.238		0.678
4-5	Tee	6538	3558	4.2533E-02	"	0.67905	0.0425	“	0.678	0.042		0.678
4-6	Pipe	6709	3729	7.0543E-02	"	0.67905	0.0573	“	0.678	0.057		0.678
4-7	45 Degree Elbow	6769	3783		"		0.1081	“	0.678	0.02		0.678
4-8	Pipe	6950	3910	9.5309E-02	"	0.67905		“	0.678	0.06		0.678
4-9	45 Degree Elbow [One Side Flange]	7032	3987		"			“	0.678	0.027		0.678
4-10	Gasket [Between Flanges]	7037	3991		"		0.0815	“		0.0011		0.678
5-1	Gate valve	7253	4207	6.3226E-02	"	1.21535		“	1.213	0.155		0.678
5-2	Gasket [Between Flanges]	7257	4212	3.3502E-01	"	0.67906		“		0.0011		0.678
6-1	Pipe [Both Side Flange]	8257	5212		"		0.3347	“	0.678	0.332		0.678
6-2	Gasket [Between Flanges]	8262	5216	3.3642E-01	"	0.67906		“		0.0011		0.678
7-1	Pipe [Both Side Flange]	9262	6216		"		0.3347	“	0.678	0.332		0.678
7-2	Gasket	9266	6221	6.5730E-02	"	0.67906		“		0.0011		0.678

	[Between Flanges]											
8-1	Pipe [One Side Flange]	9466	6421		"		0.2605	“	0.636	0.066		0.678
8-2	Orifice	10066	7021	1.8452E-01	"	0.61578		“	1.576	0.1462		0.678
8-3	Pipe [One Side Flange]	10266	7221	6.5731E-02	"	0.67907		“	0.636	0.066		0.678
8-4	Gasket [Between Flanges]	10271	7225		"			“		0.0011		0.678
9-1	Pipe[Both Side Flange]	10771	7725	1.6896E-01	"	0.67907	0.1674	“	0.678	0.166		0.678
9-2	Gasket [Between Flanges]	10775	7730		"			“		0.0011		0.678
10-1	Expansion Tank	11644	7934	2.1431E-01	"	0.70433	0.1926	“		0.245		0.678
10-2	Gasket [Between Flanges]	11648	7934		"			“		0.0011		0.678
11-1	Pipe [Both Side Flange]	12148	7934	1.6890E-01	"	0.67908	0.1674	“	0.678	0.166		0.678
11-2	Gasket [Between Flanges]	12153	7934		"			“		0.0011		0.678
12-1	Pipe [One Side Flange]	12453	7934	1.0044E-01	"	0.67908	0.1004	“	0.678	0.1		0.678
12-2	Tee	12580	7934	4.2518E-02	"	0.67908	0.0425	“	0.678	0.04		0.678
12-3	Pipe	12885	7934	1.0224E-01	"	0.67908	0.1022	“	0.678	0.1		0.678
12-4	90 Degree Elbow	13005	7858	4.0071E-02	"	0.67908	0.0801	“	0.678	0.04		0.678
12-5	90 Degree Elbow	13125	7782	4.0071E-02	"	0.67908	0.0801	“	0.678	0.04		0.678

12-6	Pipe[One Side Flange]	13325	7782	6.7084E-02	"	0.67908	0.0669	“	0.678	0.066		0.678
12-7	Gasket [Between Flanges]	13330	7782		"		0.0998	“		0.0011		0.678
13-1	Gate valve	13546	7782	6.3439E-02	"	1.08131		“	1.213	0.155		0.678
13-2	Gasket [Between Flanges]	13550	7782	6.7072E-02	"	0.67908		“		0.0011		0.678
14-1	Pipe [One Side Flange]	13750	7782		"		0.0837	“	0.678	0.066		0.678
14-2	Tee	13877	7782	4.2518E-02	"	0.67908	0.0425	“	0.678	0.04		0.678
14-3	Pipe [One Side Flange]	14259	7782	1.2950E-01	"	0.67908	0.1280	“	0.678	0.127		0.678
14-4	Gasket [Between Flanges]	14264	7782		"			“		0.0011		0.678
15-1	Heat Exchangner Vessel Inlet	14466	7782	3.6023E-02	"	0.67908	0.0466	“	0.678	0.05		0.678
15-2	Heat Exchangner Internal	16477	5771	6.3975E-01	"	0.12129	0.7350	“	0.121	0.03		0.678
15-3	Heat Exchangner Outlet	16679	5771	4.5359E-02	"	0.67907	0.0466	“	0.678	0.05		0.678
15-4	Gasket [Between Flanges]	16684	5771		"			“		0.0011		0.678
16-1	Pipe [One Side Flange]	16904	5771	7.3591E-02	"	0.67907	0.0736	“	0.678	0.073		0.678
16-2	90 Degree Elbow	17024	5695	4.0073E-02	"	0.67907	0.0401	“	0.678	0.04		0.678

16-3	Pipe	17809	4909	2.6299E-01	"	0.67907	0.2629	“	0.678	0.26		0.678
16-4	Tee	17936	4782	4.2521E-02	"	0.67906	0.0425	“	0.678	0.04		0.678
16-5	Pipe [One Side Flange]	18436	4282	1.6741E-01	"	0.67906	0.1674	“	0.678	0.166		0.678
16-6	Gasket [Between Flanges]	18441	4278		"		0.0866	“		0.0011		0.678
17-1	Gate valve	18657	4062	6.3671E-02	"	1.08129		“	1.213	0.155		0.678
17-2	Gasket [Between Flanges]	18661	4057	1.6741E-01	"	0.67906		“		0.0011		0.678
18-1	Pipe[One Side Flange]	19161	3557		"		0.1644	“	0.678	0.166		0.678
18-2	Tee	19288	3430	4.2522E-02	"	0.67906	0.0425	“	0.678	0.04		0.678
18-3	Pipe [One Side Flange]	19788	2930	1.6892E-01	"	0.67906	0.1674	“	0.678	0.166		0.678
18-4	Gasket [Between Flanges]	19793	2926		"			“		0.0011		0.678
19-1	Pipe [Both Side Flange]	20793	1926	3.3633E-01	"	0.67905	0.3347	“	0.678	0.332		0.678
19-2	Gasket [Between Flanges]	20797	1921		"			“		0.0011		0.678
20-1	Pipe[One Side Flange]	21297	1421	1.6741E-01	"	0.67905	0.1674	“	0.678	0.166		0.678
20-2	Tee	21424	1294	4.2523E-02	"	0.67905	0.0425	“	0.678	0.04		0.678
24-1	Pipe [One Side Flange]	22424	294	3.3633E-01	"	0.67905	0.3660	“	0.678	0.332		0.678
24-2	Gasket [Between Flanges]	22429	290		"			“		0.0011		0.678

24-3	Pipe[Both Side Flange]	23429	-710	3.3483E-01	"	0.67904	0.3347	“	0.678	0.332		0.678
24-4	Gasket [Between Flanges]	23433	-715	1.9008E-02	"	0.67904		“		0.0011		0.678
24-5	Pipe [One Side Flange]	23485	-767		"		0.0776	“	0.678	0.017		0.678
24-6	90 Degree Elbow	23605	-843	4.0076E-02	"	0.67904		“	0.678	0.04		0.678
24-7	45 Degree Elbow	23665	-843	2.5545E-02	"	0.67904		“	0.678	0.02		0.678
24-8	Pipe [One Side Flange]	23883	-843	7.2811E-02	"	0.67904	0.0727	“	0.678	0.072		0.678
24-9	Gasket [Between Flanges]	23887	-843		"		0.0815	“		0.0011		0.678
24-10	Gate valve	24103	-843	6.3492E-02	"	1.08125		“	1.213	0.155		0.678
24-11	Gasket [Between Flanges]	24108	-843	1.0058E-01	"	0.67904				0.0011		0.678
24-12	Pipe [One Side Flange]	24408	-843		"		0.1004	“	0.678	0.1		0.678
24-13	Tee	24535	-779	4.2525E-02	"	0.67904	0.0425	“	0.678	0.04		0.678
24-14	Pipe [One Side Flange]	24835	-479	1.0196E-01	"	0.67904	0.1004	“	0.678	0.1		0.678
25-1	Gasket [Between Flanges]	24839	-475		"			“		0.0011		0.678
25-2	Sump Tank	25816	0	3.5616E-01	"	3.66116	0.4437	“	8.122	0.1		0.678
25-3	Gasket [Between	25821	0		"		0.0815	“		0.0011		0.678

	Flanges]											
25-4	Gate valve	26037	0	7.4582E-02	"	1.21533		“	1.213	0.155		0.678
25-5	Gasket [Between Flanges]	26041	0	2.9414E-02	"	0.67904		“		0.0011		0.678
25-6	45 Degree Elbow [One Side Flange]	26124	0		"		0.1081	“	0.678	0.027		0.678
25-7	Pipe	26305	0	6.0501E-02	"	0.67904		“	0.678	0.06		0.678
25-8	45 Degree Elbow	26365	0	1.8364E-02	"	0.67904		“	0.678	0.02		0.678
25-9	Tee	26492	0	1.8616E-02	"	0.67904	0.0425	“	0.678	0.04		0.678
25-10	45 Degree Elbow	26552	0	1.8364E-02	"	0.67904	0.1081	“	0.678	0.02		0.678
25-11	Pipe	26732	0	6.0501E-02	"	0.67904		“	0.678	0.06		0.678
25-12	45 Degree Elbow [One Side Flange]	26815	0	2.7625E-02	"	0.67904		“	0.678	0.027		0.678
25-13	Gasket [Between Flanges]	26819	0		"			“	0.678	0.0011		0.678

Table C-7: Friction loss coefficient (II) at high-mass flow rate condition - IAEA, IPPE, KIT/IKET

Sub Part No.	Sub Part Name	Accumulated Length (mm)	Accumulated Height (mm)	IAEA			IPPE			KIT/IKET		
				Factor F(L/D)	Reference (Handbook or etc.)	Reference velocity (m/s)	Factor F(L/D)	Reference (Handbook or etc.)	Reference velocity (m/s)	Factor F(L/D)	Reference (Handbook or etc.)	Reference velocity (m/s)
1-1	Core Inlet	181	0	0.0564	Ref [5]	0.678	5.67E-02	[1], page 65, paragraph 30	6.78E-01	0.06	see contribution to	0.689
1-2	Downcomer	1403	-1223	0.3341	Ref [5]	0.134	4.08E-01	[1], Diagram 2-7	1.34E-01	0.42	report Phase-1	0.145
1-3	Lower Plenum	1616	-1300		Ref [5]		2.54E-02	[1], Diagram 2-7	1.34E-01	0.02		0.045
1-4	Core	2947	31	1.362	Ref [5]	0.920	1.71E+00	[1], page 65, paragraph 30; [2], formula (1.18)	9.21E-01	1.76		0.936
1-5	Upper Plenum	3629	713	0.2129	Ref [5]	0.678	2.35E-01	[1], page 65, paragraph 30	6.78E-01	0.17		0.689
1-6	Gasket [Between Flanges]	3633	717		Ref [5]	0.000	0.00E+00	[1], page 65, paragraph 30	6.78E-01			
2-1	Pipe [One Side Flange]	3933	1017	0.0937	Ref [5]	0.678	1.04E-01	[1], page 65, paragraph 30	6.78E-01			
2-2	Tee	4060	1144	0.0397	Ref [5]	0.678	4.39E-02	[1], page 65, paragraph 30	6.78E-01	0.23		0.689
2-3	Pipe [One Side Flange]	4360	1444	0.0937	Ref [5]	0.678	1.04E-01	[1], page 65, paragraph 30	6.78E-01			
2-4	Gasket [Between Flanges]	4365	1449		Ref [5]		0.00E+00	[1], page 65, paragraph 30	6.78E-01			
3-1	Pipe [Both Side Flange]	5365	2449	0.3123	Ref [5]	0.678	3.45E-01	[1], page 65, paragraph 30	6.78E-01	0.32		0.689
3-2	Gasket [Between	5369	2453		Ref [5]		0.00E+00	[1], page 65, paragraph 30	6.78E-01			

	Flanges]											
4-1	45 Degree Elbow [One Side Flange]	5452	2530	0.025	Ref [5]	0.678	2.85E-02	[1], Diagrams 6-1, 6-2, 2-1	6.78E-01			
4-2	Pipe	5632	2658	0.0562	Ref [5]	0.678	6.24E-02	[1], page 65, paragraph 30	6.78E-01			
4-3	45 Degree Elbow	5692	2712	0.018	Ref [5]	0.678	2.07E-02	[1], Diagrams 6-1, 6-2, 2-1	6.78E-01			
4-4	Pipe	6411	3431	0.2246	Ref [5]	0.678	2.48E-01	[1], page 65, paragraph 30	6.78E-01	0.53		0.689
4-5	Tee	6538	3558	0.0397	Ref [5]	0.678	4.39E-02	[1], page 65, paragraph 30	6.78E-01			
4-6	Pipe	6709	3729	0.0534	Ref [5]	0.678	5.91E-02	[1], page 65, paragraph 30	6.78E-01			
4-7	45 Degree Elbow	6769	3783	0.018	Ref [5]	0.678	2.07E-02	[1], Diagrams 6-1, 6-2, 2-1	6.78E-01			
4-8	Pipe	6950	3910	0.0565	Ref [5]	0.678	6.24E-02	[1], page 65, paragraph 30	6.78E-01			
4-9	45 Degree Elbow [One Side Flange]	7032	3987	0.0262	Ref [5]	0.678	2.85E-02	[1], Diagrams 6-1, 6-2, 2-1	6.78E-01			
4-10	Gasket [Between Flanges]	7037	3991		Ref [5]		0.00E+00	[1], page 65, paragraph 30	6.78E-01			
5-1	Gate valve	7253	4207	0.094	Ref [5]	0.614	1.97E-01	[1], page 65, paragraph 30	6.15E-01			
5-2	Gasket [Between Flanges]	7257	4212		Ref [5]		0.00E+00	[1], page 65, paragraph 30	6.78E-01	0.09		1.234
6-1	Pipe [Both Side Flange]	8257	5212	0.3123	Ref [5]	0.678	3.45E-01	[1], page 65, paragraph 30	6.78E-01			
6-2	Gasket [Between Flanges]	8262	5216		Ref [5]		0.00E+00	[1], page 65, paragraph 30	6.78E-01	0.32		0.689

7-1	Pipe [Both Side Flange]	9262	6216	0.3123	Ref [5]	0.678	3.45E-01	[1], page 65, paragraph 30	6.78E-01			
7-2	Gasket [Between Flanges]	9266	6221		Ref [5]		0.00E+00	[1], page 65, paragraph 30	6.78E-01	0.32		0.689
8-1	Pipe [One Side Flange]	9466	6421	0.0625	Ref [5]	0.678	6.91E-02	[1], page 65, paragraph 30	6.78E-01			
8-2	Orifice	10066	7021	0.18	Ref [5]	0.587	1.27E-01	[1], page 65, paragraph 30	5.94E-01	0.30		0.603
8-3	Pipe [One Side Flange]	10266	7221	0.0625	Ref [5]	0.678	6.91E-02	[1], page 65, paragraph 30	6.78E-01			
8-4	Gasket [Between Flanges]	10271	7225		Ref [5]		0.00E+00	[1], page 65, paragraph 30	6.78E-01			
9-1	Pipe[Both Side Flange]	10771	7725	0.1562	Ref [5]	0.678	1.73E-01	[1], page 65, paragraph 30	6.78E-01	0.16		0.689
9-2	Gasket [Between Flanges]	10775	7730		Ref [5]		0.00E+00	[1], page 65, paragraph 30	6.78E-01			
10-1	Expansion Tank	11644	7934	0.2136	Ref [5]	0.678	2.08E-01	[1], page 65, paragraph 30	6.78E-01	0.19		0.689
10-2	Gasket [Between Flanges]	11648	7934		Ref [5]		0.00E+00	[1], page 65, paragraph 30	6.78E-01			
11-1	Pipe [Both Side Flange]	12148	7934	0.1562	Ref [5]	0.678	1.73E-01	[1], page 65, paragraph 30	6.78E-01	0.16		0.689
11-2	Gasket [Between Flanges]	12153	7934		Ref [5]		0.00E+00	[1], page 65, paragraph 30	6.78E-01			
12-1	Pipe [One Side Flange]	12453	7934	0.0937	Ref [5]	0.678	1.04E-01	[1], page 65, paragraph 30	6.78E-01			
12-2	Tee	12580	7934	0.0397	Ref [5]	0.678	4.39E-02	[1], page 65, paragraph 30	6.78E-01			
12-3	Pipe	12885	7934	0.0954	Ref [5]	0.678	1.05E-01	[1], page 65,	6.78E-01			

								paragraph 30				
12-4	90 Degree Elbow	13005	7858	0.037	Ref [5]	0.678	8.27E-02	[1], Diagram 6-19	6.78E-01	0.37		0.689
12-5	90 Degree Elbow	13125	7782	0.04	Ref [5]	0.678	0.00E+00	[1], Diagram 6-19	0.00E+00			
12-6	Pipe[One Side Flange]	13325	7782	0.0625	Ref [5]	0.678	6.91E-02	[1], page 65, paragraph 30	6.78E-01			
12-7	Gasket [Between Flanges]	13330	7782		Ref [5]		0.00E+00	[1], page 65, paragraph 30	6.78E-01			
13-1	Gate valve	13546	7782	0.094	Ref [5]	0.614	5.04E-02	[1], page 65, paragraph 30	1.21E+00	0.07		0.689
13-2	Gasket [Between Flanges]	13550	7782		Ref [5]		0.00E+00	[1], page 65, paragraph 30	6.78E-01			
14-1	Pipe [One Side Flange]	13750	7782	0.0625	Ref [5]	0.678	6.91E-02	[1], page 65, paragraph 30	6.78E-01			
14-2	Tee	13877	7782	0.0397	Ref [5]	0.678	4.39E-02	[1], page 65, paragraph 30	6.78E-01	0.23		0.689
14-3	Pipe [One Side Flange]	14259	7782	0.1193	Ref [5]	0.678	1.32E-01	[1], page 65, paragraph 30	6.78E-01			
14-4	Gasket [Between Flanges]	14264	7782		Ref [5]		0.00E+00	[1], page 65, paragraph 30	6.78E-01			
15-1	Heat Exchangner Vessel Inlet	14466	7782	0.0564	Ref [5]	0.678	4.81E-02	[1], page 65, paragraph 30	6.78E-01	0.06		0.689
15-2	Heat Exchangner Internal	16477	5771	0.9957649	Ref [5]	0.121	8.31E-01	[1], page 65, paragraph 30; [2], formula (1.18)	1.21E-01	0.54		0.123
15-3	Heat Exchangner Outlet	16679	5771	0.0564	Ref [5]	0.678	4.81E-02	[1], page 65, paragraph 30	6.78E-01	0.07		0.689
15-4	Gasket	16684	5771		Ref [5]		0.00E+00	[1], page 65,	6.78E-01			

	[Between Flanges]							paragraph 30				
16-1	Pipe [One Side Flange]	16904	5771	0.0687	Ref [5]	0.678	7.59E-02	[1], page 65, paragraph 30	6.78E-01			
16-2	90 Degree Elbow	17024	5695	0.0375	Ref [5]	0.678	4.13E-02	[1], Diagrams 6-1, 6-2, 2-1	6.78E-01			
16-3	Pipe	17809	4909	0.2453	Ref [5]	0.678	2.71E-01	[1], page 65, paragraph 30	6.78E-01			
16-4	Tee	17936	4782	0.0397	Ref [5]	0.678	4.39E-02	[1], page 65, paragraph 30	6.78E-01	0.63		0.689
16-5	Pipe [One Side Flange]	18436	4282	0.1562	Ref [5]	0.678	1.73E-01	[1], page 65, paragraph 30	6.78E-01			
16-6	Gasket [Between Flanges]	18441	4278		Ref [5]		0.00E+00	[1], page 65, paragraph 30	6.78E-01			
17-1	Gate valve	18657	4062	0.094	Ref [5]	0.614	5.04E-02	[1], page 65, paragraph 30	1.21E+00			
17-2	Gasket [Between Flanges]	18661	4057		Ref [5]		0.00E+00	[1], page 65, paragraph 30	6.78E-01			
18-1	Pipe[One Side Flange]	19161	3557	0.1562	Ref [5]	0.678	1.73E-01	[1], page 65, paragraph 30	6.78E-01			
18-2	Tee	19288	3430	0.0397	Ref [5]	0.678	4.39E-02	[1], page 65, paragraph 30	6.78E-01	0.36		0.689
18-3	Pipe [One Side Flange]	19788	2930	0.1562	Ref [5]	0.678	1.73E-01	[1], page 65, paragraph 30	6.78E-01			
18-4	Gasket [Between Flanges]	19793	2926		Ref [5]		0.00E+00	[1], page 65, paragraph 30	6.78E-01			
19-1	Pipe [Both Side Flange]	20793	1926	0.3123	Ref [5]	0.678	3.45E-01	[1], page 65, paragraph 30	6.78E-01	0.32		0.689
19-2	Gasket [Between Flanges]	20797	1921		Ref [5]		0.00E+00	[1], page 65, paragraph 30	6.78E-01			

20-1	Pipe[One Side Flange]	21297	1421	0.1562	Ref [5]	0.678	1.73E-01	[1], page 65, paragraph 30	6.78E-01	0.16		0.689
20-2	Tee	21424	1294	0.0397	Ref [5]	0.678	4.39E-02	[1], page 65, paragraph 30	6.78E-01	0.04		0.689
24-1	Pipe [One Side Flange]	22424	294	0.3123	Ref [5]	0.678	3.45E-01	[1], page 65, paragraph 30	6.78E-01			
24-2	Gasket [Between Flanges]	22429	290		Ref [5]	0.678	0.00E+00	[1], page 65, paragraph 30	6.78E-01	0.64		0.689
24-3	Pipe[Both Side Flange]	23429	-710	0.3123	Ref [5]	0.678	3.45E-01	[1], page 65, paragraph 30	6.78E-01			
24-4	Gasket [Between Flanges]	23433	-715		Ref [5]		0.00E+00	[1], page 65, paragraph 30	6.78E-01			
24-5	Pipe [One Side Flange]	23485	-767	0.0162	Ref [5]	0.678	1.81E-02	[1], page 65, paragraph 30	6.78E-01			
24-6	90 Degree Elbow	23605	-843	0.0375	Ref [5]	0.678	4.13E-02	[1], Diagrams 6-1, 6-2, 2-1	6.78E-01			
24-7	45 Degree Elbow	23665	-843	0.018	Ref [5]	0.678	2.07E-02	[1], Diagrams 6-1, 6-2, 2-1	6.78E-01			
24-8	Pipe [One Side Flange]	23883	-843	0.0678	Ref [5]	0.678	7.50E-02	[1], page 65, paragraph 30	6.78E-01	0.14		0.689
24-9	Gasket [Between Flanges]	23887	-843		Ref [5]		0.00E+00	[1], page 65, paragraph 30	6.78E-01			
24-10	Gate valve	24103	-843	0.094	Ref [5]	0.614	5.04E-02	[1], page 65, paragraph 30	1.21E+00	0.07		0.689
24-11	Gasket [Between Flanges]	24108	-843		Ref [5]		0.00E+00	[1], page 65, paragraph 30	6.78E-01			
24-12	Pipe [One Side Flange]	24408	-843	0.0937	Ref [5]	0.678	1.04E-01	[1], page 65, paragraph 30	6.78E-01			
24-13	Tee	24535	-779	0.397	Ref [5]	0.678	1.15E-02	[1], page 65, paragraph 30	6.78E-01	0.38		0.689

24-14	Pipe [One Side Flange]	24835	-479	0.0937	Ref [5]	0.678	1.26E-01	[1], page 65, paragraph 30	6.78E-01			
25-1	Gasket [Between Flanges]	24839	-475		Ref [5]		0.00E+00	[1], page 65, paragraph 30	6.78E-01	0.07		0.689
25-2	Sump Tank	25816	0		Ref [5]		0.00E+00		0.00E+00			
25-3	Gasket [Between Flanges]	25821	0		Ref [5]		0.00E+00	[1], page 65, paragraph 30	6.78E-01			
25-4	Gate valve	26037	0	0.094	Ref [5]	0.611	5.04E-02	[1], page 65, paragraph 30	1.21E+00	0.12		0.689
25-5	Gasket [Between Flanges]	26041	0		Ref [5]		0.00E+00	[1], page 65, paragraph 30	6.78E-01			
25-6	45 Degree Elbow [One Side Flange]	26124	0	0.025	Ref [5]	0.678	2.85E-02	[1], Diagrams 6-1, 6-2, 2-1	6.78E-01			
25-7	Pipe	26305	0	0.0565	Ref [5]	0.678	6.24E-02	[1], page 65, paragraph 30	6.78E-01	0.12		0.689
25-8	45 Degree Elbow	26365	0	0.018	Ref [5]	0.678	2.07E-02	[1], Diagrams 6-1, 6-2, 2-1	6.78E-01			
25-9	Tee	26492	0	0.0397	Ref [5]	0.678	4.39E-02	[1], page 65, paragraph 30	6.78E-01			
25-10	45 Degree Elbow	26552	0	0.018	Ref [5]	0.678	2.07E-02	[1], Diagrams 6-1, 6-2, 2-1	6.78E-01			
25-11	Pipe	26732	0	0.0565	Ref [5]	0.678	6.24E-02	[1], page 65, paragraph 30	6.78E-01	0.39		0.689
25-12	45 Degree Elbow [One Side Flange]	26815	0	0.025	Ref [5]	0.678	2.85E-02	[1], Diagrams 6-1, 6-2, 2-1	6.78E-01			
25-13	Gasket [Between Flanges]	26819	0		Ref [5]		0.00E+00	[1], page 65, paragraph 30	6.78E-01			

Table C-8: Friction loss coefficient (III) at high-mass flow rate condition - KIT/INR, RRC KI, SNU

Sub Part No.	Sub Part Name	Accumulated Length (mm)	Accumulated Height (mm)	KIT/INR			RRC KI			SNU		
				Factor F(L/D)	Reference (Handbook or etc.)	Reference velocity (m/s)	Factor F(L/D)	Reference (Handbook or etc.)	Reference velocity (m/s)	Factor F(L/D)	Reference (Handbook or etc.)	Reference velocity (m/s)
1-1	Core Inlet	181	0	0.0597	TRACE Theory Manual	0.6774	0.100	Ref. [6]	0.678	0.0606	Colebrook-White correlation, calculated by MARS-LBE 3.11	0.6778
1-2	Downcomer	1403	-1223	0.3945	"	0.1342	0.460	Ref. [7]	0.134	0.4002	〃	0.1343
1-3	Lower Plenum	1616	-1300	0.0218	"	0.0376	0.000					
1-4	Core	2947	31	1.4170	"	0.9196	1.270	Ref. [8]	0.855	1.4355	〃	0.9198
1-5	Upper Plenum	3629	713	0.2251	"	0.6774	0.220	Ref. [6]	0.678	0.2285	〃	0.6779
1-6	Gasket [Between Flanges]	3633	717	0.0112	"	0.3397	0.000		0.678			
2-1	Pipe [One Side Flange]	3933	1017	0.0991	"	0.6774	0.096	Ref. [6]	0.678	0.1006	〃	0.6778
2-2	Tee	4060	1144	0.0419	"	0.6774	0.040	Ref. [6]	0.678			
2-3	Pipe [One Side Flange]	4360	1444	0.0991	"	0.6774	0.096	Ref. [6]	0.678	0.1006	〃	0.6778
2-4	Gasket [Between Flanges]	4365	1449	0.0112	"	0.3397	0.000		0.678			
3-1	Pipe [Both Side Flange]	5365	2449	0.3303	"	0.6774	0.322	Ref. [6]	0.678	0.3353	〃	0.6778
3-2	Gasket [Between Flanges]	5369	2453	0.0112	"	0.3397	0.000		0.678			
4-1	45 Degree Elbow [One Side Flange]	5452	2530	0.0273	"	0.6774	0.027	Ref. [9]	0.678	0.0075	〃 for one side flange	0.6778

4-2	Pipe	5632	2658	0.0597	"	0.6774	0.058	Ref. [6]	0.678	0.0606	〃	0.6778
4-3	45 Degree Elbow	5692	2712	0.0198	"	0.6774	0.019	Ref. [9]	0.678			
4-4	Pipe	6411	3431	0.2375	"	0.6774	0.231	Ref. [6]	0.678	0.2410	〃	0.6778
4-5	Tee	6538	3558	0.0419	"	0.6774	0.041	Ref. [6]	0.678			
4-6	Pipe	6709	3729	0.0565	"	0.6774	0.055	Ref. [6]	0.678	0.0574	〃	0.6778
4-7	45 Degree Elbow	6769	3783	0.0198	"	0.6774	0.019	Ref. [9]	0.678			
4-8	Pipe	6950	3910	0.0597	"	0.6774	0.058	Ref. [6]	0.678	0.0606	〃	0.6778
4-9	45 Degree Elbow [One Side Flange]	7032	3987	0.0273	"	0.6774	0.027	Ref. [9]	0.678	0.0075	〃 for one side flange	0.6778
4-10	Gasket [Between Flanges]	7037	3991	0.0112	"	0.3397	0.000					
5-1	Gate valve	7253	4207	0.0955	"	0.8661	0.070	Ref. [6]	1.213	0.0494	〃	1.2131
5-2	Gasket [Between Flanges]	7257	4212	0.0112	"	0.3397	0.000					
6-1	Pipe [Both Side Flange]	8257	5212	0.3303	"	0.6774	0.322	Ref. [6]	0.678	0.3353	〃	0.6778
6-2	Gasket [Between Flanges]	8262	5216	0.0112	"	0.3397	0.000					
7-1	Pipe [Both Side Flange]	9262	6216	0.3303	"	0.6774	0.322	Ref. [6]	0.678	0.3353	〃	0.6778
7-2	Gasket [Between Flanges]	9266	6221	0.0112	"	0.3397	0.000					
8-1	Pipe [One Side Flange]	9466	6421	0.0661	"	0.6774	0.064	Ref. [6]	0.678	0.0671	〃	0.6778
8-2	Orifice	10066	7021	0.1874	"	0.5932	0.193	Ref. [6]	0.574			

8-3	Pipe [One Side Flange]	10266	7221	0.0661	"	0.6774	0.064	Ref. [6]	0.678	0.0671	〃	0.6778
8-4	Gasket [Between Flanges]	10271	7225	0.0112	"	0.3397	0.000					
9-1	Pipe[Both Side Flange]	10771	7725	0.1652	"	0.6774	0.161	Ref. [6]	0.678	0.1676	〃	0.6778
9-2	Gasket [Between Flanges]	10775	7730	0.0112	"	0.3397	0.000					
10-1	Expansion Tank	11644	7934	0.4724	"	0.4627	0.000			0.1493	〃	0.6778
10-2	Gasket [Between Flanges]	11648	7934	0.0112	"	0.3397	0.000					
11-1	Pipe [Both Side Flange]	12148	7934	0.1652	"	0.6774	0.161	Ref. [6]	0.678	0.1676	〃	0.6778
11-2	Gasket [Between Flanges]	12153	7934	0.0112	"	0.3397	0.000					
12-1	Pipe [One Side Flange]	12453	7934	0.0991	"	0.6774	0.097	Ref. [6]	0.678	0.1006	〃	0.6778
12-2	Tee	12580	7934	0.0419	"	0.6774	0.041	Ref. [6]	0.678			
12-3	Pipe	12885	7934	0.1001	"	0.6774	0.098	Ref. [6]	0.678	0.1024	〃	0.6778
12-4	90 Degree Elbow	13005	7858	0.0396	"	0.6774	0.039	Ref. [9]	0.678			
12-5	90 Degree Elbow	13125	7782	0.0396	"	0.6774	0.039	Ref. [9]	0.678			
12-6	Pipe[One Side Flange]	13325	7782	0.0661	"	0.6774	0.064	Ref. [6]	0.678	0.0671	〃	0.6778
12-7	Gasket [Between Flanges]	13330	7782	0.0112	"	0.3397	0.000					
13-1	Gate valve	13546	7782	0.0955	"	0.8661	0.070	Ref. [6]	1.213	0.0494	〃	1.2131

13-2	Gasket [Between Flanges]	13550	7782	0.0112	"	0.3397	0.000					
14-1	Pipe [One Side Flange]	13750	7782	0.0661	"	0.6774	0.064	Ref. [6]	0.678	0.0671	〃	0.6778
14-2	Tee	13877	7782	0.0419	"	0.6774	0.041	Ref. [6]	0.678			
14-3	Pipe [One Side Flange]	14259	7782	0.1263	"	0.6774	0.123	Ref. [6]	0.678	0.1281	〃	0.6778
14-4	Gasket [Between Flanges]	14264	7782	0.0112	"	0.3397	0.000					
15-1	Heat Exchangner Vessel Inlet	14466	7782	0.0669	"	0.6774	0.110	Ref. [6]	0.678	0.0679	〃	0.6778
15-2	Heat Exchangner Internal	16477	5771	0.6135	"	0.121	0.650	Ref. [8]	0.121	0.5785	〃	0.1211
15-3	Heat Exchangner Outlet	16679	5771	0.0669	"	0.6774	0.110	Ref. [6]	0.678	0.0679	〃	0.6778
15-4	Gasket [Between Flanges]	16684	5771	0.0112	"	0.3397	0.000					
16-1	Pipe [One Side Flange]	16904	5771	0.0726	"	0.6774	0.071	Ref. [6]	0.678	0.0737	〃	0.6778
16-2	90 Degree Elbow	17024	5695	0.0396	"	0.6774	0.039	Ref. [9]	0.678			
16-3	Pipe	17809	4909	0.2595	"	0.6774	0.253	Ref. [6]	0.678	0.1934	〃	0.6778
16-4	Tee	17936	4782	0.0419	"	0.6774	0.041	Ref. [6]	0.678			
16-5	Pipe [One Side Flange]	18436	4282	0.1652	"	0.6774	0.161	Ref. [6]	0.678	0.1676	〃	0.6778
16-6	Gasket [Between Flanges]	18441	4278	0.0112	"	0.3397	0.000					

17-1	Gate valve	18657	4062	0.0955	"	0.8661	0.070	Ref. [6]	1.213	0.0494	〃	1.2131
17-2	Gasket [Between Flanges]	18661	4057	0.0112	"	0.6774	0.000					
18-1	Pipe[One Side Flange]	19161	3557	0.1652	"	0.6774	0.161	Ref. [6]	0.678	0.1676	〃	0.6778
18-2	Tee	19288	3430	0.0419	"	0.6774	0.041	Ref. [6]	0.678			
18-3	Pipe [One Side Flange]	19788	2930	0.1652	"	0.6774	0.161	Ref. [6]	0.678	0.1676	〃	0.6778
18-4	Gasket [Between Flanges]	19793	2926	0.0112	"	0.3397	0.000					
19-1	Pipe [Both Side Flange]	20793	1926	0.3303	"	0.6774	0.322	Ref. [6]	0.678	0.3353	〃	0.6778
19-2	Gasket [Between Flanges]	20797	1921	0.0112	"	0.3397	0.000					
20-1	Pipe[One Side Flange]	21297	1421	0.1652	"	0.6774	0.161	Ref. [6]	0.678	0.1676	〃	0.6778
20-2	Tee	21424	1294	0.0419	"	0.6774	0.041	Ref. [6]	0.678			
24-1	Pipe [One Side Flange]	22424	294	0.3303	"	0.6774	0.322	Ref. [6]	0.678	0.3353	〃	0.6778
24-2	Gasket [Between Flanges]	22429	290	0.0112	"	0.3397	0.000					
24-3	Pipe[Both Side Flange]	23429	-710	0.3303	"	0.6774	0.322	Ref. [6]	0.678	0.3353	〃	0.6778
24-4	Gasket [Between Flanges]	23433	-715	0.0112	"	0.3397	0.000					
24-5	Pipe [One Side Flange]	23485	-767	0.0173	"	0.6774	0.017	Ref. [6]	0.678	0.0175	〃	0.6778
24-6	90 Degree Elbow	23605	-843	0.0396	"	0.6774	0.039	Ref. [9]	0.678			

24-7	45 Degree Elbow	23665	-843	0.0198	"	0.6774	0.019	Ref. [9]	0.678			
24-8	Pipe [One Side Flange]	23883	-843	0.0717	"	0.6774	0.070	Ref. [6]	0.678	0.0728	〃	0.6778
24-9	Gasket [Between Flanges]	23887	-843	0.0112	"	0.3397	0.000					
24-10	Gate valve	24103	-843	0.0955	"	0.8661	0.070	Ref. [6]	1.213	0.0494	〃	1.2131
24-11	Gasket [Between Flanges]	24108	-843	0.0112	"	0.3397	0.000					
24-12	Pipe [One Side Flange]	24408	-843	0.0991	"	0.6774	0.097	Ref. [6]	0.678	0.1006	〃	0.6778
24-13	Tee	24535	-779	0.0419	"	0.6774	0.041	Ref. [6]	0.678			
24-14	Pipe [One Side Flange]	24835	-479	0.0991	"	0.6774	0.097	Ref. [6]	0.678	0.1006	〃	0.6778
25-1	Gasket [Between Flanges]	24839	-475	0.0112	"	0.3397	0.000					
25-2	Sump Tank	25816	0	0.0805	"	0.0206	0.000					
25-3	Gasket [Between Flanges]	25821	0	0.0112	"	0.3397	0.000					
25-4	Gate valve	26037	0	0.0955	"	0.8661	0.070	Ref. [6]	1.213	0.0494	〃	1.2131
25-5	Gasket [Between Flanges]	26041	0	0.0112	"	0.3397	0.000					
25-6	45 Degree Elbow [One Side Flange]	26124	0	0.0273	"	0.6774	0.027	Ref. [9]	0.678	0.0075	〃 for one side flange	0.6778
25-7	Pipe	26305	0	0.0597	"	0.6774	0.058	Ref. [6]	0.678	0.0606	〃	0.6778
25-8	45 Degree	26365	0	0.0198	"	0.6774	0.019	Ref. [9]	0.678			

	Elbow											
25-9	Tee	26492	0	0.0419	"	0.6774	0.041	Ref. [6]	0.678			
25-10	45 Degree Elbow	26552	0	0.0198	"	0.6774	0.019	Ref. [9]	0.678			
25-11	Pipe	26732	0	0.0597	"	0.6774	0.058	Ref. [6]	0.678	0.0606	″	0.6778
25-12	45 Degree Elbow [One Side Flange]	26815	0	0.0273	"	0.6774	0.027	Ref. [9]	0.678	0.0075	″ for one side flange	0.6778
25-13	Gasket [Between Flanges]	26819	0	0.0112	"	0.3397	0.000					

Table C-9: Form loss coefficient (I) at high-mass flow rate condition - ENEA, ERSE, GIDROPRESS, IPPE

Sub Part	ENEA			ERSE			GIDROPRESS			IPPE		
	Factor (K)	Reference (HandBook or etc.)	Reference Velocity (m/s)	Factor (K)	Reference (HandBook or etc.)	Reference Velocity (m/s)	Factor (K)	Reference (HandBook or etc.)	Reference Velocity (m/s)	Factor (K)	Reference (HandBook or etc.)	Reference Velocity (m/s)
25-13 → 1-1	0.24852	Borda-Carnot correlation by Idelchik	0.67904	1.688	(1)		0.11		0.678	0.00E+00	[1], Diagram 2-12	0.00E+00
1-1 → 1-2	0.99423	"	0.67904				1.04		0.678	1.04E+00	[1], Diagram 7-4	6.78E-01
1-2 → 1-3	0.40641	"	0.13450	1.118	“		0.018		0.678	2.50E-02	[1], Diagrams 4-2, 4-6, 4-1	1.44E-01
1-3 → 1-4	0.45568	"	0.92134				0.755		0.678	5.00E-01	[1], Diagram 3-1	9.21E-01
in 1-4	5.17890	Rehme correlation for grids	0.92134	4.699	(2)	0.920	17.3		0.678	2.26E+00	[1], Diagrams 4-14, 4-15, 4-19	1.80E+00
1-4 → 1-5	0.06917	Borda-Carnot correlation by Idelchik	0.92135				0.13		0.678	9.76E-02	[1], Diagrams 4-2, 4-6, 4-1	9.21E-01
1-5 → 1-6	0.24852	"	0.67904	0.549	(1)		0.016		0.678	1.04E-02	[1], Diagram 2-12	6.78E-01
1-6 → 2.1	0.24926	"	0.67904				0.107		0.678	0.00E+00	[1], Diagram 2-12	0.00E+00
in 2-2	0.00000			0.700	“	0.454	0.1		0.678	0.00E+00		0.00E+00
2-3 → 2-4	0.24852	Borda-Carnot correlation by Idelchik	0.67904	0.549	“		0.016		0.678	1.04E-02	[1], Diagram 2-12	6.78E-01
2-4 → 3-1	0.24926	"	0.67904				0.107		0.678	0.00E+00	[1], Diagram 2-12	0.00E+00
3-1 → 3-2	0.24852	"	0.67904	0.549	“		0.016		0.678	1.04E-02	[1], Diagram 2-12	6.78E-01

3-2 → 4-1	0.24926	"	0.67904				0.107		0.678	0.00E+00	[1], Diagram 2-12	0.00E+00
in 4-1	0.13593	45° Elbow correlation by Idelchik	0.67905	0.067	“	0.678	0.11		0.678	9.65E-02	[1], Diagrams 6-1, 6-2, 2-1	6.78E-01
in 4-3	0.13593	"	0.67905	0.067	“	0.678	0.11		0.678	9.65E-02	[1], Diagrams 6-1, 6-2, 2-1	6.78E-01
in 4-5	0.00000			0.700	“	0.678	0.1		0.678	0.00E+00		6.78E-01
in 4-7	0.13593	45° Elbow correlation by Idelchik	0.67905	0.067	“	0.678	0.11		0.678	9.65E-02	[1], Diagrams 6-1, 6-2, 2-1	6.78E-01
in 4-9	0.13593	"	0.67905	0.067	“	0.678	0.11		0.678	9.65E-02	[1], Diagrams 6-1, 6-2, 2-1	6.78E-01
4-9 → 4-10	0.24852	Borda-Carnot correlation by Idelchik	0.67906	1.679			0.016		0.678	1.04E-02	[1], Diagram 2-12	6.78E-01
4-10 → 5-1	0.22329	"	0.67906				0.107		0.678	0.00E+00	[1], Diagram 2-12	0.00E+00
in 5-1	0.89700	Valve coefficient supplied by manufacturer	1.21535		“	1.213	1.72		0.678	5.76E-01	[1], Diagrams 4-9, 4-10, 4-2, 4-6, 4-1	1.21E+00
5-1 → 5-2	0.19943	Borda-Carnot correlation by Idelchik	0.67906				0.016		0.678	1.04E-02	[1], Diagram 2-12	6.78E-01
5-2 → 6-1	0.24926	"	0.67906				0.107		0.678	0.00E+00	[1], Diagram 2-12	0.00E+00
6-1 → 6-2	0.24852	"	0.67906	0.549	“		0.016		0.678	1.04E-02	[1], Diagram 2-12	6.78E-01
6-2 → 7-1	0.24926	"	0.67906				0.107		0.678	0.00E+00	[1], Diagram 2-12	0.00E+00
7-1 → 7-2	0.24852	"	0.67906	0.549	“		0.016		0.678	1.04E-02	[1], Diagram 2-12	6.78E-01

7-2 → 8-1	0.24926	"	0.67906	0.015	“		0.107		0.678	0.00E+00	[1], Diagram 2-12	0.00E+00
in 8-2	0.46481(*) 9.8507 0.43181(*)	Orifice correlation by Idelchik	0.67906 0.59468 0.67907	2.309	(3)	1.576	7.796		0.678	1.44E+00	[1], Diagrams 4-14, 4-15, 4-19	1.58E+00
8-3 → 8-4	0.24852	Borda-Carnot correlation by Idelchik	0.67907	0.105	(1)		0.016		0.678	1.04E-02	[1], Diagram 2-12	6.78E-01
8-4 → 9-1	0.24926	"	0.67907	0.549	“		0.107		0.678	0.00E+00	[1], Diagram 2-12	0.00E+00
9-1 → 9-2	0.24852	"	0.67907	0.549	“		0.016		0.678	1.04E-02	[1], Diagram 2-12	6.78E-01
9-2 → 10-1	0.24926	"	0.67907				0.107		0.678	0.00E+00	[1], Diagram 2-12	0.00E+00
in 10-1	0.9418(*) 0.48687 (**)	"	0.679 0.831	1.684	“		1.61		0.678	1.66E+00	[1], Diagrams 6-1, 6-2, 2-1	6.78E-01
10-1 → 10-2	0.22218 (*) 0.24852	90° Elbow correlation by Idelchik	0.67908 0.67908	0.549	“		0.016		0.678	1.04E-02	[1], Diagram 2-12	6.78E-01
10-2 → 11-1	0.24926	Borda-Carnot correlation by Idelchik	0.67908				0.107		0.678	0.00E+00	[1], Diagram 2-12	0.00E+00
11-1 → 11-2	0.24852	"	0.67908	0.549	“		0.016		0.678	1.04E-02	[1], Diagram 2-12	6.78E-01
11-2 → 12-1	0.24926	"	0.67908				0.107		0.678	0.00E+00	[1], Diagram 2-12	0.00E+00
in 12-2	0.00000			0.700	“	0.678	0.1		0.678	0.00E+00		6.78E-01
in 12-4	0.22218	90° Elbow correlation by Idelchik	0.67908	0.184	“	0.678	0.17		0.678	3.22E-01	[1], Diagram 2-12	6.78E-01
in 12-5	0.22218	"	0.67908	0.184	“	0.678	0.17		0.678	0.00E+00	[1], Diagram 2-	0.00E+00

											12	
12-6 → 12-7	0.24852	Borda-Carnot correlation by Idelchik	0.67908	1.679			0.016		0.678	1.04E-02	[1], Diagram 2-12	6.78E-01
12-7 → 13-1	0.22329	"	0.67908				0.107		0.678	0.00E+00	[1], Diagram 2-12	0.00E+00
in 13-1	0.89700	Valve coefficient supplied by manufacturer	1.21539		"	1.213	1.72		0.678	5.76E-01	[1], Diagrams 4-9, 4-10, 4-2, 4-6, 4-1	1.21E+00
13-1 → 13-2	0.19943	Borda-Carnot correlation by Idelchik	0.67906				0.016		0.678	1.04E-02	[1], Diagram 2-12	6.78E-01
13-2 → 14-1	0.24926	"	0.67906				0.107		0.678	0.00E+00	[1], Diagram 2-12	0.00E+00
in 14-2	0.00000			0.700	"	0.678	0.1		0.678	0.00E+00		6.78E-01
14-3 → 14-4	0.24852	Borda-Carnot correlation by Idelchik	0.67908	1.549			0.016		0.678	1.04E-02	[1], Diagram 2-12	6.78E-01
14-4 → 15-1	0.24926	"	0.67908		"		0.107		0.678	0.00E+00	[1], Diagram 2-12	0.00E+00
15-1 → 15-2	0.49723	"	0.67908				1.03		0.678	1.03E+00	[1], Diagram 7-4	6.78E-01
in 15-2	9.03600	Rehme correlation for grids	0.12129	9.428	(2)	0.121	0.54		0.678	4.71E+00	[1], Diagrams 4-14, 4-15, 4-19	2.20E-01
15-2 → 15-3	0.35257	Borda-Carnot correlation by Idelchik	0.67907	1.049	(1)		0.79		0.678	1.03E+00	[1], Diagram 7-18	6.78E-01
15-3 → 15-4	0.24852	"	0.67907				0.016		0.678	1.04E-02	[1], Diagram 2-12	6.78E-01
15-4 → 16-1	0.24926	"	0.67907				0.107		0.678	0.00E+00	[1], Diagram 2-12	0.00E+00
in 16-2	0.22218	90° Elbow	0.67907	0.184	"	0.678	0.17		0.678	1.61E-01	[1], Diagrams 6-	6.78E-01

		correlation by Idelchik									1, 6-2, 2-1	
in 16-4	0.00000			0.700	“	0.678	0.1		0.678	0.00E+00		6.78E-01
16-5 → 16-6	0.24852	Borda-Carnot correlation by Idelchik	0.67906	1.679			0.016		0.678	1.04E-02	[1], Diagram 2-12	6.78E-01
16-6 → 17-1	0.22329	"	0.67908				0.107		0.678	0.00E+00	[1], Diagram 2-12	0.00E+00
in 17-1	0.89700	Valve coefficient supplied by manufacturer	1.21536		“	1.213	1.72		0.678	5.76E-01	[1], Diagrams 4-9, 4-10, 4-2, 4-6, 4-1	1.21E+00
17-1 → 17-2	0.19943	Borda-Carnot correlation by Idelchik	0.67906				0.016		0.678	1.04E-02	[1], Diagram 2-12	6.78E-01
17-2 → 18-1	0.24926	"	0.67906				0.107		0.678	0.00E+00	[1], Diagram 2-12	0.00E+00
in 18-2	0.00000			0.700	“	0.678	0.1		0.678	0.00E+00		6.78E-01
18-3 → 18-4	0.24852	Borda-Carnot correlation by Idelchik	0.67908	0.549	“		0.016		0.678	1.04E-02	[1], Diagram 2-12	6.78E-01
18-4 → 19-1	0.24926	"	0.67908				0.107		0.678	0.00E+00	[1], Diagram 2-12	0.00E+00
19-1 → 19-2	0.24852	"	0.67908	0.549	“		0.016		0.678	1.04E-02	[1], Diagram 2-12	6.78E-01
19-2 → 20-1	0.24926	"	0.67908				0.107		0.678	0.00E+00	[1], Diagram 2-12	0.00E+00
in 20-2	0.00000			0.700	“	0.678	0.1		0.678	0.00E+00		6.78E-01
24-1 → 24-2	0.24852	Borda-Carnot correlation by Idelchik	0.67908	0.566	“		0.016		0.678	1.04E-02	[1], Diagram 2-12	6.78E-01
24-2 → 24-3	0.24926	"	0.67908				0.107		0.678	0.00E+00	[1], Diagram 2-12	0.00E+00

24-3 → 24-4	0.24852	"	0.67905	0.549	“		0.016		0.678	1.04E-02	[1], Diagram 2-12	6.78E-01
24-4 → 24-5	0.24926	"	0.67904	0.266		0.678	0.107		0.678	0.00E+00	[1], Diagram 2-12	0.00E+00
in 24-6	0.22218	90° Elbow correlation by Idelchik	0.67904		“		0.17		0.678	1.61E-01	[1], Diagrams 6-1, 6-2, 2-1	6.78E-01
in 24-7	0.13593	45° Elbow correlation by Idelchik	0.67904				0.11		0.678	9.65E-02	[1], Diagrams 6-1, 6-2, 2-1	6.78E-01
24-8 → 24-9	0.24852	Borda-Carnot correlation by Idelchik	0.67904	1.679			0.016		0.678	1.04E-02	[1], Diagram 2-12	6.78E-01
24-9 → 24-10	0.22329	"	0.67904				0.107		0.678	0.00E+00	[1], Diagram 2-12	0.00E+00
in 24-10	0.89700	Valve coefficient supplied by manufacturer	1.21532		“	1.213	1.72		0.678	5.76E-01	[1], Diagrams 4-9, 4-10, 4-2, 4-6, 4-1	1.21E+00
24-10 → 24-11	0.19943	Borda-Carnot correlation by Idelchik	0.67904				0.016		0.678	1.04E-02	[1], Diagram 2-12	6.78E-01
24-11 → 24-12	0.24926	"	0.67904				0.107		0.678	0.00E+00	[1], Diagram 2-12	0.00E+00
in 24-13	0.22218		0.67904	0.700	“	0.678	1.43		0.678	0.00E+00	[1], Diagram 7-4	6.78E-01
24-14 → 25-1	0.24852	Borda-Carnot correlation by Idelchik	0.67904	0.549	“		0.016		0.678	1.04E-02	[1], Diagram 2-12	6.78E-01
25-1 → 25-2	0.24926	"	0.67904				0.107		0.678	0.00E+00	[1], Diagram 2-12	0.00E+00
in 25-2	0.98324(*) 0.71059 (**)	"	0.679 8.13425			8.122	1.45		0.678	0.00E+00		0.00E+00

25-2 → 25-3	0.78604	Borda-Carnot correlation by Idelchik	8.13445	1.679			0.016		0.678	1.04E-02	[1], Diagram 2-12	6.78E-01
25-3 → 25-4	0.22329	"	8.13445				0.107		0.678	0.00E+00	[1], Diagram 2-12	0.00E+00
in 25-4	0.89700	Valve coefficient supplied by manufacturer	1.21533		“	1.213	1.72		0.678	5.76E-01	[1], Diagrams 4-9, 4-10, 4-2, 4-6, 4-1	1.21E+00
25-4 → 25-5	0.19943	Borda-Carnot correlation by Idelchik	0.67904				0.016		0.678	1.04E-02	[1], Diagram 2-12	6.78E-01
25-5 → 25-6	0.24926	"	0.67904				0.107		0.678	0.00E+00	[1], Diagram 2-12	0.00E+00
in 25-6	0.13593	45° Elbow correlation by Idelchik	0.67904	0.133	“	0.678	0.11		0.678	9.65E-02	[1], Diagrams 6-1, 6-2, 2-1	6.78E-01
in 25-8	0.13593	"	0.67904			0.678	0.11		0.678	9.65E-02	[1], Diagrams 6-1, 6-2, 2-1	6.78E-01
in 25-9	0.00000			0.700	“	0.678	0.1		0.678	0.00E+00		6.78E-01
in 25-10	0.13593	45° Elbow correlation by Idelchik	0.67904	0.133	“	0.678	0.11		0.678	9.65E-02	[1], Diagrams 6-1, 6-2, 2-1	6.78E-01
in 25-12	0.13593	"	0.67904			0.678	0.11		0.678	9.65E-02	[1], Diagrams 6-1, 6-2, 2-1	6.78E-01
25-12 → 25-13	0.24926	Borda-Carnot correlation by Idelchik	0.67904				0.016		0.678	1.04E-02	[1], Diagram 2-12	6.78E-01

Table C-10: Form loss coefficient (II) at high-mass flow rate condition - KIT/IKET, KIT/INR, RRC KI, SNU

Sub Part	KIT/IKET			KIT/INR			RRC KI			SNU		
	Factor (K)	Reference (HandBook or etc.)	Reference Velocity (m/s)	Factor (K)	Reference (HandBook or etc.)	Reference Velocity (m/s)	Factor (K)	Reference (HandBook or etc.)	Reference Velocity (m/s)	Factor (K)	Reference (HandBook or etc.)	Reference Velocity (m/s)
25-13 → 1-1	1.92	see contribution to	0.689	1.92	see contribution to	0.689	0.13	Ref. [10]	0.678	0.2507	(a)	0.6778
1-1 → 1-2	0.00	report Phase-1	0.145	0.00	report Phase-1	0.145	0.726	Ref. [11]	0.134	0.6525	(a)	0.6778
1-2 → 1-3	1.00		0.045	1.00		0.045	0.93	Ref. [12]	0.134	0.3717	(a)	0.6778
1-3 → 1-4	8.70		0.936	8.70		0.936	1.4	Ref. [13]	0.855	0.0880	(a)	0.9198
in 1-4	0.00		0.689	0.00		0.689	0.705	Ref. [14]	0.826	4.0100	(b)	0.9198
1-4 → 1-5							0.025	Ref. [15]	0.678	0.0699	(a)	0.9198
1-5 → 1-6							0.115	Ref. [16]	0.678	0.2521	(a)	0.6778
1-6 → 2.1							0.13	Ref. [10]	0.678	0.2507	(a)	0.6778
in 2-2	0.05		0.689	0.05		0.689	0.7	Ref. [17]	0.678	0.7000	(c)	0.6778
2-3 → 2-4							0.115	Ref. [16]	0.678	0.2521	(a)	0.6778
2-4 → 3-1							0.13	Ref. [10]	0.678	0.2507	(a)	0.6778
3-1 → 3-2	0.00		0.689	0.00		0.689	0.115	Ref. [16]	0.678	0.2521	(a)	0.6778
3-2 → 4-1							0.13	Ref. [10]	0.678	0.2507	(a)	0.6778
in 4-1							0.068	Ref. [18]	0.678	0.1700	(a)	0.6778
in 4-3							0.068	Ref. [18]	0.678	0.1700	(c)	0.6778
in 4-5	0.49		0.689	0.49		0.689	0.7	Ref. [17]	0.678	0.7000	(c)	0.6778
in 4-7							0.068	Ref. [18]	0.678	0.1700	(c)	0.6778
in 4-9							0.068	Ref. [18]	0.678	0.1700	(c)	0.6778
4-9 → 4-10							0.115	Ref. [16]	0.678	0.2521	(a)	0.6778
4-10 → 5-1							0.13	Ref. [10]	0.678	0.2161	(a)	0.6142

in 5-1							1	Ref. [19]	1.213	0.4800	(a)	1.2131
5-1 → 5-2	1.05		1.234	1.05		1.234	0.13	Ref. [10]	0.678	0.2027	(a)	0.6142
5-2 → 6-1							0.13	Ref. [10]	0.678	0.2507	(a)	0.6778
6-1 → 6-2							0.115	Ref. [16]	0.678	0.2521	(a)	0.6778
6-2 → 7-1	0.00		0.689	0.00		0.689	0.13	Ref. [10]	0.678	0.2507	(a)	0.6778
7-1 → 7-2							0.115	Ref. [16]	0.678	0.2521	(a)	0.6778
7-2 → 8-1	0.00		0.689	0.00		0.689	0.13	Ref. [10]	0.678	0.2507	(a)	0.6778
in 8-2	10.88		0.603	10.88		0.603	2.43	Ref. [15]	0.574	8.3900	(c)	0.6778
8-3 → 8-4							0.115	Ref. [16]	0.678	0.2521	(a)	0.6778
8-4 → 9-1							0.13	Ref. [10]	0.678	0.2507	(a)	0.6778
9-1 → 9-2	0.00		0.689	0.00		0.689	0.115	Ref. [16]	0.678	0.2521	(a)	0.6778
9-2 → 10-1							0.13	Ref. [10]	0.678	0.2507	(a)	0.6778
in 10-1	1.50		0.689	1.50		0.689	1	Ref. [12]	0.678	1.3433	(a)	0.6778
10-1 → 10-2							0.2	Ref. [20]	0.678	0.2521	(a)	0.6778
10-2 → 11-1							0.13	Ref. [10]	0.678	0.2507	(a)	0.6778
11-1 → 11-2	0.00		0.689	0.00		0.689	0.115	Ref. [16]	0.678	0.2521	(a)	0.6778
11-2 → 12-1							0.13	Ref. [10]	0.678	0.2507	(a)	0.6778
in 12-2							0.7	Ref. [17]	0.678	0.7000	(c)	0.6778
in 12-4	0.39		0.689	0.39		0.689	0.096	Ref. [18]	0.678	0.1900	(c)	0.6778
in 12-5							0.096	Ref. [18]	0.678	0.1900	(c)	0.6778
12-6 → 12-7							0.115	Ref. [16]	0.678	0.2521	(a)	0.6778
12-7 → 13-1							0.13	Ref. [10]	0.678	0.2161	(a)	0.6142
in 13-1	1.05		0.689	1.05		0.689	1	Ref. [19]	1.213	0.4800	(a)	1.2131
13-1 → 13-2							0.115	Ref. [16]	0.678	0.2027	(a)	0.6142
13-2 → 14-1							0.13	Ref. [10]	0.678	0.2507	(a)	0.6778
in 14-2	0.05		0.689	0.05		0.689	0.7	Ref. [17]	0.678	0.7000	(c)	0.6778

14-3 → 14-4							0.115	Ref. [16]	0.678	0.2521	(a)	0.6778
14-4 → 15-1							0.13	Ref. [10]	0.678	0.2507	(a)	0.6778
15-1 → 15-2	1.72		0.689	1.72		0.689	0.726	Ref. [11]	0.121	0.6847	(a)	0.6778
in 15-2	5.79		0.123	5.79		0.123	6*0.99	Ref. [14]	0.121	9.0500	(b)	0.1210
15-2 → 15-3							0.2	Ref. [20]	0.121	0.3915	(a)	0.6778
15-3 → 15-4	1.97		0.689	1.97		0.689	0.115	Ref. [16]	0.678	0.2521	(a)	0.6778
15-4 → 16-1							0.13	Ref. [10]	0.678	0.2507	(a)	0.6778
in 16-2							0.096	Ref. [18]	0.678	0.1900	(c)	0.6778
in 16-4	1.37		0.689	1.37		0.689	0.7	Ref. [17]	0.678	0.7000	(c)	0.6778
16-5 → 16-6							0.115	Ref. [16]	0.678	0.2521	(a)	0.6778
16-6 → 17-1							0.13	Ref. [10]	0.678	0.2161	(a)	0.6142
in 17-1							1	Ref. [19]	1.213	0.4800	(a)	1.2131
17-1 → 17-2							0.115	Ref. [16]	0.678	0.2027	(a)	0.6142
17-2 → 18-1							0.13	Ref. [10]	0.678	0.2507	(a)	0.6778
in 18-2	0.05		0.689	0.05		0.689	0.7	Ref. [17]	0.678	0.7000	(c)	0.6778
18-3 → 18-4							0.115	Ref. [16]	0.678	0.2521	(a)	0.6778
18-4 → 19-1							0.13	Ref. [10]	0.678	0.2507	(a)	0.6778
19-1 → 19-2	0.00		0.689	0.00		0.689	0.115	Ref. [16]	0.678	0.2521	(a)	0.6778
19-2 → 20-1	0.00		0.689	0.00		0.689	0.13	Ref. [10]	0.678	0.2507	(a)	0.6778
in 20-2	0.05		0.689	0.05		0.689	0.7	Ref. [17]	0.678	0.7000	(c)	0.6778
24-1 → 24-2							0.115	Ref. [16]	0.678	0.2521	(a)	0.6778
24-2 → 24-3	0.00		0.689	0.00		0.689	0.13	Ref. [10]	0.678	0.2507	(a)	0.6778
24-3 → 24-4							0.115	Ref. [16]	0.678	0.2521	(a)	0.6778
24-4 → 24-5							0.13	Ref. [10]	0.678	0.2507	(a)	0.6778
in 24-6							0.096	Ref. [18]	0.678	0.1900	(c)	0.6778
in 24-7							0.068	Ref. [18]	0.678	0.1700	(c)	0.6778

24-8 → 24-9	0.28		0.689	0.28		0.689	0.115	Ref. [16]	0.678	0.2521	(a)	0.6778
24-9 → 24-10							0.13	Ref. [10]	0.678	0.2161	(a)	0.6142
in 24-10	1.05		0.689	1.05		0.689	1	Ref. [19]	1.213	0.4800	(a)	1.2131
24-10 → 24-11							0.115	Ref. [16]	0.678	0.2027	(a)	0.6142
24-11 → 24-12							0.13	Ref. [10]	0.678	0.2507	(a)	0.6778
in 24-13	1.30		0.689	1.30		0.689	0.7	Ref. [17]	0.678	2.8000	(c)	0.6778
24-14 → 25-1							0.115	Ref. [16]	0.678	0.2521	(a)	0.6778
25-1 → 25-2	1.15		0.689	1.15		0.689	0.13	Ref. [10]	0.678	0.2507	(a)	0.6778
in 25-2							1	Ref. [12]	0.678			
25-2 → 25-3							0.115	Ref. [16]	0.678	0.2521	(a)	0.6778
25-3 → 25-4							0.13	Ref. [10]	0.678	0.2161	(a)	0.6142
in 25-4	0.25		0.689	0.25		0.689	1	Ref. [19]	1.213	0.4800	(a)	0.6778
25-4 → 25-5							0.115	Ref. [16]	0.678	0.2027	(a)	0.6142
25-5 → 25-6							0.13	Ref. [10]	0.678	0.2507	(a)	0.6778
in 25-6	0.25		0.689	0.25		0.689	0.068	Ref. [18]	0.678	0.1700	(c)	0.6778
in 25-8							0.068	Ref. [18]	0.678	0.1700	(c)	0.6778
in 25-9							0.7	Ref. [17]	0.678	0.7000	(c)	0.6778
in 25-10	0.36		0.689	0.36		0.689	0.068	Ref. [18]	0.678	0.1700	(c)	0.6778
in 25-12							0.068	Ref. [18]	0.678	0.1700	(c)	0.6778
25-12 → 25-13							0.115	Ref. [16]	0.678	0.2521	(a)	0.6778

Table C-11: Form loss coefficient of IAEA at low-and high-mass flow rate condition

Sub Part	IAEA – Low flow rate			IAEA – High flow rate		
	Factor (K)	Reference (HandBook or etc.)	Reference Velocity (m/s)	Factor (K)	Reference (HandBook or etc.)	Reference Velocity (m/s)
in 25-13	0.22	Ref [5]	0.163	0.19	Ref [5]	0.678
1-1 → 1-2	1.11	Ref [5]	0.163	1.11	Ref [5]	0.678
1-2 → 1-3	0.91	Ref [5]	0.032	0.91	Ref [5]	0.134
1-3 → 1-4	0.42	Ref [6]	0.222	0.42	Ref [6]	0.920
in 1-4	3.54	Ref [5]	0.222	3.54	Ref [5]	0.920
1-4 → 1-5	0.07	Ref [5]	0.222	0.07	Ref [5]	0.920
1-5 → 1-6	0		0.163	0		
in 1-6	0.22	CFD analysis, Ref [4]	0.163	0.19	CFD analysis, Ref [4]	0.678
in 2-2	0.15	CFD analysis, Ref [4]	0.163	0.25	CFD analysis, Ref [4]	0.678
2-3 → 2-4	0		0.163	0		0.000
in 2-4	0.22	CFD analysis, Ref [4]	0.163	0.19	CFD analysis, Ref [4]	0.678
3-1 → 3-2	0		0.163	0		
in 3-2	0.22	CFD analysis, Ref [4]	0.163	0.19	CFD analysis, Ref [4]	0.678
in 4-1	0.11	Ref [5]	0.163	0.11	Ref [5]	0.678
in 4-3	0.11	Ref [5]	0.163	0.11	Ref [5]	0.678
in 4-5	0.15	CFD analysis, Ref [4]	0.163	0.25	CFD analysis, Ref [4]	0.678
in 4-7	0.11	Ref [5]	0.163	0.11	Ref [5]	0.678
in 4-9	0.11	Ref [5]	0.163	0.11	Ref [5]	0.678
4-9 → 4-10	0		0.163	0		0.678
in 4-10	0.22	CFD analysis, Ref [4]	0.163	0.19	CFD analysis, Ref [4]	0.678
in 5-1	1.04	Ref [5]	0.147	1.04	Ref [5]	0.614
5-1 → 5-2	0		0.163	0		

in 5-2	0.22	CFD analysis, Ref [4]	0.163	0.19	CFD analysis, Ref [4]	0.678
6-1 → 6-2	0		0.163	0		
in 6-2	0.22	CFD analysis, Ref [4]	0.163	0.19	CFD analysis, Ref [4]	0.678
7-1 → 7-2	0		0.163	0		
in 7-2	0.22	CFD analysis, Ref [4]	0.163	0.19	CFD analysis, Ref [4]	0.678
8-1 → 8-5*	0		0.163	0		
in 8-5	0.22	CFD analysis, Ref [4]	0.163	0.19	CFD analysis, Ref [4]	0.678
in 8-2	6	Ref [5]	0.141	6	Ref [5]	0.587
8-2 → 8-6*	0		0.163	0		
in 8-6	0.22	CFD analysis, Ref [4]	0.163	0.19	CFD analysis, Ref [4]	0.678
8-3 → 8-4	0		0.163	0		
in 8-4	0.22	CFD analysis, Ref [4]	0.163	0.19	CFD analysis, Ref [4]	0.678
9-1 → 9-2	0		0.163	0		
in 9-2	0.22	CFD analysis, Ref [4]	0.163	0.19	CFD analysis, Ref [4]	0.678
in 10-1	1.61	Ref [5]	0.163	1.61	Ref [5]	0.678
10-1 → 10-2	0		0.163	0		
in 10-2	0.22	CFD analysis, Ref [4]	0.163	0.19	CFD analysis, Ref [4]	0.678
11-1 → 11-2	0		0.163	0		
in 11-2	0.22	CFD analysis, Ref [4]	0.163	0.19	CFD analysis, Ref [4]	0.678
in 12-2	0.15	CFD analysis, Ref [4]	0.163	0.25	CFD analysis, Ref [4]	0.678
in 12-4	0.17	Ref [5]	0.163	0.17	Ref [5]	0.678
in 12-5	0.17	Ref [5]	0.163	0.17	Ref [5]	0.678
12-6 → 12-7	0		0.163	0		0.678
in 12-7	0.22	CFD analysis, Ref [4]	0.163	0.19	CFD analysis, Ref [4]	0.678
in 13-1	1.04	Ref [5]	0.147	1.04	Ref [5]	0.614
13-1 → 13-2	0	Ref [5]	0.163	0		

in 13-2	0.22	CFD analysis, Ref [4]	0.163	0.19	CFD analysis, Ref [4]	0.678
in 14-2	0.15	CFD analysis, Ref [4]	0.163	0.25	CFD analysis, Ref [4]	0.678
14-3 → 14-4	0		0.163	0		
in 14-4	0.22	CFD analysis, Ref [4]	0.163	0.19	CFD analysis, Ref [4]	0.678
15-1 → 15-2	1.1	Ref [5]	0.163	1.1	Ref [5]	0.678
in 15-2	9.1	Ref [6]	0.029	9.1	Ref [6]	0.121
15-2 → 15-3	2.2	CFD analysis, Ref [4]	0.163	2.2	CFD analysis, Ref [4]	0.678
15-3 → 15-4	0		0.163	0		
in 15-4	0.22	CFD analysis, Ref [4]	0.163	0.19	CFD analysis, Ref [4]	0.678
in 16-2	0.17	Ref [5]	0.163	0.17	Ref [5]	0.678
in 16-4	0.15	CFD analysis, Ref [4]	0.163	0.25	CFD analysis, Ref [4]	0.678
16-5 → 16-6	0		0.163	0		
16-5 → 17-1	0.107	Ref [5]	0.163	0.107	Ref [5]	0.678
in 17-1	1.04	Ref [5]	0.147	1.04	Ref [5]	0.614
17-1 → 17-2	0		0.163	0		
in 17-2	0.22	CFD analysis, Ref [4]	0.163	0.19	CFD analysis, Ref [4]	0.678
in 18-2	0.15	CFD analysis, Ref [4]	0.163	0.25	CFD analysis, Ref [4]	0.678
18-3 → 18-4	0		0.163	0		
in 18-4	0.22	CFD analysis, Ref [4]	0.163	0.19	CFD analysis, Ref [4]	0.678
19-1 → 19-2	0		0.163	0		
in 19-2	0.22	CFD analysis, Ref [4]	0.163	0.19	CFD analysis, Ref [4]	0.678
in 20-2	0.15	CFD analysis, Ref [4]	0.163	0.25	CFD analysis, Ref [4]	0.678
24-1 → 24-2	0		0.163	0		
in 24-2	0.22	CFD analysis, Ref [4]	0.163	0.19	CFD analysis, Ref [4]	0.678
24-3 → 24-4	0		0.163	0		
in 24-4	0.22	CFD analysis, Ref [4]	0.163	0.19	CFD analysis, Ref [4]	0.678

in 24-6	0.17	Ref [5]	0.163	0.17	Ref [5]	0.678
in 24-7	0.11	Ref [5]	0.163	0.11	Ref [5]	0.678
24-8 → 24-9	0		0.163	0		
in 24-9	0.22	CFD analysis, Ref [4]	0.163	0.19	CFD analysis, Ref [4]	0.678
in 24-10	1.04	Ref [5]	0.147	1.04	Ref [5]	0.614
24-10 → 24-14*	0		0.163	0		
in 24-14	0.22	CFD analysis, Ref [4]	0.163	0.19	CFD analysis, Ref [4]	0.678
in 24-12	0.15	CFD analysis, Ref [4]	0.163	0.25	CFD analysis, Ref [4]	0.678
24-13 → 25-1	0		0.163	0		
in 25-1	0.22	CFD analysis, Ref [4]	0.163	0.19	CFD analysis, Ref [4]	0.678
in 25-2	0		0.163	0		
25-2 → 25-3***	0.84	Ref [5]	1.956	0.84	Ref [5]	8.137
in 25-3	0.22	CFD analysis, Ref [4]	0.163	0.19	CFD analysis, Ref [4]	0.678
in 25-4	1.04	Ref [5]	0.147	1.04	Ref [5]	0.614
25-4 → 25-5	0		0.163	0		
in 25-5	0.22	CFD analysis, Ref [4]	0.163	0.19	CFD analysis, Ref [4]	0.678
in 25-6	0.11	Ref [5]	0.163	0.11	Ref [5]	0.678
in 25-8	0.11	Ref [5]	0.163	0.11	Ref [5]	0.678
in 25-9	0.15	CFD analysis, Ref [4]	0.163	0.25	CFD analysis, Ref [4]	0.678
in 25-10	0.11	Ref [5]	0.163	0.11	Ref [5]	0.678
in 25-12	0.11	Ref [5]	0.163	0.11	Ref [5]	0.678